AD-A258 257

CUMENTATION PAGE

Form Approved
OMB No 0704-0188

1. AGENCY USE ONLY (Leave blank)	2. REPORT DATE	3. REPORT TYPE AND DATES COVERED
	1992	XXXXXXXDISSERTATION

4. TITLE AND SUBTITLE
Robust Multivariable Feedback Design for Uncertain Linear Systems

5. FUNDING NUMBERS

6. AUTHOR(S)
Mark C. Crews, Captain

7. PERFORMING ORGANIZATION NAME(S) AND ADDRESS(ES)
AFIT Student Attending: University of Oxford

8. PERFORMING ORGANIZATION REPORT NUMBER
AFIT/CI/CIA-92-025D

9. SPONSORING / MONITORING AGENCY NAME(S) AND ADDRESS(ES)
AFIT/CI
Wright-Patterson AFB OH 45433-6583

10. SPONSORING / MONITORING AGENCY REPORT NUMBER

11. SUPPLEMENTARY NOTES

12a. DISTRIBUTION / AVAILABILITY STATEMENT
Approved for Public Release IAW 190-1
Distributed Unlimited
ERNEST A. HAYGOOD, Captain, USAF
Executive Officer

12b. DISTRIBUTION CODE

13. ABSTRACT (Maximum 200 words)

14. SUBJECT TERMS	15. NUMBER OF PAGES 215
	16. PRICE CODE

17. SECURITY CLASSIFICATION OF REPORT	18. SECURITY CLASSIFICATION OF THIS PAGE	19. SECURITY CLASSIFICATION OF ABSTRACT	20. LIMITATION OF ABSTRACT

ROBUST MULTIVARIABLE FEEDBACK DESIGN FOR UNCERTAIN LINEAR SYSTEMS

Mark Conrad Crews

Merton College

This thesis is submitted in partial fulfillment of the requirements for the degree of Doctor of Philosophy at the University of Oxford, Trinity Term, 1992.

For

Christy

Courtney

Natalie

Christopher

and

Rachel

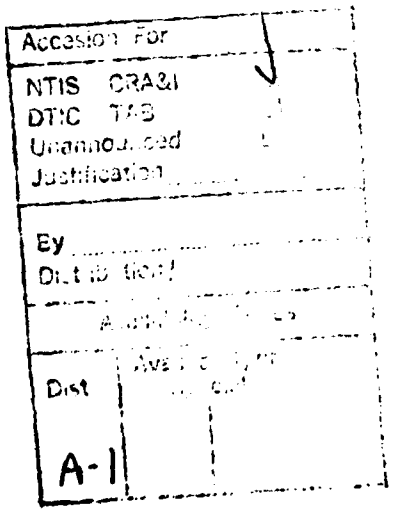

Robust Multivariable Feedback Design for Uncertain Linear Systems

Mark Conrad Crews
Merton College, Oxford

Thesis Submitted for D. Phil degree Trinity Term 1992

Abstract

Realistic control strategies must address the inevitable uncertainty which accompanies nominal system descriptions. Even though uncertainty can often be characterized mathematically, effective robust control techniques have been slow to appear. This work investigates robust control methods directed at both the analysis and design of multivariable feedback systems in the presence of system uncertainty.

The first part of the thesis examines perturbed interaction from the generalized Nyquist/characteristic locus perspective. This work establishes that, for a given class of uncertainty and a specific class of gain-limited controllers, feedback compensation can be optimally deployed to reduce perturbed interaction. Subsequently, this treatment exploits the geometric eigen-structure embodied in the characteristic locus framework along with the appropriate stationary conditions in order to characterize the worst case uncertainty which produces the largest interaction as measured by the perturbed misalignment angles. Furthermore, the structure of the worst case perturbation has a particularly simple representation which facilitates the determination of the worst case interaction based on simple open-loop quantities. These results together with the previous development of the E-Contour method complete the overall development of the characteristic locus approach as a convenient robust analysis tool.

In order to address robust design, the thesis transitions from the characteristic locus perspective to the H^∞ framework. During this process, this work produces new mathematical theory pertaining to H^∞ optimization. Initially, this work presents a useful characterization of the degrees of freedom contained in the H^∞ problem. For a special class of transfer functions, the degrees of freedom are deployed to attain gramian stationarity which, in turn, produces matched error systems which have singular value total flatness. Moreover, gramian stationarity also produces totally stable complementary maximizing vector projections which reduce the computational burden during super-optimization. The computational efficiency of the algorithm is further enhanced with a minimal, explicit realization of the core recursion term. These results are subsequently extended to cover the general class of transfer function matrices.

Finally, this thesis develops a robust shifted H^∞ design technique to maximize the worst case relative stability margin. It is shown that when upper bounds on the size of additive uncertainty are known, maximizing the tolerance to uncertainty does not form a useful design objective as compared to maximizing the relative stability margin. The specific cost function required to maximize the relative stability margin is formulated along with the required theory for its optimization. This work concludes by enumerating the design process and presenting illustrative examples.

ACKNOWLEDGEMENTS

I would like to publicly express my sincere gratitude to my wife *Christy* for her encouragement, devotion, and love during the course of this work. Her unfailing belief in my abilities both sustained and inspired me. I'm also thankful for her frequently-used ability to function as a "single parent" to our four children, *Courtney*, *Natalie*, *Christopher*, and *Rachel*. Both she and they sacrificed much time without a husband and father in order to see this work through. Indeed, this work could not have been completed if it were not for their kind patience and support for which I am deeply indebted.

My parents, *John and Joan Crews*, have inspired me in numerous ways as well. My father's heroism and humility serve to remind me what true greatness is. My mother's love and nurturing are blessings that I've been fortunate to experience. I'm truly grateful for their guidance and direction over the years.

I would also like to thank my remarkably gifted supervisor, *Dr. Basil Kouvaritakis*, to whom I owe much. His insightful questioning and his strong analytic capabilities served as a model which I sought to emulate in my work. Moreover, his enthusiasm for teaching and interacting with students are qualities which I hope to adopt and similarly share with my students when I begin teaching again.

I would also like to express my appreciatiation to *Dr. Denis Mustafa* for his many helpful comments.

Finally, I would like to acknowledge some special friends I've had the privilege of meeting during my stay in Great Britain. My colleagues, *João Basilio*, *Anton Chang*, *Anthony Rossiter*, *Jianguo Wang*, *Grevin Williams*, and *Tae-Woong Yoon* have all shared a bit of their respective worlds with me and I've come to learn about and appreciate each of their cultures. *John and Iris Cummings* have certainly enriched my family's experiences in England and they shall be sorely missed when we return to America.

Contents

Chapter 1

Introduction

1.1 A perspective on feedback control theory

In order to place the present work in the proper context of control engineering, it is necessary to trace briefly some of the more important historical developments leading to the current understanding of feedback control theory. Without doubt, feedback is the most fundamental, requisite structure upon which control theory rests. From the first recorded applications by the Greeks of feedback in the form of float regulator mechanisms circa 300 B.C. [Dorf, *1989*] to the numerous present day applications in aerospace, astronautics, industry, etc., feedback has been a prime mover in enabling technological advances by providing the means to control systems. For instance, James Watts' invention of the fly-ball steam engine speed governor in 1769 enabled self-regulation via feedback and hence, provided considerable impetus to the industrial revolution in terms of more efficient power generation [Ingpen and Wilkinson, 1991].

Feedback control theory began to be formalized mathematically by James Clerk Maxwell whose 1868 treatise on Watts' fly-ball steam engine speed governor employed a differential equation model of the governor [Maxwell, 1868; Wiener, 1948]. Although the work of Maxwell marks a significant milestone, present day feedback control theory begins essentially with the invention of the negative feedback amplifier by Black in the late 1920's [Siebert, 1986]. The negative feedback amplifier not only enabled a 500-fold increase in long distance communication capability, but it also heralded a new type of frequency domain analysis by Black's colleagues Bode and Nyquist. Bode's feedback analysis in 1927 provided a unique relationship between the

gain and phase of minimum phase transfer functions subsequently exploited to yield the concepts of gain and phase margins of feedback systems. Nyquist's contribution in 1932 was to provide a simple open-loop experimental test to determine closed-loop (i.e. feedback) system stability. Moreover, Nyquist's method also provided a convenient graphical means to assess closed-loop behaviour based on the open-loop frequency response. By the early 1950's, rigorous control tools such as Nyquist plots, Bode gain/phase diagrams, and Evan's root-locus technique had evolved to the point that the frequency domain approach provided a unified and coherent framework from which analysis and design could be based, albeit only for single-input single-output (SISO) control systems.

In the 1960's, the time domain feedback control approach emerged as a dominant force with R. Kalman's treatment of the linear multivariable, or multiple-input multiple-output (MIMO), optimization problem [Kalman et al., 1964]. Kalman's development of the Linear Quadratic (LQ) method involved the optimization of a weighted quadratic performance index and this implied that a linear controller could be chosen to be the best of its type and therefore, *optimal.* Furthermore, in contrast to previous design methods, the LQ method gave a synthesis procedure to compute *an* optimal stabilizing state-feedback controller thereby reducing the amount of empirical knowledge required by the designer [Anderson and Moore, 1989]. Finally, Kalman's work relating state-space models to transfer functions produced the important concepts of controllability and observability of feedback systems [Kalman, 1964].

Since the LQ requirement of complete state accessibility was generally not met in practice, Luenberger devised a state observer to reconstruct the states from output measurements. The requirement for uncorrupted output measurements by the Luenberger observer was followed by the more realistic extension of Kalman and Bucy who derived a stochastic state estimator now well known as the Kalman-Bucy filter [Van Trees, 1968]. Furthermore, the white Gaussian noise assumption used in the Kalman-Bucy filter, enabled the subsequent development of the Linear Quadratic

Gaussian (LQG) method of optimal state-feedback control.

Due to LQG's inability to deal with imprecise mathematical descriptions and devise meaningful quadratic performance indices for many multivariable processes, the late 1960's and 1970's witnessed a resurgence in the extension of frequency domain techniques to multivariable systems. Initial work sought to diagonalize the system transfer function matrix in order to decouple the system into single loops to permit the application of the well known SISO techniques. In order to alleviate the difficulties in achieving complete decoupling of the system, Rosenbrock permitted a degree of interaction in his development of the inverse Nyquist array (INA) method which was based on Gershgorin's theorem for locating matrix eigenvalues [Rosenbrock, 1974]. Although the INA method was simple to understand and use when diagonal dominance was easily achieved, the INA controllers were often difficult to design and intrinsically conservative as a result of the accompanying sufficient (but not necessary) stability test. Such issues began to be redressed by the development of MacFarlane's Characteristic Locus Method (CLM) [MacFarlane, 1980]. The Characteristic Locus Method was based on the generalized Nyquist stability criterion for MIMO systems which provided a necessary and sufficient closed-loop stability assessment based on the open-loop eigenfunction frequency response plots called *characteristic loci.* The eigenfunctions were shown to be analytic functions of frequency almost everywhere on the complex plane and thus, the corresponding characteristic loci could be used to determine the nominal and relative stability of MIMO systems in a manner analogous to the use of Nyquist plots for SISO systems. By working in the eigenframe of the system, the Characteristic Locus Method enabled SISO design techniques to be employed on individual MIMO loops and therefore, the generalized Nyquist/characteristic locus structure provided a convenient and appropriate framework for accomplishing feedback controller design.

1.2 Feedback control theory for uncertain systems

The methods of the previous section have provided much insight into dynamic feedback system behaviour as well as mathematically rigorous design methodologies; however, they all presuppose a completely known system (with the partial exception of the LQG method). In order to extend these methods to include more realistic control problems, much research over the last two decades has been directed at the issue of uncertainty in the mathematical model of the system or plant. *Robust* control methods address plant uncertainty by using suitable uncertainty characterizations in order to satisfy not only nominal stability and performance requirements, but also robust stability and performance objectives as well. In this context, the frequency domain control tools have achieved preeminence due to their effectiveness in incorporating various uncertainty characterizations. Moreover, these methods have re-established links to the earlier work of Bode and Nyquist. Before considering the status of the current robust multivariable frequency domain techniques, it is useful to survey the LQG time domain approach from an uncertainty robustness perspective.

The LQ optimal control method initially addressed "robustness" with precise statements regarding guaranteed stability margins [Safonov and Athans, 1977]; however, Doyle and Stein subsequently demonstrated that LQ designs could result in relatively poor stability margins [Doyle, 1978; Doyle and Stein, 1979]. Next, in order to regain the desirable stability margins offered by LQG designs, Doyle and Stein developed a Loop Transfer Recovery (LTR) procedure [Doyle and Stein, 1981]; however, the LQG/LTR procedure was guaranteed to work only with minimum phase plants. Furthermore, from an uncertainty robustness perspective, the LQG/LTR approach only admitted well-defined white Gaussian noise processes acting on the plant and measurements. Thus, the LQG/LTR formulation has been unable to incorporate the uncertainty characterizations essential for robust design, although the technique has earned further value as a frequency domain loop-shaping tool [Maciejowski, 1989].

Of the frequency domain techniques presented in the previous section, the generalized Nyquist/CLM with its concomitant necessary and sufficient stability criterion was found to be appropriate for extension to robust applications. Previous problems with eigenvalue sensitivity were addressed by Daniel and Kouvaritakis with their development of the *E-Contour* method to locate the exact eigenvalue inclusion regions in the complex plane [Daniel and Kouvaritakis, 1984; Daniel and Kouvaritakis, 1985]. The perturbed characteristic locus bands produced by plotting the E-Contour regions over a preselected set of frequencies enabled an immediate generalized Nyquist stability assessment of the uncertain system. Significantly, these results were subsequently extended by Kouvaritakis and Latchman to cater for the structured uncertainty case which exploits bounds on the individual uncertainty transfer function matrix elements [Kouvaritakis and Latchman, 1985; Kouvaritakis and Latchman, 1986; Daniel et al., 1986]. These results confirmed that the generalized Nyquist technique could provide an important robust analysis tool; however, the corresponding robust design procedure is continuing to be developed as discussed next.

Similar to the SISO Nyquist technique, the generalized Nyquist framework allowed robust design objectives to be formulated in terms of shaping the characteristic loci about the critical point. Based on this strategy, Kouvaritakis and Trimboli developed a robust generalized Nyquist design technique to construct a robust proportional-plus-integral (PI) controller by optimizing the characteristic loci locations at successive frequency points [Kouvaritakis and Trimboli, 1989; Trimboli, 1989]. Moreover, the optimizations were obtained by exploiting the geometric alignment properties, based on the Major Principal Direction Alignment Principle (MPDA) [Kouvaritakis and Latchman, 1985], of the relevant matrices at each frequency point. Although this work underscored the potential of robust characteristic locus design, it imposed artificial constraints in the design process in order to ensure nominal stability. Furthermore, in comparison with the CLM design process, the corresponding robust design technique did not address the issue of interaction although the present work has made significant progress in this direction as seen in

the sequel.

The most active area of current robust design research has focused on the evolving H^∞ optimal control methodology initiated by Zames to counter the inadequate LQG robustness properties which were derived from the unrealistic additive white noise assumptions [Zames, 1981]. By incorporating unstructured uncertainty characterizations (i.e. the uncertainty is characterized by a scalar modulus bounding function) in the H^∞ optimization problem, H^∞ optimal control theory has yielded solutions to both the additive uncertainty robustness problem [Glover, 1986] as well as the mixed disturbance rejection performance and multiplicative output uncertainty robustness problem [Doyle, 1984; Francis, 1987]. The way in which the H^∞ optimization problem includes the unstructured uncertainty characterizations is by casting the problem in terms of the minimization of the H^∞-norm (defined for a transfer function matrix $G(s)$ as $\|G(s)\|_\infty = \sup_\omega \overline{\sigma}[G(j\omega)]$) of weighted transfer function matrices. The weighting functions themselves either contain the unstructured uncertainty characterization or reflect the desired performance objectives.

H^∞ optimal design is essentially a synthesis procedure which yields robust controllers in a fashion reminiscent of LQG synthesis. The H^∞ optimal control problem is initially formulated as a nonlinear minimization ranging over the entire class of internally stabilizing controllers and subsequently transformed into an affine minimization via the Youla parametrization of stabilizing controllers [Youla et al., 1976; Doyle, 1984]. This latter optimization ranges over an unknown stable transfer function matrix and is, like the previous optimization, weighted by the appropriate uncertainty characterization. The optimization process can be viewed as a distance problem in which the stable function (i.e. the H^∞ optimal function) is chosen to be the closest to the given unstable function. This distance problem was first solved analytically by Nehari [Nehari, 1957] for the SISO case and by Adamjan, Arov, and Krein [Adamjan et al., 1978] for the MIMO case. Subsequently, Glover characterized the optimal solutions using state-space formulae for the special MIMO case in which the unknown stable transfer function matrix has the same dimensions as

the known unstable transfer function matrix, namely the 1-block problem [Glover, 1984]. More general (i.e. 2- and 4-block) H^∞ MIMO problems can be computed algorithmically using the γ-iteration technique whereby a prespecified tolerance governs the sufficiency of the "near H^∞ optimal" solution [Chu et al., 1986; Glover and Doyle, 1988]. More recently, [Doyle et al., 1989] have given a solution to general H^∞ problems directly in terms of two Riccati equations, completely bypassing the Youla parametrization and Hankel approximation.

In comparison with the distance interpretation of H^∞ optimization, H^∞ optimization can also be viewed as a model-matching problem in which the H^∞ optimal "model" is chosen to "match" the known "model" so that the norm of the difference between the models is minimized over all frequency. The resulting H^∞ optimal solution to the model-matching (or distance) problem has long been known to be generally nonunique and in order to restore uniqueness, Young proposed a Strengthened Model-Matching Problem (SMMP) in which *all* of the singular values of the H^∞ cost function are minimized in lexicographic order thereby producing *super-optimality* [Young, 1986a]. Although Young also developed an operator theoretic "existence" algorithm to achieve super-optimality, its practical implementation was questionable and so other researchers [Tsai et al., 1988; Limebeer et al., 1989] presented practical, realizable super-optimization algorithms cast in the state-space framework. In addition to the mathematical motivation for achieving super-optimality (i.e. to restore solution uniqueness), others [Foo and Postlethwaite, 1986; Kwakernaak, 1986; Postlethwaite et al., 1989] have also supplied associated engineering motivation. This is summarized in [Tsai et al., 1990] which asserts that because the super-optimal s-numbers (i.e. the actual values of the super-optimal singular values which are constant over all frequency) reflect the energy gains between appropriately defined input and output spaces, "greater robustness" results from the minimization of all of the H^∞ cost function singular values, not just the largest.

1.3 Structure of Thesis

1.3.1 Objectives

The previous two sections have provided a foundation on which the work presented in this thesis builds. This work is directed at advancing the theory and development of *robust multivariable control methods* pertaining to perturbed interaction, H^∞ super-optimization, and H^∞ design for the maximization of relative stability.

This work initially seeks to understand if perturbed multivariable interaction is inherently an open-loop property optimally minimized by a prefilter after deploying feedback to minimize closed-loop uncertainty. If this were the case for example, it would eliminate any possible robust extension of the high frequency nominal CLM design process in which feedback is deployed to reduce interaction as measured by the misalignment angles (i.e. the angles of misalignment between corresponding eigenvector/standard basis vector pairs). The results of the former undertaking may be inferred by the very presence of this work's next objective which is to characterize the worst case uncertainty which yields the maximum interaction as measured by the misalignment angles.

In the characteristic locus framework, E-Contours can be generated from either structured or unstructured uncertainty characterizations and hence, provide a convenient means of assessing both nominal and relative stability; however, E-Contours supply only partial information regarding the interaction of perturbed systems. Therefore, this work seeks to provide a complete perturbed interaction assessment by characterizing the worst case uncertainty which maximizes the misalignment angles. The fulfillment of this objective would clearly provide an efficient and convenient tool for the appraisal of perturbed interaction based on open-loop quantities. Moreover, it could provide the basis for the extension of the high frequency nominal CLM design process to robust CLM design.

Even though the E-Contour method defines the worst case relative stability margin, it cannot as yet accommodate design with respect to the worst case (i.e. min-

imum) relative stability margin. Therefore, this work shifts from the characteristic locus perspective to the H^∞ optimal framework with the objective of achieving the optimal design procedure as measured by the relative stability margin. Concurrently, this work aims to distinguish between the possibly ambiguous concepts of tolerance to uncertainty and relative stability. This distinction would both clarify these concepts and define the conditions under which one or the other should be pursued in design. The objective of design for the maximization of relative stability, which this work pursues, requires the formulation of a specific cost function to reflect this objective. This in turn requires the specification of the theoretical constraints associated with the optimization followed by the actual mechanics and enumeration of the design process.

Related to the objective of maximizing relative stability using H^∞ design is the objective of characterizing and using the degrees of freedom within the H^∞ optimization problem. This work seeks to characterize uniquely the degrees of freedom in a manner which facilitates their use in achieving several well-defined mathematical properties, some of which are defined for the first time in this work. Initially, the degrees of freedom will be deployed within a special class of systems to obtain both singular value total flatness as well as completely stable projections in the context of super-optimization. Subsequently, the degrees of freedom will be deployed to obtain either singular value near flatness or minimal antistable projections in the context of super-optimization.

1.3.2 Overview of Thesis

The work presented in this thesis falls into two principal categories pertaining to the characteristic locus perspective and the H^∞ optimal perspective, respectively. Accordingly, the thesis is organized into two parts as outlined below:

Chapter 1 : Introduction

Part I : Robust analysis from the characteristic locus perspective: perturbed interaction

Chapter 2 : An overview of the generalized Nyquist/characteristic locus approach

Chapter 3 : The minimization of interaction in the presense of uncertainty and controller gain limitations

Chapter 4 : Uncertainty and interaction in linear multivariable feedback systems

Part II : Robust design from the H^∞ perspective: super-optimization and relative stability margin maximization

Chapter 5 : An overview of H^∞ optimal techniques

Chapter 6 : Characterization and use of the degrees of freedom in the H^∞ problem

Chapter 7 : Using the degrees of freedom in the general case

Chapter 8 : An evaluation of super-optimality as a control tool: a relative stability perspective

Chapter 9 : H^∞ design for the maximization of relative stability

Chapter 10 : Conclusions and future work

The thesis begins in Chapter 2 by presenting an overview of the generalized Nyquist/characteristic locus approach. Initially, the structured and unstructured uncertainty models are defined along with their associated perturbed stability conditions. This is followed by a brief description of the E-Contour method which will be useful for later assessments of both stability and relative stability. Next, a summary of the nominal and robust aspects of the generalized Nyquist/characteristic locus approach is presented and particular emphasis is placed on how the design process addresses interaction.

With the generalized Nyquist/characteristic locus approach in proper perspective, Chapter 3 examines the issue of perturbed interaction in order to counter the widely-held belief that multivariable interaction is an open-loop property optimally

minimized by a prefilter after deploying feedback to minimize closed-loop uncertainty. A specific example is given to illustrate that for a given class of gain-limited controllers and a specific class of structured uncertainty, interaction is optimally addressed by the feedback compensator rather than the decoupling prefilter/uncertainty minimizing feedback compensator combination.

By considering the appropriate stationary conditions, Chapter 4 characterizes the worst case perturbation which produces the largest interaction in terms of misalignment angles. This information together with the modulus information derived from the E-Contours can be deployed to supplement the nominal plots of eigenvalue-moduli and misalignment angles versus frequency with plots of bands of possible eigenvalue-moduli and possible misalignment angles versus frequency. The combination of resulting plots provides a convenient graphical means of assessing interaction in the presence of uncertainty.

The transition to robust H^∞ optimal design begins in Chapter 5 with an overview of the relevant aspects of the H^∞ optimization problem. Here, the standard H^∞ problem is presented and internal stability is defined along with the Youla stabilizing controller parametrization. Finally, the relationship between the H^∞ problem and Hankel approximation is outlined in order to lay the groundwork for the theoretical treatment of the following chapter.

Chapter 6 presents a useful characterization of the degrees of freedom contained in the H^∞ problem. For the special class of transfer function matrices considered, the degrees of freedom can be deployed to yield stationarity of either the observability or controllability approximation system gramians. This stationarity, in turn, produces *matched* error systems (i.e. the error system's controllability or observability pairs are identical to the right or left maximizing vector, respectively) which have the *singular value total flatness* property, defined for the first time in this work. Moreover, in the context of a super-optimal algorithm, the approximation system gramian stationarity also produces totally stable complementary maximizing vector projections which in turn lessens the computational burden of the attendant super-optimal algorithm.

The computational efficiency of the algorithm is further enhanced with a minimal, explicit realization of the core recursion term.

The results of Chapter 6 are extended in Chapter 7 to cover the general class of transfer function matrices. Here, the degrees of freedom are deployed to yield either singular value near flatness or minimal antistable projections in the context of super-optimization. In order to reduce state inflation and allow the possibility of early termination of the super-optimal algorithm, a strict norm constraint on the degree of freedom parameter is required. This constraint is met through a composite Riccati equation formed by merging the gramian stationary conditions with their respective Riccati equations. Furthermore, this special Riccati equation has a unique closed-form solution (independent of the partitioned eigenvectors of the Hamiltonian matrix) which may be expressed in terms of the known Markov-type parameters defined by the characterization of the degrees of freedom in the H^∞ problem.

Chapter 8 considers a simple class of H^∞ super-optimal controllers from a relative stability perspective.

Chapter 9 presents a newly developed design technique to maximize the worst case relative stability margin. Here, the distinction is made between the objectives of tolerance to uncertainty and relative stability. This distinction is accompanied with an outline of the conditions under which one or the other should be pursued in design. It is argued that relative stability forms the more sensible objective when there exists an accurate uncertainty envelope function as is often the case in practice. The specific cost function required to maximize the relative stability margin is formulated. Next, the theory required for the optimization of the cost function is developed and finally, the design process itself is given along with illustrative examples.

A summary of the work is provided in Chapter 10 together with proposals for future research.

1.3.3 Notation

The following notational conventions shall be used throughout the thesis:

SISO	:	Single-Input/Single-Output
MIMO	:	Multiple-Input/Multiple-Output
CLM	:	Characteristic Locus Method
E-Contour	:	Plot of the Eigenvalue inclusion region Contour
MPDA	:	Major Principal Direction Alignment
LQG	:	Linear Quadratic Gaussian
SMMP	:	Strengthened Model Matching Problem
inf	:	infimum
sup	:	supremum
max	:	maximum
min	:	minimum
$\mathbf{x}^t$	:	the transpose of vector $\mathbf{x}$
$\mathbf{x}^T$	:	the transpose of vector $\mathbf{x}$
$\mathbf{x}^*$	:	the complex-conjugate transpose of vector $\mathbf{x}$
$\mathbf{e}_i$	:	the i^{th} standard basis vector
$\|\mathbf{x}\|$	:	Euclidean norm of vector $\mathbf{x}$ defined by $\sqrt{\mathbf{x}^*\mathbf{x}}$
A^T	:	the transpose of matrix A
$\lambda[A]$	:	an eigenvalue of matrix A
$\mathbf{w}$	:	a right eigenvector
$\mathbf{v}^T$	:	a left eigenvector
$\rho(A)$	:	the spectral radius of matrix A defined as the magnitude of the maximum modulus eigenvalue
$\sigma[A]$	:	a singular value of matrix A
$\overline{\sigma}[A]$	:	the maximum singular value of matrix A
$\underline{\sigma}[A]$	:	the minimum singular value of matrix A
$\overline{x}[A]$	:	the major principal output direction of matrix A
$\underline{x}[A]$	:	the minor principal output direction of matrix A
$\overline{y}[A]$	:	the major principal input direction of matrix A
$\underline{y}[A]$	:	the minor principal input direction of matrix A

$\overline{x}[A] \| \overline{y}[B]$: the MPDA property between the output major principal direction of matrix A and the input major principal direction of matrix B whereby $\overline{x}[A] = e^{(j\alpha)}\overline{y}[B]$ for some real scalar constant α

R_+ : a nonnegative real scalar

$R_+^{n\times n}$: the set of $n \times n$ matrices with nonnegative real entries

Δ : an additive perturbation

$\mathbf{D_u}$: the unstructured class of additive uncertainty

$\mathbf{D_s}$: the structured class of additive uncertainty

H^2 : the Hardy space of stable transfer functions with bounded H^2 norm (see below)

$\|G(s)\|_2$: H^2 norm of transfer function matrix $G(s)$ defined as $\left[\frac{1}{2\pi}\int_{-\infty}^{\infty} \mathrm{tr}\left[G(j\omega)G^T(-j\omega)\right] d\omega\right]^{1/2}$

H^∞ : the Hardy space of stable proper transfer functions with bounded H^∞ norm (see below)

$\|G(s)\|_\infty$: H^∞ norm of transfer function matrix $G(s)$ defined as $\sup_\omega \overline{\sigma}[G(j\omega)]$

RH_+^∞ : the class of real rational stable transfer functions

RH_-^∞ : the class of real rational unstable transfer functions

$G(s) = \left[\begin{array}{c|c} A & B \\ \hline C & D \end{array}\right]$: state-space representation of transfer function matrix G(s)

$G^*(s)$: the complex-conjugate transpose of the transfer function matrix $G(s)$ given by $G^*(s) = G^T(-s)$

$A \leq B$: Part I: the matrix elements satisfy $|a_{ij}| \leq b_{ij}\ \forall i,j\ :\ b_{ij} \in R_+$
Part II: the matrix A-B is negative semi-definite

Given the following algebraic Riccati equation:

$$A^TX + XA - XBB^TX + C^TC = 0$$

we say that the solution X is ***stabilizing*** if Real $\left\{\lambda_i\left[A - BB^TX\right]\right\} < 0\ \forall\ i$.

Part I

Robust analysis from the characteristic locus perspective: perturbed interaction

Chapter 2

An overview of the generalized Nyquist/characteristic locus approach

2.1 Introduction

The classical SISO approach initiated by Bode and Nyquist has enjoyed widespread support over the years due in large part to the insight and intuition provided by the Bode gain/phase plots and Nyquist diagrams. For example, the Nyquist diagram gives the designer immediate visual feedback concerning not only closed-loop stability, but also concerning stability margins, steady-state performance, and the transient response as well. The intuition revealed by the Nyquist diagram has, as mentioned in the previous chapter, found a natural extension to multivariable systems via characteristic transfer functions (or eigenfunctions) and the generalized Nyquist stability criterion. The frequency response plots of the characteristic transfer functions produce the characteristic loci which, in turn, convey similar insights to those provided by the Nyquist diagram.

The characteristic transfer functions can be viewed as generalizations of SISO transfer functions; however, they must be accessed through the spectral decomposition of the system transfer function matrix. Therefore, in order to apply SISO design techniques to the characteristic transfer functions, the Characteristic Locus Method (CLM) [MacFarlane, 1980] was developed. After accessing the characteristic transfer functions through the eigenframe of the system, the CLM approach employs SISO techniques to shape each characteristic locus (i.e. the frequency response plot of each characteristic transfer function) as if it were an ordinary Nyquist locus and, in this

way, the CLM approach achieves the required stability via the generalized Nyquist stability criterion and desired dynamic performance objectives via proximity to the critical point.

In the presence of modelling and identification errors the CLM approach must be modified to deal with robust stability and performance issues. In particular, perturbations cause the characteristic loci to vary from their nominal locations which implies a potential loss of stability and performance objectives. However, uncertainty may be addressed by E-Contours (i.e. the boundaries of the eigenvalue inclusion regions) and subsequently plotted at preselected frequency points to produce perturbed characteristic locus bands. These plots provide an immediate graphical assessment of both stability and relative stability as depicted by critical point encirclements and the gain/phase margins respectively.

The primary purpose of this chapter is give an account of the generalized Nyquist/characteristic locus framework in order to give the proper perspective from which to view the first portion of the thesis dealing with perturbed interaction. In support of this larger aim, this chapter also provides background material pertaining to structured and unstructured uncertainty models together with the associated perturbed stability conditions. This is followed by a succinct description of the E-Contour method which will be particularly helpful in later assessments of both stability and relative stability. Finally, a summary of the pertinent aspects of the generalized Nyquist/characteristic locus approach is presented and particular emphasis is placed on how the design process addresses interaction.

2.2 Background

2.2.1 Uncertainty

Robust analysis and design techniques have the fundamental aim of addressing the inevitable uncertainty which accompanies nominal system models. The sources of model uncertainty are manifold and can often be attributed to unmodelled dynamics,

the omission of higher order dynamics, and/or component variations which cause the system to vary in unpredictable ways. Regardless of the source of uncertainty, robust design methods require a model which characterizes the uncertainty associated with a system. Consider the multivariable system of Fig. 2.1. This figure illustrates how

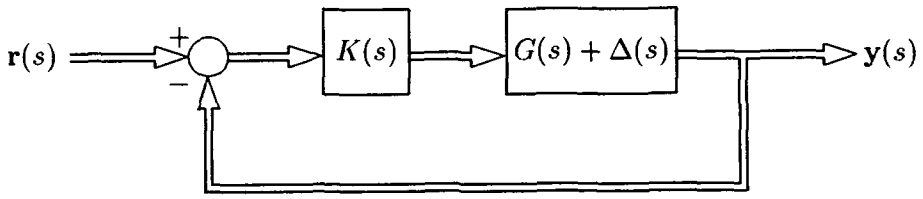

Figure 2.1: Perturbed multivariable system

the actual plant $\tilde{G}(s)$ may be modelled as the sum of the nominal transfer function matrix $G(s)$ and an additive perturbation matrix $\Delta(s)$:

$$\tilde{G}(s) = G(s) + \Delta(s)$$

where the perturbation $\Delta(s)$ accounts for the uncertainty associated with the nominal system model $G(s)$. The degree of knowledge about system uncertainty dictates whether the perturbation matrix $\Delta(s)$ has structure or not.

Unstructured uncertainty

When information concerning the individual elements of the perturbation matrix $\Delta(s)$ is either unavailable or unnecessary for the specific problem, the uncertainty information can still be conveyed through a rough perturbation size which normally takes the form of an upper-norm bound on the perturbation matrix $\Delta(s)$:

$$\overline{\sigma}\left[\Delta(j\omega)\right] \leq |p(j\omega)| = \delta(\omega) \qquad \forall \quad \omega \tag{2.1}$$

where $p(s)$ is a scalar *modulus function* whose modulus, given by $\delta(\omega)$, bounds the largest principal gain of the perturbation over all frequency. Such a characterization falls within the *unstructured* class of uncertainty $\mathbf{D_u}$ which may be expressed at each

frequency $s = j\omega$ as:

$$\Delta \in \mathbf{D_u} \triangleq \{\Delta : \overline{\sigma}[\Delta] \leq |p|,\ \delta = |p|,\ \delta \in R_+\} \tag{2.2}$$

where R_+ is a nonnegative real number. Moreover, since (2.2) pertains to each frequency ω, this characterization is valid for the entire frequency spectrum. Clearly, the perturbation matrix $\Delta(s)$ has no explicit structure since there is no explicit magnitude or phase information associated with the individual perturbation matrix elements. Even though the unstructured uncertainty is conveyed as a rough perturbation size, it is nonetheless convenient to use in analyzing both perturbed stability and perturbed eigenvalues as will be observed after the following discussion of a more detailed characterization of uncertainty.

Structured uncertainty

In many practical situations, more specific information is available regarding the magnitude of uncertainty between various input/output pairs. When such information is available, the individual elements of the perturbation matrix $\Delta(s)$ can be bounded as:

$$|\Delta_{kl}(j\omega)| \leq |d_{kl}(j\omega)| = p_{kl}(\omega) \qquad \forall \quad \omega \tag{2.3}$$

where $d_{kl}(s)$ is a scalar modulus function whose magnitude, given by $p_{kl}(\omega)$, bounds the modulus of the kl^{th} element of $\Delta(s)$. Such a characterization falls within the *structured* class of uncertainty $\mathbf{D_s}$ which may be written at each frequency $s = j\omega$ as:

$$\Delta \in \mathbf{D_s} \triangleq \left\{\Delta : |\Delta_{kl}| \leq p_{kl}\ ,\ p_{kl} = |d_{kl}|\ ,\ P \in R_+^{m\times m}\right\} \tag{2.4}$$

where $R_+^{m\times m}$ is the set of $m \times m$ matrices with nonnegative real entries and the kl^{th} element of the modulus matrix P is denoted by p_{kl}. Similar to the characterization of the unstructured uncertainty class, (2.4) is valid over the entire frequency spectrum. However, in contrast to the unstructured uncertainty characterization, adding structure to the perturbation matrix typically allows "tighter" assessments of per-

turbed stability and perturbed eigenvalue inclusion regions by exploiting geometric relationships between the plant and perturbation transfer function matrices.

2.2.2 Perturbed stability

The delineation between structured and unstructured uncertainty is important in assessing robust stability because, in general, stability analyses which use only unstructured perturbations tend to be more conservative than necessary. However, the unstructured information allows a relatively simple analysis yielding convenient stability evaluations. After examining the unstructured perturbation analysis, a structured uncertainty analysis follows which illustrates how the perturbed stability assessment can be tightened by employing the Major Principal Direction Alignment (MPDA) principle [Kouvaritakis and Latchman, 1985].

Perturbed stability with unstructured uncertainty

Consider the system of Fig. 2.1 in which the nominal plant G[1] is subject to an additive unstructured perturbation, Δ, with bounded norm $\overline{\sigma}[\Delta] \leq \delta$. Assuming nominal closed-loop stability and that the nominal plant G and the perturbed plant $G + \Delta$ have the same number of unstable poles, closed-loop stability requires the following equivalent conditions:

$$\begin{aligned} |I + (G + \Delta)K| &\neq 0 \\ |I + GK + \Delta K| &\neq 0 \\ |I + \Delta K(I + GK)^{-1}| \cdot |I + GK| &\neq 0 \end{aligned}$$

The latter equation can be manipulated to yield a more useful robust stability condition as will be seen below. Since the nominal plant and controller are assumed to be stable under unity feedback, it is true that:

$$|I + GK| \neq 0$$

[1]For notational convenience, the frequency dependence of the transfer function matrices will be implicit in Sections 2.2.2 and 2.2.3.

Using this and by letting $M = K(I + GK)^{-1}$, the previous stability criterion can be rewritten as:

$$|I + \Delta M| \neq 0$$

This equation can be further modified by use of the eigenvalue shift theorem and the fact that a determinant equals the product of its eigenvalues to produce:

$$|\lambda_{\max}(M\Delta)| = \rho(M\Delta) < 1 \tag{2.5}$$

Hence, the spectral radius provides an upper perturbed stability bound. However, since the unstructured perturbation is bounded in norm by δ, the subsequent inequality relating singular values and eigenvalues can be employed to yield the following stability requirement expressed in terms of singular values:

$$\rho(M\Delta) \leq \overline{\sigma}(M\Delta) \leq \overline{\sigma}(M)\overline{\sigma}(\Delta) < 1 \tag{2.6}$$

This result can be rewritten to give the following equivalent, necessary and sufficient conditions for robust stability in the presence of an unstructured additive perturbation:

$$\begin{aligned} \overline{\sigma}(M) = \overline{\sigma}\left[K(I + GK)^{-1}\right] &< \frac{1}{\delta} \\ \underline{\sigma}\left[K^{-1} + G\right] &> \delta \end{aligned} \tag{2.7}$$

where $M = K(I + GK)^{-1} = [K^{-1} + G]^{-1}$ was reintroduced into the top inequality and the singular value relationship $\overline{\sigma}(M) = 1/\underline{\sigma}(M^{-1})$ was employed. The final form of the robust stability requirement given by (2.7) is particularly useful in the context of unstructured uncertainty analyses; however, it can be tightened further using MPDA analysis in the case of structured uncertainty. Essentially, MPDA also casts the stability criterion of (2.5) in terms of singular values but uses scaling matrices to tighten the bound as will be seen next.

Perturbed stability with structured uncertainty

The previous analysis using unstructured uncertainty applies equally to the case of structured uncertainty since the norm information can easily be derived from the

given structured uncertainty class. However, the stability result may be tightened further by exploiting the uncertainty structure in conjunction with the MPDA property in (2.6). In minimizing the upper singular value bound on the spectral radius $\rho(M\Delta)$, MPDA deploys scaling matrices L and R to attain the major principal direction alignment property between the scaled matrix $\mathbf{M} = R^{-1}ML^{-1}$ and the worst case scaled perturbation matrix, $\mathbf{\Delta} = \Phi LPR\Psi$ where $\Phi = \text{diag}\left\{e^{j\phi_1}, e^{j\phi_2}, \ldots, e^{j\phi_m}\right\}$ and $\Psi = \text{diag}\left\{e^{j\psi_1}, e^{j\psi_2}, \ldots, e^{j\psi_m}\right\}$ are appropriate phase matrices [Kouvaritakis and Latchman, 1985]. Recalling that $\rho(M\Delta) < 1$ for perturbed system stability, MPDA permits the rewriting of this constraint in the following form:

$$\begin{aligned} \rho(\mathbf{M\Delta}) &= \overline{\sigma}(R^{-1}ML^{-1})\overline{\sigma}(LPR) < 1 \\ &\Leftrightarrow \underline{\sigma}\left[L(K^{-1}+G)R\right] > \overline{\sigma}(LPR) \end{aligned} \tag{2.8}$$

where $M^{-1} = K^{-1} + G$ and P is defined by (2.4). The attainment of the MPDA property in (2.8) provides the tightest necessary and sufficient robust stability criterion since the optimal scaling matrices L and R effectively maximize the ratio $\underline{\sigma}\left[L(K^{-1}+G)R\right]/\overline{\sigma}(LPR)$ for the worst case perturbation $\mathbf{\Delta}$.

2.2.3 Eigenvalue inclusion region Contours: E-Contours

In order to extend the graphical Nyquist-type criterion to perturbed systems, it is necessary to characterize how perturbed eigenvalues deviate from their nominal values. For a given perturbation, the perturbed eigenvalues will lie within eigenvalue inclusion regions bounded by *E-Contours* which form simply connected curves that expand with the size of the perturbation [Daniel and Kouvaritakis, 1984; Daniel and Kouvaritakis, 1985]. To follow the analysis, consider the following definition of a perturbed eigenvalue in the context of the system of Fig. 2.1:

$$\begin{aligned} |\tilde{\lambda}I - (G+\Delta)K| &= 0 \\ |\tilde{\lambda}I - GK - \Delta K| &= 0 \\ |I - \Delta K(\tilde{\lambda}I - GK)^{-1}| \cdot |\tilde{\lambda}I - GK| &= 0 \end{aligned}$$

where $\tilde{\lambda}$ represents the perturbed eigenvalue. Provided that $|\tilde{\lambda}I - GK| \neq 0$[2], the perturbed eigenvalue condition becomes:

$$\rho(M\Delta) \geq 1 \tag{2.9}$$

where $M = K(\tilde{\lambda}I - GK)^{-1}$. Interestingly, the formulation of (2.9) parallels the previous robust stability analysis with the exception of the reversed inequality.

For the case of unstructured uncertainty, the following singular value analysis provides the relationship needed to define exact eigenvalue inclusion region boundaries or E-Contours:

$$\begin{aligned} \rho(M\Delta) = \rho(K(\tilde{\lambda}I - GK)^{-1}\Delta) &\geq 1 \\ \Rightarrow \quad \underline{\sigma}\left[G - \tilde{\lambda}K^{-1}\right] &\leq \delta \end{aligned} \tag{2.10}$$

This last condition can be used to define each E-Contour as the solution of the following equation:

$$\underline{\sigma}\left[G - \left(\lambda + \rho e^{j\theta}\right)K^{-1}\right] = \overline{\sigma}\left[\Delta\right] \tag{2.11}$$

where ρ defines the radius from each nominal eigenvalue λ needed to achieve equality of (2.11) at angle θ. Thus, (2.11) provides the basis for an algorithm which may be solved for ρ as θ varies from 0° to 360° [Daniel and Kouvaritakis, 1985]. The solutions may then be sorted into closed simple curves which define the E-Contour boundary.

For the case of structured uncertainty, the MPDA property can be applied to (2.9) to convert the inequality of (2.10) to equality and hence decrease the size of the E-Contours. The governing E-Contour equation for the structured uncertainty case is:

$$\underline{\sigma}\left[L(G - \left(\lambda + \rho e^{j\theta}\right)K^{-1})R\right] = \overline{\sigma}\left[LPR\right] \tag{2.12}$$

where scaling matrices L and R are positive diagonal matrices introduced to achieve MPDA. Analogous to the perturbed stability result using structured uncertainty, the attainment of the MPDA property in (2.12) provides the tightest (i.e. smallest) E-Contours since the optimal scaling matrices L and R effectively maximize the ratio $\underline{\sigma}\left[L(K^{-1} + G)R\right]/\overline{\sigma}(LPR)$ for the worst case perturbation $\mathbf{\Delta}$.

[2]The contrary would imply $\tilde{\lambda}$ is a nominal eigenvalue.

2.3 Open and closed-loop relationships

The previous discussion of uncertainty characterizations, perturbed stability, and E-Contours, allows us to focus on the final aim of this chapter which is to give an account of the generalized Nyquist/characteristic locus framework. We begin by defining the characteristic transfer functions and then see how they can be accessed through the spectral decomposition. Next, we examine the open- and closed-loop relationships followed by a discussion of stability and performance objectives. Finally, an overview of the CLM approach is given along with an enumeration of the design steps.

A multivariable system with square $m \times m$ transfer matrix, $G(s)$, possesses m scalar, characteristic transfer functions, $g_i(s)$, which are the branches of the algebraic function $g(s)$ defined by the following characteristic equation [MacFarlane and Postlethwaite, 1977a]:

$$|g(s)I - G(s)| = 0 \tag{2.13}$$

Frequency response plots of the m characteristic transfer functions, $g_i(s)$, are produced by letting s vary over the standard D-Contour. These frequency response plots are Nyquist-like in appearance and are called the characteristic loci[3]. Before examining how the characteristic loci are used in analysis and design, first consider how the characteristic transfer functions arise in the spectral and dyadic decompositions.

Associated with each characteristic transfer function (or eigenvalue), $g_i(s)$, is both a characteristic direction (or right eigenvector) $\mathbf{w}_i(s)$ and dual characteristic direction (or left eigenvector) $\mathbf{v}_i^t(s)$[4]. For an $m \times m$ open-loop transfer function matrix $G(s)$, all of these characteristic components are related by the following spectral and dyadic decompositions, respectively:

$$G(s) \;=\; W(s)\Lambda_g(s)V(s) \tag{2.14}$$

[3]Strictly speaking, the characteristic loci are a composite of the frequency response plots of the $g_i(s)$ where the algebraic function $g(s)$ has as its domain separate copies of the complex plane joined at the branch cut(s) to form a Riemann surface [MacFarlane, 1980].

[4]True for all $s \neq$ branchpoint.

$$= \sum_{i=1}^{m} g_i(s)\mathbf{w}_i(s)\mathbf{v}_i^t(s) \tag{2.15}$$

where $W(s)$ is a matrix whose columns contain the right eigenvectors $\mathbf{w}_i(s)$, $V(s)$ is a matrix whose rows contain the left eigenvectors $\mathbf{v}_i^t(s)$, and $\Lambda_g(s)$ is a diagonal matrix composed of the characteristic functions $g_i(s)$. Both (2.14) and (2.15) employ the following eigenvalue/eigenvector properties:

$$G(s)\mathbf{w}_i(s) = g_i(s)\mathbf{w}_i(s) \qquad \mathbf{v}_i^t(s)G(s) = g_i(s)\mathbf{v}_i^t(s) \qquad \mathbf{v}_i^t(s)\mathbf{w}_i(s) = 1 \tag{2.16}$$

which are valid for $i = 1, \ldots, m$.

With scalar precompensation and under unity feedback as shown in Fig. 2.2, the

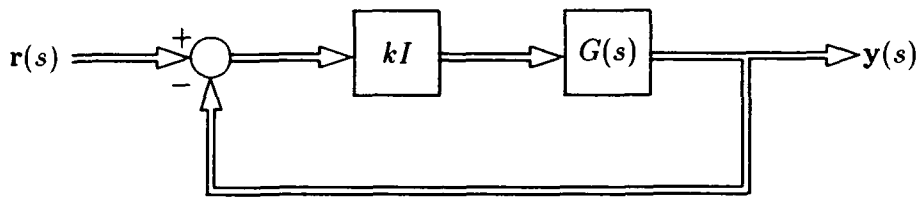

Figure 2.2: Multivariable system with scalar precompensation and unity feedback

closed-loop transfer function matrix, $T(s)$, becomes:

$$\begin{aligned} T(s) &= [I + kG(s)]^{-1} kG(s) \\ &= W(s)[I + k\Lambda_g(s)]^{-1} k\Lambda_g(s)V(s) \\ &= W(s)\Lambda_t(s)V(s) \qquad (2.17) \\ &= \sum_{i=1}^{m} \frac{g_i(s)k}{1 + g_i(s)k}\mathbf{w}_i(s)\mathbf{v}_i^t(s) \qquad (2.18) \end{aligned}$$

where $W(s)$ and $V(s)$ are identical to those defined for the open-loop system and $\Lambda_t(s)$ is a diagonal matrix composed of the closed-loop transfer functions $t_i(s) = \frac{g_i(s)k}{1+g_i(s)k}$. Comparison of the closed-loop decompositions with those of the open-loop reveals that they share a common eigenvector direction set but differ in their characteristic transfer functions. However, the special relationship between these characteristic transfer functions permits the exploration of system stability, gain, accuracy, and interaction as explained next beginning with the application of the generalized Nyquist stability criterion.

2.3.1 Nominal stability

The immediacy and convenience of the generalized Nyquist criterion lies in the geometric interpretation it provides for multivariable stability based on the open-loop characteristic loci. Application of the generalized Nyquist criterion to the system of Fig. 2.2 implies that this system is closed-loop stable if and only if the net sum of counterclockwise encirclements of the "special" critical point $[(-1/k) + j0]$ by the characteristic loci $g_i(j\omega)$ equals the number of open-loop unstable poles [MacFarlane and Postlethwaite, 1977b; MacFarlane and Postlethwaite, 1977a]. Hence, the open-loop characteristic loci provide an immediate graphical assessment of nominal closed-loop stability.

2.3.2 Relative stability

As mentioned earlier, the characteristic loci have been shown to be analytic almost everywhere in the complex plane; therefore, the conformal mapping from the s-plane to the $G(s)$-plane establishes a relationship between the proximity of the dominant closed-loop poles to the imaginary-axis and the proximity of the characteristic loci to the critical point [Cameron and Kouvaritakis, 1979]. Thus, the characteristic loci can be employed to assess relative stability in terms of the gain and phase margins. The gain margin, for example, can be found by determining the "special" critical point $[(-1/k)+j0]$ which has minimum modulus, yet gives the proper number of encirclements; the corresponding value of k provides a measure of the system's gain margin. In addition to enabling nominal and relative stability assessments via frequency response plots, the characteristic transfer functions also have a characteristic gain interpretation useful for dividing the frequency spectrum into particular frequency ranges as will be seen next.

2.3.3 Characteristic gain

The modulus of the characteristic transfer functions can be used to define characteristic gains which are useful in dividing the frequency spectrum into low, intermediate, and high frequency ranges. As will be seen subsequently, this frequency division facilitates the design of frequency dependent characteristic transfer function compensators. The frequency spectrum can be segregated into low, high, and intermediate frequency ranges according to the following rules:

$$|g_i(j\omega)| \begin{cases} \gg 1 & \Rightarrow \text{low frequency range} \\ \ll 1 & \Rightarrow \text{high frequency range} \\ \text{otherwise} & \Rightarrow \text{intermediate frequency range} \end{cases} \tag{2.19}$$

In addition to defining these frequency ranges, the characteristic transfer functions may also be used in assessing accuracy.

2.3.4 Accuracy

It is well known that for scalar systems high controller gain yields good tracking accuracy; this can easily be related to the multivariable case by considering the closed-loop dyadic expansion of (2.18). In general, the components of input signal $\mathbf{r}(j\omega)$ will be projected onto the different characteristic directions and the output will not resemble the input. This is seen by placing $\mathbf{r}(j\omega)$ at the input of the system as shown in Fig. 2.2 and writing the closed-loop dyadic expansion for output $\mathbf{y}(j\omega)$:

$$\begin{aligned} \mathbf{y}(j\omega) &= G(j\omega)\mathbf{r}(j\omega) \\ &= \sum_{i=1}^{m} \frac{g_i(j\omega)k}{1+g_i(j\omega)k} \mathbf{w}_i(j\omega)\mathbf{v}_i^t(j\omega)\mathbf{r}(j\omega) \end{aligned} \tag{2.20}$$

Hence, in general $\mathbf{y} \neq \mathbf{r}$ and the input will not be reproduced at the output.

One way of improving output accuracy is revealed by (2.20). Namely, increasing the compensator gain, k, has the following effect:

$$\frac{g_i(j\omega)k}{1+g_i(j\omega)k} \approx 1 \quad \Rightarrow \quad \mathbf{y}(j\omega) \approx \sum_{i=1}^{m} \mathbf{w}_i(j\omega)\mathbf{v}_i^t(j\omega)\mathbf{r}(j\omega) = \mathbf{r}(j\omega) \tag{2.21}$$

Thus, increasing the compensator gain improves tracking accuracy. However, this simple solution may conflict with other design objectives such as maintaining system stability as explained in the subsequent section.

2.3.5 Interaction

In the context of the characteristic locus framework, interaction may be characterized in terms of:

(1) the magnitude of the characteristic loci; and/or

(2) the misalignment angles between the open-loop characteristic vector set and the standard basis vector set; and/or

(3) the near equality of the characteristic loci.

Since the plant uncertainty is modelled as an additive perturbation $\Delta(s)$, the problem of characterizing perturbed interaction becomes one of determining the effect of the perturbation on the characteristic loci moduli and on the angular misalignment between the eigenvectors and the standard basis vectors. Property (1) relating to the moduli of the characteristic loci is generally pertinent in the low frequency range due to steady state accuracy requirements discussed in the previous section. In contrast, Property (2) relating to the misalignment angles of the characteristic vectors is generally pertinent in the high frequency range due to the natural attenuation present in most physical systems, noise considerations, and compensator gain limitations imposed by stability requirements. In the intermediate frequency range, both (1) and (2) can play an important role in assessing multivariable interaction. Property (3) above will be ignored because it is rather restrictive; due to differences in the dynamics of the various system loops it is unlikely that $g_i(s) \approx g_j(s)$ for $j \neq i$ would form a sensible design objective. Since the present work will be subsequently concerned with characterizing the worst case uncertainty corresponding to the worst case (i.e. largest) misalignment angles, the focus here will be on the description of interaction expressed in terms of the misalignment angles.

The condition for low interaction in the high frequency range can be expressed equivalently by the requirement that each eigenvector of the plant $G(s)$ make a small angle with a different standard basis vector. In order to understand how this interaction measure arises, consider the condition of *no* interaction which is met when the i^{th} input excites the i^{th} output exclusively. This condition is also equivalent to the condition that $\mathbf{e}_i$, the i^{th} standard basis vector, be an eigenvector of the closed-loop transfer function matrix $T(s)$ given by (2.17) and hence by (2.14) an eigenvector of the open-loop transfer function matrix $G(s)$ also. Although this condition would guarantee the existence of no interaction at all, a near alignment of the eigenvector, say $\mathbf{w}_i$, with the standard basis vector $\mathbf{e}_i$ would imply low interaction in the i^{th} loop of the closed-loop system. A quantitative measure of the degree of alignment between the two vectors $\mathbf{e}_i$ and $\mathbf{w}_j$ at a particular frequency is given by:

$$\cos \phi_i \triangleq \max_j \frac{|\mathbf{e}_i^t \mathbf{w}_j|}{\|\mathbf{e}_i\| \|\mathbf{w}_j\|} \tag{2.22}$$

where the angle ϕ_i is termed the *misalignment angle*. For all but highly interactive systems, (2.22) associates a unique eigenvector $\mathbf{w}_j$ to each standard basis vector $\mathbf{e}_i$ and it can be assumed that the eigenvectors have been ordered so that $\mathbf{e}_i$ makes the smallest misalignment angle with $\mathbf{w}_i$.

In the sequel, the concern will be with analyzing how additive uncertainty affects multivariable interaction as measured by the misalignment angles. It will be seen that this analysis together with the previous development of the E-Contour method, can be used to provide a convenient, complete assessment of perturbed interaction from the characteristic locus perspective. Prior to this, however, the Characteristic Locus Method will be enumerated below.

2.4 Characteristic Locus Method

As stated previously, the Characteristic Locus Method [MacFarlane, 1980] seeks to extend some of the ideas behind single-loop feedback design such as the Nyquist stability criterion and the use of simple compensators to achieve desired stability

margins, steady-state performance, and transient response. The generalized Nyquist stability criterion has already been shown to depend on the frequency response plots of the characteristic transfer functions, namely the characteristic loci. It remains to be seen how simple compensators are designed to achieve various performance objectives. Basically, this is done using the approximately commutative controller which enables the manipulation of the characteristic loci as if they were ordinary Nyquist loci.

2.4.1 Approximately commutative controller

The goal of the approximately commutative[5] controller is to shape the characteristic loci to achieve system stability and meet performance specifications regarding relative stability, accuracy and interaction [MacFarlane and Kouvaritakis, 1977]. The manipulation of individual characteristic loci could be easily achieved if a controller could be designed with the same characteristic direction set (or eigenframe) as the system. In other words, if the square $m \times m$ transfer function matrix, $G(s)$, has spectral decomposition $G(s) = W(s)\Lambda_g(s)V(s)$, then a controller which has spectral decomposition $K(s) = W(s)\Lambda_k(s)V(s)$ can shape the individual characteristic loci in the following way:

$$\begin{aligned} G(s)K(s) &= W(s)\Lambda_g(s)V(s)W(s)\Lambda_k(s)V(s) \\ &= W(s)\Lambda_g(s)\Lambda_k(s)V(s) \\ &= W(s)\Lambda_{gk}(s)V(s) \end{aligned}$$

where $\Lambda_{gk}(s) = \text{diag}\{g_i(s)k_i(s)\}$. Thus, each scalar controller $k_i(s)$ could be designed to shape the corresponding characteristic loci. Although such simple scalar controllers would be desirable, in practice, the overall structure is difficult to implement because components of the characteristic direction set matrix $W(s)$ are almost invariably irrational functions. Moreover, for $m > 2$, the eigenvectors are not known explicitly.

[5]The controller is commutative because both pre and post multiplication of G by the controller transfer function matrix produce the same result as outlined in the main discussion.

A practical alternative is to construct a controller whose eigenframe approximates the system eigenframe at a particular frequency, s_o. Such a controller, called an approximately commutative controller, is given by:

$$\begin{aligned} K(s) &= \hat{W}\Lambda_k(s)\hat{V} \\ &\approx W(s_o)\Lambda_k(s)V(s_o) \end{aligned}$$

where $\hat{W} \approx W(s_o)$ and $\hat{V} \approx V(s_o)$ are constant, real matrix approximations to the characteristic direction set and dual characteristic direction set, respectively. The particular frequency s_o is chosen during the design procedure outlined below. One reason for using the real approximations lies in the simplicity of the resulting implementation which consists only of amplifier networks devoid of dynamic elements [Maciejowski, 1989]. The procedure for obtaining the real approximations to the direction sets is given by the ALIGN algorithm [Kouvaritakis, 1988].

The approximately commutative controller permits control of the system in the frequency range about s_o by approximating the eigenframe of the system at frequency s_o. The equations which govern the open-loop behaviour in this frequency range are given by:

$$\begin{aligned} G(s)K(s) &= W(s)\Lambda_g(s)V(s)\hat{W}\Lambda_k(s)\hat{V} \\ &\approx W(s)\Lambda_{gk}(s)V(s_o) \end{aligned}$$

where use is made of $V(s)\hat{W} \approx I$. Thus, the individual products of the characteristic transfer functions $g_i(s)$ with the corresponding compensators $k_i(s)$ can be used to shape the loci to meet stability and performance requirements as subsequently outlined in the CLM design procedure.

2.5 Characteristic locus design

In order to manipulate the characteristic loci to meet the stability, accuracy, and interaction requirements, the Characteristic Locus Method specifies controller design at each of the three frequency ranges defined by (2.19). Subsequently, the overall

controller is realized as a combination of the three frequency dependent controllers. The CLM design procedure is outlined in the steps below [MacFarlane, 1980; Kouvaritakis, 1988]:

1. **High Frequency Range** ($\omega \geq \omega_h$): In the high frequency range, interaction cannot be reduced with high compensator gain. Therefore, some form of compensation other than increased gain must be deployed to reduce interaction. In the high frequency range, the requirement that the k^{th} input excite only the k^{th} output is equivalent to the requirement that the eigenvectors parallel the standard basis vectors. This can be accomplished by requiring $G(j\omega_h)K_h \approx D$ where K_h is the constant high frequency compensator and D is a diagonal matrix. Thus, the high frequency compensator is designed to satisfy:

$$K_h \approx DG^{-1}(j\omega_h) \tag{2.23}$$

   This compensator is given by applying the ALIGN algorithm to find an approximate real inverse to $DG^{-1}(j\omega_h)$.

2. **Intermediate Frequency Range** ($\omega_l < \omega < \omega_h$): In the intermediate frequency range, the primary concern is with improving the relative stability margins about the critical point. This is done by designing an intermediate frequency compensator, $K_m(s)$, as an approximately commutative controller which operates on the combined system $G(s)K_h$. The ALIGN algorithm is used to approximate the eigenframe of this system in order to apply classical scalar phase lead or phase lag shaping techniques to the characteristic loci. To reduce the interference of the intermediate frequency design phase with that of the previous step, an attempt is made to ensure that $\lim_{\omega \to \omega_h} K_m(j\omega) = I$. At the completion of this step, the compensated system is $G(s)K_hK_m(s)$.

3. **Low Frequency Range** ($\omega \leq \omega_l$): In the low frequency range, the main concern is with steady state accuracy. As noted previously in the discussion of accuracy, high gains cause the output to accurately follow the input. To both increase and balance the gains of the characteristic loci, proportional-plus-integral (PI) action is used in the low frequency compensator which has the following form:

$$\frac{\alpha}{s}K_l(s) + I \tag{2.24}$$

where α is chosen to control the transition from low to intermediate frequency. Similar to the previous step, the low frequency compensator is designed as an approximately commutative controller which operates on the combined system $G(s)K_hK_m(s)$.

4. **Characteristic Locus Controller**: The overall characteristic locus controller is realized as the following combination of previously designed compensators:

$$K(s) = K_hK_m(s)\left(\frac{\alpha}{s}K_l(s) + I\right) \tag{2.25}$$

Thus, the characteristic locus controller manipulates both the characteristic directions and transfer functions to achieve stability, reduced interaction, and improved performance.

2.6 Summary

This chapter has given an overview of the generalized Nyquist/characteristic locus framework so that the perturbed interaction investigation which follows may be viewed from this perspective. To achieve this, background material relating to uncertainty models, perturbed stability conditions, and the E-Contour method was presented. Finally, a summary of the relevant aspects of the generalized Nyquist/characteristic locus approach was given with particular emphasis on interaction.

Chapter 3

The minimization of interaction in the presense of uncertainty and controller gain limitations

3.1 Introduction

The problem of interaction in linear time-invariant multivariable systems has been examined extensively from many differing perspectives for quite some time. A description of the status of noninteracting control prior to 1971 is given in [Morse and Wonham, 1971] and an analysis of decoupling from a geometric perspective is presented in [Wonham, 1979]. More recent work has focused on employing state feedback to achieve decoupling [Descusse et al., 1984; Descusse et al., 1988] while additional research has examined the simultaneous problem of disturbance rejection by output feedback and decoupling [Desoer and Nasli Gündes, 1986; da Silva and Leite, 1992; Chang and Rhodes, 1975; Fabian and Wonham, 1975]. These latter approaches in conjunction with others [Horowitz, 1963; Horowitz, 1982] have emphasised a two-degree-of-freedom design structure in which the feedback compensator is deployed to stabilize an uncertain system while the prefilter is used to decouple the resulting stabilized system. Clearly, such approaches are most effective whenever feedback can be deployed to reduce system uncertainty to such an extent that decoupling can be achieved through pre-filtering. However, in many practical situations, physical limitations on the available/permissible amount of feedback gain imply that, at least over a range of frequencies, open-loop uncertainty will persist in the closed-loop. In cases like these, the use of a decoupling pre-filter will not necessarily suppress in-

teraction to an acceptable level. The persistence of closed-loop interaction has been implicitly acknowledged in the design strategy of the Characteristic Locus (Generalized Nyquist) Method [MacFarlane, 1980; Kouvaritakis and Trimboli, 1989] where, as seen in the previous chapter, decoupling feedback is deployed in the high frequency range where gain is necessarily limited.

The main objective of the present chapter is to give an example which demonstrates that feedback compensation can attain better performance in terms of reduced interaction when there are compensator gain limitations and the nominal plant is subject to additive uncertainty. In line with this aim, this chapter seeks to develop only the means of completing the counter-example rather developing the entire methodology. In the particular example given, the decoupling feedback compensator will be seen to provide greater relative decoupling as compared to a two-degree-of-freedom structure in which the feedback compensator is designed to minimize the closed-loop uncertainty and the prefilter is designed to minimize interaction. Although two-degree-of-freedom approaches simplify the design process through the separation of robustness and decoupling issues, they do so at the potential cost of excessive interaction. The conclusion to be drawn here is that realistic design strategies which address the simultaneous problems of robust stabilization and decoupling should incorporate a more general approach in which both the feedback compensator and prefilter are either simultaneously deployed or deployed over different frequency ranges in order to achieve the concurrent objectives of robust stabilization and optimal decoupling.

3.2 Preliminaries

The preliminaries of this section pertain to the simple multivariable example considered in the following section. In particular, the example studied will be a two-input/two-output system whose values are known at a particular frequency. Since the present concern is primarily with interaction, it will be assumed that stability is implicitly ensured by the design process. This assumption is particularly perti-

nent, for example, when considering generalized Nyquist design techniques which initially address high frequency interaction and subsequently ensure robust stability [Kouvaritakis and Trimboli, 1989]. Additionally, in order to reduce the number of computations required to optimize the cost functions given below, it will also be assumed that the plant $G(s)$ at the specified frequency contains only real elements.

The nominal multivariable feedback system of Fig. 3.1 has three associated transfer functions: (1) the *sensitivity function* $S(s)$, (2) the *controller sensitivity function* $R(s)$, and (3) the *complementary sensitivity function* $T(s)$. The nominal models

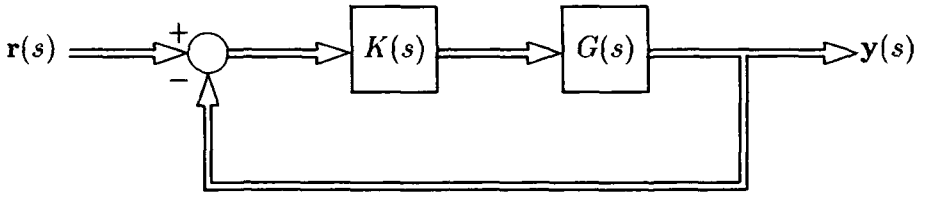

Figure 3.1: Nominal multivariable feedback system

are given as:

$$S = (I + GK)^{-1} \tag{3.1}$$

$$R = K(I + GK)^{-1} \tag{3.2}$$

$$T = GK(I + GK)^{-1} \tag{3.3}$$

When the nominal plant G is subject to additive uncertainty Δ, the true plant is represented by $G + \Delta$ as depicted in Fig. 3.2. The perturbed complementary

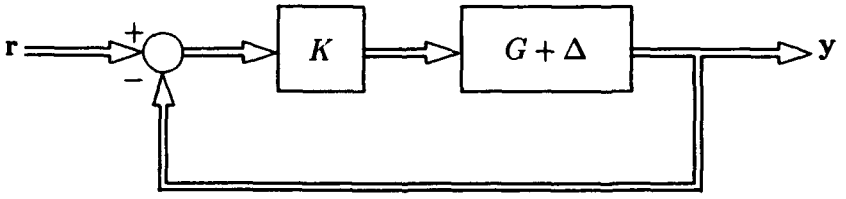

Figure 3.2: One-degree-of-freedom multivariable system with additive uncertainty

sensitivity function corresponding to Fig. 3.2 is represented by:

$$\begin{aligned} T+\tilde{T} &= (G+\Delta)K(I+(G+\Delta)K)^{-1} \\ &= T+S\left(I-(I+\Delta R)^{-1}\right) \end{aligned} \tag{3.4}$$

where S and R represent the nominal sensitivity and controller sensitivity functions given by (3.1) and (3.2), respectively. From (3.4), it is clear that contribution of the additive uncertainty Δ to the closed-loop complementary sensitivity function is given by $\tilde{T} = S\left(I-(I+\Delta R)^{-1}\right)$.

The specific class of additive structured uncertainty $\mathbf{D_s}$ considered in the sequel is characterized as:

$$\Delta \in \mathbf{D_s} \triangleq \left\{\Delta : |\Delta| \leq P = \begin{pmatrix} 0 & p \\ 0 & 0 \end{pmatrix},\ 0 \leq p\right\} \tag{3.5}$$

where p is a nonnegative real number. Thus, the uncertainty class given by (3.5) has uncertainty exclusively in the $(1,2)$ element and for simplicity, all perturbations within the defined class $\mathbf{D_s}$ will be compactly represented as:

$$\Delta = \delta \mathbf{e}_1 \mathbf{e}_2^T \quad \text{where} \quad \delta = \rho e^{j\theta} \quad \text{and} \quad 0 \leq \rho \leq p \tag{3.6}$$

Moreover, ρ and θ are the modulus and phase, respectively, of the uncertainty element δ and $\mathbf{e}_1$ and $\mathbf{e}_2$ are standard basis vectors corresponding to the respective columns of the 2×2 identity matrix.

In the following discussion, it will be useful to define the stabilizing feedback controller class $\mathcal{K}$ with limited lower and upper gains specified by the following notation:

$$\mathcal{K}_\alpha^\beta \triangleq \{K :\ 0 \leq \alpha \leq \underline{\sigma}[K] \leq \overline{\sigma}[K] \leq \beta\} \tag{3.7}$$

where α and β represent the lower and upper gain limits, respectively, of the feedback controller K. Additionally, the notation $\overline{\sigma}[\,\cdot\,]$ denotes the maximum singular value of $[\,\cdot\,]$ while $\underline{\sigma}[\,\cdot\,]$ denotes the minimum singular value of $[\,\cdot\,]$.

For the specific 2×2 case, a simple measure of the interaction present in the i^{th} loop of the perturbed closed-loop transfer function $T+\tilde{T}$ is given by the following

measure:

$$\tau = \max\left\{\left|\frac{\left(T+\tilde{T}\right)_{21}}{\left(T+\tilde{T}\right)_{11}}\right|, \left|\frac{\left(T+\tilde{T}\right)_{12}}{\left(T+\tilde{T}\right)_{22}}\right|\right\} \tag{3.8}$$

where the subscript ij denotes the corresponding element (i,j) and τ denotes the maximum interaction in either the first or second loop. Hence, τ measures the maximum ratio of the i^{th} column off-diagonal element to the i^{th} column diagonal element. It is straightforward to rewrite this interaction measure in the following more compact fashion:

$$\tau_1 = \max_{i=1,2}\left|\frac{\mathbf{e}_i^T E\left(T+\tilde{T}\right)\mathbf{e}_i}{\mathbf{e}_i^T\left(T+\tilde{T}\right)\mathbf{e}_i}\right| \tag{3.9}$$

where the subscript associated with τ_1 denotes the one-degree-of-freedom interaction measure and E is the 2×2 identity matrix with reversed columns. Similarly, by employing a prefilter F as shown in Fig. 3.3, the resulting two-degree-of-freedom interaction measure becomes:

$$\tau_2 = \max_{i=1,2}\left|\frac{\mathbf{e}_i^T E\left(T+\tilde{T}\right)F\mathbf{e}_i}{\mathbf{e}_i^T\left(T+\tilde{T}\right)F\mathbf{e}_i}\right| \tag{3.10}$$

where the prefilter F simply post multiplies the perturbed closed-loop transfer function matrix $T+\tilde{T}$.

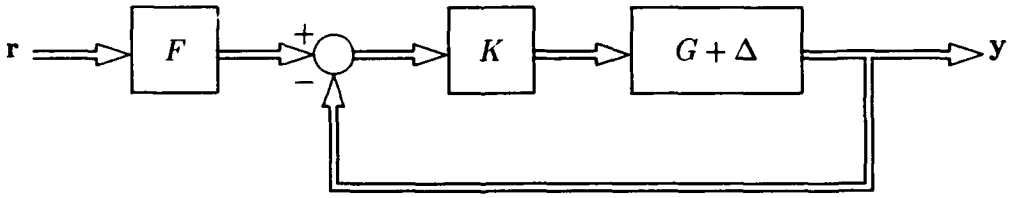

Figure 3.3: Two-degree-of-freedom multivariable system with additive uncertainty

In the two-degree-of-freedom design structure of Fig. 3.3, the feedback compensator K_2 which minimizes uncertainty in the perturbed closed-loop system $T+\tilde{T}$ satisfies the following cost function:

$$K_2 := \min_{K \in \mathcal{K}_a^s} \max_{\Delta \in \mathbf{D}_s} \frac{\overline{\sigma}\left[\tilde{T}\right]}{\overline{\sigma}\left[T\right]} \tag{3.11}$$

where the controller class $\mathcal{K}_\alpha^\beta$ is defined by (3.7) and the notation "$a := f(a)$" denotes that "a" is assigned the optimal value defined by the optimization function "$f(a)$". The presence of the denominator term $\overline{\sigma}[T]$ in (3.11) precludes the occurrence of the trivial case $K_2 = 0$ and for the simple 2×2 example to be considered, it is straightforward to show that the numerator term $\overline{\sigma}\left[\tilde{T}\right]$ satisfies the following relationship:

$$\overline{\sigma}\left[\tilde{T}\right] = \left|\frac{\delta}{1 + \delta \mathbf{e}_2^T R \mathbf{e}_1}\right| \|S\mathbf{e}_1\| \left\|\mathbf{e}_2^T R\right\| \tag{3.12}$$

where δ denotes the $(1,2)$ element of the perturbation matrix Δ. Using (3.12), it is also straightforward to show that the worst case uncertainty which achieves the maximization in (3.11) lies on the boundary of the class $\mathbf{D}_s$ and is purely real:

$$\Delta_{wc_2} = \pm p \mathbf{e}_1 \mathbf{e}_2^T \tag{3.13}$$

where the subscript 2 associates this worst case perturbation with the two-degree-of-freedom controller K_2. Hence, referring to (3.6) the worst case uncertainty Δ_{wc_2} has maximum modulus (i.e. $|\delta| = p$) and either positive or negative sign (i.e. $\theta = 0$ or $\theta = \pi$). Clearly, this characterization of the worst case uncertainty significantly reduces the number of computations required to optimize (3.11).

Further examination of (3.12) reveals that the feedback controller K_2 which minimizes the uncertainty cost function (3.11) has the following general structure:

$$K_2 = \begin{pmatrix} \boldsymbol{k}^T \\ \mathbf{o}^T \end{pmatrix} \tag{3.14}$$

where $\boldsymbol{k}^T$ is a 2-element (nonzero) row vector and $\mathbf{o}^T$ is a 2-element zero row vector. Here, it is implicitly assumed that the feedback controller K_2 is in the controller class $\mathcal{K}_\alpha^\beta$ with lower gain limit $\alpha = 0$ and upper gain limit $\beta > 0$ [c.f. (3.7)]. The optimal controller structure given by (3.14) becomes apparent by writing the controller sensitivity function as the product $R = KS$ and observing that the second standard basis vector $\mathbf{e}_2$ premultiplies the controller K in the optimization function numerator term (3.12). Thus, the feedback controller of (3.14) yields $\overline{\sigma}\left[\tilde{T}\right] = 0$ and therefore completely removes uncertainty in the feedback loop.

Given the general compensator structure of (3.14), it is of interest to determine the optimal prefilter (c.f. Fig. 3.3), designated F_2, which minimizes the closed-loop two-degree-of-freedom interaction measure τ_2 given by (3.10). By writing the 2×2 prefilter as stacked column vectors (i.e. $F_2 = [\boldsymbol{f}_1 \boldsymbol{f}_2]$), the closed-loop interaction measure τ_2 becomes

$$\tau_2 = \max_{i=1,2} \left| \frac{\mathbf{e}_i^T E G \mathbf{e}_1 \boldsymbol{k}^T [\boldsymbol{f}_1 \boldsymbol{f}_2] \mathbf{e}_i}{\mathbf{e}_i^T G \mathbf{e}_1 \boldsymbol{k}^T [\boldsymbol{f}_1 \boldsymbol{f}_2] \mathbf{e}_i} \right| \tag{3.15}$$

Additionally, if the elements of the nominal plant G are denoted by g_{ij}, then (3.15) implies that τ_2 is given by:

$$\tau_2 = \max \left\{ \left| \frac{g_{21}}{g_{11}} \right|, \left| \frac{g_{11}}{g_{21}} \right| \right\} \tag{3.16}$$

where it is implicitly assumed that $g_{11} \neq 0$ and $g_{21} \neq 0$. Clearly, minimal interaction results when $|g_{11}| = |g_{21}|$ and this yields the value of the two-degree-of-freedom interaction measure $\tau_2 = 1$. Interestingly, (3.16) implies that interaction depends entirely on the nominal plant G and is completely independent of the prefilter F_2.

In order to permit the two-degree-of-freedom prefilter to influence the closed-loop interaction measure, it is necessary to modify the rank deficient controller of (3.14). Thus, in lieu of attaining minimal closed-loop uncertainty (i.e. $\overline{\sigma}\left[\hat{T}\right] = 0$), the optimization (3.11) must consider the class of stabilizing controllers $\mathcal{K}_\alpha^\beta$ where the controllers considered are constrained to have a lower gain limit α which satisfies $0 < \alpha \leq \beta$.

Upon determining the two-degree-of-freedom feedback compensator K_2 which minimizes closed-loop uncertainty according to (3.11) with $\alpha \neq 0$, the optimal decoupling prefilter F_2 is chosen to satisfy:

$$F_2 := \min_F \tau_2 \tag{3.17}$$

where τ_2 is given by (3.10).

In contrast to the two-degree-of-freedom optimizations presented above, the optimal decoupling one-degree-of-freedom feedback compensator designated K_1 satisfies the following optimization:

$$K_1 := \min_{K \in \mathcal{K}_\alpha^\beta} \tau_1 \tag{3.18}$$

where τ_1 is given by (3.9) and $\mathcal{K}_\alpha^\beta$ represents the feedback controller class defined by (3.7). In general, the optimal decoupling controller is not constrained to have some lower gain limit $\alpha \neq 0$ as was the case in the two-degree-of-freedom structure, therefore we may take $\alpha = 0$.

This discussion of the assumptions, optimization functions, constraints, and uncertainty and controller classes enables the study of the simple example presented in the next section. This example demonstrates the main point of this chapter, namely that interaction is *not always* optimally dealt with by a decoupling prefilter after the minimization of closed-loop uncertainty.

3.3 Example

Consider the 2×2 nominal plant model G whose matrix value at a specific frequency ω is given by:

$$G = \begin{pmatrix} -0.7000 & -0.0500 \\ 0.1000 & 0.1000 \end{pmatrix}$$

and which is subject to an additive structured uncertainty Δ within the structured uncertainty class $\mathbf{D_s}$ defined by (3.6) in which $|\delta| \leq 0.1$. It should be noted that both G and Δ have been arbitrarily chosen for this example. From the analysis of the previous section, it is known that the worst case uncertainty which maximizes the closed-loop uncertainty is given by $\Delta_{wc_2} = \pm 0.1 \mathbf{e}_1 \mathbf{e}_2^T$. Additionally, the controller class $\mathcal{K}_\alpha^\beta$ will be assumed to have a lower gain limit given by $\alpha = 0.1$ and an upper gain limit given by $\beta = 1$. It is possible to parameterize the controllers and pre-filter in terms of their respective singular value decompositions and perform an exhaustive search over the parameterizations; this simple optimization technique will be employed to solve each optimization problem.

Exhaustively searching over the parameterization of feedback compensators to minimize the closed-loop uncertainty in accordance with (3.11) yields the following

optimal "two-degree-of-freedom-feedback-compensator":

$$K_2 = \begin{pmatrix} 0.1324 & -0.9889 \\ 0.0905 & 0.0795 \end{pmatrix}$$

This feedback compensator gives the optimal worst case value of uncertainty reduction $\overline{\sigma}\left[\tilde{T}_2\right]/\overline{\sigma}\left[T_2\right] = 0.0131$ and clearly, K_2 has done well by way of reducing the closed-loop uncertainty. In addition, the controller K_2 is on the boundary of the controller class $\mathcal{K}_{0.1}^1$ since $\underline{\sigma}\left[K_2\right] = 0.1$ and $\overline{\sigma}\left[K_2\right] = 1$. Interestingly, the uncertainty value $\overline{\sigma}\left[\tilde{T}_2\right]/\overline{\sigma}\left[T_2\right]$ is independent of the sign of the uncertainty $\pm 0.1\mathbf{e}_1\mathbf{e}_2^T$.

By employing the optimal uncertainty reducing controller K_2 and exhaustively searching over the parametrization of prefilters to minimize the two-degree-of-freedom interaction measure τ_2 defined by (3.10), the following optimal decoupling prefilter is obtained:

$$F_2 = \begin{pmatrix} 0.3080 & -0.4510 \\ 0.9240 & -0.0678 \end{pmatrix}$$

Using the prefilter F_2 in conjunction with the controller K_2 yields the following value of the two-degree-of-freedom interaction measure:

$$\tau_2 = 1.2112 \tag{3.19}$$

As with $\overline{\sigma}\left[\tilde{T}_2\right]/\overline{\sigma}\left[T_2\right]$, the optimal value of τ_2 is independent of the sign of the uncertainty $\pm 0.1\mathbf{e}_1\mathbf{e}_2^T$.

In comparison, by exhaustively searching over the parametrization of feedback compensators to minimize the one-degree-of-freedom interaction measure τ_1 defined by (3.9), the following optimal compensator was found:

$$K_1 = \begin{pmatrix} -0.9968 & 0.0525 \\ -0.0795 & -0.6514 \end{pmatrix}$$

The corresponding value of closed-loop interaction is given by:

$$\tau_1 = 0.6363 \tag{3.20}$$

and analogous to the previous two-degree-of-freedom results, the interaction measure τ_1 (based on the optimal decoupling controller K_1) is independent of the sign of

$\pm 0.1 \mathbf{e}_1 \mathbf{e}_2^T$. By way of uncertainty reduction, the controller K_1 yielded the value $\overline{\sigma}\left[\tilde{T}_1\right] / \overline{\sigma}\left[T_1\right] = 0.0999$; however, K_1 was chosen to optimize perturbed decoupling rather than uncertainty reduction. In order to confirm the decoupling optimality of K_1, the range of prefilters was scanned to minimize the two-degree-of-freedom interaction measure τ_2 defined by (3.10) but with K_1 used in place of K_2. Not surprisingly, the optimal decoupling prefilter F_1 paired with the optimal decoupling compensator K_1 turns out to be the identity matrix (i.e. $F_1 = I$) and this further confirms that interaction has been optimized by the feedback compensator K_1.

Comparison of the interaction measures $\tau_1 = 0.6363$ and $\tau_2 = 1.2112$ given in (3.20) and (3.19), respectively, clearly demonstrates the improved decoupling performance afforded by the one-degree-of-freedom compensator K_1.

3.4 Summary

This chapter has demonstrated, by way of example, that controller gain limitations in conjunction with plant uncertainty may require optimal decoupling through feedback compensation rather than through a decoupling prefilter. Although two-degree-of-freedom approaches simplify the design process through the separation of robustness and decoupling issues, they do so at the potential cost of excessive interaction over the range of frequencies in which feedback gain is necessarily limited. Under these situations, feedback compensation may not sufficiently reduce the effects of uncertainty to enable optimal pre-filtering; therefore, in such cases, decoupling feedback must be deployed over the appropriate frequency range.

Chapter 4

Uncertainty and interaction in linear multivariable feedback systems

4.1 Introduction

One of the main objectives in feedback control design is to minimize the effects of uncertainty in system dynamics. It is not surprising therefore that, over the last two decades, much research effort has been directed in this area with a particular concern for the multivariable case. As a result there are now a wealth of results relating to multivariable stability and tolerance to uncertainty, accuracy of tracking, disturbance rejection, etc.; however, one aspect of multivariable behaviour that appears to have been overlooked is interaction. In the context of the characteristic locus framework (c.f. Section 2.3.5), interaction is characterized in terms of:

(1) the moduli of the characteristic loci; and/or

(2) the misalignment angles between the open-loop characteristic vector set and the standard basis vector set.

Naturally, an assessment of interaction is of no use in situations where feedback can be deployed to reduce plant uncertainty to such an extent that decoupling can be accomplished via pre-filtering. However, as demonstrated in the previous chapter, limitations on the available/permissible amount of compensator gain imply that, at least over a range of frequencies, open-loop uncertainty will persist in the closed-loop. In such cases, the use of a decoupling pre-filter will not necessarily result in a non-interactive system and, as a consequence, it is useful to have the capability of evaluating closed-loop interaction in terms of open-loop parameters, particularly

with regard to the effects of uncertainty. For the case where the plant uncertainty is modelled as an additive perturbation $\Delta(s)$ on a nominal transfer function matrix $G(s)$, the problem of assessing interaction becomes one of determining the effect of $\Delta(s)$ on the moduli of the eigenvalues of $G(s)+\Delta(s)$ and on the angular displacement of the eigenvectors of $G(s)+\Delta(s)$ with respect to the standard basis vectors. For the structured uncertainty class $\mathbf{D_s}$ [c.f. (2.4)] considered in the present investigation, the E-Contour method based on the MPDA property [c.f. (2.12)] can be deployed to determine upper and lower bounds on the perturbed eigenvalue moduli and, therefore, contribute to an assessment of interaction in terms of (1) above. Unfortunately, the E-Contour method provides no tangible information on the effects of uncertainty on eigenvector/standard basis vector misalignment; hence, this work seeks to bridge this gap by enabling an assessment of perturbed interaction in terms of (2) above.

It will be shown that by considering the appropriate stationary conditions, the perturbation which maximizes interaction in terms of eigenvector misalignment, hereafter referred to as the worst case perturbation, lies on the boundary of the structured uncertainty class $\mathbf{D_s}$ (i.e. each element δ_{ij} of Δ has maximum modulus). Furthermore, the stationary conditions will be shown to enable the further characterization of the worst case perturbation phase structure in terms of diagonal phase matrices which pre- and post-multiply the uncertainty class boundary matrix. This enables the development of a simple and efficient algorithm for the determination of the worst and best case perturbed interaction as measured by the maximum and minimum values of the misalignment angles, respectively, at a set of preselected frequencies. This information together with the modulus information derived from the E-Contours can be deployed to supplement the nominal plots of eigenvalue-moduli and misalignment angles versus frequency with plots of bands of possible eigenvalue-moduli and possible angles versus frequency. The resulting plots provide a convenient means of assessing interaction in the presence of uncertainty. The strength of this approach is its convenience: it relates closed-loop interaction to simple open-loop attributes. The overall interaction assessment can be supplemented further with

upper bounds on interaction [Kouvaritakis and Trimboli, 1988]. In this case, an appropriate modification of the algorithm presented will yield interaction bounds which take full account of model uncertainty and still enable one to relate closed-loop interaction to simple open-loop geometric properties. The results are illustrated by means of a numerical example and a study carried out on the model of an open-loop unstable chemical reactor. Throughout this discussion, the assumption will be made that the eigenvalues of the uncertain transfer function $G(s) + \Delta(s)$, evaluated at any frequency, if repeated will be simple. This assumption does constitute a limitation to the approach because non-simple eigenvalues can only occur when the corresponding eigenvectors become pa.allel. In such a case however, interaction will be excessive and a precise quantification of interaction would be of little practical use.

4.2 Background

The two open-loop attributes listed in the previous section which characterize closed-loop interaction are also useful in specifying the corresponding conditions under which the closed-loop system of Fig. 4.1 will exhibit *low* closed-loop interaction;

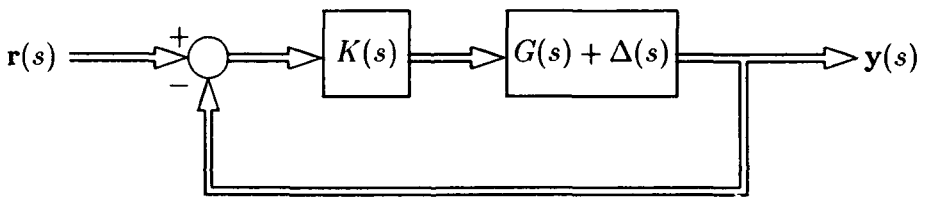

Figure 4.1: Multivariable system with additive perturbation

these are:

(*i*) the moduli of the eigenvalues of $G(s)$ is large; and/or

(*ii*) each eigenvector of $G(s)$ makes a small angle with a different standard basis vector.

The physical reasons underlying these conditions can be explained in terms of the characteristic locus framework.

Recall from Chapter 2 that the open-loop transfer function matrix $G(s)$ has an associated algebraic function $g(s)$ defined by (2.13). Moreover, everywhere, except at its branch points, the algebraic function $g(s)$ has m distinct characteristic transfer functions[1] (or branches), $g_i(s)$, each having an associated distinct right and dual left-eigenvector $\mathbf{w}_i(s)$ and $\mathbf{v}_i^t(s)$ with the following properties [c.f. (2.16)]:

$$G(s)\mathbf{w}_i(s) = g_i(s)\mathbf{w}_i(s) \qquad \mathbf{v}_i^t(s)G(s) = g_i(s)\mathbf{v}_i^t(s) \qquad \mathbf{v}_i^t(s)\mathbf{w}_i(s) = 1 \tag{4.1}$$

These properties, in turn, define the dyadic decompositions of the open- and closed-loop transfer function matrices $G(s)$ and $T(s)$ given by (2.15) and (2.18), respectively, which at any given frequency become:

$$G = \sum_{i=1}^{m} g_i \mathbf{w}_i \mathbf{v}_i^t \qquad \text{and} \qquad T = \sum_{i=1}^{m} \frac{g_i}{1+g_i} \mathbf{w}_i \mathbf{v}_i^t \tag{4.2}$$

From (4.1) and (4.2) it is easy to understand how *condition (i) above yields the* following low closed-loop interaction result:

$$\text{if} \quad |g_i| \gg 1 \quad \forall\, i \quad \text{then} \quad T \approx I$$

Thus, large eigenvalue moduli yield low closed-loop interaction.

The physical reasoning underlying low closed-loop interaction condition (ii) above was explained in Section 2.3.5 where it was observed that the condition of *no* interaction requires that the i^{th} standard basis vector $\mathbf{e}_i$ be an eigenvector $\mathbf{w}_i$ of both the open- and closed-loop transfer function matrices G and T as given by (4.2). Consequently, a quantification of closed-loop interaction is given by the *misalignment angle*, ϕ_i, which measures the angular difference between $\mathbf{e}_i$ and $\mathbf{w}_j$ as:

$$\cos\phi_i \triangleq \max_j \frac{|\mathbf{e}_i^t \mathbf{w}_j|}{\|\mathbf{e}_i\| \|\mathbf{w}_j\|} \tag{4.3}$$

Additionally, for all but highly interactive systems, (4.3) associates a unique eigenvector $\mathbf{w}_j$ to each standard basis vector $\mathbf{e}_i$; henceforth for convenience it will be

[1] m is the number of plant inputs and outputs.

assumed that the eigenvectors have been ordered so that $\mathbf{e}_i$ makes the smallest misalignment angle with $\mathbf{w}_i$. This pairing of $\mathbf{e}_i$ to a unique $\mathbf{w}_i$ will be unambiguous unless $\phi_i > 45°$ for some i, when more than one pairing may be possible. But clearly in such a case (i.e. when $\phi_i > 45°$) the i^{th} loop will be expected to be highly interactive and a measure of the amount of interaction present would not convey any useful information.

Due to steady state accuracy requirements, the characteristic gains of the open-loop system (after compensation) must be made large, thus at low frequencies, condition (i) relating to the eigenvalue moduli will be pertinent in the assessment of closed-loop interaction. Conversely at high frequencies, due to the natural attenuation present in most physical systems, constraints on control input levels, noise considerations as well possible conflicts with the requirement for stability, condition (i) will not apply and condition (ii) pertaining to the eigenvector misalignment will be applicable. At the cross over from low to high frequencies (namely at intermediate frequencies) both conditions (i) and (ii) can play an important role in the assessment of interaction.

A convenient way to combine and present the information relevant to conditions (i) and (ii) is to plot, for each eigenvector $\mathbf{w}_i$, the eigenvalue modulus $|g_i|$ versus frequency ω and the misalignment angle ϕ_i again versus frequency ω. As explained earlier, these plots may be supplemented by plots of upper bounds on interaction in terms of the open-loop eigen-properties of the transfer function matrix [Kouvaritakis and Trimboli, 1988]. In particular, if the reference signal $\mathbf{r}$ of Fig. 4.1 is in the direction of the i^{th} standard basis vector $\mathbf{e}_i$, then the reference signal may be written as $\mathbf{r}(j\omega) = r_o(j\omega)\mathbf{e}_i$, where $r_o(j\omega)$ is a scalar function of frequency ω; for convenience in the sequel the argument $(j\omega)$ shall be dropped. If $\mathbf{y}$ denotes the corresponding output, then the quantity $\|\mathbf{y} - (\mathbf{e}_i^t\mathbf{y})\mathbf{e}_i\|$ gives an exact measure of interaction at a particular frequency ω, which can be shown to be bounded from above as:

$$\frac{\|\mathbf{y} - (\mathbf{e}_i^t\mathbf{y})\mathbf{e}_i\|}{|r_o|} \leq U_1 \leq U_2 \tag{4.4}$$

with

$$U_1 = \|W_i\| \max_j |t_j - t_i| \|V_i \mathbf{e}_i\| \qquad \text{and} \qquad U_2 = \mathcal{K}_i(W) \max_j |t_j - t_i| \sin(\phi_i) \quad (4.5)$$

where W and V are the matrices of right- and left-eigenvectors, $\mathbf{w}_i$ and $\mathbf{v}_i^t$, W_i is W with its i^{th} column stricken; V_i is V with its i^{th} row stricken; t_i is the i^{th} closed-loop eigenvalue defined by $t_i = \frac{g_i}{1+g_i}$; and $\mathcal{K}_i(W)$ is the partial spectral condition number of the eigenvector matrix defined as $\mathcal{K}_i(W) \triangleq \|W_i\| \|V_i\|$. Clearly, excepting the 2×2 case when $U_1 = U_2$, U_1 gives a tighter bound on interaction. However, U_2 has a simpler geometric interpretation and is more closely related to the qualitative approach discussed earlier in the section. In particular, it provides further (quantitative) justification for the low interaction conditions (i) and (ii) listed earlier: under condition (i) the open-loop eigenvalue moduli are large (i.e. $|g_i| \gg 1$) so that the closed-loop eigenvalue moduli are approximately unity (i.e. $|t_i| = 1 + O(1/|g_i|)$) from which the maximum value of $|t_j - t_i|$ is of order $O(1/|g_i|)$; under condition (ii) the misalignment angle ϕ_i is small thus leading to a small value of $\sin(\phi_i)$ and therefore a small value of U_2 in (4.5). Thus, providing that the eigenvector matrix W is not ill-conditioned (it is noted that $\mathcal{K}_i(W) \leq \|W\| \|V\|$), the plots of eigenvalue-moduli $|g_i|$ and misalignment angles ϕ_i versus frequency provide a sensible graphical means of assessing interaction. These can be enhanced by a third plot, namely that of the partial condition number $\mathcal{K}_i(W)$ versus frequency, in order to account for eigenvector conditioning. For a purely quantitative assessment one can revert to a plot of U_1 or U_2 against frequency. Uncertainty in the model transfer function G will affect the plots of $|g_i|$, ϕ_i and $\mathcal{K}_i(W)$, and it is the present endeavour to derive suitable algorithms for the computation of upper (and lower) bounds on these quantities and Section 4.3 initiates this work with a study of the effect of uncertainty on the eigenvector misalignment angles. Subsequently, algorithms for the computation of worst case and best case bounds on $|g_i|$, $\mathcal{K}_i(W)$, and U_2 are considered briefly in Section 4.4.

4.3 Misalignment angles in the presence of additive perturbations

4.3.1 The uncertainty class

Recall from the discussion in Section 2.2.1 that uncertainty arises from many sources such as imprecise knowledge of physical parameters (e.g. masses, friction coefficients, etc.) or errors during a model identification stage (such as would be caused by the presence of measurement noise and/or unmodelled dynamics). In such cases, the transfer function matrix $G(s)$ can only be thought of as a nominal description of the plant dynamics and a more realistic representation of the plant dynamics is given by:

$$\tilde{G}(s) = G(s) + \Delta(s) \tag{4.6}$$

where the additive perturbation $\Delta(s)$ is introduced in an attempt to account for the model uncertainty. Using physical arguments (concerning the possible range of parameter values) or invoking some reasonable assumptions concerning the identification process (for example that the measurement noise is either normally distributed or is bounded) it is possible to stipulate element-by-element bounds on the uncertainty $\Delta(j\omega)$:

$$|\Delta_{rs}(j\omega)| \leq p_{rs}(j\omega) \qquad \forall\, \omega \tag{4.7}$$

where $\Delta_{rs}(j\omega)$ denotes any complex-valued (r,s) element of $\Delta(j\omega)$ and $p_{rs}(j\omega)$ denotes the corresponding nonnegative real function which bounds the element modulus. Thus, the implied class of possible perturbations considered here lies within the structured class of uncertainty $\mathbf{D_s}$ defined by (2.4). The problem of assessing perturbed interaction now becomes one of determining the effect of the perturbation $\Delta(j\omega)$ on the misalignment angles ϕ_i of (4.3); clearly the perturbed eigenvectors $\tilde{\mathbf{w}}_i$ and the perturbed misalignment angles $\tilde{\phi}_i$ being considered are those relating to the perturbed plant $\tilde{G}(s)$ (rather than the nominal plant $G(s)$) and to emphasize the distinction between nominal and perturbed quantities, tildes have been added.

Hereon, the primary interest will be in determining the maximum and minimum values that the perturbed misalignment angles $\tilde{\phi}_i$ attain over the structured class of uncertainty $\mathbf{D_s}$.

4.3.2 The stationary conditions

At any given frequency ω, let each (r,s) element of the perturbation Δ be represented as

$$\delta_{rs} = \rho_{rs}\exp(j\theta_{rs}) \qquad \text{for} \quad 0 \leq \rho_{rs} \leq p_{rs} \quad \text{and} \quad 0 \leq \theta_{rs} < 2\pi \tag{4.8}$$

where p_{rs} is the maximum modulus which δ_{rs} can assume. Clearly, the perturbed transfer function matrix $\tilde{G}$ as well as its eigenvalues $\tilde{g}_i$ and eigenvectors $\tilde{\mathbf{w}}_i$ will be functions of both the perturbation modulus ρ_{rs} and phase θ_{rs}. Furthermore, unless $\tilde{G}$ has a non-simple Jordan form (i.e. $\tilde{G}$ is not diagonalizable), both $\tilde{g}_i$ and $\tilde{\mathbf{w}}_i$ will both be differentiable with respect to ρ_{rs} and θ_{rs}. Non-simple Jordan forms are of no interest presently since these arise when two or more eigenvectors become parallel; this can only happen for $\tilde{\phi}_i > 45°$ (for some i) when the system under consideration is highly interactive and, as mentioned earlier, an exact measure of interaction is of no practical value in such a case. Thus, the derivative of the perturbed eigenvector $\tilde{\mathbf{w}}_i$ with respect to the perturbation element radius ρ_{rs} and the phase θ_{rs} can be assumed to be well defined and, hence, it is reasonable at this stage to look for the stationary conditions of the misalignment angles $\tilde{\phi}_i$ with a view to determining the maximum and minimum values over the set of $\Delta \in \mathbf{D_s}$.

For notational convenience $\tilde{g}_i$, $\tilde{\mathbf{w}}_i$, and $\mathbf{e}_i$ will be denoted by $\tilde{g}$, $\tilde{\mathbf{w}}$, and $\mathbf{e}$ respectively. Using this notation and under the assumption that the perturbed eigenvectors have been scaled such that:

$$\mathbf{e}^t\tilde{\mathbf{w}} = 1 \tag{4.9}$$

the perturbed misalignment angle definition reduces to:

$$\cos(\tilde{\phi}) = \frac{1}{\|\tilde{\mathbf{w}}\|} \tag{4.10}$$

This in turn implies that the maxima and minima of $\tilde{\phi}$ are given by the maxima and minima, respectively, of

$$\|\tilde{\mathbf{w}}\|^2 = \tilde{\mathbf{w}}^*\tilde{\mathbf{w}} \tag{4.11}$$

where $(\cdot)^*$ denotes transposition and complex conjugation. Letting $(\cdot)'$ denote differentiation with respect to x, where x can be either ρ_{rs} or θ_{rs}, then differentiation of the perturbed transfer function matrix $\tilde{G}$ may be written as:

$$\tilde{G}' = \exp(j\theta_{rs})\mathbf{e}_r\mathbf{e}_s{}^t \qquad \text{for} \quad x = \rho_{rs} \tag{4.12a}$$

$$\tilde{G}' = j\rho_{rs}\exp(j\theta_{rs})\mathbf{e}_r\mathbf{e}_s{}^t \qquad \text{for} \quad x = \theta_{rs} \tag{4.12b}$$

On the other hand, the perturbed eigenvector norm-squared derivative is given by:

$$\left(\|\tilde{\mathbf{w}}\|^2\right)' = 2\text{Real}\left\{\tilde{\mathbf{w}}^*\tilde{\mathbf{w}}'\right\} \tag{4.13}$$

so that in order to find the stationary points of the perturbed misalignment angle $\tilde{\phi}$, it is necessary to differentiate the perturbed eigenvector $\tilde{\mathbf{w}}$ with respect to x. This can be accomplished by differentiating the eigenvalue/eigenvector defining equation in order to obtain:

$$\tilde{G}'\tilde{\mathbf{w}} + \tilde{G}\tilde{\mathbf{w}}' = \tilde{g}'\tilde{\mathbf{w}} + \tilde{g}\tilde{\mathbf{w}}' \tag{4.14}$$

from which it follows that:

$$\tilde{V}_i\tilde{G}'\tilde{\mathbf{w}} + \tilde{V}_i\tilde{G}\tilde{\mathbf{w}}' = \tilde{g}'\tilde{V}_i\tilde{\mathbf{w}} + \tilde{g}\tilde{V}_i\tilde{\mathbf{w}}' \tag{4.15}$$

or

$$(\tilde{g}I - \tilde{\Lambda}_i)\tilde{V}_i\tilde{\mathbf{w}}' = \tilde{V}_i\tilde{G}'\tilde{\mathbf{w}} \tag{4.16}$$

where $\tilde{V}_i$ is the left-eigenvector matrix whose rows are the left eigenvectors $\tilde{\mathbf{v}}_j^t$ for all $j \neq i$, and where $\tilde{\Lambda}_i$ is the corresponding diagonal eigenvalue matrix formed from the eigenvalues $\tilde{g}_j$ for all $j \neq i$. In deriving the above, the following facts have been used:

$$\tilde{V}_i\tilde{G} = \tilde{\Lambda}_i\tilde{V}_i \qquad \text{and} \qquad \tilde{V}_i\tilde{\mathbf{w}} = 0 \tag{4.17}$$

Projection of the perturbed eigenvector derivative $\tilde{\mathbf{w}}'$ onto its eigenvector basis set yields:

$$\tilde{\mathbf{w}}' = \tilde{W}_i\boldsymbol{\alpha} + \beta\tilde{\mathbf{w}} \tag{4.18}$$

where $\tilde{W}_i$ is the right eigenvector matrix whose column vectors are the right eigenvectors $\tilde{\mathbf{w}}_j$ for all $j \neq i$ (taken in the same order as in $\tilde{V}_i$ and $\tilde{\Lambda}_i$), $\boldsymbol{\alpha}$ is a complex vector in C^{m-1} and β is a complex scalar in C. In order to solve for $\boldsymbol{\alpha}$, substitute (4.18) into (4.16) to obtain:

$$\boldsymbol{\alpha} = (\tilde{g}I - \tilde{\Lambda}_i)^{-1}\tilde{V}_i\tilde{G}'\tilde{\mathbf{w}} \tag{4.19}$$

from which:

$$\tilde{\mathbf{w}}' = M\tilde{G}'\tilde{\mathbf{w}} + \beta\tilde{\mathbf{w}} \qquad \text{with} \qquad M \triangleq \tilde{W}_i(\tilde{g}I - \tilde{\Lambda}_i)^{-1}\tilde{V}_i \tag{4.20}$$

In order to solve for β, observe that eigenvector scaling constraint (4.9) implies that:

$$\mathbf{e}^t\tilde{\mathbf{w}}' = 0 \tag{4.21}$$

and this, together with (4.20) (and constraint (4.9)) gives the desired final expression for the eigenvector derivative:

$$\tilde{\mathbf{w}}' = M\tilde{G}'\tilde{\mathbf{w}} - (\mathbf{e}^tM\tilde{G}'\tilde{\mathbf{w}})\tilde{\mathbf{w}} \tag{4.22}$$

This enables the following statement of the stationary conditions of the perturbed misalignment angle, $\tilde{\phi}$:

Theorem 4.1 (Misalignment angle stationary conditions)
Under the assumption that the spectral decomposition of $\tilde{G}$ has a simple Jordan form and with the definitions given above, the stationary conditions for the misalignment angle of perturbed eigenvector $\tilde{\mathbf{w}}$ and its corresponding standard basis vector $\mathbf{e}$ are given as:

$$\text{Real}\left\{\exp(j\theta_{rs})\left[\tilde{\mathbf{w}}^*M\mathbf{e}_r\mathbf{e}_s{}^t\tilde{\mathbf{w}} - (\mathbf{e}^tM\mathbf{e}_r\mathbf{e}_s{}^t\tilde{\mathbf{w}})\tilde{\mathbf{w}}^*\tilde{\mathbf{w}}\right]\right\} = 0 \quad \text{wrt} \quad \rho_{rs} \tag{4.23a}$$

$$\text{Real}\left\{j\exp(j\theta_{rs})\left[\tilde{\mathbf{w}}^*M\mathbf{e}_r\mathbf{e}_s{}^t\tilde{\mathbf{w}} - (\mathbf{e}^tM\mathbf{e}_r\mathbf{e}_s{}^t\tilde{\mathbf{w}})\tilde{\mathbf{w}}^*\tilde{\mathbf{w}}\right]\right\} = 0 \quad \text{wrt} \quad \theta_{rs} \tag{4.23b}$$

Proof: This follows directly from (4.12a), (4.12b), (4.13), and (4.22) when the derivatives of the perturbed eigenvector norm-squared $\|\tilde{\mathbf{w}}\|^2$ with respect to ρ_{rs} and θ_{rs} are set equal to zero. ■

Corollary 4.1 (Worst case perturbation on the boundary of the class $\mathbf{D_s}$) *The maximum perturbed misalignment angle $\tilde{\phi}$ over $\Delta \in \mathbf{D_s}$ does not occur at a stationary point and is hence achieved on the boundary of the structured uncertainty class $\mathbf{D_s}$.*

Proof: Perturbed misalignment angle maxima over the class of perturbations $\Delta \in \mathbf{D_s}$ must concurrently satisfy both (4.23a) and (4.23b) and thus must satisfy:

$$[\tilde{\mathbf{w}}^* M \mathbf{e}_r \mathbf{e}_s{}^t \tilde{\mathbf{w}} - (\mathbf{e}^t M \mathbf{e}_r \mathbf{e}_s{}^t \tilde{\mathbf{w}}) \tilde{\mathbf{w}}^* \tilde{\mathbf{w}}] = 0 \tag{4.24}$$

for all r and s, namely:

$$\tilde{\mathbf{w}}^* M - \mathbf{e}^t M \tilde{\mathbf{w}}^* \tilde{\mathbf{w}} = \mathbf{0}^t \tag{4.25}$$

In the above, the obvious assumption that $\mathbf{e}_s{}^t \tilde{\mathbf{w}} \neq 0$ for at least one s has been made. Now, given the structure of M as defined by (4.20) this last condition implies:

$$\tilde{\mathbf{w}}^* - \tilde{\mathbf{w}}^* \tilde{\mathbf{w}} \mathbf{e}^t = \sigma \tilde{\mathbf{v}}^t \tag{4.26}$$

where σ is some complex constant. Post-multiplication of (4.26) by $\tilde{\mathbf{w}}$ and use of the duality condition $\tilde{\mathbf{v}}^t \tilde{\mathbf{w}} = 1$ together with the eigenvector scaling constraint of (4.9) imply that either of the following must hold:

$$\sigma = 0 \quad \text{or} \quad \tilde{\mathbf{w}} = \mathbf{e} \tag{4.27}$$

which can only arise when $\tilde{\phi} = 0$, and this clearly cannot be a maximum. ■

An obvious consequence of this proof is the following corollary:

Corollary 4.2 (Misalignment angle extrema on the boundary of $\mathbf{D_s}$) *If the misalignment angle is nonzero (i.e. $\tilde{\phi} > 0$) for all possible perturbations in the class $\Delta \in \mathbf{D_s}$ then both the maximum and minimum values of the misalignment angle $\tilde{\phi}$ will be attained on the boundary of the uncertainty class $\mathbf{D_s}$.*

4.3.3 The structure of the worst case perturbation Δ_{wc}

The degrees of freedom available in the representation of the structured uncertainty $\Delta \in \mathbf{D_s}$ defined by (4.8) are far too many to permit an efficient application of a maximization algorithm, even for the simple 2×2 case. Clearly, additional information concerning the structure of the worst case perturbation Δ_{wc} would be very useful. As a first step in this direction consider the following re-statement of Corollary 4.1:

Lemma 4.1 (Characterization of the worst case perturbation moduli)
The worst case perturbation $\Delta \in \mathbf{D_s}$ which maximizes the eigenvector misalignment angle $\tilde{\phi}$ is comprised of elements which assume their maximum modulus:

$$\delta_{rs} = p_{rs} \exp(j\theta_{rs}) \quad \forall \ r,s \quad \text{and} \quad 0 \leq \theta_{rs} < 2\pi \tag{4.28}$$

where p_{rs} are the upper bounds defining the uncertainty class $\mathbf{D_s}$ (as per (4.7)).

Proof: The perturbation Δ of the lemma simply gives a characterization of all elements on the boundary of the uncertainty class $\mathbf{D_s}$. ■

With each perturbation element modulus ρ_{rs} being replaced by its upper bound p_{rs}, the only remaining degrees of freedom in the worst case perturbation characterization are the element-by-element phase angles θ_{rs}. But even so, the number of variables involved is still too large (e.g. four angles even for the simple 2×2 case) to enable the development of a practicable maximization algorithm. With this objective in mind, the following result reduces the number of angles which must be scanned by giving a simplified characterization of the worst (best) case perturbation Δ which maximizes (minimizes) the eigenvector misalignment angle.

Lemma 4.2 (Phase conditions for the worst case and best case perturbation)
Let φ_r and ψ_s be defined as

$$\varphi_r = \text{phase} \left\{ \left(\tilde{\mathbf{w}}^* - \tilde{\mathbf{w}}^* \tilde{\mathbf{w}} \mathbf{e}^t \right) M \mathbf{e}_r \right\} \qquad \psi_s = \text{phase} \left\{ \mathbf{e}_s^t \tilde{\mathbf{w}} \right\} \tag{4.29}$$

then the stationary condition with respect to the structured perturbation of Lemma 4.1 is:

$$\theta_{rs} + \varphi_r + \psi_s = \tau_{rs}\pi \tag{4.30}$$

with τ_{rs} being either 0 or 1.

Proof: Of the two stationary conditions of Theorem 4.1 only (4.23b) applies on the boundary of the structured uncertainty class $\mathbf{D_s}$ and with the definitions of the lemma this condition becomes:

$$\text{Real}\{j\exp(j\theta_{rs})\mu_r\exp(j\varphi_r)\sigma_s\exp(j\psi_s)\} = 0 \tag{4.31}$$

where μ_r and σ_s denote the magnitudes corresponding to the phase arguments of (4.29). Since (4.31) is a direct consequence of (4.23b), the result of the lemma holds. ■

Theorem 4.2 (Structure of the worst case and best case perturbation) *The worst case perturbation Δ_{wc} for which the misalignment angle $\tilde{\phi}$ attains a maximum over the structured uncertainty class $\mathbf{D_s}$ is characterized by Lemma 4.1 with $\tau_{rs} = 0$ and has the following general structure:*

$$\Delta_{wc} = \Phi P \Psi \tag{4.32}$$

where Φ and Ψ are diagonal phase matrices defined by:

$$\Phi = \text{diag}\{\exp(-j\varphi_r)\} \qquad \text{and} \qquad \Psi = \text{diag}\{\exp(-j\psi_s)\} \tag{4.33}$$

Additionally, the diagonal phase elements φ_r and ψ_s are defined by (4.29) and P is the boundary matrix comprised of the nonnegative element bounds p_{rs} which define the structured uncertainty class $\mathbf{D_s}$. Furthermore, for a nonzero misalignment angle $\tilde{\phi} > 0$ over all possible perturbations in the class $\mathbf{D_s}$, the best case perturbation Δ_{bc} for which the misalignment angle $\tilde{\phi}$ attains a minimum will have the structure of (4.32) with the sign reversed:

$$\Delta_{bc} = -\Delta_{wc} \tag{4.34}$$

Proof: For a fixed nonzero perturbation modulus ρ_{rs}, the maximizing (i.e. worst case) perturbation phase θ_{rs} is defined by the following stationary condition:

$$\frac{\partial\tilde{\phi}}{\partial\theta_{rs}} = 0 \tag{4.35}$$

where it is assumed for the moment that the perturbation elements δ_{ij} are fixed for all $i \neq r$ and $j \neq s$. Equation (4.35) implies a functional dependence of the maximizing perturbation phase θ_{rs} on the perturbation modulus ρ_{rs} which may be expressed as:

$$\theta_{rs} = f_{rs}(\rho_{rs}) \tag{4.36}$$

and so the function f_{rs} defines the locus of misalignment angle maxima as the perturbation element modulus ρ_{rs} varies. Now clearly the maximum misalignment angle $\tilde{\phi}$ defined by (4.35) will be monotonically increasing as the perturbation element modulus ρ_{rs} increases, and so the slope of the misalignment angle $\tilde{\phi}$ versus the perturbation element modulus ρ_{rs} is positive:

$$\frac{d\tilde{\phi}}{d\rho_{rs}}\Big|_{\theta_{rs}=f_{rs}(\rho_{rs})} > 0 \tag{4.37}$$

In general, the derivative of the misalignment angle $\tilde{\phi}$ with respect to the perturbation element modulus ρ_{rs} is given by:

$$\frac{d\tilde{\phi}}{d\rho_{rs}} = \frac{\partial\tilde{\phi}}{\partial\rho_{rs}} + \frac{\partial\tilde{\phi}}{\partial\theta_{rs}}\frac{d\theta_{rs}}{d\rho_{rs}} \tag{4.38}$$

and this, on the locus of the misalignment angle maxima, by (4.35) becomes:

$$\frac{d\tilde{\phi}}{d\rho_{rs}} = \frac{\partial\tilde{\phi}}{\partial\rho_{rs}} \tag{4.39}$$

However, by the positive slope condition given by (4.37), (4.39) further implies that at the misalignment angle maximum, the partial derivative of the misalignment angle $\tilde{\phi}$ with respect to the perturbation element modulus ρ_{rs} is given by:

$$\frac{\partial\tilde{\phi}}{\partial\rho_{rs}} > 0 \tag{4.40}$$

Using this partial derivative condition in conjunction with (4.23a) yields:

$$\text{Real}\left\{\exp(j\theta_{rs})\left[\tilde{\mathbf{w}}^{*}M\mathbf{e}_{r}\mathbf{e}_{s}^{t}\tilde{\mathbf{w}} - (\mathbf{e}^{t}M\mathbf{e}_{r}\mathbf{e}_{s}^{t}\tilde{\mathbf{w}})\tilde{\mathbf{w}}^{*}\tilde{\mathbf{w}}\right]\right\} > 0$$

which, with the notation of Lemma 4.2, reduces to

$$\text{Real}\{\exp(j\theta_{rs})\mu_r \exp(j\varphi_r)\sigma_s \exp(j\psi_s)\} > 0 \tag{4.41}$$

This taken together with (4.30) gives the worst case perturbation structure given in (4.32). The proof of the best case perturbation structure is similar and therefore omitted. ■

4.3.4 Numerical solution and illustrative example

Algorithms

Theorem 4.2 gives a complete description of the worst case perturbation and thus could form the basis of a numerical algorithm for the determination of the maximum misalignment angle $\tilde{\phi}$ over the structured uncertainty class $\mathbf{D_s}$. It must be pointed out however that the set of equations to be solved, namely (4.30) with $\tau_{rs} = 0$, is both non-linear and implicitly so because of the dependence of φ_r and ψ_s on θ_{ij}. Clearly therefore, a closed-form solution is not available and a numerical algorithm (say a Newton-Raphson type of algorithm) can be deployed. Alternatively on account of the explicit knowledge of the derivatives of $\tilde{\phi}$ with respect to θ_{rs}, the problem of maximizing the misalignment angle $\tilde{\phi}$ could be solved by any of the efficient gradient methods (say the conjugate gradient optimization method [Golub and Van Loan, 1983]). Of course on account of the $(m-1)^2$ constraints implied by (4.30) the number of variables involved in the maximization is not m^2 (the number of elements in Δ) but rather $m^2 - (m-1)^2 = 2m-1$. In order to see this rewrite (4.30) in vector form as:

$$\theta_2 = L\theta_1 \tag{4.42}$$

where θ_1 contains $2m-1$ and θ_2 contains the remaining $(m-1)^2$ of the phases of elements of Δ; L is an $(m-1)^2 \times (2m-1)$ matrix whose elements are 0, or 1 or -1. Clearly, the misalignment angle $\tilde{\phi}$ need be maximized only over θ_1 and the relevant vector of derivatives will be given by:

$$\nabla(\tilde{\phi}) = \nabla_{\theta_1}(\tilde{\phi}) + L\nabla_{\theta_2}(\tilde{\phi}) \tag{4.43}$$

where $\nabla_{\theta_1}(\cdot)$ and $\nabla_{\theta_2}(\cdot)$ denote partial differentiation with respect to the elements of θ_1 and θ_2 respectively.

The 2×2 case

By way of illustration consider next the 2×2 case for which (4.30) assumes a particularly simple form.

Theorem 4.3 (Worst case perturbation for the 2×2 case)
For the 2×2 case the angles φ_r and ψ_s of Lemma 4.2 assume the form:

$$\varphi_1 = -\alpha - \pi; \quad \varphi_2 = -\alpha - \beta; \quad \psi_1 = 0; \quad \psi_2 = \beta \tag{4.44}$$

where

$$\alpha = \text{phase}\ \{\tilde{g}_1 - \tilde{g}_2\}; \qquad \beta = \text{phase}\ \left\{\mathbf{e}_2^t \tilde{\mathbf{w}}\right\} \tag{4.45}$$

and hence the worst case perturbation assumes the form:

$$\Delta_{wc} = \exp(j\alpha) \begin{pmatrix} -p_{11} & -p_{12}\exp(-j\beta) \\ p_{21}\exp(j\beta) & p_{22} \end{pmatrix} \tag{4.46}$$

Proof: This follows by expressing the elements of the vectors $(\tilde{\mathbf{w}}^* - \tilde{\mathbf{w}}^*\tilde{\mathbf{w}}\mathbf{e}^t)M\mathbf{e}_r$ and $\mathbf{e}_s{}^t\tilde{\mathbf{w}}$ of Lemma 4.2 in terms of the eigenvalues and eigenvectors of $\tilde{G}$ which, for the 2×2 case, can be derived explicitly in terms of the elements of $\tilde{G}$. ■

It is interesting to note that Δ_{wc} above has been characterized in terms of only two angles which is one less than the $2m - 1 = 3$ degrees of freedom that would have been predicted from the discussion above. The reason for this is that the phases φ_r and ψ_s are constrained by the relationship:

$$(\tilde{\mathbf{w}}^* - \tilde{\mathbf{w}}^*\tilde{\mathbf{w}}\mathbf{e}^t)M\tilde{\mathbf{w}} = 0 \tag{4.47}$$

which for the 2×2 case implies that

$$\varphi_1 + \psi_1 = \varphi_2 + \psi_2 - \pi \tag{4.48}$$

[In the general $m \times m$ case the phase constraint given by (4.47) does not lead to a simple equation for φ_r and ψ_s and has thus been ignored]. Now to obtain numerical solutions one could solve the simple but nevertheless non-linear equations given in (4.44) and (4.45), or alternatively one could use a conjugate gradient algorithm based on the derivatives of $\tilde{\phi}$, which for the special structure of Δ_{wc} given in (4.46) reduces to:

$$\frac{d\tilde{\phi}}{d\alpha} = \frac{2}{\|\tilde{\mathbf{w}}\|^2\sqrt{\|\tilde{\mathbf{w}}\|^4 - 4}}\text{Imag}\left\{\tilde{\mathbf{w}}^* M\Delta_{wc}\tilde{\mathbf{w}} - \mathbf{e}^t M\Delta_{wc}\tilde{\mathbf{w}}\tilde{\mathbf{w}}^*\tilde{\mathbf{w}}\right\}$$

$$\frac{d\tilde{\phi}}{d\beta} = \frac{2}{\|\tilde{\mathbf{w}}\|^2\sqrt{\|\tilde{\mathbf{w}}\|^4 - 4}}\text{Imag}\left\{\tilde{\mathbf{w}}^* M\Delta_{o}\tilde{\mathbf{w}} - \mathbf{e}^t M\Delta_{o}\tilde{\mathbf{w}}\tilde{\mathbf{w}}^*\tilde{\mathbf{w}}\right\}$$

where

$$\Delta_o = \exp(j\alpha)\begin{pmatrix} 0 & p_{12}\exp(-j\beta) \\ p_{21}\exp(j\beta) & 0 \end{pmatrix} \tag{4.49}$$

Alternatively, due to the very small number of degrees of freedom, namely 2, an exhaustive search type of algorithm is perfectly feasible and this is the method chosen in the illustrative example below.

A numerical example

Consider a system transfer function matrix which at a specific frequency is given by:

$$G = \begin{pmatrix} 4.00 + j6.41 & -1.62 - j1.35 \\ 0.923 + j2.83 & -2.90 + j5.28 \end{pmatrix}$$

with corresponding spectral decomposition:

$$G = W\Lambda V =$$

$$\begin{pmatrix} 1 & 0.23+j0.18 \\ 0.14+j0.39 & 1 \end{pmatrix}\begin{pmatrix} 4.3-j5.6 & 0 \\ 0 & -3.2+j6.2 \end{pmatrix}\begin{pmatrix} 0.95+j0.11 & -0.20-j0.19 \\ -0.09-j0.39 & 0.95+j0.11 \end{pmatrix}$$

Direct calculation of the nominal misalignment angles yields:

$$\phi_1 = \cos^{-1}\left(\frac{1}{\sqrt{1 + |0.14 + j0.39|^2}}\right) = 22.5° \tag{4.50}$$

$$\phi_2 = \cos^{-1}\left(\frac{1}{\sqrt{1 + |0.23 + j0.18|^2}}\right) = 16.3° \tag{4.51}$$

Given an additive structured perturbation $\Delta \in \mathbf{D_s}$ whose corresponding elements are bounded in modulus by:

$$|\Delta| \leq \begin{pmatrix} 0.483 & 1.100 \\ 1.840 & 0.881 \end{pmatrix} \tag{4.52}$$

it is of interest to examine the corresponding impact on the misalignment angles of the system. Equation (4.46) gives the phase constraints which yields the maximum misalignment angle. Scanning over the possible values of α and β yields the worst case perturbation Δ_{wc} (corresponding to the first misalignment angle) as:

$$\Delta_{wc} = \begin{pmatrix} -0.452 + j0.170 & -0.177 + j1.09 \\ 1.40 + j1.20 & 0.827 - j0.304 \end{pmatrix} = e^{-j20.2} \begin{pmatrix} -0.483 & -1.10e^{-j60.8} \\ 1.84e^{j60.8} & 0.881 \end{pmatrix}$$

This was produced with $\alpha = -20.2°$ and $\beta = 60.8°$. The misalignment angles resulting from this perturbation are:

$$\tilde{\phi}_1 = 42.8° \qquad \tilde{\phi}_2 = 16.28° \tag{4.53}$$

Comparison of (4.50) and (4.51) with (4.53) demonstrates how the phase orientations of the worst case perturbation dramatically increase the misalignment angle under consideration.

4.4 The overall assessment of perturbed interaction

To complete the assessment of interaction, it is necessary to evaluate how the uncertainty affects the eigenvalue moduli $|g_i|$, the partial condition number $\mathcal{K}_i(W)$, and the interaction bound U_2. Each of these are considered in turn below.

4.4.1 Uncertainty and the modulus condition $|g_i|$

Eigenvalues are notorious for their sensitivity to perturbations and, as a result, the plots of the nominal eigenvalue moduli $|g_i|$ may not convey accurate information. This problem can be overcome by employing the E-Contour method (c.f. Section 2.2.3) since E-Contours define tight perturbed eigenvalue inclusion regions and

hence, provide a convenient means of determining non-conservative upper and lower bounds for the moduli of the perturbed eigenvalues $|\tilde{g}_i|$. Thus, this information can be superimposed on the plots of the moduli of the nominal eigenvalues $|g_i|$ to assess the effects of uncertainty on the eigenvalue modulus condition.

4.4.2 Uncertainty and the partial condition number $\mathcal{K}_i(W)$

Once again it is of interest to establish upper and lower bounds on the partial condition number $\mathcal{K}_i(\tilde{W})$ with the intention of superimposing these on the nominal plots of $\mathcal{K}_i(W)$. As was the case with the misalignment angles, the maximum of $\mathcal{K}_i(\tilde{W})$ does not occur at a stationary point and hence it is achieved on the boundary of the perturbation class. This assertion can be explained by the ensuing simple arguments. The values of $\mathcal{K}_i(\tilde{W})$ range from 1 (when the set $\tilde{\mathbf{w}}_j \; \forall \; j \neq i$, is orthonormal) to ∞, (when two or more eigenvectors, $\tilde{\mathbf{w}}_j, \tilde{\mathbf{w}}_k$ for $j, k \neq i$, become parallel). Now by assumption, the eigenvalues $\tilde{g}_i$ and hence the eigenvectors $\tilde{\mathbf{w}}_i$ are analytic functions of the elements of the perturbation Δ; the possibility of the eigenvalues $\tilde{g}_i$ becoming repeated and non-simple has been precluded. Hence $\tilde{\mathbf{w}}_j^* \tilde{\mathbf{w}}_k$, viewed as a function of δ_{rs}, a single element of Δ, is analytic over the disc defined by $|\delta_{rs}| \leq p_{rs}$, and so attains both its maximum and minimum modulus on the boundary, namely the circle $|\delta_{rs}| = p_{rs}$. However the modulus of $\tilde{\mathbf{w}}_j^* \tilde{\mathbf{w}}_k$ is precisely equal to the cosine of the angle between $\tilde{\mathbf{w}}_j$ and $\tilde{\mathbf{w}}_k$, and so $\mathcal{K}_i(\tilde{W})$ attains its maximum and minimum values on the boundary of δ_{rs}, and hence on the boundary of the uncertainty class $\mathbf{D_s}$. The problem of determining the maximum and minimum of $\mathcal{K}_i(\tilde{W})$ over $\mathbf{D_s}$ therefore reduces to an optimization problem over the perturbation angles θ_{rs}; as with the algorithm for the worst (and best) case misalignment angles, here also it is easy to compute the gradient of $\mathcal{K}_i(\tilde{W})$ with respect to the θ_{rs} and so it is possible to implement an efficient steepest descent algorithm; however, the detailed procedure will not be given here. It is pointed out that for the 2×2 case, $\mathcal{K}_i(\tilde{W})$ reduces to $\|V_i\|$ for $j \neq i$ and, in parallel with the misalignment angle analysis of Section 4.3.4, it is possible to determine the structure of the worst (and best) case perturbation.

4.4.3 Uncertainty and the bound U_2

The plots of the misalignment angles, together with the eigenvalue moduli and partial condition number plots convey all the necessary information for a graphical assessment of interaction. However if one were interested in a strictly quantitative assessment, then worst- and best-case upper bounds on U_2 could be sought. By definition $U_2 = \mathcal{K}_i(\tilde{W}) \max_j |\tilde{t}_i - \tilde{t}_j| \sin(\tilde{\phi}_i)$ [c.f. (4.5)], and so far it has been established that algorithms can be generated to quantify the dependence of both the partial condition number $\mathcal{K}_i(\tilde{W})$ and the misalignment angle $\tilde{\phi}_i$ (and hence $\sin(\tilde{\phi}_i)$) on the perturbation Δ. All that is needed is a corresponding algorithm to find the largest distance between any two closed-loop eigenvalues, i.e. $\max_j |\tilde{t}_i - \tilde{t}_j|$. But, providing that the E-Contours (and the eigenvalue regions defined by them) avoid the point $-1+j0$ (a necessary condition for stability), then $\max_j |\tilde{t}_i - \tilde{t}_j|$ also attains its maximum and minimum on the boundary of the uncertainty class $\mathbf{D_s}$. This follows from two simple points: i) viewing the eigenvalues $\tilde{g}_i$ as a mapping from the uncertainty class $\mathbf{D_s}$ to the complex plane it is the case that boundary points of the eigenvalue regions have unique pre-images in $\mathbf{D_s}$ [Kouvaritakis and Latchman, 1985]; ii) under the assumption that the perturbed eigenvalue regions avoid the point $(-1+j0)$, the map of the E-Contours under the closed-loop eigenvalue transformation $\tilde{t}_i = \tilde{g}_i/(1+\tilde{g}_i)$ form simple closed curves and define bounded regions which contain all possible values for the closed-loop eigenvalues $\tilde{t}_i$. The computation of a worst- and best-case bound on $\max_j |\tilde{t}_i - \tilde{t}_j|$, therefore, follows trivially from the construction of the E-Contours; E-Contours of course are a prerequisite for the assessment of closed-loop stability in the presence of uncertainty.

4.4.4 The overall assessment

For well conditioned eigenvectors (i.e. low $\mathcal{K}_i(\tilde{W})$) the moduli plots of Section 4.4.1 together with the misalignment angle plots of Section 4.3 give a convenient means of assessing (qualitatively) closed-loop interaction in terms of simple open-loop geometric properties. Thus for example, if at a particular frequency, the eigenvalue

moduli, the partial condition number, and the misalignment angles obey the bounds $|\tilde{g}_i| > 10$, $\mathcal{K}_i(\tilde{W}) < 2$ and $\tilde{\phi}_i < 20°$, then the overall bound on interaction will be small (of the order of 0.1 or less) and the closed-loop system can be predicted to be largely non-interactive at that frequency. Conversely, if the misalignment angles are large (say 40°) and the eigenvalue moduli $\tilde{g}_i$ are not large (say $|\tilde{g}_i| \approx 2$) then (providing that pairwise the eigenvalues $\tilde{g}_i$ are not nearly equal) significant closed-loop interaction will be expected; even for the best partial condition number $\mathcal{K}_i(\tilde{W}) = 1$, the bound of interaction could be as large as 0.86. The strength of this assessment is that it relates (by simple graphical means) closed-loop interaction to simple open-loop geometric properties. Should a more quantitative assessment be needed then the bound on U_2 proposed in Section 4.4.3 could be plotted. The calculation here is still based on open-loop quantities with the exception of the term $\max_j |\tilde{t}_i - \tilde{t}_j|$; however due to the diagonal nature of the eigenvalue matrix of $\tilde{G}$, the relationship between $\tilde{t}_i$ and $\tilde{g}_i$ is no more complicated than the corresponding relationship between the open- and closed-loop transfer functions of scalar systems.

4.4.5 Chemical reactor study

Consider an open-loop unstable chemical reactor with transfer function matrix:

$$G = \frac{3}{s^4 + 11.67s^3 + 15.75s^2 - 88.31s + 5.514} \cdot \begin{pmatrix} 6.292s^3 + 65.34s^2 + 179.66s + 63.62 & 29.2s + 263.3 \\ -18.86s - 30.30 & 5.679s^3 + 42.67s^2 - 68.84s - 106.8 \end{pmatrix} \tag{4.54}$$

and additive perturbation, Δ, with modulus, $|\Delta|$, given by:

$$|\Delta| \leq \begin{pmatrix} \left|\frac{17.82}{s^2+6.36s+20.25}\right| & \left|\frac{5.39}{s^2+4.95s+12.25}\right| \\ \left|\frac{5.39}{s^2+4.95s+12.25}\right| & \left|\frac{17.82}{s^2+6.36s+20.25}\right| \end{pmatrix}$$

It is noted that the transfer function matrix of (4.54) (and the corresponding perturbation bounds) have incorporated in them a high frequency pre-compensator the details of which can be found in [MacFarlane and Kouvaritakis, 1977].

The effect of the perturbation Δ on the relevant frequency plots are shown in Fig. 4.2. In particular, Figs. 4.2(a) and 4.2(b) depict the uncertainty in the moduli of the first and second characteristic loci, namely the loci that correspond to the eigenvectors which best align with $\mathbf{e}_1$ and $\mathbf{e}_2$, respectively. The solid lines of the figure correspond to the nominal plots whereas the dashed and dotted lines correspond to the maximum and minimum values of the eigenvalue moduli, respectively. The information concerning these maximum and minimum values is readily available from the E-Contour plots shown in Fig. 4.2(f). Furthermore, this figure indicates that the perturbed eigen-loci will give a net sum of two anticlockwise encirclements of the critical point; this being precisely the requirement for the stability of the perturbed closed-loop system. As pointed out previously, for a full assessment of interaction it is necessary to compute the effects of the perturbation Δ on both the misalignment angles and the partial eigenvector condition numbers. The misalignment angle plots were obtained using the algorithm of Section 4.3.4 and are shown in Figs. 4.2(c) and 4.2(d). The worst and best case misalignment angles are depicted by the dashed and dotted lines, respectively. These plots are supplemented by the condition number information which is plotted in Fig. 4.2(e); this plot was obtained via the algorithm discussed in Section 4.4.2 and the dashed line here portrays the worst case condition number behaviour. It is pointed out that in the 2×2 case, $\mathcal{K}_1(\tilde{W}) = \mathcal{K}_2(\tilde{W}) = 1/|\det(\tilde{W})|$; therefore, only one plot is needed for both loops.

Fig. 4.2 shows clearly that the effect of uncertainty is significant and cannot be ignored when assessing closed-loop interaction. In particular, the poor conditioning of the model at low frequencies (the nominal value for $\mathcal{K}_1(W) = \mathcal{K}_2(W)$ at 0.01 rad./sec. is about 5) results in large eigenvalue variations as shown by the E-Contours of Fig. 4.2(f) as well as the modulus plots of Figs. 4.2(a) and 4.2(b). Poor conditioning is also reflected in large variations of the condition number itself. It is interesting to note that the eigenvector variations reflected by the partial condition number values do not have a significant impact on the low frequency misalignment angles; this appears to be a paradox, but is perfectly possible given the complex na-

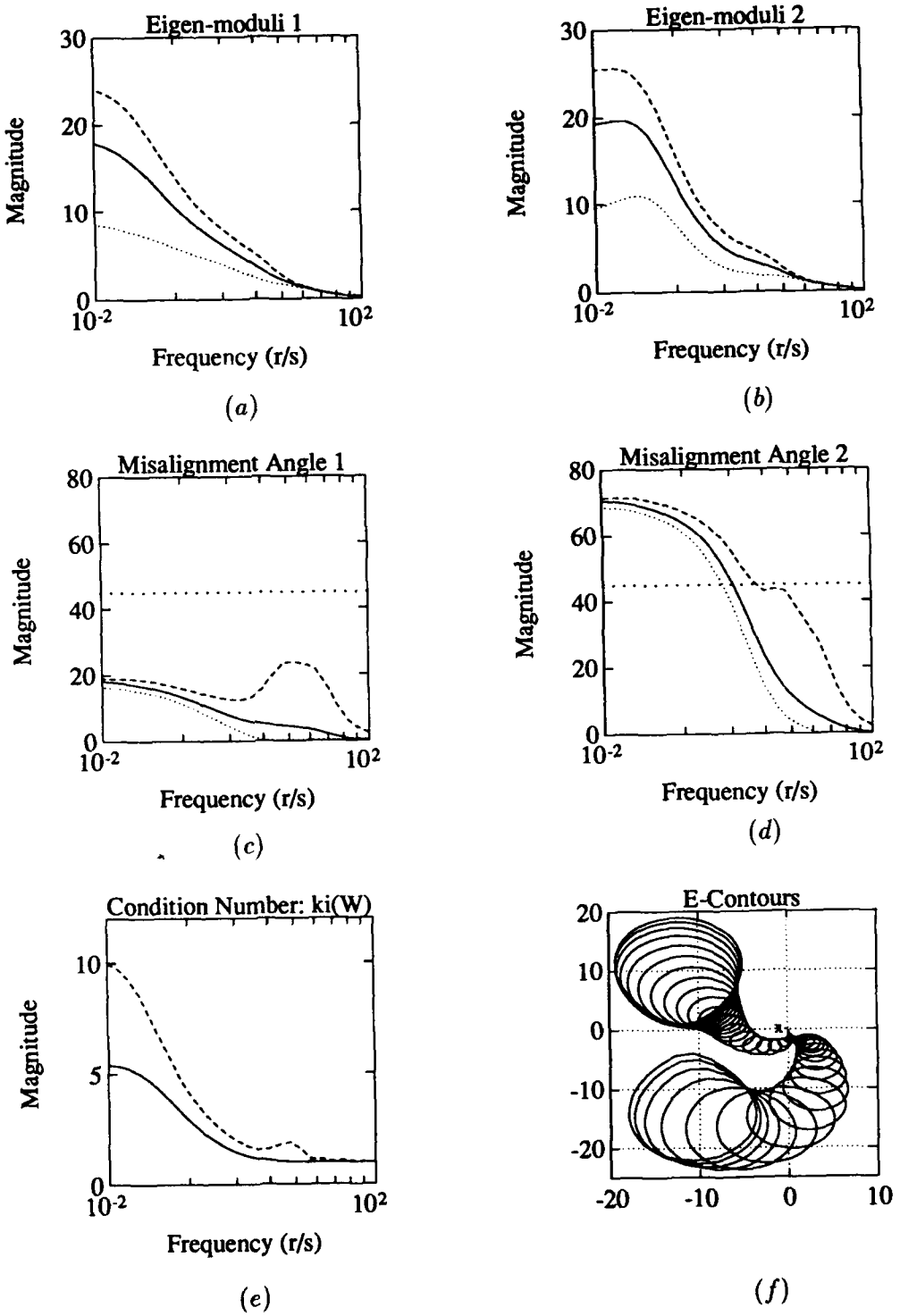

Figure 4.2: Perturbed chemical reactor study: Plots (a) and (b) depict the magnitude of the characteristic loci. Plots (c) and (d) depict the misalignment angles. Plot (e) shows the partial condition number while plot (f) shows the perturbed characteristic loci bands. Maximum: (dashed) Nominal: (solid) Minimum: (dotted)

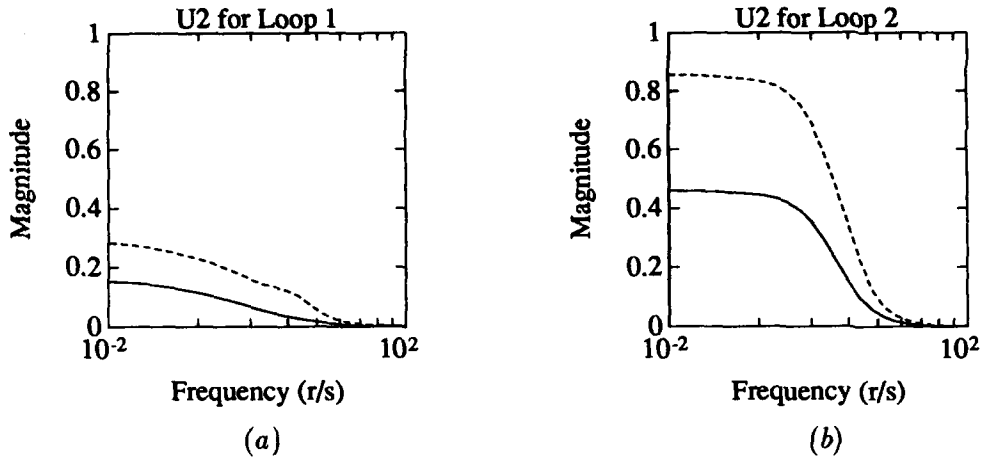

Figure 4.3: Perturbed chemical reactor study: Plots (a) and (b) depict interaction bound U_2 for loops 1 and 2 respectively. Perturbed Maximum: (dashed) Nominal: (solid)

ture of $\tilde{\mathbf{w}}_1$ and $\tilde{\mathbf{w}}_2$ at the frequencies concerned. Conversely at high frequencies, say at about 10 rad./sec. the nominal model is well conditioned ($\mathcal{K}_1(W) = \mathcal{K}_2(W) \approx 1$) and thus the eigenvalues are not sensitive (the variations of $\tilde{g}_i$, as shown in Fig. 4.2(f), and of their moduli, as shown in Figs. 4.2(a) and 4.2(b), are comparable to the size of the perturbation class); however the eigenvalue insensitivity does not guarantee eigenvector insensitivity as indeed is demonstrated by the variations in both the condition number and the misalignment angles.

The overall assessment one can derive from an inspection of Fig. 4.2 is as follows. A significant amount of interaction is expected in loop 2 both at low frequencies (say $\omega < 0.1$ rad./sec.) and intermediate frequencies ($0.1 < \omega < 5$ rad./sec.); for example at $\omega = 0.01$, since both $|\tilde{g}_1|$ and $|\tilde{g}_2|$ are at least about 10, $|\tilde{t}_1 - \tilde{t}_2|$ will be of the order of 0.1, while the worst case condition number is 10, hence the bound on interaction will be given by the sine of the worst case misalignment angle $\tilde{\phi}_2$ which (sine) is of the order of 1. On the other hand loop 1 is expected to be considerably less interactive over all frequencies; for example at $\omega = 0.01$, using similar arguments to the one presented above, a rough estimate of the bound on the interaction present in loop 1 is given by the sine of the worst case misalignment angle $\tilde{\phi}_1$ which (sine) is of the order of 0.3. These predictions are indeed borne out by the plots of

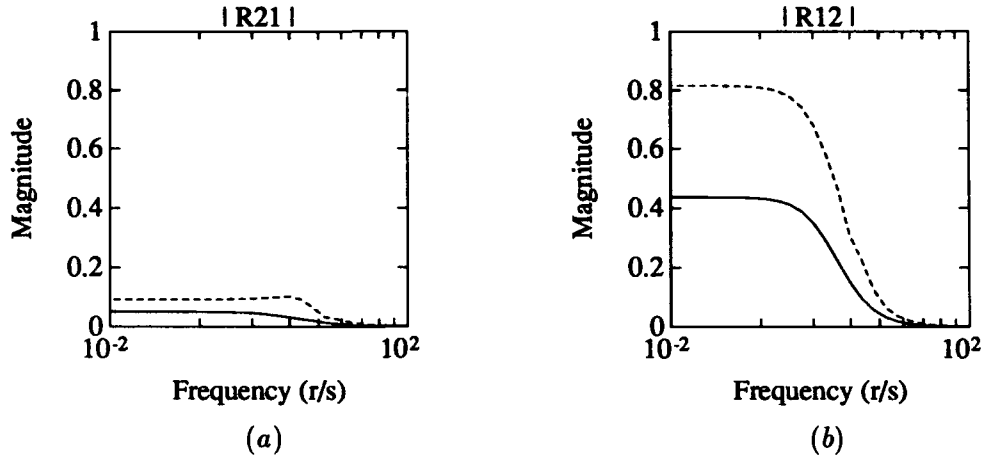

Figure 4.4: Perturbed chemical reactor study: Plots (a) and (b) depict the magnitude of the off-diagonal elements of closed-loop transfer function matrix, R. Perturbed Maximum: (dashed) Nominal: (solid)

Figs. 4.3(a) and 4.3(b) which depict the variations with frequency of the interaction bound U_2 for loops 1 and 2 respectively; once again the solid line refers to nominal values whereas the dashed line shows the worst case bound. The validity of this assessment of closed-loop interaction can be checked against the plots of Figs. 4.4(a) and 4.4(b) which show the actual amount of closed-loop interaction as measured by the size of the off-diagonal elements of the closed-loop transfer function matrix for the perturbed open-loop model; the worst case values for this figure (shown by the dashed line) were obtain by an exhaustive search algorithm which, even for this 2×2 case, required a considerable amount of computational effort. A comparison of Figs. 4.3 and 4.4 shows that the graphical/geometric assessment gave realistic bounds on interaction. In particular, at low frequencies the bound of interaction for loop 1 was somewhat conservative but over intermediate and high frequencies for loop 1 and over all frequencies for loop 2 the bounds were particularly tight. Furthermore due to its geometric nature, the approach allows one to trace the causes of interaction to simple open-loop properties such as the orientation of eigenvectors with respect to the standard basis vectors and to one another as well as to the modulus of the open-loop characteristic gains.

4.5 Summary

The uncertainty associated with the nominal models of multivariable systems can have significant effects on aspects of feedback behaviour such as stability, relative stability, accuracy of tracking etc. as discussed in a plethora of papers published over the last two decades. Uncertainty can also affect the interactive properties of a feedback configuration, and the examination of this problem formed the main aim of this chapter. The worst case uncertainty was characterized and this characterization subsequently facilitated the determination of the worst case eigenvector misalignment. When using the perturbed misalignment angle information in conjunction with the information about the perturbed eigenvalue moduli and the perturbed partial condition numbers, it is possible to use open-loop data to assess the worst case closed-loop interaction. The theory developed also applies to the best case perturbation, and so one can deduce upper and lower bounds on closed-loop interaction. The suitability and strength of this approach was demonstrated by way of a numerical study carried out on the model of open-loop unstable chemical reactor.

Part II

Robust design from the H^∞ perspective: super-optimization and relative stability margin maximization

Chapter 5

An overview of H^∞ optimal techniques

The previous portion of the thesis dealing with interaction and uncertainty was best viewed from the characteristic locus framework since the associated geometry of the system eigenframe enabled the use of simple open-loop quantities to analyze closed-loop interaction. Indeed the preceding work on interaction in conjunction with the E-Contour method completes the development of the characteristic locus approach as a convenient *robust analysis* tool; however, the characteristic locus framework cannot as yet accommodate general robust design. For example, even though the E-Contour method defines the worst case relative stability margin, it cannot presently be adapted for design with respect to the worst case (i.e. minimum) relative stability margin. Therefore, the remaining portion of the work shifts to the investigation of H^∞ optimal control methods in order to pursue this *robust design* objective. Moreover, in the course of pursuing this goal, this work produces new mathematical theory pertaining to H^∞ optimization. Consequently, in order to support the ensuing H^∞ theoretical development as well as the succeeding H^∞ robust design presentation, this chapter presents an overview of H^∞ optimal techniques.

5.1 Introduction

H^∞[1] optimal techniques are relatively new frequency domain approaches [Zames, 1981; Zames and Francis, 1983] which, in the previous decade, have yielded solutions to such problems as the additive unstructured uncertainty robustness prob-

[1] H^∞ represents the Hardy subspace which contains functions $F(s)$ which are both analytic and bounded in Real(s) > 0, the ∞ in H^∞ represents the infinity norm defined on the subspace [Francis, 1987].

lem [Glover, 1986] and the mixed disturbance rejection performance and multiplicative output uncertainty robustness problem [Doyle, 1984; Francis, 1987]. These successful applications of H^∞ theory to specific robust control problems have resulted primarily because the relevant H^∞ optimization function not only incorporates the unstructured uncertainty characterization, but also because it generates an internally stabilizing controller. To see how the H^∞ optimization function incorporates unstructured uncertainty, it is only necessary to point out that the scalar modulus function which bounds the unstructured uncertainty [c.f. (2.1)] can be used to weight the appropriate transfer function matrix. The way in which the H^∞ optimization function generates an internally stabilizing controller is far from obvious, yet has an elegant solution in terms of the Youla parametrization [Youla et al., 1976]. In addition to these key ingredients, the robustness to additive unstructured uncertainty problem can be converted (by applying norm-preserving operations) to a Hankel approximation problem and, subsequently, solved explicitly using Glover's state-space formulae [Glover, 1984]. At this point, *an*[2] H^∞ optimal solution (i.e. an optimal Hankel approximation) can be used to construct the corresponding H^∞ controller. This design process is covered in more detail in the following overview of H^∞ design.

5.2 An overview of H^∞ design

H^∞ design formulates closed-loop design objectives which can be subsequently achieved by minimizing the H^∞ norm. Before examining the H^∞ design formulation however, we first need to define the H^∞ norm and the relevant closed-loop transfer functions. The H^∞ norm is defined as:

$$\|E(s)\|_\infty = \sup_\omega \overline{\sigma}\,[E(j\omega)] \tag{5.1}$$

Here, $E(s)$ represents a real-rational, proper, transfer function matrix; the notation $E(s) \in RH_+^\infty$ will be used to denote when this class of matrices is *stable*, whereas,

[2]The H^∞ optimal solution is generally nonunique and therefore contains degrees of freedom which the next two chapters characterize and use.

the notation $E(s) \in RH_-^\infty$ will be used to denote when this class of matrices is *unstable*. In general, $E(s)$ will contain both stable and unstable components one of which is known and the other of which must be determined using H^∞ optimization techniques to be addressed in the sequel.

In order to see how H^∞ closed-loop design objectives are formed, consider the multivariable feedback system of Fig. 5.1. This system[3] has three associated

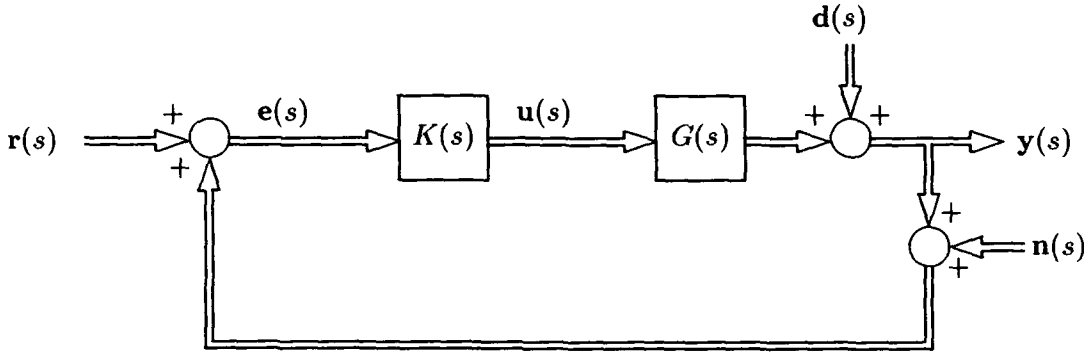

Figure 5.1: Multivariable system with positive unity feedback subject to disturbances and noise

transfer function matrices which directly affect stability and performance [Hvostov, 1990]. First, the *sensitivity* function, defined as $S(s) = [I - G(s)K(s)]^{-1}$, governs the system's ability to track commands and reject output disturbances. Next, the *complementary sensitivity* function, defined as $T(s) = G(s)K(s)\,[I - G(s)K(s)]^{-1}$, governs the system's tolerance to multiplicative output uncertainty as well as the ability to reject noise. Finally, the *controller sensitivity* function, defined as $R(s) = K\,[I(s) - G(s)K(s)]^{-1}$, governs the system's tolerance to additive uncertainty as well as the control activity. H^∞ design formulates control objectives by appropriately weighting one or more of these sensitivity functions. For example, a

[3]This system has positive feedback which is the convention used in most H^∞ literature.

useful H^∞ optimization problem is formulated as [Chiang and Safonov, 1988]:

$$\min_{Stabilizing K} \left\| \begin{array}{c} w_1(s)S(s) \\ w_2(s)R(s) \\ w_3(s)T(s) \end{array} \right\|_\infty \tag{5.2}$$

where the H^∞ optimal controller, $K(s)$, is that which not only minimizes the H^∞ norm but stabilizes the closed-loop system as well. Additionally, (5.2) confirms that the H^∞ design objectives enter the problem formulation through the weighting functions $w_1(s)$, $w_2(s)$, and $w_3(s)$ which shape the respective sensitivity functions.

The general H^∞ optimization given by (5.2) represents the *standard H^∞ problem* [Francis, 1987] which can be obtained by a simple loop transformation of Fig. 5.1 as depicted in Fig. 5.2[4]. In this figure, the input $\mathbf{w} = \begin{pmatrix} \mathbf{r} \\ \mathbf{d} \\ \mathbf{n} \end{pmatrix}$ is the generalized sig-

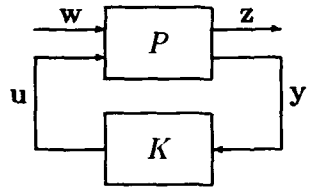

Figure 5.2: Standard H^∞ problem

nal vector of commands, disturbances, and noise while the output $\mathbf{z} = \begin{pmatrix} \mathbf{e} \\ \mathbf{u} \\ \mathbf{y} \end{pmatrix}$ is the generalized signal vector of tracking errors, control inputs, and measured outputs. Additionally, $\mathbf{u}$ is the control input signal vector and $\mathbf{y}$ is the measured output signal vector. Fig. 5.2 also defines a *generalized plant* transfer matrix P which maps the input signals to the output signals in the following manner:

$$\begin{aligned} P\begin{pmatrix} \mathbf{w} \\ \mathbf{u} \end{pmatrix} &= \begin{pmatrix} \mathbf{z} \\ \mathbf{y} \end{pmatrix} \\ &= \begin{pmatrix} P_{11} & P_{12} \\ P_{21} & P_{22} \end{pmatrix} \begin{pmatrix} \mathbf{w} \\ \mathbf{u} \end{pmatrix} \\ &\rightarrow \mathbf{z} = P_{11}\mathbf{w} + P_{12}\mathbf{u} \qquad (5.3) \\ &\rightarrow \mathbf{y} = P_{21}\mathbf{w} + P_{22}\mathbf{u} \qquad (5.4) \end{aligned}$$

[4]For notational convenience, the argument s will be dropped throughout the remainder of this chapter.

Thus, P_{11} and P_{12} are the transfer functions which map commands, disturbances, noise, and control signals to tracking errors, actuator commands, and the output. Likewise, P_{21} and P_{22} are the transfer functions which map commands, disturbances, noise, and control signals to the measured output. Here, P_{22} simply represents the nominal plant G and thus, the generalized plant P provides a convenient means of capturing additional aspects the design problem. The generalized plant/controller configuration of Fig. 5.2 also permits the standard H^∞ problem (5.2) to be rendered in an alternative representation discussed next.

The input-output map from $\mathbf{w}$ to $\mathbf{z}$ may be represented with a *linear fractional transformation* which may be obtained from (5.3) and (5.4) along with the fact that $\mathbf{u} = K\mathbf{y}$ in Fig. 5.2 to give:

$$\begin{aligned} \mathbf{z} &= \left[P_{11} + P_{12}K(I - P_{22}K)^{-1}P_{21}\right]\mathbf{w} \\ \mathbf{z} &= F_l(P,K)\mathbf{w} \end{aligned}$$

Thus, the linear fractional transformation $F_l(P,K)$ serves as a mapping from the generalized inputs to the generalized outputs. With this representation, the general H^∞ norm minimization problem given by (5.2) can be rewritten in the following compact form of the standard problem:

$$\min_{Stabilizing K} \|F_l(P,K)\|_\infty \tag{5.5}$$

where the controller K stabilizes the closed-loop containing the nominal plant P_{22}. Remarkably, both the assessment of the stabilization of the closed-loop and the minimization of the H^∞ optimization function (5.5) are concurrently simplified by using the Youla parametrization of internally stabilizing controllers which will be examined after defining internal stability.

5.2.1 Internal stability

An explicit characterization of internal stability is useful because it intrinsically accounts for possible right half-plane pole cancellations between the plant G[5] and the

[5] G in this context is identical to P_{22}.

controller K. In particular, if the closed-loop system is stable at each internal node, overall stability follows. Consider the system shown in Fig. 5.3. In this figure,

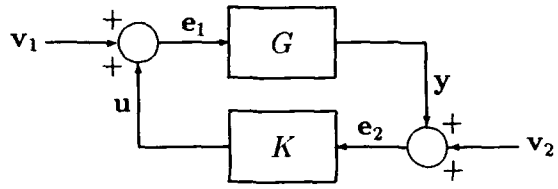

Figure 5.3: Block diagram for internal stability definition

$\mathbf{v}_1$ and $\mathbf{v}_2$ are superfluous inputs introduced to define internal stability. Specifically, internal stability implies that if $\mathbf{v}_1$ and $\mathbf{v}_2$ are bounded "inputs", then the corresponding "outputs" $\mathbf{e}_1$ and $\mathbf{e}_2$ will remain bounded. Consequently, the transfer function from the inputs $\begin{pmatrix}\mathbf{v}_1\\ \mathbf{v}_2\end{pmatrix}$ to the outputs $\begin{pmatrix}\mathbf{e}_1\\ \mathbf{e}_2\end{pmatrix}$ must be stable for internal stability to hold. Algebraic manipulation of the governing equations yields:

$$\begin{pmatrix}\mathbf{v}_1\\ \mathbf{v}_2\end{pmatrix} = \begin{pmatrix} I & -K\\ -G & I\end{pmatrix}\begin{pmatrix}\mathbf{e}_1\\ \mathbf{e}_2\end{pmatrix} \tag{5.6}$$

In order to write the outputs in terms of the inputs, the transfer matrix of (5.6) must be invertible in RH_+^∞ and its inverse is given as [Kailath, 1980]:

$$\begin{pmatrix} I & -K\\ -G & I\end{pmatrix}^{-1} = \begin{pmatrix} I+K(I-GK)^{-1}G & K(I-GK)^{-1}\\ (I-GK)^{-1}G & (I-GK)^{-1}\end{pmatrix} \tag{5.7}$$

For internal stability, it is necessary and sufficient to check that each of the four entries in (5.7) are in RH_+^∞ [Francis, 1987]. This internal stability characterization forms the basis for the following parametrization of all stabilizing controllers for a given plant.

5.2.2 Stabilizing controller parametrization

The parametrization of all controllers K which stabilize a given plant G can be achieved through the following *fractional representations* [Desoer et al., 1980; Moore et al., 1990]:

$$K = UV^{-1} = \tilde{V}^{-1}\tilde{U} \tag{5.8}$$

$$G = NM^{-1} = \tilde{M}^{-1}\tilde{N} \tag{5.9}$$

where U, V, $\tilde{U}$, $\tilde{V}$, M, N, $\tilde{M}$, and $\tilde{N}$ are in RH_+^∞ with (U,V) and (M,N) pairwise right coprime[6] in RH_+^∞ and $(\tilde{U},\tilde{V})$ and $(\tilde{M},\tilde{N})$ pairwise left coprime in RH_+^∞. Right coprimeness requires the removal of the greatest common right divisor while the converse applies for left coprimeness. A useful characterization of right coprimeness is given by the Bezout Identity [Kailath, 1980]. This identity states that U and V are right coprime in RH_+^∞ if and only if there exist stable functions X and Y such that:

$$XU + YV = I$$

A similar identity can be used to characterize left coprimeness. These coprime characterizations and the fractional representations of (5.8) and (5.9) are fundamental to the following parametrization of all controllers K which stabilize a given plant G.

The fractional representations of (5.8) and (5.9) can be employed in (5.6), subsequently inverted, and factored into coprime parts to yield the following equivalent internal stability requirements:

$$\begin{pmatrix} I & -K \\ -G & I \end{pmatrix}^{-1} \in RH_+^\infty \quad \begin{pmatrix} M & U \\ N & V \end{pmatrix}^{-1} \in RH_+^\infty \quad \begin{pmatrix} \tilde{V} & -\tilde{U} \\ -\tilde{N} & \tilde{M} \end{pmatrix}^{-1} \in RH_+^\infty$$

Using the Bezout Identity and the definitions of (5.8) and (5.9), it can be shown that the latter two requirements satisfy:

$$\begin{pmatrix} \tilde{V} & -\tilde{U} \\ -\tilde{N} & \tilde{M} \end{pmatrix} \begin{pmatrix} M & U \\ N & V \end{pmatrix} = \begin{pmatrix} I & 0 \\ 0 & I \end{pmatrix} \tag{5.10}$$

This important relation can be combined with the fractional representations of (5.8) and (5.9) as well as the following state-space realizations for M, N, $\tilde{M}$, and $\tilde{N}$ to give the general observer-based structure of all stabilizing controllers. First, consider the state-space representations of the plant coprime factors given below [Nett et al., 1984]:

$$M = \left(\begin{array}{c|c} A+BF & B \\ \hline F & I \end{array}\right) \qquad N = \left(\begin{array}{c|c} A+BF & B \\ \hline C+DF & D \end{array}\right) \tag{5.11}$$

[6]The right coprimeness in RH_+^∞ of U and V, for example, implies that U and V have no common unstable zeros.

$$\tilde{M} = \left(\begin{array}{c|c} A+HC & H \\ \hline C & I \end{array}\right) \qquad \tilde{N} = \left(\begin{array}{c|c} A+HC & B+HD \\ \hline C & D \end{array}\right) \tag{5.12}$$

where $G = NM^{-1} = \tilde{M}^{-1}\tilde{N} = \left[\begin{array}{c|c} A & B \\ \hline C & D \end{array}\right]$. Additionally, F is stabilizing state feedback and H is stabilizing output injection which, when obtained in the following way [Doyle, 1984]:

$$F = -B^T X_c \quad \text{where } X_c \text{ satisfies} \quad X_c A + A^T X_c - X_c B B^T X_c = 0 \tag{5.13}$$

$$H = -Y_o C^T \quad \text{where } Y_o \text{ satisfies} \quad Y_o A^T + A Y_o - Y_o C^T C Y_o = 0 \tag{5.14}$$

make M and $\tilde{M}$ *inner*, respectively. In particular, these inner transfer function matrices are special *all pass* systems that satisfy $M^T(-s)M(s) = \tilde{M}(s)\tilde{M}^T(-s) = I$; this property will be useful in performing subsequent norm-preserving operations. Thus, the state-space representations of (5.11) and (5.12) in conjunction with (5.10) give the following observer-based controller structure which is the central form of all stabilizing controllers [Doyle, 1984]:

$$K_o = \left(\begin{array}{c|c} A+BF+HC+HDF & -H \\ \hline F & 0 \end{array}\right) \tag{5.15}$$

The controller subscript indicates that K_o is the "central" stabilizing controller and it will be seen below that additional dynamics can be added to this basic controller form to obtain additional degrees of design freedom. However, it should be restated that (5.10) encapsulates the requirement for internal stability in terms of fractional representations which are suitable for the parametrization of all stabilizing controllers of a given plant. In order to generalize the internally stabilizing controller result of (5.15) to include *all* internally stabilizing controllers, we require the Youla parametrization [Youla et al., 1976; Doyle, 1984].

The Youla parametrization characterizes all stabilizing feedback controllers for a given plant. It can be stated in the following way: Let $K_o = U_o V_o^{-1} = \tilde{V}_o^{-1}\tilde{U}_o$ be the fractional representations of the controller such that the internal stability requirement encapsulated in (5.10) holds. For any transfer function $Q \in RH_+^\infty$,

define the following transfer function matrices:

$$U = U_o + MQ, \qquad V = V_o + NQ \tag{5.16}$$

$$\tilde{U} = \tilde{U}_o + Q\tilde{M}, \qquad \tilde{V} = \tilde{V}_o + Q\tilde{N} \tag{5.17}$$

Then $K = UV^{-1} = \tilde{V}^{-1}\tilde{U}$ characterizes *all* stabilizing controllers for a given plant $G = NM^{-1} = \tilde{M}^{-1}\tilde{N}$. The proof that this parametrization is stabilizing follows by substituting (5.16) and (5.17) into (5.10). The proof that this parametrization generates the entire class of stabilizing controllers is straightforward and can be found in [Doyle, 1984].

This parametrization based on the Youla parameter Q has powerful implications in the H^∞ design procedure. Consider the impact on the standard H^∞ norm minimization problem of (5.5). Using the fractional representations for K and P_{22}[7] given by (5.16) and (5.17), the original H^∞ problem may be transformed using the following steps:

$$\begin{aligned}
\min_{K \in RH_+^\infty} \|F_l(P,K)\|_\infty &= \min_{K \in RH_+^\infty} \left\| P_{11} + P_{12}K(I - P_{22}K)^{-1}P_{21} \right\|_\infty \\
&= \min_{Q \in RH_+^\infty} \left\| P_{11} + P_{12}\left(U_o\tilde{M} + MQ\tilde{M}\right)P_{21} \right\|_\infty \\
&= \min_{Q \in RH_+^\infty} \left\| (P_{11} + P_{12}U_o\tilde{M}P_{21}) + P_{12}MQ\tilde{M}P_{21} \right\|_\infty \\
&= \min_{Q \in RH_+^\infty} \|T_{11} + T_{12}QT_{21}\|_\infty \\
&= \min_{Q \in RH_+^\infty} \|F_l(T,Q)\|_\infty
\end{aligned} \tag{5.18}$$

where $K(I - P_{22}K)^{-1} = \left(U_o\tilde{M} + MQ\tilde{M}\right)$,

$$T_{11} = (P_{11} + P_{12}U_o\tilde{M}P_{21}) \qquad T_{12} = P_{12}M$$

$$T_{21} = \tilde{M}P_{21} \qquad T_{22} = 0$$

Thus the original H^∞ norm minimization problem has been transformed from a nonlinear minimization over $K \in RH_+^\infty$ to an affine minimization over $Q \in RH_+^\infty$. The final linear fractional transformation, $F_l(T,Q)$, is in the form of the *model-matching problem* in which the "model" transfer function T_{11} is to be matched by

[7] Recall that $P_{22} = G$.

the cascade transfer function $-T_{12}QT_{21}$ with the constraint that all four functions are in RH_+^∞ [Francis, 1987].

5.2.3 Hankel approximation

The model-matching problem can be converted into a *distance problem* which, in turn, can be solved by Hankel approximation theory. The conversion of the model-matching problem begins with the application of norm-preserving operations and factorizations to the model-matching terms of (5.18). This results in a difference of two terms: one which is stable and one which is antistable. This[8] can be written as:

$$\min_{Q \in RH_+^\infty} \|T_{11} + T_{12}QT_{21}\|_\infty = \min_{F \in RH_+^\infty} \|G - F\|_\infty$$

where G[9] is the known antistable transfer function and F is the unknown stable transfer function to be optimally determined. Note that G will not usually equal T_{11} and F will not usually equal $-T_{12}QT_{21}$ as a result of the norm-preserving operations and factorizations. In addition, the stable "free" transfer function Q remains embedded within F since Q is in RH_+^∞. Thus, the model-matching problem above is equivalent to a distance problem whereby the distance from the known antistable transfer function $G \in RH_-^\infty$ is minimized by the optimal choice of the unknown stable transfer function $F \in RH_+^\infty$.

Hankel approximation theory can be used to solve the distance problem by characterizing the unknown stable function (i.e. the approximation) in terms of the known antistable function [Safonov and Verma, 1985]. In particular, it is well known that the optimal approximation has a minimum distance from the antistable function and the specific value of the minimum distance is given by the Hankel norm defined as [Glover, 1984]:

$$\min_{F \in RH_+^\infty} \|G - F\|_\infty = \|G^*\|_H \tag{5.19}$$

[8] In the 1-block problem.

[9] G here is to be distinguished from the plant transfer function matrix. This conforms to the notation given in [Glover, 1984].

where $G^*(s) \triangleq G^T(-s)$ is a completely stable, proper transfer function in RH_+^∞ and H is the Hankel matrix associated with G^*. In addition, the controllability and observability gramians, denoted X and Y respectively, are given as [Francis, 1987]:

$$X \triangleq \int_0^\infty e^{At} B B^T e^{A^T t} dt$$

$$Y \triangleq \int_0^\infty e^{A^T t} C^T C e^{At} dt$$

Here, the state-space component matrices A, B, and C are those associated with stable transfer function G^*. Furthermore, it is straightforward to show (by using the appropriate matrix differential equations) that the gramians satisfy the following Lyapunov equations:

$$AX + XA^T + BB^T = 0 \tag{5.20}$$

$$YA^T + AY + C^T C = 0 \tag{5.21}$$

With these gramians definitions, the value of the Hankel norm of (5.19) can be obtained as:

$$\|G^*\|_H = \sqrt{\rho(XY)} \tag{5.22}$$

where $\rho(\cdot)$ denotes spectral radius. This basic relationship between the Hankel norm and the controllability and observability gramians can be derived by considering how the Hankel operator maps past inputs (controls) to future outputs (observations) [Francis and Doyle, 1987]. The role played by the gramians is fundamental in producing an explicit state-space realization for the closest antistable transfer function to the given stable transfer function; however, the gramians must first be balanced [Moore, 1981].

The gramians of a completely controllable, completely observable, stable, and balanced state-space realization are equal, real, and diagonal and are given by [Pernebo and Silverman, 1982; Laub et al., 1987]:

$$X = Y = \Sigma = \text{diag}\{\sigma_i\}$$

where the σ_i's are the ordered Hankel singular values (e.g. $\sigma_1 = \sqrt{\rho(XY)}$). If the system is initially unbalanced, the gramian diagonalization can be obtained by using a similarity transformation $M = \Sigma^{-1/2}U^*R$ where $Y = R^*R$ is a Cholesky factorization of Y, $RXR^* = U\Sigma^2U^*$, and U is unitary [Glover, 1984, p. 1129]. Subsequently, both gramians can be diagonalized in the following manner:

$$MXM^* = M^{*^{-1}}YM^{-1} = \Sigma$$

When the balanced gramian is partitioned, it permits the conformal partitioning of the state-space matrices associated with the stable transfer function G^*. Furthermore, this partitioning facilitates the derivation of a state-space realization of the closest unstable transfer function to the given stable transfer function.

The explicit state-space realization of the solution to the Hankel approximation problem has been provided by Glover [Glover, 1984]. An outline of the solution begins with the H^∞ norm minimization problem:

$$\min_{F \in RH_+^\infty} \|G - F\|_\infty$$

where $G \in RH_-^\infty$ is a completely unstable (analytic in Real$(s) \leq 0$) strictly proper transfer function. The H^∞ optimal solution $F \in RH_+^\infty$ achieves an all pass error equal to the Hankel norm: $\min_{F \in RH_+^\infty} \|G - F\|_\infty = \|G^*\|_H$. Moreover, the explicit state-space realization of *an*[10] H^∞ optimal solution F is derived from the state-space realization of G^*. The specific state-space formulae will be presented in the following chapter along with a characterization of the degrees of freedom contained therein. After employing the state-space formulae to determine F, the optimal transfer function $Q \in RH_+^\infty$ may be constructed where Q is defined by the H^∞ norm minimization problem of (5.18). Subsequently, substituting the parameter Q in the Youla parametrization of (5.16) and (5.17) and using (5.8) determines the optimal controller transfer function K. This overview of H^∞ design is briefly set forth in the following robustness to additive unstructured uncertainty problem.

[10] In general there are an infinity of H^∞ optimal solutions. The selection of a unique solution based on additional objectives will be the subject of the following two chapters.

5.3 H^∞ optimal control: robustness to additive uncertainty

Consider the perturbed multivariable system of Fig. 5.4 in which the additive unstructured uncertainty is bounded by $\overline{\sigma}[\Delta] < \delta$. Given the objective of designing

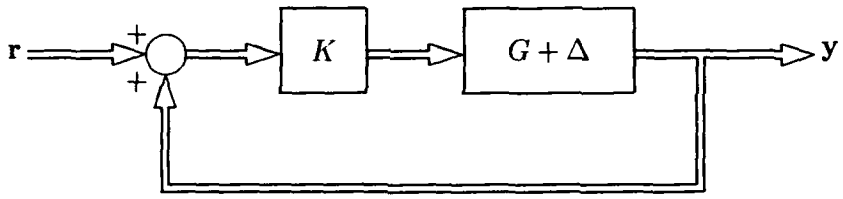

Figure 5.4: H^∞ additive uncertainty model

an H^∞ controller which stabilizes the loop for all possible perturbations of the plant, the optimal H^∞ controller is given by:

$$\min_{K \in RH_+^\infty} \|\delta K(I - GK)^{-1}\|_\infty \leq 1 \tag{5.23}$$

where $K(I-GK)^{-1}$ is the controller sensitivity function. Moreover, the requirement that the norm be less than or equal to one can be easily derived from spectral radius stability criterion of (2.5). Using the Youla parametrization of (5.16) and (5.17), the nonlinear optimization(5.23) is converted into the following affine optimization:

$$\begin{aligned}
&\min_{Q \in RH_+^\infty} \|\delta UV^{-1}(I - \tilde{M}^{-1}\tilde{N}UV^{-1})^{-1}\|_\infty \\
&= \min_{Q \in RH_+^\infty} \|\delta U\left[(\tilde{M}V_o - \tilde{N}U_o) + (\tilde{M}N - \tilde{N}M)Q\right]^{-1}\tilde{M}\|_\infty \\
&= \min_{Q \in RH_+^\infty} \|\delta U\left[I + 0\right]^{-1}\tilde{M}\|_\infty \\
&= \min_{Q \in RH_+^\infty} \|\delta(U_o + MQ)\tilde{M}\|_\infty
\end{aligned}$$

where use has been made of the internal stability requirement of (5.10). Subsequently, the determination of the output injection H [c.f. (5.14)] allows the removal of $\tilde{M}$ from the minimization by making $\tilde{M}$ inner. Finally, the Hankel norm approximation may be written as:

$$\min_{Q \in RH_+^\infty} \|\delta M^{-1}U_o + \delta Q\|_\infty \leq 1$$

Notice that the unstructured perturbation δ can be viewed as a scalar weighting function which simply scales the norm. Hereon, the problem can be converted to a Hankel approximation problem and finally solved using Glover's state-space formula. Additional details of this process will be explored in more depth in the following chapter.

5.4 Summary

This chapter served to re-orient this work toward H^∞ optimal techniques in order to lay the groundwork for the ensuing H^∞ theoretical development as well as the H^∞ robust design presentation. An overview of the H^∞ optimal methods was given by considering the general formulation of the H^∞ optimization problem and observing that the design objectives are mathematically embodied in the weighting functions which multiply the appropriate sensitivity transfer matrix. After formulating the H^∞ optimization, the Youla parametrization of internally *stabilizing controllers* was presented. This elegant parametrization not only ensured closed-loop stability, but also simplified the actual optimization problem through conversion to a Hankel approximation problem. Moreover, in the robustness to additive unstructured uncertainty problem, it was noted that the Hankel approximation could be expressed in terms of Glover's state-space formulae; these formulae will be explicitly enumerated in the following chapter along with a characterization and use of their implicit degrees of freedom.

Chapter 6

Characterization and use of the degrees of freedom in the H^∞ problem

6.1 Introduction

It has been known for some time that the H^∞ approach can be used to design robust feedback controllers which maintain stability in the presence of plant uncertainty [Zames, 1981; Zames and Francis, 1983]. Not surprisingly, H^∞ robust design methods have received considerable attention over the past few years. Underpinning those methods is Glover's seminal work on optimal Hankel approximations [Glover, 1984] which gives explicit state-space formulae that yield an H^∞ optimal solution. However, as mentioned in the preceding chapter, there are infinitely many transfer function matrices which qualify as H^∞ optimal solutions; in order to restore uniqueness, a strengthening of the H^∞ optimization problem, labelled the H^∞ super-optimization problem, was presented in [Young, 1986b] and subsequently reliable state-space algorithms were presented in [Tsai et al., 1988; Limebeer et al., 1989].

The present objective is to characterize the degrees of freedom contained in the H^∞ optimal solution so that they may be used to obtain desirable properties in the Hankel approximation. In particular, for a special class of transfer function matrices, it will be shown that the degrees of freedom can be deployed to obtain stationarity of either the controllability or the observability approximation gramians. Remarkably, for the specified class of transfer function matrices, the stationary conditions for the gramians of the approximation system impose flatness on *all* of the error system singular values. Although the error system singular values are simultaneously ma-

nipulated and made flat (as a function of frequency), they do not in general attain their super-optimal values. Hence, it may be necessary to submit the error system to a super-optimal algorithm in order to minimize the remaining singular values, and, in this context, the degrees of freedom can be used to *match* the error system to either the left or right maximizing vector. It will be shown that the matched error systems produce completely stable projections when multiplied by the complementary maximizing vectors. Clearly, this feature has obvious implications (a reduction in the computational burden) for any attendant super-optimal algorithm.

The main thrust of this work is not the development of a super-optimal algorithm, but rather the exploitation of the H^∞ optimal solution degrees of freedom to advantage, which advantage is sometimes so great that near super-optimality is attained in one H^∞ optimal solution iteration. As will be seen, a natural by-product of using the H^∞ optimal solution degrees of freedom is the emergence of an alternative super-optimal algorithm; the super-optimal solution is unique and hence, the algorithm presented clearly must overlap with earlier work [Tsai et al., 1988; Limebeer et al., 1989]. The super-optimal solution can be computed in many different ways, however, by using the degrees of freedom as subsequently presented, there is a concomitant lessening of the computational burden. If super-optimality is desired, the proposed algorithm uses the H^∞ optimal solution degrees of freedom to attain total flatness within each cycle of iteration and to eliminate (suppress) all unstable poles in the special case considered or maximal number in the general case.

This work begins in the next section by presenting the H^∞ 1-block optimization problem as well as the H^∞ optimal solution to that problem. In addition, the salient features of the super-optimal solution as they relate to the present work are depicted. Subsequently, a characterization of the degrees of freedom contained within the H^∞ optimal solution is given along with an important Hankel singular value relationship. Section 6.3 begins by exploring how the degrees of freedom may be used to obtain desirable properties in the H^∞ optimal solution. In order to present the results in a logical sequence from the simplest case to the most general, the focus is initially

restricted to the special class of transfer function matrices in which the number of states equals the number of inputs and outputs. [It is acknowledged that this class is very special and is therefore unrealistic from a practical viewpoint, however it is initially considered in order to gain insight.] For this class, it is possible to identify the desirable approximation system properties such as gramian stationarity, error system singular value flatness, and stable complementary maximizing vector projections. Finally, these properties will be highlighted using two examples studied previously in the literature [Young, 1986a; Tsai et al., 1988; Limebeer et al., 1989].

6.2 Background

The H^∞ 1-block optimization problem is given by[1]

$$\min_{F(s)\in RH_-^\infty} \|G(s) - F(s)\|_\infty \tag{6.1}$$

where $G(s)$ *is a stable function in* RH_+^∞ *and* $F(s)$ *is an* antistable approximation in RH_-^∞. In [Glover, 1984, Theorem 6.3 and Corollary 7.3], explicit state-space formulae were provided which solve the H^∞ 1-block optimization problem in terms of a Hankel approximation. These formulae, hereafter referred to as the *Central Glover Solution* are formalized in the following lemma.

Lemma 6.1 (Central Glover Solution)

Given a stable transfer function $G(s) \in RH_+^\infty$ *with minimal, balanced state-space realization* $G(s) = \left[\begin{array}{c|c} A & B \\ \hline C & D \end{array}\right]$ *and equal, diagonal controllability and observability gramians* $X = Y$ *which satisfy the following Lyapunov equations*

$$AX + XA^T + BB^T = 0 \tag{6.2}$$

$$A^TY + YA + C^TC = 0 \tag{6.3}$$

[1]The form given here differs from that given in (5.19) where $G(s) \in RH_-^\infty$ and $F(s) \in RH_+^\infty$; however, (6.1) conforms to the way in which the problem is stated in [Glover, 1984].

partition A, B, and C conformally with X and Y in the following manner:

$$X = Y = \begin{pmatrix} \sigma_1 & 0 \\ 0 & \Sigma_2 \end{pmatrix} \quad \Rightarrow \quad \left[\begin{array}{c|c} A & B \\ \hline C & D \end{array}\right] = \left[\begin{array}{cc|c} a_{11} & A_{12} & B_1 \\ A_{21} & A_{22} & B_2 \\ \hline C_1 & C_2 & D \end{array}\right] \tag{6.4}$$

where $\Sigma_2 = \mathrm{diag}\{\sigma_2, \ldots, \sigma_n\}$ *and* $\sigma_1 > \sigma_2 \geq \ldots \geq \sigma_n > 0$. *The* H^∞ *optimal solution* $F(s) \in RH_-^\infty$ *of (6.1) has the state-space realization* $F(s) = \left[\begin{array}{c|c} \tilde{A} & \tilde{B} \\ \hline \tilde{C} & \tilde{D} \end{array}\right]$ *given by:*

$$\begin{aligned} \tilde{A} &= \Gamma^{-1}(\sigma_1^2 A_{22}^T + \Sigma_2 A_{22} \Sigma_2 - \sigma_1 C_2^T U B_2^T) \\ \tilde{B} &= \Gamma^{-1}(\Sigma_2 B_2 + \sigma_1 C_2^T U) \\ \tilde{C} &= C_2 \Sigma_2 + \sigma_1 U B_2^T \\ \tilde{D} &= D - \sigma_1 U \end{aligned}$$

where $\Gamma = \Sigma_2^2 - \sigma_1^2 I$ *and* U *is a matrix satisfying:*

$$(i) \quad B_1 = -C_1^T U \tag{6.5}$$

$$(ii) \quad U^T U \leq I \tag{6.6}$$

Additionally, the balanced realization and conformal partitioning yield the following useful formulae. First, (6.2) implies

$$(1) \quad B_1 B_1^T = -2\sigma_1 a_{11} \tag{6.7}$$

$$(2) \quad A_{12}\Sigma_2 + \sigma_1 A_{21}^T + B_1 B_2^T = 0 \tag{6.8}$$

$$(3) \quad A_{22}\Sigma_2 + \Sigma_2 A_{22}^T + B_2 B_2^T = 0 \tag{6.9}$$

Similarly, (6.3) implies

$$(1) \quad C_1^T C_1 = -2\sigma_1 a_{11} \tag{6.10}$$

$$(2) \quad \sigma_1 A_{12} + A_{21}^T \Sigma_2 + C_1^T C_2 = 0 \tag{6.11}$$

$$(3) \quad \Sigma_2 A_{22} + A_{22}^T \Sigma_2 + C_2^T C_2 = 0 \tag{6.12}$$

The error system $G_e(s) = G(s) - F(s)$ *has associated controllability and observability gramians given by* X_e *and* Y_e *respectively, which satisfy the following Lyapunov*

equations

$$A_e X_e + X_e A_e^T + B_e B_e^T = 0 \tag{6.13}$$

$$A_e^T Y_e + Y_e A_e + C_e^T C_e = 0 \tag{6.14}$$

where

$$A_e = \begin{pmatrix} A & 0 \\ 0 & \tilde{A} \end{pmatrix}, \quad B_e = \begin{pmatrix} B \\ \tilde{B} \end{pmatrix}, \quad C_e = \begin{pmatrix} C & -\tilde{C} \end{pmatrix}, \quad D_e = D - \tilde{D} \tag{6.15}$$

Furthermore, the error system controllability and observability gramians are given by

$$X_e = \begin{pmatrix} \sigma_1 & 0 & 0 \\ 0 & \Sigma_2 & I \\ 0 & I & \tilde{X} \end{pmatrix} \qquad Y_e = \begin{pmatrix} \sigma_1 & 0 & 0 \\ 0 & \Sigma_2 & -\Gamma \\ 0 & -\Gamma & \tilde{Y} \end{pmatrix} \tag{6.16}$$

where the approximation system controllability and observability gramians are given by

$$\tilde{A}\tilde{X} + \tilde{X}\tilde{A}^T + \tilde{B}\tilde{B}^T = 0 \tag{6.17}$$

$$\tilde{A}^T\tilde{Y} + \tilde{Y}\tilde{A} + \tilde{C}^T\tilde{C} = 0 \tag{6.18}$$

For clarity of presentation, the assumption has been made in the above that the maximum Hankel singular value σ_1 is distinct. This assumption will be made throughout this chapter and the next with the understanding that the results can be extended to the case when σ_1 is repeated and simple. In the case that U of (6.5) and (6.6) is unitary, it turns out that $\tilde{X} = \Sigma_2\Gamma^{-1}$ and $\tilde{Y} = \Sigma_2\Gamma$ as shown in [Glover, 1984, Theorem 6.3]. The validity of these substitutions follows directly by expanding (6.13) and (6.14) and solving for the (2,2) blocks. Prior to characterizing the degrees of freedom contained in the Central Glover Solution, the pertinent background relating to the H^∞ super-optimal solution will be reviewed.

Conditions (6.5) and (6.6) do not define a unique matrix U and so there exist infinitely many central optimal approximation systems for all but the scalar case. To restore uniqueness, super-optimality seeks to find the unique extension $F(s)$ such that the sequence of s-numbers

$$s_1^\infty(G(s) - F(s)), s_2^\infty(G(s) - F(s)), s_3^\infty(G(s) - F(s)), \ldots \tag{6.19}$$

is minimized with respect to lexicographic ordering where for any $G(s) \in RL^\infty$

$$s_i^\infty(G(s)) = \sup_\omega \sigma_i(G(j\omega)) \tag{6.20}$$

and $\sigma_i(G(s))$, represents the i^{th} singular value of matrix $G(s)$. Thus, the H^∞ super-optimal approach seeks to minimize the supremum over ω of all the error system singular values other than the largest which is minimized implicitly as part of the Central Glover Solution and given as $s_1^\infty(G(s) - F(s)) = \sigma_1$. The H^∞ super-optimal approach has been solved using state-space representations of maximizing vectors in block diagonalizing algorithms [Tsai et al., 1988; Limebeer et al., 1989] and the relevant details are examined next.

The H^∞ super-optimal approach constructs inner maximizing vectors as well as their complements in order to block diagonalize the transfer function $G(s) - F(s)$ contained in the H^∞ cost function (6.1). In terms of the error system returned by the Central Glover Solution $G_e(s) = G(s) - F(s)$, the maximizing vectors $\mathbf{x}(s) \in RH_2$ and $\mathbf{y}(s) \in RH_2$ form a Schmidt pair [Young, 1983] which satisfy

$$G_e(s)\mathbf{x}(-s) = \sigma_1 \mathbf{y}(s) \qquad \text{and} \qquad \|\mathbf{x}(s)\|_2 = \|\mathbf{y}(s)\|_2 \tag{6.21}$$

Given the state-space representation for $G(s) = \left[\begin{array}{c|c} A & B \\ \hline C & D \end{array}\right] \in RH_+^\infty$, the maximizing vectors are made inner and augmented by conformal, inner, orthogonal complements (labelled $\mathbf{x}_\perp(s)$ and $\mathbf{y}_\perp(s)$). The maximizing vectors and their orthogonal complements are paramount in reducing the problem dimension so that the transfer function $G_e(s) = G(s) - F(s)$ can be iteratively block diagonalized thereby permitting direct application of the Central Glover Solution at each subsequent iteration. For example, the following illustrates the block diagonalization of the dimension reduction process.

$$\begin{aligned} \|G_e(s)\|_\infty &= \left\| \begin{bmatrix} \mathbf{y}^T(-s) \\ \mathbf{y}_\perp{}^T(-s) \end{bmatrix} G_e(s) \begin{bmatrix} \mathbf{x}(-s) & \mathbf{x}_\perp(-s) \end{bmatrix} \right\|_\infty \\ &= \left\| \begin{bmatrix} \sigma_1 & 0 \\ 0 & \mathbf{y}_\perp{}^T(-s) G_e(s) \mathbf{x}_\perp(-s) \end{bmatrix} \right\|_\infty \end{aligned}$$

where $\mathbf{y}_\perp{}^T(-s)G_e(s)\mathbf{x}_\perp(-s)$ defines the dimensionally-reduced system. At this point, it is necessary to introduce superscripts to identify the quantities gener-

ated during each iteration of the super-optimal algorithm. Hence, if the iteration count begins at zero, all of the quantities above would have the superscript zero (i.e. $G_e(s)$ becomes $G_e^{(0)}(s)$). Using this convention, the dimensionally-reduced system (or *projection*) generated during the $(i-1)^{\text{th}}$ iteration is denoted $\left[\mathbf{y}_\perp{}^{T\,(i-1)}(-s)G_e^{(i-1)}(s)\mathbf{x}_\perp{}^{(i-1)}(-s)\right]$. In order to prepare for the next iteration (i.e. the $(i)^{\text{th}}$ iteration), this projection is split into stable and antistable parts labelled $G^{(i)}$ and $Q^{(i)}$, respectively. These are given as

$$G^{(i)}(s) = \left[\mathbf{y}_\perp{}^{T\,(i-1)}(-s)G_e^{(i-1)}(s)\mathbf{x}_\perp{}^{(i-1)}(-s)\right]_+ \in RH_+^\infty \tag{6.22}$$

$$Q^{(i)}(s) = \left[\mathbf{y}_\perp{}^{T\,(i-1)}(-s)G_e^{(i-1)}(s)\mathbf{x}_\perp{}^{(i-1)}(-s)\right]_- \in RH_-^\infty \tag{6.23}$$

Subsequently, the Central Glover Solution is employed to generate an antistable approximation $F^{(i)}(s)$ to the stable component $G^{(i)}(s)$. Finally, the antistable component $Q^{(i)}(s)$ must be added to the approximation $F^{(i)}(s)$ and subsequently multiplied by the complementary maximizing vectors of previous iterations to form the intermediate super-optimal solution $F_{so}^{(i)}(s)$ at this stage.

This description of super-optimality lays the groundwork for the presentation in the subsequent sections which, for the special case studied in Section 6.3, results in $Q^{(i)}(s) = 0$ and, for the more general case studied in the next chapter, results in the minimal number of states contained in $Q^{(i)}(s)$. Before discussing these results further, a characterization of the degrees of freedom contained in the Central Glover Solution is in order.

Lemma 6.2 (Central Glover Solution degrees of freedom)

The structure of U which satisfies $B_1 = -C_1^T U$ of (6.5) and $U^T U \leq I$ of (6.6) may be written as:

$$U = (\hat{C}_1 \quad \hat{C}_1^{\perp}) \begin{pmatrix} 1 & 0 \\ 0 & \mathbf{P} \end{pmatrix} \begin{pmatrix} -\hat{B}_1 \\ \hat{B}_1^{\perp} \end{pmatrix} \tag{6.24}$$

where $\hat{B}_1 = B_1/\|B_1\| \quad \hat{B}_1^{\perp}\hat{B}_1^T = 0 \quad \hat{B}_1^{\perp}\hat{B}_1^{\perp T} = I \quad \|\mathbf{P}\| \leq 1$

$\hat{C}_1 = C_1/\|C_1\| \quad \hat{C}_1^{\perp T}\hat{C}_1 = 0 \quad \hat{C}_1^{\perp T}\hat{C}_1^{\perp} = I$

Proof: (See Appendix 6A.)

The parameter $\mathbf{P}$ of (6.24) completely characterizes the degrees of freedom contained within the Central Glover Solution. Observe that by setting $\mathbf{P} = 0$, the matrix U_o of [Glover, 1984] (Corollary 7.3) is obtained. The following restatement of the Central Glover Solution clearly exposes the way in which the free parameter $\mathbf{P}$ threads through the state-space formulae.

$$\tilde{A} = \Gamma^{-1}(\mathbf{A} - \sigma_1 \mathbf{C}^T \mathbf{P} \mathbf{B}) \tag{6.25}$$

$$\tilde{B} = \Gamma^{-1}(\Sigma_2 B_2 - \sigma_1 C_2^T \hat{C}_1 \hat{B}_1 + \sigma_1 \mathbf{C}^T \mathbf{P} \hat{B}_1^{\perp}) \tag{6.26}$$

$$= (\tfrac{1}{\beta} A_{12}^T \quad \Gamma^{-1}(\sigma_1 \mathbf{C}^T \mathbf{P} + \Sigma_2 \mathbf{B}^T)) \begin{pmatrix} -\hat{B}_1 \\ \hat{B}_1^{\perp} \end{pmatrix} \tag{6.27}$$

$$\tilde{C} = C_2 \Sigma_2 - \sigma_1 \hat{C}_1 \hat{B}_1 B_2^T + \sigma_1 \hat{C}_1^{\perp} \mathbf{P} \mathbf{B} \tag{6.28}$$

$$= (\hat{C}_1 \quad \hat{C}_1^{\perp}) \begin{pmatrix} -\frac{1}{\beta} A_{21}^T \Gamma \\ \sigma_1 \mathbf{P} \mathbf{B} + \mathbf{C} \Sigma_2 \end{pmatrix} \tag{6.29}$$

$$\tilde{D} = D + \sigma_1 \hat{C}_1 \hat{B}_1 - \sigma_1 \hat{C}_1^{\perp} \mathbf{P} \hat{B}_1^{\perp} \tag{6.30}$$

$$= D - (\hat{C}_1 \quad \hat{C}_1^{\perp}) \begin{pmatrix} \sigma_1 & 0 \\ 0 & \sigma_1 \mathbf{P} \end{pmatrix} \begin{pmatrix} -\hat{B}_1 \\ \hat{B}_1^{\perp} \end{pmatrix} \tag{6.31}$$

where

$$\mathbf{A} = \sigma_1^2 A_{22}^T + \Sigma_2 A_{22} \Sigma_2 + \sigma_1 C_2^T \hat{C}_1 \hat{B}_1 B_2^T \qquad (n-1) \times (n-1) \tag{6.32}$$

$$\mathbf{B} = \hat{B}_1^{\perp} B_2^T \qquad (m-1) \times (n-1) \tag{6.33}$$

$$\mathbf{C} = \hat{C}_1^{\perp T} C_2 \qquad (m-1) \times (n-1) \tag{6.34}$$

$$\beta = \|B_1\| = \|C_1\| = \sqrt{-2a_{11}\sigma_1} \tag{6.35}$$

Here, m and n are the number of inputs/outputs and states, respectively, in G and the hat ($\hat{}$) represents quantities which have been normalized to have unit norm. Clearly, $\mathbf{A}$ represents the components of the Central Glover Solution state matrix $\tilde{A}$ which do not multiply the parameter $\mathbf{P}$. Moreover, because $\mathbf{B}$ and $\mathbf{C}$ directly multiply $\mathbf{P}$, they will play an increasingly important role in accessing the degrees of freedom contained within $\mathbf{P}$. Before accessing these degrees of freedom however, the definitions above will first be employed to show that the Hankel singular values Σ_2 satisfy the Riccati equations given in the following lemma.

Lemma 6.3 (Hankel singular value property)
Let $G(s)$ be a stable transfer function matrix and let $\Sigma_2 = \text{diag}\{\sigma_2, \ldots, \sigma_n\}$ where $\sigma_1 > \sigma_2 \geq \ldots \geq \sigma_n > 0$ are the Hankel singular values of $G(s)$. The Hankel singular values Σ_2 satisfy the following Riccati equations:

$$(i) \quad \Sigma_2\mathbf{A}^T + \mathbf{A}\Sigma_2 + \Sigma_2\mathbf{B}^T\mathbf{B}\Sigma_2 + \sigma_1^2\mathbf{C}^T\mathbf{C} + \frac{1}{\beta^2}\Gamma A_{12}^T A_{12}\Gamma = 0 \qquad (6.36)$$

$$(ii) \quad \Sigma_2\mathbf{A} + \mathbf{A}^T\Sigma_2 + \Sigma_2\mathbf{C}^T\mathbf{C}\Sigma_2 + \sigma_1^2\mathbf{B}^T\mathbf{B} + \frac{1}{\beta^2}\Gamma A_{21} A_{21}^T\Gamma = 0 \qquad (6.37)$$

where $\mathbf{A}$, $\mathbf{B}$, $\mathbf{C}$, and β are given by (6.32) through (6.35).

Proof: (Appendix 6A.)

6.3 Using the degrees of freedom in the square case

The structure of matrix U given by (6.24) clearly exposes the Central Glover Solution degrees of freedom in terms of the parameter $\mathbf{P}$ and here, the degrees of freedom are given up in order to attain desirable properties in the Central Glover Solution. This chapter focuses on the special class of stable transfer function matrices $G(s)$ in which the number of states equals the number of inputs and outputs (i.e. when $n = m = p$ and B and C full rank), hereafter referred to as the *square case*. The reasoning for this is twofold: first, the presentation of the state-space algebra is unhindered by

discussions of nullity and second, the desirable Central Glover Solution properties such as error system singular value flatness and stable complementary maximizing vector projections are most clearly seen in this case. Initially the simplest, nontrivial square case is explored; this case contains two states, two inputs, and two outputs. For this simple case, super-optimality may be obtained in the context of the Central Glover Solution by solving a *simple* quadratic equation involving the free parameter $\mathbf{P}$. To illustrate the strength of this result, an example studied previously in [Young, 1986a; Tsai et al., 1988] will be employed.

6.3.1 Two-state square case

The two-state square case has two inputs and two outputs and constitutes the simplest of transfer function matrices which possess a degree of freedom within the Central Glover Solution. In particular, for this case, both the free parameter $\mathbf{P}$ and the approximation system state matrix $\tilde{A}$ are scalars. Moreover, for this simple case, the second singular value of the error system is only a function of frequency ω and the parameter $\mathbf{P}$. Since a super-optimal solution of order 1 is known to exist and be unique [Limebeer et al., 1989], the value of the parameter $\mathbf{P}$ (for $\|\mathbf{P}\| < 1$) which makes the second singular value of the error system flat will also define the unique super-optimal solution; i.e. for this case total flatness defines super-optimality [c.f. (6B.3)].

Theorem 6.1 (Quadratic super-optimality)

For the condition $\|\mathbf{P}\| \leq 1$ in the two-state square case, the values of the parameter $\mathbf{P}$ which attain total flatness of the error system singular values are given by either $\mathbf{P} = \pm 1$ or $\mathbf{P} = \mathbf{P}_{so}$ where $\mathbf{P}_{so}$ is given by:

$$\mathbf{P}_{so} = (\sigma_1 \mathbf{BC})^{-1} \left(\mathbf{A} + \sqrt{\mathbf{A}^2 - (\sigma_1 \mathbf{BC})^2} \right) \tag{6.38}$$

Additionally, $\mathbf{A}, \mathbf{B}$, and $\mathbf{C}$ are defined in (6.32) through (6.34) and are all scalars. Furthermore, $\mathbf{P}_{so}$ is the value of the parameter $\mathbf{P}$ which yields the super-optimal error system whereas the values of $\mathbf{P} = \pm 1$ yield an error system which is all-pass.

The two s-numbers of the super-optimal error system are given by:

$$s_1^{\infty} = \sigma_1 \qquad s_2^{\infty} = \sigma_1 |\mathbf{P}_{so}| \tag{6.39}$$

Proof: (See Appendix 6B.)

Remark 6.1 Note that an inspection of (6.25) together with the facts that $\tilde{A} > 0$ and $|\mathbf{P}| \leq 1$ imply that the discriminant of (6.38) satifies $\mathbf{A}^2 - (\sigma_1 \mathbf{BC})^2 > 0$ so that the parameter $\mathbf{P}_{so}$ is always real.

The following result is an immediate consequence of the definitions of the controllability and observability gramians of the approximation system (i.e. of $F(s)$).

Corollary 6.1 (2-state approximation gramian stationarity)
Under the condition that the Hankel singular values $\{\sigma_1, \sigma_2\}$ of $G(s)$ are distinct, the controllability and observability gramians $\tilde{X}$, $\tilde{Y}$ of the approximation system $F(s)$, as well as their product $\tilde{X}\tilde{Y}$, each have two stationary points with respect to the parameter $\mathbf{P}$ corresponding to the two roots of the following quadratic equation:

$$\mathbf{P}^2 - \mathbf{P}\left(\frac{2\mathbf{A}}{\sigma_1 \mathbf{BC}}\right) + 1 = 0 \tag{6.40}$$

The root $\mathbf{P}_{so}$ given in (6.38) of Theorem 6.1 defines the unique minimum of the negative approximation system gramians $-\tilde{X}$ and $-\tilde{Y}$ as well as their product $\tilde{X}\tilde{Y}$.

Proof: (See Appendix 6B.)

Thus for the simple 2-state square case, the stationary condition for $\tilde{X}$ and $\tilde{Y}$ defines the value of the parameter $\mathbf{P}$ which yields total flatness of the error system singular values. In the next section, it will be shown that this observation carries over to the general square case. First, it is interesting to record the observation below:

Corollary 6.2 (Error system gramian trace stationarity)

For the 2-state square case, the product of the error system controllability and observability gramians defined by (6.16) assumes the form:

$$X_e Y_e = \begin{pmatrix} \sigma_1^2 & 0 & 0 \\ 0 & \sigma_1^2 I & \tilde{Y} - \Sigma_2 \Gamma \\ 0 & \Sigma_2 - \tilde{X}\Gamma & \tilde{X}\tilde{Y} - \Gamma \end{pmatrix} \tag{6.41}$$

and clearly one of its eigenvalues is σ_1^2. Furthermore, the parameter $\mathbf{P}_{so}$ given in (6.38) of Theorem 6.1 defines the global minimum of the trace of $X_e Y_e$.

Proof: (See Appendix 6B.)

It has been shown [Moore, 1981; Wicks and DeCarlo, 1990] that the eigenvalues of the product of the controllability and observability gramians are indicators of energy dissipation in particular directions, hence, the maximum eigenvalue bounds the maximum energy dissipation in any direction. It is interesting therefore to note from Theorem 6.1 and its Corollaries that the super-optimal parameter $\mathbf{P}_{so}$ emerges as the solution which minimizes the product of the approximation system gramians $\tilde{X}\tilde{Y}$ (and hence its eigenvalue, given that both $\tilde{X}$ and $\tilde{Y}$ are scalar) and also as the solution that minimizes the sum of the eigenvalues of $X_e Y_e$.

In addition to minimizing the product of the approximation gramians for the two-state square case, Theorem 6.1 permits the *a priori* characterization of the super-optimal Hankel approximation $F_{so}(s) = \left[\begin{array}{c|c} \tilde{A}_{so} & \tilde{B}_{so} \\ \hline \tilde{C}_{so} & \tilde{D}_{so} \end{array}\right]$ in terms of the known stable transfer function $G(s) = \left[\begin{array}{c|c} A & B \\ \hline C & D \end{array}\right]$ and $\mathbf{P}_{so}$. For example, substituting the super-optimal value of $\mathbf{P}_{so}$ given by (6.38) into (6.25) reveals that the H^∞ optimal eigenvalue $\tilde{A}$ becomes the H^∞ super-optimal eigenvalue $\tilde{A}_{so} = -\Gamma^{-1}\sqrt{\mathbf{A}^2 - (\sigma_1 \mathbf{BC})^2}$. The strength and simplicity of the result encapsulated in Theorem 6.1 is illustrated below.

Example 6.1 The example studied in [Young, 1986a; Tsai et al., 1988] is a two-state square system with stable transfer function $G(s)$ given by the following minimal balanced realization

$$G(s) \doteq \left[\begin{array}{cc|c} a_{11} & A_{12} & B_1 \\ A_{21} & A_{22} & B_2 \\ \hline C_1 & C_2 & D \end{array}\right] = \left[\begin{array}{cc|cc} -1.6928 & -0.5422 & -3.3737 & -0.5886 \\ 0.8853 & -0.3072 & 0.5506 & 0.7521 \\ \hline -3.2160 & 0.1425 & -3.7321 & -1.0000 \\ -1.1171 & -0.9212 & -3.7321 & 1.0000 \end{array}\right]$$

The corresponding Hankel singular values and the parameters of Theorem 6.1 which are independent of $\mathbf{P}$ are given as

$$\{\sigma_1, \Sigma_2\} = \{3.4641, 1.4142\} \qquad \mathbf{A} = -4.7262 \qquad \mathbf{B} = -0.6463 \qquad \mathbf{C} = 0.9140$$

Computing the two roots of Equation (6.40) and taking the root which satisfies $\|\mathbf{P}\| \leq 1$ yields the super-optimal value of the parameter $\mathbf{P}$ together with the corresponding matrix U as

$$\mathbf{P}_{so} = 0.2277 \qquad U = \begin{pmatrix} -0.9116 & -0.2385 \\ -0.3753 & 0.1516 \end{pmatrix}$$

The state-space representation of the super-optimal approximation $F_{so}(s) \in RH_+^\infty$ then follows from Lemma 6.1

$$F_{so}(s) = \left[\begin{array}{c|cc} 0.4260 & 0.1526 & 0.0462 \\ \hline 2.1588 & -0.5740 & -0.1738 \\ 1.6236 & -2.4318 & 0.4749 \end{array}\right]$$

and its associated s-numbers are $s_1^\infty = 3.4641$ and $s_2^\infty = \sigma_1|\mathbf{P}_{so}| = 0.7889$.

This simple example illustrates how characterizing the Central Glover Solution degrees of freedom and relinquishing them in an optimal fashion enables significant computational savings. In particular, the simple quadratic equation root given by (6.38), supplants previous super-optimal algorithmic requirements to compute two Riccati equations, compute two Central Glover Solutions, and implement subsequent minimal realization algorithms [Tsai et al., 1988].

6.3.2 n-state square case

Corollary 6.1 demonstrated that the results of Theorem 6.1 can be obtained by differentiating the product of the scalar approximation system controllability and observability gramians to find their corresponding stationary point. However, in larger dimensioned square cases, the approximation gramians are matrix valued and differentiation of their product quickly becomes cumbersome. Alternatively, each gramian may be differentiated and the following lemma generates the desired stationary conditions in terms of the free parameter $\mathbf{P}$.

Lemma 6.4 (Approximation gramian stationarity)
The necessary and sufficient conditions for the stationarity of the approximation controllability and observability gramians in terms of the free parameter $\mathbf{P}$ *are given by:*

$$\tilde{X}\mathbf{B}^T = \Gamma^{-1}\left(\sigma_1\mathbf{C}^T\mathbf{P}_{\tilde{X}} + \Sigma_2\mathbf{B}^T\right) \tag{6.42}$$

$$\mathbf{C}\Gamma^{-1}\tilde{Y} = \sigma_1\mathbf{P}_{\tilde{Y}}\mathbf{B} + \mathbf{C}\Sigma_2 \tag{6.43}$$

where $\mathbf{P}_{\tilde{X}}$ *and* $\mathbf{P}_{\tilde{Y}}$ *are associated with controllability and observability gramian stationarity, respectively.*

Proof: (See Appendix 6B.)

Lemma 6.4 provides motivation for not setting the parameter $\mathbf{P} = 0$ which might otherwise seem the natural choice. The next theorem builds on the stationary conditions of Lemma 6.4 by giving the corresponding solutions for the controllability and observability gramians in terms of their matrix Riccati equations.

Theorem 6.2 (Approximation gramian solutions)

The approximation system controllability and observability gramians $\tilde{X}$ and $\tilde{Y}$, respectively, may be obtained as the destabilizing solutions of the following Riccati equations:

$$\Gamma^{-1}\left(\mathbf{A}+\Sigma_2\mathbf{B}^T\mathbf{B}\right)\tilde{X}+\tilde{X}\left(\mathbf{A}^T+\mathbf{B}^T\mathbf{B}\Sigma_2\right)\Gamma^{-1}-\tilde{X}\mathbf{B}^T\mathbf{B}\tilde{X}+\frac{1}{\beta^2}A_{12}^TA_{12} = 0 \quad (6.44)$$

$$\left(\mathbf{A}^T+\Sigma_2\mathbf{C}^T\mathbf{C}\right)\Gamma^{-1}\tilde{Y}+\tilde{Y}\Gamma^{-1}\left(\mathbf{A}+\mathbf{C}^T\mathbf{C}\Sigma_2\right)-\tilde{Y}\Gamma^{-1}\mathbf{C}^T\mathbf{C}\Gamma^{-1}\tilde{Y}+\frac{1}{\beta^2}\Gamma A_{21}A_{21}^T\Gamma = 0 \quad (6.45)$$

Moreover, if $\mathbf{B}$ *and* $\mathbf{C}$ *are square and nonsingular, then the degrees of freedom* $\mathbf{P}_{\tilde{X}}$ *and* $\mathbf{P}_{\tilde{Y}}$ *may be obtained from the gramians* $\tilde{X}$ *and* $\tilde{Y}$ *as:*

$$\mathbf{P}_{\tilde{X}} = \frac{1}{\sigma_1}\mathbf{C}^{T^{-1}}\Gamma\left(\tilde{X}-\Sigma_2\Gamma^{-1}\right)\mathbf{B}^T \quad (6.46)$$

$$\mathbf{P}_{\tilde{Y}} = \frac{1}{\sigma_1}\mathbf{C}\Gamma^{-1}\left(\tilde{Y}-\Sigma_2\Gamma\right)\mathbf{B}^{-1} \quad (6.47)$$

Proof: (See Appendix 6B.)

Note that $\tilde{X}$ and $\tilde{Y}$ are computed using their respective destabilizing Riccati solutions because they correspond to the antistable approximation. For the square case, the symmetric Riccati equations (6.44) and (6.45) take on simpler forms which permit direct access to the free parameter $\mathbf{P}$. These are presented in the following corollary.

Corollary 6.3 (Nonsymmetric Riccati equations)

For the n−state square case, the parameters $\mathbf{P}_{\tilde{X}}$ *and* $\mathbf{P}_{\tilde{Y}}$ *which attain stationarity for the approximation system controllability and observability gramians* $\tilde{X}$ *and* $\tilde{Y}$*, respectively, may be obtained as the destabilizing solution of the following nonsymmetric Riccati equations:*

$$(i) \quad \mathbf{A}_{\mathbf{C}}^T\mathbf{P}_{\tilde{X}}+\mathbf{P}_{\tilde{X}}\mathbf{A}_{\mathbf{B}}^T-\mathbf{P}_{\tilde{X}}\mathbf{R}\mathbf{P}_{\tilde{X}}-\mathbf{R}^T=0 \quad (6.48)$$

$$(ii) \quad \mathbf{A}_{\mathbf{C}}\mathbf{P}_{\tilde{Y}}+\mathbf{P}_{\tilde{Y}}\mathbf{A}_{\mathbf{B}}-\mathbf{P}_{\tilde{Y}}\mathbf{R}\mathbf{P}_{\tilde{Y}}-\mathbf{R}^T=0 \quad (6.49)$$

where $\mathbf{A_B} = \mathbf{B}\Gamma^{-1}\mathbf{A}\mathbf{B}^{-1}$ $\mathbf{A_C} = \mathbf{C}\Gamma^{-1}\mathbf{A}^T\mathbf{C}^{-1}$ $\mathbf{R} = \sigma_1\mathbf{B}\Gamma^{-1}\mathbf{C}^T$

Proof: (See Appendix 6B.)

Observe that for the two-state square case, both nonsymmetric Riccati equations of Corollary 6.3 can be simplified to yield the quadratic form given in (6.40) and thus, Corollary 6.3 can be viewed as the direct matrix extension of the quadratic equation associated with Theorem 6.1. In addition, although Corollary 6.3 states that two Riccati equations must be solved, only one Hamiltonian matrix must be constructed as follows. Consider the matrix H given by:

$$H = \begin{pmatrix} \mathbf{A_B} & -\mathbf{R} \\ \mathbf{R}^T & -\mathbf{A_C} \end{pmatrix}$$

and the similarity transformation T given by:

$$T = \begin{pmatrix} \sigma_1\mathbf{B} & 0 \\ 0 & \mathbf{C}\Gamma^{-1} \end{pmatrix}$$

Then, application of similarity transformation T to H yields:

$$T^{-1}HT = \begin{pmatrix} \Gamma^{-1}\mathbf{A} & -\Gamma^{-1}\mathbf{C}^T\mathbf{C}\Gamma^{-1} \\ \sigma_1^2\mathbf{B}^T\mathbf{B} & -\mathbf{A}^T\Gamma^{-1} \end{pmatrix}$$

which is Hamiltonian. Hence we can write the spectral decomposition of H as [Potter, 1966; Mårtensson, 1971]:

$$H = \begin{pmatrix} \mathbf{A_B} & -\mathbf{R} \\ \mathbf{R}^T & -\mathbf{A_C} \end{pmatrix} = \begin{pmatrix} W_{11} & W_{12} \\ W_{21} & W_{22} \end{pmatrix} \begin{pmatrix} -\Lambda & 0 \\ 0 & \Lambda \end{pmatrix} \begin{pmatrix} W_{11} & W_{12} \\ W_{21} & W_{22} \end{pmatrix}^{-1}$$

where the product on the right hand side describes the spectral decomposition of H suitably partitioned so that all of the strictly positive eigenvalues are in Λ. Then, the parameters $\mathbf{P}_{\hat{X}}$ and $\mathbf{P}_{\hat{Y}}$ may be obtained as

$$\mathbf{P}_{\hat{X}} = \left(W_{11}W_{21}^{-1}\right)^T \quad \text{and} \quad \mathbf{P}_{\hat{Y}} = W_{22}W_{12}^{-1}$$

The two different approximations $F_{\hat{X}}(s)$ and $F_{\hat{Y}}(s)$ based on the two Central Glover Solutions using the parameters $\mathbf{P}_{\hat{X}}$ and $\mathbf{P}_{\hat{Y}}$ of Theorem 6.2, respectively, are

given as

$$F_{\tilde{X}}(s) = \left[\begin{array}{c|c} \tilde{A}_{\tilde{X}} & \tilde{B}_{\tilde{X}} \\ \hline \tilde{C}_{\tilde{X}} & \tilde{D}_{\tilde{X}} \end{array}\right]$$
$$= \begin{pmatrix} \hat{C}_1 & \hat{C}_1^{\perp} \end{pmatrix} \left[\begin{array}{c|cc} \Gamma^{-1}\left(\mathbf{A}-\Gamma\left(\tilde{X}-\Sigma_2\Gamma^{-1}\right)\mathbf{B}^T\mathbf{B}\right) & \frac{1}{\beta}A_{12}^T & \tilde{X}\mathbf{B}^T \\ \hline -\frac{1}{\beta}A_{21}^T\Gamma & \sigma_1 & 0 \\ \sigma_1\mathbf{P}_{\tilde{X}}\mathbf{B}+\mathbf{C}\Sigma_2 & 0 & \sigma_1\mathbf{P}_{\tilde{X}} \end{array}\right] \begin{pmatrix} -\hat{B}_1 \\ \hat{B}_1^{\perp} \end{pmatrix} \tag{6.50}$$

$$F_{\tilde{Y}}(s) = \left[\begin{array}{c|c} \tilde{A}_{\tilde{Y}} & \tilde{B}_{\tilde{Y}} \\ \hline \tilde{C}_{\tilde{Y}} & \tilde{D}_{\tilde{Y}} \end{array}\right]$$
$$= \begin{pmatrix} \hat{C}_1 & \hat{C}_1^{\perp} \end{pmatrix} \left[\begin{array}{c|cc} \Gamma^{-1}\left(\mathbf{A}-\mathbf{C}^T\mathbf{C}\Gamma^{-1}\left(\tilde{Y}-\Sigma_2\Gamma\right)\right) & \frac{1}{\beta}A_{12}^T & \Gamma^{-1}\left(\sigma_1\mathbf{C}^T\mathbf{P}_{\tilde{Y}}+\Sigma_2\mathbf{B}^T\right) \\ \hline -\frac{1}{\beta}A_{21}^T\Gamma & \sigma_1 & 0 \\ \mathbf{C}\Gamma^{-1}\tilde{Y} & 0 & \sigma_1\mathbf{P}_{\tilde{Y}} \end{array}\right] \begin{pmatrix} -\hat{B}_1 \\ \hat{B}_1^{\perp} \end{pmatrix} \tag{6.51}$$

where (6.42) and (6.43) have been used in concert with (6.25) through (6.29) in defining $(\tilde{A}_{\tilde{X}}, \tilde{B}_{\tilde{X}})$ and $(\tilde{A}_{\tilde{Y}}, \tilde{C}_{\tilde{Y}})$ respectively. Additionally, $\begin{pmatrix} \hat{C}_1 & \hat{C}_1^{\perp} \end{pmatrix}$ and $\begin{pmatrix} -\hat{B}_1 \\ \hat{B}_1^{\perp} \end{pmatrix}$ have been pulled out on either side to expose the internal dynamics.

Equipped with the approximation gramian solutions given by Theorem 6.2, it will be shown how these may be used to construct maximizing vectors. Although state-space representations for maximizing vectors have been given previously in [Tsai et al., 1988; Limebeer et al., 1989], the constructions given below show how to choose the unique parameters $\mathbf{P}_{\tilde{X}}$, $\mathbf{P}_{\tilde{Y}}$ and the associated unique Central Glover Solutions which each produce an entirely stable projection. As will be shown in the square case, either of these approximations given by (6.50) or (6.51) may be used to construct an error system which is *matched* respectively to either the right or left maximizing vector. Here "matched" means that the error system constructed using $F_{\tilde{X}}(s)$ will have the same controllability pair $(\tilde{A}_{\tilde{X}}, \tilde{B}_{\tilde{X}})$ as the right maximizing vector while the error system based on $F_{\tilde{Y}}(s)$ will have the same observability pair

$(\tilde{A}_{\tilde{Y}}, \tilde{C}_{\tilde{Y}})$ as the left maximizing vector. This can be seen clearly in the next lemma which defines the maximizing vectors and relates them to the approximation systems $F_{\tilde{X}}(s)$ and $F_{\tilde{Y}}(s)$.

Lemma 6.5 (Maximizing vectors)

The unique, inner left and right maximizing vectors, labelled $\mathbf{x}^T(s)$ *and* $\mathbf{y}(s)$ *respectively, are given by*

$$\mathbf{x}^T(s) = \left[\begin{array}{c|c} \overline{A}_{\tilde{X}} & \overline{B}_{\tilde{X}} \\ \hline -\hat{B}_1\overline{B}_{\tilde{X}}^T\tilde{X}^{-1} & \hat{B}_1 \end{array}\right] = \left[\begin{array}{c|c} \overline{A}_{\tilde{X}} & \overline{B}_{\tilde{X}} \\ \hline -\frac{1}{\beta}A_{12}\tilde{X}^{-1} & \hat{B}_1 \end{array}\right] \tag{6.52}$$

$$\mathbf{y}(s) = \left[\begin{array}{c|c} \overline{A}_{\tilde{Y}} & -\tilde{Y}^{-1}\overline{C}_{\tilde{Y}}^T\hat{C}_1 \\ \hline \overline{C}_{\tilde{Y}} & \hat{C}_1 \end{array}\right] = \left[\begin{array}{c|c} \overline{A}_{\tilde{Y}} & \frac{1}{\beta}\tilde{Y}^{-1}\Gamma A_{21} \\ \hline \overline{C}_{\tilde{Y}} & \hat{C}_1 \end{array}\right] \tag{6.53}$$

where the controllability and observability pairs $(\overline{A}_{\tilde{X}}, \overline{B}_{\tilde{X}})$ *and* $(\overline{A}_{\tilde{Y}}, \overline{C}_{\tilde{Y}})$ *are given by*

$$\overline{A}_{\tilde{X}} = \Gamma^{-1}\left(\mathbf{A} - \Gamma\left(\tilde{X} - \Sigma_2\Gamma^{-1}\right)\mathbf{B}^T\mathbf{B}\right) \tag{6.54}$$

$$\overline{B}_{\tilde{X}} = \left(\frac{1}{\beta}A_{12}^T \quad \tilde{X}\mathbf{B}^T\right)\begin{pmatrix} -\hat{B}_1 \\ \hat{B}_1^{\perp} \end{pmatrix} \tag{6.55}$$

$$\overline{A}_{\tilde{Y}} = \Gamma^{-1}\left(\mathbf{A} - \mathbf{C}^T\mathbf{C}\Gamma^{-1}\left(\tilde{Y} - \Sigma_2\Gamma\right)\right) \tag{6.56}$$

$$\overline{C}_{\tilde{Y}} = \left(\hat{C}_1 \quad \hat{C}_1^{\perp}\right)\begin{pmatrix} -\frac{1}{\beta}A_{21}^T\Gamma \\ \mathbf{C}\Gamma^{-1}\tilde{Y} \end{pmatrix} \tag{6.57}$$

$\tilde{X}$ is the approximation system controllability gramian given by (6.17), $\tilde{Y}$ is the approximation system observability gramian given by (6.18), and β is a scalar given by (6.35). Moreover, for the $n-$state square case,

$$(\overline{A}_{\tilde{X}}, \overline{B}_{\tilde{X}}) = (\tilde{A}_{\tilde{X}}, \tilde{B}_{\tilde{X}}) \quad \text{and} \quad (\overline{A}_{\tilde{Y}}, \overline{C}_{\tilde{Y}}) = (\tilde{A}_{\tilde{Y}}, \tilde{C}_{\tilde{Y}}) \tag{6.58}$$

Proof: (See Appendix 6B.)

Although the controllability and observability pairs are interchangeable for the square case, they are not so in general and to maintain a clear delineation between the maximizing vectors and the approximation systems, the maximizing vectors will have an associated overbar while the approximation systems will continue to have an associated tilde. Indeed, the maximizing vectors of Lemma 6.5 apply to the most general systems as do their complementary parts given in the following lemma.

Lemma 6.6 (Complementary maximizing vectors)

Given the maximizing vectors of Lemma 6.5, the complementary inner parts are given by

$$\mathbf{x}_\perp{}^T(s) = \left[\begin{array}{c|c} \overline{A}_{\tilde{X}} & \overline{B}_{\tilde{X}} \\ \hline -\hat{B}_1^\perp \overline{B}_{\tilde{X}}^T \tilde{X}^{-1} & \hat{B}_1^\perp \end{array}\right] = \left[\begin{array}{c|c} \overline{A}_{\tilde{X}} & \overline{B}_{\tilde{X}} \\ \hline -\mathbf{B} & \hat{B}_1^\perp \end{array}\right] \tag{6.59}$$

$$\mathbf{y}_\perp(s) = \left[\begin{array}{c|c} \overline{A}_{\tilde{Y}} & -\tilde{Y}^{-1}\overline{C}_{\tilde{Y}}{}^T \hat{C}_1^\perp \\ \hline \overline{C}_{\tilde{Y}} & \hat{C}_1^\perp \end{array}\right] = \left[\begin{array}{c|c} \overline{A}_{\tilde{Y}} & -\Gamma^{-1}\mathbf{C}^T \\ \hline \overline{C}_{\tilde{Y}} & \hat{C}_1^\perp \end{array}\right] \tag{6.60}$$

where $\tilde{X}$ is the approximation system controllability gramian given by (6.17) and $\tilde{Y}$ is the approximation system observability gramian given by (6.18). Moreover, as with the maximizing vectors of Lemma 6.5 in the n−state square case, the complementary maximizing vectors have matched dynamics as given by (6.58).

Proof: (See Appendix 6B.)

Since maximizing vectors are unique [Young, 1983], the expressions above are simply alternative descriptions of those given previously in [Tsai et al., 1988; Limebeer et al., 1989]. However, the treatment given here differs in that the resulting maximizing vector state-space formulae are closely related to the Central Glover Solution state-space formulae and therefore, as presented below, facilitate both an understanding of the projection operation and lead to significant algorithmic simplifications. In particular, it will be shown how the state-space formulae for the maximizing vector complements $\mathbf{x}_\perp(s)$ and $\mathbf{y}_\perp(s)$ facilitate the determination of matching error systems which produce totally stable projections as outlined in the following theorem.

Theorem 6.3 (Totally stable projections)

For the n−state square case, the two unique error systems $G_{e_{\hat{X}}}(s)$ and $G_{e_{\hat{Y}}}(s)$ based on the approximations $F_{\hat{X}}(s) = \left[\begin{array}{c|c} \hat{A}_{\hat{X}} & \hat{B}_{\hat{X}} \\ \hline \hat{C}_{\hat{X}} & \hat{D}_{\hat{X}} \end{array}\right]$ and $F_{\hat{Y}}(s) = \left[\begin{array}{c|c} \hat{A}_{\hat{Y}} & \hat{B}_{\hat{Y}} \\ \hline \hat{C}_{\hat{Y}} & \hat{D}_{\hat{Y}} \end{array}\right]$ given by the solutions $\mathbf{P}_{\hat{X}}$ and $\mathbf{P}_{\hat{Y}}$ corresponding to (6.44) and (6.45), respectively, yield the following totally stable, dimensionally-reduced projections:

$$G_{\hat{X}}^{(1)}(s) = \mathbf{y}_{\perp}{}^{T\,(0)}(-s)G_{e_{\hat{X}}}^{(0)}(s)\mathbf{x}_{\perp}{}^{(0)}(-s) = \left[\begin{array}{c|c} -\overline{A}_{\hat{Y}}^{T} & -\sigma_1^2\mathbf{B}^T(I - \mathbf{P}_{\hat{Y}}{}^T\mathbf{P}_{\hat{X}}) \\ \hline \mathbf{C}\Gamma^{-1} & \sigma_1\mathbf{P}_{\hat{X}} \end{array}\right] \tag{6.61}$$

$$G_{\hat{Y}}^{(1)}(s) = \mathbf{y}_{\perp}{}^{T\,(0)}(-s)G_{e_{\hat{Y}}}^{(0)}(s)\mathbf{x}_{\perp}{}^{(0)}(-s) = \left[\begin{array}{c|c} -\overline{A}_{\hat{X}}^{T} & \mathbf{B}^T \\ \hline -\sigma_1^2(I - \mathbf{P}_{\hat{Y}}\mathbf{P}_{\hat{X}}{}^T)\mathbf{C}\Gamma^{-1} & \sigma_1\mathbf{P}_{\hat{Y}} \end{array}\right] \tag{6.62}$$

Proof: (See Appendix 6B.)

Not only does Theorem 6.3 confirm the stable projection property of the uniquely matched error systems $G_{e_{\hat{X}}}(s)$ and $G_{e_{\hat{Y}}}(s)$, but it also yields fewer computations in super-optimal algorithms as they would apply to square systems. First, the use of either projection of Theorem 6.3 obviates the need to multiply the error system by the complementary maximizing vectors and subsequently separate the product into stable and antistable components since the projections given are both stable and minimal. Furthermore, the minimality of these stable projections alleviates the computationally burdensome chore of determining minimal realizations of the projected systems. Finally, the stable projection property of Theorem 6.3 in concert with the quadratic super-optimality result of Theorem 6.1 implies that super-optimality may be achieved with one less Central Glover Solution iteration than required by previous algorithms. These results are contained in the following super-optimal algorithm:

Super-optimal Algorithm I (Square Case):
Given a stable n−state transfer function matrix $G^{(0)}(s)$, find the super-optimal extension $F_{so}(s)$. In the following, superscripts are used to represent the iteration value.

Step 1. Initialization:

a. Compute $\mathbf{P}_{\tilde{X}}$ and $\mathbf{P}_{\tilde{Y}}$ in accordance with Theorem 6.2.

b. Construct the matched Central Glover Solution $F_l^{(0)}(s)$ using either (6.50) or (6.51) where the subscript "l" identifies which of the two approximation systems will be constructed according to the following rule:

$$l = \begin{cases} \tilde{X} & \text{if} \quad \|\mathbf{P}_{\tilde{X}}\| \leq \|\mathbf{P}_{\tilde{Y}}\| \\ \tilde{Y} & \text{if} \quad \|\mathbf{P}_{\tilde{X}}\| > \|\mathbf{P}_{\tilde{Y}}\| \end{cases}$$

c. Construct the totally stable projection $G_l^{(1)}(s)$ using Theorem 6.3.

d. Calculate and save the complementary maximizing vectors $\mathbf{x}_\perp{}^{T\ (0)}(s)$ and $\mathbf{y}_\perp{}^{(0)}(s)$ using Lemma 6.6.

e. Set $F_{so}^{(0)}(s) = F_l^{(0)}(s)$.

Step 2. Iteration: for $i = 1$ to $n-3$ do the following:

a. For each iteration, compute the matched Central Glover Solution, the complementary maximizing vectors, and the corresponding totally stable projection similar to above.

b. Accumulate the super-optimal extension as:

$$F_{so}^{(i)}(s) = F_{so}^{(i-1)}(s) + \left[\prod_{j=0}^{i-1} \mathbf{y}_\perp{}^{(j)}(s)\right] F_l^{(i)}(s) \left[\prod_{k=i-1}^{0} \mathbf{x}_\perp{}^{T\ (k)}(s)\right]$$

Step 3. Completion:

a. Construct the approximation $F_l^{(n-2)}(s)$ based on the quadratic parameter $\mathbf{P}_{so}$ given in Theorem 6.1.

b. Complete the overall super-optimal extension as:

$$F_{so}(s) = F_{so}^{(n-3)}(s) + \left[\prod_{j=0}^{n-3} \mathbf{y}_\perp{}^{(j)}(s)\right] F_l^{(n-2)}(s) \left[\prod_{k=n-3}^{0} \mathbf{x}_\perp{}^{T\ (k)}(s)\right]$$

The totally stable projection property of Theorem 6.3 allowed the development of the previous super-optimal algorithm and, although this algorithm takes advantage of the stable projection property, further progress can be made in reducing the state

inflation of the super-optimal solution. To see how further reduction results, consider the following expansion of the super-optimal solution:

$$\begin{aligned} F_{so}(s) = F^{(0)}(s) \\ &+ \mathbf{y}_\perp{}^{(0)}(s)\, F^{(1)}(s)\, \mathbf{x}_\perp{}^{T\,(0)}(s) \\ &+ \mathbf{y}_\perp{}^{(0)}(s)\, \mathbf{y}_\perp{}^{(1)}(s)\, F^{(2)}(s)\, \mathbf{x}_\perp{}^{T\,(1)}(s)\, \mathbf{x}_\perp{}^{T\,(0)}(s) \\ &+ \cdots \\ &+ \mathbf{y}_\perp{}^{(0)}(s) \cdots \mathbf{y}_\perp{}^{(n-3)}(s)\, F^{(n-2)}(s)\, \mathbf{x}_\perp{}^{T\,(n-3)}(s) \cdots \mathbf{x}_\perp{}^{T\,(0)}(s) \end{aligned} \tag{6.63}$$

where n is the number of states in the square system $G(s)$. For notational convenience, the subscripts $\tilde{X}$ and $\tilde{Y}$ normally appended to the approximation system $F(s)$ have been dropped with the implicit understanding that the approximation system $F(s)$ is based on either $\mathbf{P}_{\tilde{X}}$ or $\mathbf{P}_{\tilde{Y}}$. Moreover, for increased notational compactness, momentarily drop the dependence on frequency, s, and rewrite the above as:

$$\begin{aligned} F_{so} &= F^{(0)} + \mathbf{y}_\perp{}^{(0)} \Big[F^{(1)} + \mathbf{y}_\perp{}^{(1)} \Big[\cdots \\ &\qquad \cdots [F^{(n-3)} + \mathbf{y}_\perp{}^{(n-3)} F^{(n-2)} \mathbf{x}_\perp{}^{T\,(n-3)}] \cdots \Big] \mathbf{x}_\perp{}^{T\,(1)} \Big] \mathbf{x}_\perp{}^{T\,(0)} \\ &= S^{(0)} \Big[S^{(1)} \Big[\cdots S^{(n-3)} \Big[F^{(n-2)} \Big] \cdots \Big] \Big] \end{aligned} \tag{6.64}$$

where $S^{(r)}[\,\cdot\,]$ is defined as:

$$S^{(r)}[\,\cdot\,] = F^{(r)}(s) + \mathbf{y}_\perp{}^{(r)}(s)\, [\,\cdot\,]\, \mathbf{x}_\perp{}^{T\,(r)}(s) \tag{6.65}$$

A recursion similar to (6.64) was defined previously in [Limebeer et al., 1989], however, the recursion defined by (6.64) requires one less iteration and there are *no* antistable terms. Clearly, the *core* term within the innermost square brackets fits a pattern which matches the outer layers of the recursion; hence, a minimal realization for the *core* term would greatly reduce the resulting state inflation in assembling the super-optimal solution. The next lemma gives such a minimal realization for the core term.

Lemma 6.7 (Core term minimal realization)

An expression for the minimal realization for the core term of (6.64) based on $F_{\tilde{Y}}(s)$ is given by:

$$S^{(r)}\left[F^{(r+1)}(s)\right] = \left[\begin{array}{cc|c} \overline{A}_{\tilde{Y}} & \overline{B}_{\tilde{Y}}\tilde{C}_{\tilde{Y}} & \overline{B}_{\tilde{Y}}\tilde{D}_{\tilde{Y}}\overline{D}_{\tilde{X}} + \tilde{B}_{\tilde{Y}}^{(r)} \\ 0 & \tilde{A}_{\tilde{Y}} & \tilde{B}_{\tilde{Y}}\overline{D}_{\tilde{X}} - T\overline{B}_{\tilde{X}} \\ \hline \overline{C}_{\tilde{Y}} & \overline{D}_{\tilde{Y}}\tilde{C}_{\tilde{Y}} & \overline{D}_{\tilde{Y}}\tilde{D}_{\tilde{Y}}\overline{D}_{\tilde{X}} + \tilde{D}_{\tilde{Y}}^{(r)} \end{array}\right] \tag{6.66}$$

where for notational convenience, $\overline{C}_{\tilde{X}}$, $\overline{D}_{\tilde{X}}$, $\overline{B}_{\tilde{Y}}$, and $\overline{D}_{\tilde{Y}}$ are implicitly defined by (6.59) and (6.60) as:

$$\overline{C}_{\tilde{X}} = -\mathbf{B} \qquad \text{and} \qquad \overline{D}_{\tilde{X}} = \hat{B}_1^{\perp} \tag{6.67}$$

$$\overline{B}_{\tilde{Y}} = -\Gamma^{-1}\mathbf{C}^T \qquad \text{and} \qquad \overline{D}_{\tilde{Y}} = \hat{C}_1^{\perp} \tag{6.68}$$

Moreover, all "overbarred" quantities in (6.66) are those associated with the complementary maximizing vectors at the $(r)^{\text{th}}$ iteration level, while the "tilded" quantities are those associated with the matched, projected approximation system at the $(r+1)$ iteration level; there are two notable exceptions, $\tilde{B}_{\tilde{Y}}^{(r)}$ and $\tilde{D}_{\tilde{Y}}^{(r)}$, associated with the $(r)^{\text{th}}$ iteration level and this is clearly indicated by the superscript. Finally, T solves the following Sylvester equation:

$$\tilde{A}_{\tilde{Y}}\, T - T\, \overline{A}_{\tilde{X}} + \tilde{B}_{\tilde{Y}}\, \overline{C}_{\tilde{X}} = 0 \tag{6.69}$$

Proof: (See Appendix 6B.)

Although Lemma 6.7 was based on $F_{\tilde{Y}}(s)$, an equally valid minimal core realization based on $F_{\tilde{X}}(s)$ results simply by exchanging the subscript $\tilde{Y}$ for $\tilde{X}$ in <u>all</u> "tilded" terms. An immediate consequence of Lemma 6.7 and (6.64) is that the total number of states in the super-optimal solution $n_{F_{so}(s)}$ is limited to be:

$$n_{F_{so}(s)} \leq \sum_{i=1}^{n_{G(s)}-1} i = \left(\frac{1}{2}\right) n_{G(s)}\left(n_{G(s)} - 1\right) \tag{6.70}$$

where $n_{G(s)}$ represents the number of states in $G(s)$. A further consequence of Lemma 6.7 is the simplified and efficient super-optimal algorithm presented below:

Super-optimal Algorithm II (Square Case):
Given a stable $n-$state $G^{(0)}(s)$, find the super-optimal extension $F_{so}(s)$. In the following, superscripts are used to represent the iteration value.

Step 1. Computation and Storage: for $i = 0$ to $n-2$ do the following:

a. Calculate and save the complementary maximizing vectors ${\mathbf{x}_\perp}^{T\,(i)}(s)$ and ${\mathbf{y}_\perp}^{(i)}(s)$.

b. Calculate and save $\tilde{B}_{\tilde{Y}}^{(i)}$ and $\tilde{D}_{\tilde{Y}}^{(i)}$.

Step 2. Core System Computation:

a. Compute $F_{\tilde{Y}}^{(n-2)}(s)$ using Theorem 6.1.

Step 3. Super-Optimal Assimilation: for $i = n-3$ down to 0 do the following:

a. Retrieve the complementary maximizing vectors ${\mathbf{x}_\perp}^{T\,(i)}(s)$ and ${\mathbf{y}_\perp}^{(i)}(s)$ from storage.

b. Retrieve $\tilde{B}_{\tilde{Y}}^{(i)}$ and $\tilde{D}_{\tilde{Y}}^{(i)}$ from storage.

c. Solve Sylvester equation (6.69) for T.

d. Form the system $S^{(i)}\left[F^{(i+1)}(s)\right]$ in accordance with Lemma 6.7.

Step 4. The super-optimal extension is given by $F_{so}(s) = S^{(0)}\left[F^{(1)}(s)\right]$.

Before demonstrating the efficacy of the above algorithm, the unusual singular value total flatness property associated with the matched error systems will be explored. With hindsight, it is seems quite remarkable that the matching property of $G_{\tilde{X}}(s)$ and $G_{\tilde{Y}}(s)$ also affords singular value total flatness over all frequencies. This singular value total flatness property, henceforth referred to as *total flatness*, differs from the normal definition of all-passness in that the both parahermitian forms $G_{e_{\tilde{X}}}^T(-s)G_{e_{\tilde{X}}}(s)$ and $G_{e_{\tilde{Y}}}(s)G_{e_{\tilde{Y}}}^T(-s)$ *do not* lose their dynamic components $[A_e, B_e, C_e]$ through either unobservability or uncontrollability. However, complete decoupling is achieved for the projected parahermitian forms ${\mathbf{x}_\perp}^T(s)G_{e_{\tilde{X}}}^T(-s)G_{e_{\tilde{X}}}(s)\mathbf{x}_\perp(-s)$ and ${\mathbf{y}_\perp}^T(-s)G_{e_{\tilde{Y}}}(s)G_{e_{\tilde{Y}}}^T(-s)\mathbf{y}_\perp(s)$; this property permits the proof of total flatness for the matched error systems $G_{e_{\tilde{X}}}(s)$ and $G_{e_{\tilde{Y}}}(s)$.

Theorem 6.4 (Singuiar value total flatness)

For the n−state square case, the error systems $G_{e_{\tilde{X}}}(s)$ *and* $G_{e_{\tilde{Y}}}(s)$ *based on the approximations* $F_{\tilde{X}}(s) = \left[\begin{array}{c|c} \tilde{A}_{\tilde{X}} & \tilde{B}_{\tilde{X}} \\ \hline \tilde{C}_{\tilde{X}} & \tilde{D}_{\tilde{X}} \end{array}\right]$ *and* $F_{\tilde{Y}}(s) = \left[\begin{array}{c|c} \tilde{A}_{\tilde{Y}} & \tilde{B}_{\tilde{Y}} \\ \hline \tilde{C}_{\tilde{Y}} & \tilde{D}_{\tilde{Y}} \end{array}\right]$ *given by the solutions* $\mathbf{P}_{\tilde{X}}$ *and* $\mathbf{P}_{\tilde{Y}}$ *corresponding to (6.46) and (6.47) respectively, have constant singular values given as*

$$\sigma_1\left[G_{e_{\tilde{X}}}(j\omega)\right] = \sigma_1, \quad \sigma_{(i+1)}\left[G_{e_{\tilde{X}}}(j\omega)\right] = \sigma_1 \cdot \sigma_i\left[\mathbf{P}_{\tilde{X}}\right] \quad \forall\,\omega, \quad \text{for i} = 1,\ldots,n-1 \tag{6.71}$$

$$\sigma_1\left[G_{e_{\tilde{Y}}}(j\omega)\right] = \sigma_1, \quad \sigma_{(i+1)}\left[G_{e_{\tilde{Y}}}(j\omega)\right] = \sigma_1 \cdot \sigma_i\left[\mathbf{P}_{\tilde{Y}}\right] \quad \forall\,\omega, \quad \text{for i} = 1,\ldots,n-1 \tag{6.72}$$

where $\sigma_k[G]$ *represents the* k^{th} *singular value of matrix* G.

Proof: (See Appendix 6B.)

Although the parameters $\mathbf{P}_{\tilde{X}}$ and $\mathbf{P}_{\tilde{Y}}$ impose total flatness on the matched error system singular values, the actual values of the singular values do not in general attain their super-optimal values with the notable exception of the two-state square case. For square systems with more than two states, the square case super-optimal algorithm uses the matched systems based on $\mathbf{P}_{\tilde{X}}$ and $\mathbf{P}_{\tilde{Y}}$ to further minimize the error system singular values. To illustrate this as well as the error system total flatness property, consider the following example studied previously in [Limebeer et al., 1989].

Example 6.2 The example given in [Limebeer et al., 1989] is a three-state square system given by stable transfer function $G^{(0)}(s)$ which has the following minimal realization:

$$G^{(0)}(s) = \left[\begin{array}{ccc|ccc} -1 & 1 & 0 & 1 & 2 & 0 \\ 0 & -2 & 0 & 1 & 1 & 1 \\ 0 & 0 & -3 & 2 & 2 & 1 \\ \hline 1 & -1 & 2 & 0 & 0 & 0 \\ 2 & 3 & 0 & 0 & 0 & 0 \\ 1 & -5 & -1 & 0 & 0 & 0 \end{array}\right]$$

with corresponding Hankel singular values:

$$\begin{pmatrix} \sigma_1 & 0 \\ 0 & \Sigma_2 \end{pmatrix} = \begin{pmatrix} 4.6925 & 0 & 0 \\ 0 & 1.4132 & 0 \\ 0 & 0 & 0.3097 \end{pmatrix}$$

The Central Glover Solution parameters of Theorem 6.2 are given as

$$\mathbf{A} = \begin{pmatrix} -0.3909 & -6.8279 \\ 1.3264 & -0.6070 \end{pmatrix}$$

$$\mathbf{B} = \begin{pmatrix} -0.9914 & -0.0613 \\ 1.2633 & -0.8364 \end{pmatrix}$$

$$\mathbf{C} = \begin{pmatrix} -0.5836 & -1.2291 \\ -2.0900 & 0.3614 \end{pmatrix}$$

Substitution of these values into (6.44) and (6.45) yields the approximation system gramians from which $\mathbf{P}_{\tilde{X}}$ and $\mathbf{P}_{\tilde{Y}}$ can be computed using Theorem 6.2 as

$$\mathbf{P}_{\tilde{X}} = \begin{pmatrix} -0.0387 & 0.0060 \\ -0.1300 & 0.1790 \end{pmatrix} \quad \text{and} \quad \|\mathbf{P}_{\tilde{X}}\| = 0.2230$$

$$\mathbf{P}_{\tilde{Y}} = \begin{pmatrix} -0.0299 & -0.0054 \\ -0.1272 & 0.1821 \end{pmatrix} \quad \text{and} \quad \|\mathbf{P}_{\tilde{Y}}\| = 0.2226$$

Since $\|\mathbf{P}_{\tilde{Y}}\| < \|\mathbf{P}_{\tilde{X}}\|$, parameter $\mathbf{P}_{\tilde{Y}}$ is used to construct the corresponding matrix U defined by (6.24) and given as

$$U_{\tilde{Y}} = \begin{pmatrix} -0.2465 & -0.3536 & -0.0598 \\ -0.4312 & -0.6365 & -0.2188 \\ 0.2802 & 0.2219 & 0.3070 \end{pmatrix}$$

The resulting Central Glover Solution is given by the following state-space description of $F_{\tilde{Y}}^{(0)}(s) \in RH_+^\infty$

$$F_{\tilde{Y}}^{(0)}(s) = \left[\begin{array}{c|c} \tilde{A}_{\tilde{Y}} & \tilde{B}_{\tilde{Y}} \\ \hline \tilde{C}_{\tilde{Y}} & \tilde{D}_{\tilde{Y}} \end{array}\right] \approx \left[\begin{array}{cc|ccc} 1.7746 & 0.4110 & 0.0340 & 0.0506 & 0.0200 \\ -0.0390 & 2.7557 & 0.0297 & 0.0429 & 0.0140 \\ \hline -2.8136 & -1.9598 & 1.1569 & 1.6592 & 0.2808 \\ -6.0081 & -4.0641 & 2.0234 & 2.9866 & 1.0266 \\ 1.5604 & 1.4285 & -1.3147 & -1.0413 & -1.4408 \end{array}\right]$$

As predicted by Theorem 6.4, the error system singular values are flat over all frequency and are given as [c.f. (6.72)]

$$\left\{\sigma_1\left[G_{e_{\hat{Y}}}\right], \sigma_2\left[G_{e_{\hat{Y}}}\right], \sigma_3\left[G_{e_{\hat{Y}}}\right]\right\} = \{4.6925, 1.0443, 0.12910\} \tag{6.73}$$

Further minimization of the error system singular values may be obtained using the square case super-optimal algorithm which requires only one further Central Glover Solution iteration. The stable projection to be submitted to the final Central Glover Solution iteration is computed using (6.62) and is given as

$$G_{\hat{Y}}^{(1)}(s) = \mathbf{y}_\perp{}^{T\,(0)}(-s) G_{e_{\hat{Y}}}^{(0)}(s) \mathbf{x}_\perp{}^{(0)}(-s) = \left[\begin{array}{c|c} -\overline{A}_{\hat{X}} & \mathbf{B}^T \\ \hline -s^2(I - \mathbf{P}_{\hat{Y}}\mathbf{P}_{\hat{X}}{}^T)\mathbf{C}\Gamma^{-1} & \sigma_1 \mathbf{P}_{\hat{Y}} \end{array}\right]$$

$$= \left[\begin{array}{cc|cc} -1.7720 & 0.0451 & -0.9914 & 1.2633 \\ -0.4108 & -2.7582 & -0.0613 & -0.8364 \\ \hline -0.6344 & -1.2341 & -0.1402 & -0.0251 \\ -2.1816 & 0.3526 & -0.5971 & 0.8547 \end{array}\right]$$

Since the projected system is a two-state square system, the quadratic formula associated with Theorem 6.1 may be deployed for which $\mathbf{P}_{so} = 0.1236$ and for this, the remaining s-numbers become $s_2^\infty = 1.0442$ and $s_3^\infty = 0.12911$. Thus, the super-optimal s-numbers are given by

$$\{s_1^\infty, s_2^\infty, s_3^\infty\} = \{4.6925, 1.0442, 0.12911\} \tag{6.74}$$

Interestingly, for this example near super-optimality was attained by giving up the degrees of freedom in the Central Glover Solution to achieve observability gramian stationarity in accordance with (6.45) of Theorem 6.2. In fact, the second and third singular values[2] of error system $G_{e_{\hat{Y}}}$ differed from the corresponding super-optimal s-numbers by only 0.01%; moreover, the third singular value was actually *less* than the third super-optimal s-number. Furthermore, the resulting approximation system $F_{\hat{Y}}{}^{(0)}(s)$ is less complex than the super-optimal solution $F_{so}(s)$ since the former requires only two states as compared to the latter which requires three states. Finally,

[2]The first singular value equals the first s-number as a result of the Central Glover Solution.

it should be noted that even for this small example, the super-optimal approximation obtained with the square case super-optimal algorithm based on both the stable projection property of Theorem 6.3 and the quadratic super-optimal result of Theorem 6.1 resulted in processing 9 fewer states than would otherwise be required if the returned projections were nonminimal with antistable and stable components.

6.4 Summary

This chapter presented a useful characterization of the degrees of freedom available in the Hankel approximation as solved by the Central Glover Solution. Subsequently, this characterization allowed the degrees of freedom to be expressed simply in terms of the parameter $\mathbf{P}$ which could, in turn, be accessed through the predefined parameters $\mathbf{A}$, $\mathbf{B}$, and $\mathbf{C}$. Initially, the degrees of freedom were deployed to attain super-optimality in the two-state square-case by solving for the parameter $\mathbf{P}$ as the root of a simple quadratic equation. Next, the degrees of freedom were used in the context of larger square-case systems to attain approximation gramian stationarity. Here it was pointed out that the degree of freedom parameter $\mathbf{P}$ which yielded gramian stationarity could be obtained indirectly from a symmetric Riccati equation based on either the controllability or the observability approximation system gramian. Alternatively, the degree of freedom parameter $\mathbf{P}$ which yielded gramian stationarity could also be obtained directly from a nonsymmetric Riccati equation based on either the controllability or the observability approximation system gramian. In the course of using the degree of freedom parameter $\mathbf{P}$, a new super-optimal algorithm emerged as a natural by-product and was based on the matched error systems whose observability or controllability dynamics matched those of either the left or right maximizing vectors. By expressing the maximizing vectors and their orthogonal complements in terms of the approximation system, we were able to obtain a minimal realization of the completely stable projection and hence gain significant computational savings. In addition to the completely stable projection property, the matched error systems

also achieved singular value total flatness defined for the first time in this work. Finally, further significant super-optimal simplifications were achieved through the minimal core term expression of the super-optimal approximation. The efficacy and strength of these results were demonstrated in two examples studied previously in the literature [Young, 1986a; Tsai et al., 1988; Limebeer et al., 1989].

6A Appendix

Proof of Lemma 6.2: (Central Glover Solution degrees of freedom)

Without loss of generality, U can be written as the product of two square full rank matrices:

$$U = (\hat{C}_1 \quad \hat{C}_1^{\perp}) \begin{pmatrix} \alpha \\ \mathcal{B} \end{pmatrix}$$

Substitution of this into (6.5) yields

$$\alpha = \frac{-B_1}{C_1^T \hat{C}_1} = \frac{-B_1}{\|C_1\|} = \frac{-B_1}{\|B_1\|} = -\hat{B}_1$$

since $\|C_1\| = \|B_1\|$. The second requirement of U embodied in (6.6) together with the above implies

$$U^T U = (-\hat{B}_1^T \quad \mathcal{B}^T) \begin{pmatrix} -\hat{B}_1 \\ \mathcal{B} \end{pmatrix} = \hat{B}_1^T \hat{B}_1 + \mathcal{B}^T \mathcal{B} \leq I \qquad (6A.1)$$

If unknown $\mathcal{B}$ is written (without loss of generality) as

$$\mathcal{B} = (\rho \quad \mathbf{P}) \begin{pmatrix} -\hat{B}_1 \\ \hat{B}_1^{\perp} \end{pmatrix}$$

the pre- and post-multiplication of (6A.1) by $\hat{B}_1$ and $\hat{B}_1^T$, respectively, implies $\rho = 0$ while pre- and post-multiplication of (6A.1) by $\hat{B}_1^{\perp}$ and $\hat{B}_1^{\perp T}$ implies $\|\mathbf{P}\| \leq 1$. ■

Proof of Lemma 6.3: (Hankel singular value property)

By the definitions of Lemma 6.1, the product $\tilde{B}\tilde{B}^T$ is given by

$$\begin{aligned} \tilde{B}\tilde{B}^T &= \Gamma^{-1}(\Sigma_2 B_2 + \sigma_1 C_2^T U)(B_2^T \Sigma_2 + \sigma_1 U^T C_1)\Gamma^{-1} \\ &= \Gamma^{-1}(-\Sigma_2(A_{22}\Sigma_2 + \Sigma_2 A_{22}^T)\Sigma_2 + \sigma_1 \Sigma_2 B_2 U^T C_2 + \sigma_1 C_2^T U B_2^T \Sigma_2 \\ &\quad + \sigma_1^2 C_2^T U U^T C_2)\Gamma^{-1} \end{aligned}$$

where use of (6.9) has been made. Further rearrangement yields

$$\begin{aligned} \tilde{B}\tilde{B}^T &= \Gamma^{-1}\big[-(\sigma_1^2 A_{22}^T + \Sigma_2 A_{22}\Sigma_2 - \sigma_1 C_2^T U B_2^T)\Sigma_2 \\ &\quad -\Sigma_2(\sigma_1^2 A_{22} + \Sigma_2 A_{22}^T \Sigma_2 - \sigma_1 B_2 U^T C_2) \end{aligned}$$

$$
\begin{aligned}
&+\sigma_1^2(A_{22}^T\Sigma_2 + \Sigma_2 A_{22}) + \sigma_1^2 C_2^T UU^T C_2\Big]\Gamma^{-1} \\
&= \Gamma^{-1}\left[-\Gamma\tilde{A}\Sigma_2 - \Sigma_2\tilde{A}^T\Gamma - \sigma_1^2 C_2^T C_2 + \sigma_1^2 C_2^T UU^T C_2\right]\Gamma^{-1} \\
&= -\tilde{A}(\Sigma_2\Gamma^{-1}) - (\Sigma_2\Gamma^{-1})\tilde{A}^T - \sigma_1^2\Gamma^{-1}C_2^T(I - UU^T)C_2\Gamma^{-1} \\
\Rightarrow \quad &\tilde{A}(\Sigma_2\Gamma^{-1}) + (\Sigma_2\Gamma^{-1})\tilde{A}^T + \tilde{B}\tilde{B}^T + \sigma_1^2\Gamma^{-1}C_2^T(I - UU^T)C_2\Gamma^{-1} = 0
\end{aligned}
\tag{6A.2}
$$

By the definition for $\tilde{B}$ given in (6.27), $\tilde{B}\tilde{B}^T$ may equally be written as

$$
\tilde{B}\tilde{B}^T = \Gamma^{-1}\left(\frac{1}{\beta^2}\Gamma A_{12}^T A_{12}\Gamma + \Sigma_2\mathbf{B}^T\mathbf{B}\Sigma_2 + \sigma_1\mathbf{C}^T\mathbf{P}\mathbf{B}\Sigma_2 + \sigma_1\Sigma_2\mathbf{B}^T\mathbf{P}^T\mathbf{C} + \sigma_1^2\mathbf{C}^T\mathbf{P}\mathbf{P}^T\mathbf{C}\right)\Gamma^{-1}
\tag{6A.3}
$$

Use of both (6A.3) and substitution of the definition for $\tilde{A}$ given in (6.25) into (6A.2) yields (after pre- and post-multiplication by Γ)

$$
\begin{aligned}
&(\mathbf{A} - \sigma_1\mathbf{C}^T\mathbf{P}\mathbf{B})\Sigma_2 + \Sigma_2(\mathbf{A}^T - \sigma_1\mathbf{B}^T\mathbf{P}^T\mathbf{C}) + \frac{1}{\beta^2}\Gamma A_{12}^T A_{12}\Gamma \ldots \sigma_1\mathbf{B}^T\mathbf{B}\Sigma_2 \\
&\quad +\sigma_1\mathbf{C}^T\mathbf{P}\mathbf{B}\Sigma_2 + \sigma_1\Sigma_2\mathbf{B}^T\mathbf{P}^T\mathbf{C} + \sigma_1^2\mathbf{C}^T\mathbf{P}\mathbf{P}^T\mathbf{C} + \sigma_1^2 C_2^T(I - UU^T)C_2 \\
&= \mathbf{A}\Sigma_2 - \sigma_1\mathbf{C}^T\mathbf{P}\mathbf{B}\Sigma_2 + \Sigma_2\mathbf{A}^T - \sigma_1\Sigma_2\mathbf{B}^T\mathbf{P}^T\mathbf{C} \\
&\quad +\frac{1}{\beta^2}\Gamma A_{12}^T A_{12}\Gamma + \Sigma_2\mathbf{B}^T\mathbf{B}\Sigma_2 + \sigma_1\mathbf{C}^T\mathbf{P}\mathbf{B}\Sigma_2 + \sigma_1\Sigma_2\mathbf{B}^T\mathbf{P}^T\mathbf{C} + \sigma_1^2\mathbf{C}^T\mathbf{P}\mathbf{P}^T\mathbf{C} \\
&\quad +\sigma_1^2 C_2^T C_2 - \sigma_1^2 C_2^T\hat{C}_1\hat{C}_1^T C_2 - \sigma_1^2 C_2^T\hat{C}_1^{\perp}\mathbf{P}\mathbf{P}^T\hat{C}_1^{\perp T}C_2 \\
&= 0
\end{aligned}
$$

where the structure of U given in (6.24) has been employed. Cancelling terms and using the definition that $\mathbf{C} = \hat{C}_1^{\perp T}C_2$ and the identity $\hat{C}_1^{\perp}\hat{C}_1^{\perp T} = I - \hat{C}_1\hat{C}_1^T$ establishes (6.36). The proof for (6.37) begins with $\tilde{C}^T\tilde{C}$ and follows a similar structure and is thus omitted. ■

6B Appendix

Proof of Theorem 6.1: (Quadratic super-optimality)

Using the definitions (6.25) through (6.31), the error system $G_e(s) = G(s) - F(s)$ satisfies the following equation:

$$\frac{1}{\sigma_1^2} G_e^T(-s) G_e(s) =$$

$$\begin{pmatrix} -\hat{B}_1 \\ \hat{B}_1^\perp \end{pmatrix}^T \left[\begin{array}{cc|cc} (-\mathbf{A}^T+\sigma_1\mathbf{B}^T\mathbf{P}^T\mathbf{C})\Gamma^{-1} & \mathbf{B}^T(I-\mathbf{P}^T\mathbf{P})\mathbf{B} & 0 & -\mathbf{B}^T(I-\mathbf{P}^T\mathbf{P}) \\ 0 & \Gamma^{-1}(\mathbf{A}-\sigma_1\mathbf{C}^T\mathbf{P}\mathbf{B}) & \frac{1}{\beta}A_{12}^T & \Gamma^{-1}(\sigma_1\mathbf{C}^T\mathbf{P}+\Sigma_2\mathbf{B}^T) \\ \hline \frac{1}{\beta}A_{12} & 0 & 1 & 0 \\ (\sigma_1\mathbf{P}^T\mathbf{C}+\mathbf{B}\Sigma_2)\Gamma^{-1} & (I-\mathbf{P}^T\mathbf{P})\mathbf{B} & 0 & \mathbf{P}^T\mathbf{P} \end{array}\right] \begin{pmatrix} -\hat{B}_1 \\ \hat{B}_1^\perp \end{pmatrix}$$

where the norm preserving unitary matrix $\begin{pmatrix} -\hat{B}_1 \\ \hat{B}_1^\perp \end{pmatrix}^T$ and its transpose have been pulled out on the left and right respectively. Clearly, the total flatness of $G_e(s)$ is equivalent to the total flatness of:

$$\boldsymbol{G}(s) = \left[\begin{array}{c|c} \mathcal{A} & \mathcal{B} \\ \hline \mathcal{C} & \mathcal{D} \end{array}\right]$$

$$= \left[\begin{array}{cc|cc} (-\mathbf{A}^T+\sigma_1\mathbf{B}^T\mathbf{P}^T\mathbf{C})\Gamma^{-1} & \mathbf{B}^T(I-\mathbf{P}^T\mathbf{P})\mathbf{B} & 0 & -\mathbf{B}^T(I-\mathbf{P}^T\mathbf{P}) \\ 0 & \Gamma^{-1}(\mathbf{A}-\sigma_1\mathbf{C}^T\mathbf{P}\mathbf{B}) & \frac{1}{\beta}A_{12}^T & \Gamma^{-1}(\sigma_1\mathbf{C}^T\mathbf{P}+\Sigma_2\mathbf{B}^T) \\ \hline \frac{1}{\beta}A_{12} & 0 & 1 & 0 \\ (\sigma_1\mathbf{P}^T\mathbf{C}+\mathbf{B}\Sigma_2)\Gamma^{-1} & (I-\mathbf{P}^T\mathbf{P})\mathbf{B} & 0 & \mathbf{P}^T\mathbf{P} \end{array}\right] \tag{6B.1}$$

In turn, this is equivalent to the condition:

$$\boldsymbol{G}(s)\boldsymbol{y}(s) = \boldsymbol{\sigma}\boldsymbol{y}(s) \tag{6B.2}$$

where $\boldsymbol{\sigma}$ denotes either of the two constant singular values of $\boldsymbol{G}(s)$ while $\boldsymbol{y}(s)$ denotes the corresponding frequency dependent principal directions. Next write the following power series expansions for $\boldsymbol{G}(s)$ and $\boldsymbol{y}(s)$

$$\boldsymbol{G}(s) = \sum_{i=0}^{\infty} \mathcal{G}_i s^{-i} \qquad \text{and} \qquad \boldsymbol{y}(s) = \sum_{i=0}^{\infty} y_i s^{-i}$$

where $\mathcal{G}_0 = \mathcal{D}$ and $\mathcal{G}_i = \mathcal{C}\mathcal{A}^{i-1}\mathcal{B} \;\; \forall\, i \geq 1$. Substitution of these into (6B.2) and equating the coefficients of s^{-i} for $i = 0, 1, 2$ yields the condition:

$$\left(\mathbf{P}^2 - 1\right)\left(\mathbf{P}^2 - \mathbf{P}\left(\frac{2\mathbf{A}}{\sigma_1\mathbf{BC}}\right) + 1\right) = 0 \qquad \text{(6B.3)}$$

The detailed steps in the derivation of (6B.3) are lengthy but straightforward and will be omitted. Finally, (6B.3) together with the bound $\|\mathbf{P}\| \leq 1$ from (6.24) gives the solution in (6.38); note that the solutions $\mathbf{P} = \pm 1$ are ignored since these values can easily be shown to yield the all-pass solution which is clearly not super-optimal.

To complete the proof, observe that the s-numbers may be obtained from the super-optimal "D-matrix" which in this case is the matrix $\sigma_1 U$, and given the structure of matrix U in (6.24), the super-optimal singular values are clearly given by $\sigma_1 \times \{1, |\mathbf{P}|\}$. ■

Proof of Corollary 6.1: (2-State approximation gramian stationarity)

For the two-input/two-output square case, $\tilde{X}$ and $\tilde{Y}$ are scalars and satisfy (6.17) and (6.18), respectively, so that

$$\tilde{X} = \frac{-\tilde{B}\tilde{B}^T}{2\tilde{A}} =$$

$$-\Gamma^{-1}\left\{\frac{\frac{1}{\beta^2}\Gamma A_{12}^T A_{12}\Gamma + \Sigma_2\mathbf{B}^T\mathbf{B}\Sigma_2 + \sigma_1^2\mathbf{C}^T\mathbf{P}\mathbf{P}^T\mathbf{C} + \sigma_1\mathbf{C}^T\mathbf{P}\mathbf{B}\Sigma_2 + \sigma_1\Sigma_2\mathbf{B}^T\mathbf{P}^T\mathbf{C}}{2\Gamma^{-1}(\mathbf{A} - \sigma_1\mathbf{C}^T\mathbf{P}\mathbf{B})}\right\}\Gamma^{-1}$$

$$\tilde{Y} = \frac{-\tilde{C}^T\tilde{C}}{2\tilde{A}} =$$

$$-\left\{\frac{\frac{1}{\beta^2}\Gamma A_{21} A_{21}^T\Gamma + \Sigma_2\mathbf{C}^T\mathbf{C}\Sigma_2 + \sigma_1^2\mathbf{B}^T\mathbf{P}^T\mathbf{P}\mathbf{B} + \sigma_1\mathbf{B}^T\mathbf{P}^T\mathbf{C}\Sigma_2 + \sigma_1\Sigma_2\mathbf{C}^T\mathbf{P}\mathbf{B}}{2\Gamma^{-1}(\mathbf{A} - \sigma_1\mathbf{C}^T\mathbf{P}\mathbf{B})}\right\}$$

where the definitions for $\tilde{A}$, $\tilde{B}$, and $\tilde{C}$ as given in (6.25) through (6.29) have been employed. Use of Lemma 6.3 in conjunction with the fact that $\mathbf{A}$, $\mathbf{B}$, $\mathbf{C}$ and Σ_2 are scalars produces the following simplified forms of the approximation system gramians and their derivatives with respect to $\mathbf{P}$.

$$\tilde{X} = \frac{\sigma_1^2\Gamma^{-2}\mathbf{C}^2(1 - \mathbf{P}^2)}{2\Gamma^{-1}(\mathbf{A} - \sigma_1\mathbf{P}\mathbf{B}\mathbf{C})} + \Sigma_2\Gamma^{-1} \quad \text{and} \quad \tilde{X}' = \frac{\sigma_1^3\Gamma^{-2}\mathbf{B}\mathbf{C}^3\left(\mathbf{P}^2 - \mathbf{P}\left(\frac{2\mathbf{A}}{\sigma_1\mathbf{B}\mathbf{C}}\right) + 1\right)}{2\Gamma^{-1}(\mathbf{A} - \sigma_1\mathbf{P}\mathbf{B}\mathbf{C})^2}$$

$$\tilde{Y} = \frac{\sigma_1^2\mathbf{B}^2(1 - \mathbf{P}^2)}{2\Gamma^{-1}(\mathbf{A} - \sigma_1\mathbf{P}\mathbf{B}\mathbf{C})} + \Sigma_2\Gamma \quad \text{and} \quad \tilde{Y}' = \frac{\sigma_1^3\mathbf{B}^3\mathbf{C}\left(\mathbf{P}^2 - \mathbf{P}\left(\frac{2\mathbf{A}}{\sigma_1\mathbf{B}\mathbf{C}}\right) + 1\right)}{2\Gamma^{-1}(\mathbf{A} - \sigma_1\mathbf{P}\mathbf{B}\mathbf{C})^2}$$

Clearly, stationarity of the individual gramians occurs only when $\mathbf{P}$ satisfies the quadratic equation given in (6.40). Detailed calculation of the derivative of the approximation gramian product $(\tilde{X}\tilde{Y})' = \tilde{X}'\tilde{Y} + \tilde{X}\tilde{Y}'$ shows that the derivative of $(\tilde{X}\tilde{Y})$ can only vanish for values of $\mathbf{P}$ which satisfy either (6.40) or the following quadratic equation:

$$\mathbf{P}^2 - \mathbf{P}\left(\frac{\Sigma_2}{\sigma_1 \mathbf{BC}}\right)\left(\mathbf{B}^2 + \mathbf{C}^2\right) - 1 - \left(\frac{\Sigma_2 \mathbf{A}}{\sigma_1^2 \mathbf{B}^2 \mathbf{C}^2}\right)\left(\mathbf{B}^2 + \mathbf{C}^2\right) = 0 \qquad \text{(6B.4)}$$

However, the discriminant of this quadratic can be shown (through use of the identities (6.36) and (6.37)) to always be negative; hence the roots of (6B.4) are complex and therefore inadmissible. Thus, $\tilde{X}$, $\tilde{Y}$, and $\tilde{X}\tilde{Y}$ share common stationary points, and those are defined by (6.40); of these only one lies in the range $-1 \leq \mathbf{P} \leq 1$, and is given by the value of $\mathbf{P}_{so}$ of Theorem 6.1. Double differentiation of $\tilde{X}$ and $\tilde{Y}$ readily establishes that at $\mathbf{P}_{so}$ both $-\tilde{X}$ and $-\tilde{Y}$ and hence $\tilde{X}\tilde{Y}$ go through a minimum. ■

Proof of Corollary 6.2: (Error system gramian trace stationarity)

Equation (6.41) follows directly from (6.16) and for the 2-state case yields:

$$\text{Trace}\,[X_e Y_e] = \tilde{X}\tilde{Y} - \Gamma + 2\sigma_1^2$$

Thus the stationary properties of the trace of the error system gramian product $X_e Y_e$ are the same as those of the approximation system gramian product $\tilde{X}\tilde{Y}$. ■

Proof of Lemma 6.4: (Approximation gramian stationarity)

Differentiation of (6.18) with respect to the $(i,j)^{\text{th}}$ element of $\mathbf{P}$ yields:

$$\begin{aligned}
\tilde{A}^T\tilde{Y}' + \tilde{Y}'\tilde{A} &= -\left(\left(\tilde{A}^T\right)'\tilde{Y} + \tilde{Y}\tilde{A}' + \left(\tilde{C}^T\right)'\tilde{C} + \tilde{C}^T\tilde{C}'\right) \\
&= -\sigma_1 \mathbf{B}^T \mathbf{e}_j \mathbf{e}_i^T \mathbf{C}\Gamma^{-1}\tilde{Y} - \sigma_1 \tilde{Y}\Gamma^{-1}\mathbf{C}^T \mathbf{e}_i \mathbf{e}_j^T \mathbf{B} \\
&\quad + \sigma_1 \mathbf{B}^T \mathbf{e}_j \mathbf{e}_i^T \hat{C}_1^{\perp T} \begin{pmatrix} \hat{C}_1 & \hat{C}_1^{\perp} \end{pmatrix} \begin{pmatrix} -\frac{1}{\beta} A_{21}^T \Gamma \\ \sigma_1 \mathbf{PB} + \mathbf{C}\Sigma_2 \end{pmatrix} \\
&\quad + \begin{pmatrix} -\frac{1}{\beta}\Gamma A_{21} & \sigma_1 \mathbf{B}^T \mathbf{P}^T + \Sigma_2 \mathbf{C}^T \end{pmatrix} \begin{pmatrix} \hat{C}_1^T \\ \hat{C}_1^{\perp T} \end{pmatrix} \sigma_1 \hat{C}_1^{\perp} \mathbf{e}_i \mathbf{e}_j^T \mathbf{B}
\end{aligned}$$

$$= -\sigma_1 \mathbf{B}^T \mathbf{e}_j \mathbf{e}_i^T \left(\mathbf{C}\Gamma^{-1}\tilde{Y}\right) - \sigma_1 \left(\tilde{Y}\Gamma^{-1}\mathbf{C}^T\right) \mathbf{e}_i \mathbf{e}_j^T \mathbf{B}$$
$$+\sigma_1 \mathbf{B}^T \mathbf{e}_j \mathbf{e}_i^T (\sigma_1 \mathbf{P}\mathbf{B} + \mathbf{C}\Sigma_2) + \left(\sigma_1 \mathbf{B}^T \mathbf{P}^T + \Sigma_2 \mathbf{C}^T\right) \sigma_1 \mathbf{e}_i \mathbf{e}_j^T \mathbf{B} \quad (6B.5)$$

where the definitions of $\tilde{A}$ and $\tilde{C}$ given by (6.25) and (6.29), respectively, have been employed. From (6B.5) it is clear that the stationarity of $\tilde{Y}$ (i.e. $\tilde{Y}' = 0$) yields the following condition:

$$\mathbf{B}^T \mathbf{e}_j \mathbf{e}_i^T \mathbf{N} = -\mathbf{N}^T \mathbf{e}_i \mathbf{e}_j^T \mathbf{B}$$

where $\mathbf{N} = \left(\mathbf{C}\Gamma^{-1}\tilde{Y}\right) - (\sigma_1 \mathbf{P}\mathbf{B} + \mathbf{C}\Sigma_2)$. This condition in turn implies that either $\mathbf{B}^T \mathbf{e}_j = 0$ or $\mathbf{N}^T \mathbf{e}_i = 0$; however, the obvious assumption that B defined in (6.4) is full rank implies that $\mathbf{B}^T \mathbf{e}_j \neq 0$ and hence we conclude that $\mathbf{N}^T \mathbf{e}_i = 0$. Moreover, this must be true for all i and thus (6.43) must hold. Condition (6.43) is also sufficient because it makes the right hand side of (6B.5) zero and thus yields:

$$\tilde{A}^T \tilde{Y}' + \tilde{Y}' \tilde{A} = 0$$

For the completely unstable approximation system state matrix $\tilde{A}$ (i.e. Real $\left[\lambda_i\left(\tilde{A}\right)\right] > 0 \; \forall \, i$), this equation has the unique solution $\tilde{Y}' = 0$. ■

Proof of Theorem 6.2: (Approximation gramian solutions)

Substitution of the definitions for $\tilde{A}$ and $\tilde{B}$ given by (6.25) and (6.27), respectively, into (6.17) yields

$$\Gamma^{-1}(\mathbf{A} - \sigma_1 \mathbf{C}^T \mathbf{P}\mathbf{B})\tilde{X} + \tilde{X}(\mathbf{A}^T - \sigma_1 \mathbf{B}^T \mathbf{P}^T \mathbf{C})\Gamma^{-1}$$
$$+\frac{1}{\beta^2} A_{12}^T A_{12} + \Gamma^{-1}(\sigma_1 \mathbf{C}^T \mathbf{P} + \Sigma_2 \mathbf{B}^T)(\sigma_1 \mathbf{P}^T \mathbf{C} + \mathbf{B}\Sigma_2)\Gamma^{-1} \quad (6B.6)$$
$$= \Gamma^{-1}(\mathbf{A} - \sigma_1 \mathbf{C}^T \mathbf{P}\mathbf{B})\left(\tilde{X} - \Sigma_2\Gamma^{-1}\right) + \left(\tilde{X} - \Sigma_2\Gamma^{-1}\right)(\mathbf{A}^T - \sigma_1 \mathbf{B}^T \mathbf{P}^T \mathbf{C})\Gamma^{-1}$$
$$+\sigma_1^2 \Gamma^{-1} \mathbf{C}^T (\mathbf{P}\mathbf{P}^T - I)\mathbf{C}\Gamma^{-1} = 0 \quad (6B.7)$$

where use of Lemma 6.3 has been made. Furthermore, by substitution of the specific value $\mathbf{P}_{\tilde{X}}$ of $\mathbf{P}$ given in (6.42), the above reduces (after some cancellations) to

$$\Gamma^{-1}\mathbf{A}\left(\tilde{X} - \Sigma_2\Gamma^{-1}\right) + \left(\tilde{X} - \Sigma_2\Gamma^{-1}\right)\mathbf{A}^T\Gamma^{-1}$$
$$-\sigma_1^2 \Gamma^{-1} \mathbf{C}^T \mathbf{C}\Gamma^{-1} - \sigma_1^2 \Gamma^{-1} \mathbf{C}^T \mathbf{P}_{\tilde{X}} \mathbf{P}_{\tilde{X}}{}^T \mathbf{C}\Gamma^{-1} = 0 \quad (6B.8)$$

Finally, by using $\sigma_1\Gamma^{-1}\mathbf{C}^T\mathbf{P}_{\tilde{X}} = (\tilde{X} - \Sigma_2\Gamma^{-1})\mathbf{B}^T$ as implied by (6.42) in conjunction with the Hankel singular value property given by (6.36), Riccati Equation (6.44) is obtained. In the square case, $\mathbf{C}$ is generally invertible, thus, (6.42) may be solved explicitly for $\mathbf{P}_{\tilde{X}}$ yielding (6.46). The proof of Riccati Equation (6.45) is parallel and therefore omitted. ■

Proof of Corollary 6.3: (Nonsymmetric Riccati equations)

Using the Hankel singular value property of (6.37), Riccati Equation (6.45) may be rewritten as:

$$\begin{aligned}&\mathbf{A}^T\Gamma^{-1}\left(\tilde{Y} - \Sigma_2\Gamma\right) + \left(\tilde{Y} - \Sigma_2\Gamma\right)\Gamma^{-1}\mathbf{A} \\ &\quad - \left(\tilde{Y} - \Sigma_2\Gamma\right)\Gamma^{-1}\mathbf{C}^T\mathbf{C}\Gamma^{-1}\left(\tilde{Y} - \Sigma_2\Gamma\right) - \sigma_1^2\mathbf{B}^T\mathbf{B} = 0\end{aligned}$$

Next, pre- and post-multiply this equation by $\mathbf{C}\mathbf{A}^{T^{-1}}$ and $\mathbf{A}^{-1}\mathbf{C}^T$, respectively, to obtain

$$\begin{aligned}&\mathbf{C}\Gamma^{-1}\left(\tilde{Y} - \Sigma_2\Gamma\right)\mathbf{A}^{-1}\mathbf{C}^T + \mathbf{C}\mathbf{A}^{T^{-1}}\left(\tilde{Y} - \Sigma_2\Gamma\right)\Gamma^{-1}\mathbf{C}^T \\ &\quad -\mathbf{C}\mathbf{A}^{T^{-1}}\left(\tilde{Y} - \Sigma_2\Gamma\right)\Gamma^{-1}\mathbf{C}^T\mathbf{C}\Gamma^{-1}\left(\tilde{Y} - \Sigma_2\Gamma\right)\mathbf{A}^{-1}\mathbf{C}^T \\ &\quad - \left(\sigma_1\mathbf{C}\mathbf{A}^{T^{-1}}\mathbf{B}^T\right)\left(\sigma_1\mathbf{B}\mathbf{A}^{-1}\mathbf{C}^T\right) \\ &= 0 \qquad\qquad (6B.9)\end{aligned}$$

Further simplification follows using the stationary condition of (6.43) which implies

$$\mathbf{C}\Gamma^{-1}\left(\tilde{Y} - \Sigma_2\Gamma\right) = \sigma_1\mathbf{P}_{\tilde{Y}}\mathbf{B}$$

Using this in (6B.9) produces

$$\mathbf{P}_{\tilde{Y}}\mathbf{M}^T + \mathbf{M}\mathbf{P}_{\tilde{Y}}{}^T - \mathbf{M}\mathbf{P}_{\tilde{Y}}{}^T\mathbf{P}_{\tilde{Y}}\mathbf{M}^T - \mathbf{M}\mathbf{M}^T = 0 \qquad (6B.10)$$

where $\mathbf{M} = \left(\sigma_1\mathbf{C}\mathbf{A}^{T^{-1}}\mathbf{B}^T\right)$. Next, pre- and post-multiply this by $\mathbf{M}^{-1}$ and $\mathbf{M}^{T^{-1}}$, respectively, to obtain

$$\mathbf{M}^{-1}\mathbf{P}_{\tilde{Y}} + \mathbf{P}_{\tilde{Y}}{}^T\mathbf{M}^{T^{-1}} - \mathbf{P}_{\tilde{Y}}{}^T\mathbf{P}_{\tilde{Y}} - I = 0$$

Subsequent pre-multiplication of this by $\mathbf{R}^T$, where $\mathbf{R} = \sigma_1 \mathbf{B}\Gamma^{-1}\mathbf{C}^T$, yields

$$\mathbf{R}^T\mathbf{M}^{-1}\mathbf{P}_{\hat{Y}} + \mathbf{R}^T\mathbf{P}_{\hat{Y}}{}^T\mathbf{M}^{T^{-1}} - \mathbf{R}^T\mathbf{P}_{\hat{Y}}{}^T\mathbf{P}_{\hat{Y}} - \mathbf{R}^T = 0$$

Finally, it is straightforward to show that the symmetry of the observability gramian $\hat{Y}$ implies the symmetry of the product $\mathbf{P}_{\hat{Y}}\mathbf{R} = \mathbf{R}^T\mathbf{P}_{\hat{Y}}{}^T$ where $\mathbf{R}$ is defined as above. Using this and cancelling the corresponding terms in the product $\mathbf{R}^T\mathbf{M}^{-1}$ yields (6.49). The proof of (6.48) is similar and therefore omitted. ■

Proof of Lemma 6.5: (Maximizing vectors)

The product $\mathbf{y}^T(-s)\mathbf{y}(s)$ is given as

$$\mathbf{y}^T(-s)\mathbf{y}(s) = \left[\begin{array}{cc|c} -\overline{A}_{\hat{Y}}^T & \overline{C}_{\hat{Y}}^T\overline{C}_{\hat{Y}} & \overline{C}_{\hat{Y}}^T\hat{C}_1 \\ 0 & \overline{A}_{\hat{Y}} & -\hat{Y}^{-1}\overline{C}_{\hat{Y}}^T\hat{C}_1 \\ \hline \hat{C}_1^T\overline{C}_{\hat{Y}}\hat{Y}^{-1} & \hat{C}_1^T\overline{C}_{\hat{Y}} & \hat{C}_1^T\hat{C}_1 \end{array}\right]$$

where $\overline{A}_{\hat{Y}}$ and $\overline{C}_{\hat{Y}}$ are as given if (6.56) and (6.57) respectively. Subsequent application of the state similarity transformation $\begin{pmatrix} I & \hat{Y} \\ 0 & I \end{pmatrix}$ yields

$$\begin{aligned} \mathbf{y}^T(-s)\mathbf{y}(s) &= \left[\begin{array}{cc|c} -\overline{A}_{\hat{Y}}^T & \overline{A}_{\hat{Y}}^T\hat{Y} + \hat{Y}\overline{A}_{\hat{Y}} + \overline{C}_{\hat{Y}}^T\overline{C}_{\hat{Y}} & \overline{C}_{\hat{Y}}^T\hat{C}_1 - \overline{C}_{\hat{Y}}^T\hat{C}_1 \\ 0 & \overline{A}_{\hat{Y}} & -\hat{Y}^{-1}\overline{C}_{\hat{Y}}^T\hat{C}_1 \\ \hline \hat{C}_1^T\overline{C}_{\hat{Y}}\hat{Y}^{-1} & \hat{C}_1^T\overline{C}_{\hat{Y}} - \hat{C}_1^T\overline{C}_{\hat{Y}} & 1 \end{array}\right] \\ &= \left[\begin{array}{cc|c} -\overline{A}_{\hat{Y}}^T & 0 & 0 \\ 0 & \overline{A}_{\hat{Y}} & -\hat{Y}^{-1}\overline{C}_{\hat{Y}}^T\hat{C}_1 \\ \hline \hat{C}_1^T\overline{C}_{\hat{Y}}\hat{Y}^{-1} & 0 & 1 \end{array}\right] = 1 \end{aligned}$$

where $\overline{A}_{\hat{Y}}^T\hat{Y} + \hat{Y}\overline{A}_{\hat{Y}} + \overline{C}_{\hat{Y}}^T\overline{C}_{\hat{Y}} = 0$ follows directly by substituting the definitions for $(\overline{A}_{\hat{Y}}, \overline{C}_{\hat{Y}})$ to obtain Riccati Equation (6.45) of Theorem 6.2. This proves the innerness of $\mathbf{y}(s)$; the innerness of $\mathbf{x}(s)$ follows similar lines but involves $\overline{A}_{\hat{X}}$, $\overline{B}_{\hat{X}}$, and $\hat{X}$ in place of $\overline{A}_{\hat{Y}}$, $\overline{C}_{\hat{Y}}$, and $\hat{Y}$ respectively. To prove the maximizing property, it will be shown that

$$\frac{1}{\sigma_1^2}G_e^T(-s)G_e(s)\mathbf{x}(-s) = \mathbf{x}(-s) \quad \text{and} \quad \frac{1}{\sigma_1^2}\mathbf{y}^T(-s)G_e(s)G_e^T(-s) = \mathbf{y}^T(-s) \quad \text{(6B.11)}$$

where $G_e(s) = G(s) - F(s)$. The definitions (6.25) through (6.31) yield:

$$\frac{1}{\sigma_1^2}G_e^T(-s)G_e(s) =$$

$$\begin{pmatrix} -\hat{B}_1 \\ \hat{B}_1^\perp \end{pmatrix}^T \left[\begin{array}{cc|cc} (-\mathbf{A}^T+\sigma_1\mathbf{B}^T\mathbf{P}^T\mathbf{C})\Gamma^{-1} & \mathbf{B}^T(I-\mathbf{P}^T\mathbf{P})\mathbf{B} & 0 & -\mathbf{B}^T(I-\mathbf{P}^T\mathbf{P}) \\ 0 & \Gamma^{-1}(\mathbf{A}-\sigma_1\mathbf{C}^T\mathbf{P}\mathbf{B}) & \frac{1}{\beta}A_{12}^T & \Gamma^{-1}(\sigma_1\mathbf{C}^T\mathbf{P}+\Sigma_2\mathbf{B}^T) \\ \hline \frac{1}{\beta}A_{12} & 0 & 1 & 0 \\ (\sigma_1\mathbf{P}^T\mathbf{C}+\mathbf{B}\Sigma_2)\Gamma^{-1} & (I-\mathbf{P}^T\mathbf{P})\mathbf{B} & 0 & \mathbf{P}^T\mathbf{P} \end{array}\right] \begin{pmatrix} -\hat{B}_1 \\ \hat{B}_1^\perp \end{pmatrix} \tag{6B.12}$$

where the norm preserving unitary matrix $\begin{pmatrix} -\hat{B}_1 \\ \hat{B}_1^\perp \end{pmatrix}^T$ and its transpose have been pulled out on the left and right respectively. In order to simplify the notation, write $\frac{1}{\sigma_1^2}G_e^T(-s)G_e(s)$ as

$$\frac{1}{\sigma_1^2}G_e^T(-s)G_e(s) = \begin{pmatrix} -\hat{B}_1 \\ \hat{B}_1^\perp \end{pmatrix}^T \left[\begin{array}{c|c} \mathcal{A} & \mathcal{B} \\ \hline \mathcal{C} & \mathcal{D} \end{array}\right] \begin{pmatrix} -\hat{B}_1 \\ \hat{B}_1^\perp \end{pmatrix}$$

where the definitions of $\mathcal{A}$, $\mathcal{B}$, $\mathcal{C}$, and $\mathcal{D}$ are implied from context by (6B.12). Next, write

$$\begin{aligned} \mathbf{x}(-s) &= \begin{pmatrix} -\hat{B}_1 \\ \hat{B}_1^\perp \end{pmatrix}^T \left[\begin{array}{c|c} -\overline{A}_{\tilde{X}}^T & -\frac{1}{\beta}\tilde{X}^{-1}A_{12}^T \\ \hline \frac{1}{\beta}A_{12} & \\ (\sigma_1\mathbf{P}_{\tilde{X}}{}^T\mathbf{C}+\mathbf{B}\Sigma_2)\Gamma^{-1} & -\mathbf{e}_1 \end{array}\right] \\ &= \begin{pmatrix} -\hat{B}_1 \\ \hat{B}_1^\perp \end{pmatrix}^T \left[\begin{array}{c|c} -A_x & -B_x \\ \hline C_x & D_x \end{array}\right] \end{aligned} \tag{6B.13}$$

where $\mathbf{e}_1$ is the first standard basis vector and the definitions of A_x, B_x, C_x, and D_x are implied from context by (6B.13). With these definitions, the maximizing property of (6B.11) implies the following

$$\left[\begin{array}{c|c} \mathcal{A} & \mathcal{B} \\ \hline \mathcal{C} & \mathcal{D} \end{array}\right]\left[\begin{array}{c|c} -A_x & -B_x \\ \hline C_x & D_x \end{array}\right] = \left[\begin{array}{cc|c} \mathcal{A} & \mathcal{B}C_x & \mathcal{B}D_x \\ 0 & -A_x & -B_x \\ \hline \mathcal{C} & \mathcal{D}C_x & \mathcal{D}D_x \end{array}\right] = \left[\begin{array}{c|c} -A_x & -B_x \\ \hline C_x & D_x \end{array}\right]$$

Apply the state similarity transformation $\begin{pmatrix} I & T \\ 0 & I \end{pmatrix}$ to obtain

$$\left[\begin{array}{c|c} -A_x & -B_x \\ \hline C_x & D_x \end{array}\right] \equiv \left[\begin{array}{cc|c} \mathcal{A} & \mathcal{A}T+TA_x+\mathcal{B}C_x & \mathcal{B}D_x+TB_x \\ 0 & -A_x & -B_x \\ \hline \mathcal{C} & \mathcal{C}T+\mathcal{D}C_x & \mathcal{D}D_x \end{array}\right] \tag{6B.14}$$

where state similarity transformation matrix T has the conformally partitioned form $T = \binom{T_1}{T_2}$. Equation (6B.14) is equivalent to the following four conditions:

$$(1) \quad \mathcal{A}T + T\mathcal{A}_x + \mathcal{B}C_x = 0 \tag{6B.15}$$

$$(2) \quad \mathcal{B}D_x + T\mathcal{B}_x = 0 \tag{6B.16}$$

$$(3) \quad \mathcal{C}T + \mathcal{D}C_x = C_x \tag{6B.17}$$

$$(4) \quad \mathcal{D}D_x = D_x \tag{6B.18}$$

Next, these four conditions will be proved in turn. Thus, with $\tilde{X}$ being the controllability gramian of (6.17), choose

$$T = \begin{pmatrix} T_1 \\ T_2 \end{pmatrix} = \begin{pmatrix} 0 \\ \tilde{X} \end{pmatrix} \tag{6B.19}$$

Condition 1: Substitution of the definitions of the relevant matrices of (6B.15) yields

$$(i) \quad -\tilde{A}^T T_1 + \mathbf{B}^T(I - \mathbf{P}^T\mathbf{P})\mathbf{B}T_2 + T_1\overline{A}_{\tilde{X}}^T - \mathbf{B}^T(I - \mathbf{P}^T\mathbf{P})\mathbf{B}\tilde{X} = 0$$

$$(ii) \quad \tilde{A}T_2 + T_2\overline{A}_{\tilde{X}}^T + \frac{1}{\beta^2}A_{12}^T A_{12} + \Gamma^{-1}(\sigma_1\mathbf{C}^T\mathbf{P} + \Sigma_2\mathbf{B}^T)\mathbf{B}\tilde{X} = 0$$

Clearly, (i) is solved by the choice of $T_1 = 0$ and $T_2 = \tilde{X}$ given in (6B.19). Next, to prove (ii), substitute the definitions for $\tilde{A}$ and $\overline{A}_{\tilde{X}}$ given in (6.25) and (6.54), respectively, and subsequently carry out the multiplication of the third term to get

$$\Gamma^{-1}(\mathbf{A} - \sigma_1\mathbf{C}^T\mathbf{P}\mathbf{B})T_2 + T_2\left[\Gamma^{-1}\left(\mathbf{A} - \Gamma\left(\tilde{X} - \Sigma_2\Gamma^{-1}\right)\mathbf{B}^T\mathbf{B}\right)\right]^T + \frac{1}{\beta^2}A_{12}^T A_{12} + \sigma_1\Gamma^{-1}\mathbf{C}^T\mathbf{P}\mathbf{B}\tilde{X} + \Sigma_2\Gamma^{-1}\mathbf{B}^T\mathbf{B}\tilde{X} = 0$$

With $T_2 = \tilde{X}$ and further simplification, this results in the controllability gramian Riccati equation (6.44) and thus Condition 1 has been met.

Condition 2: Substitution of the definitions of the relevant matrices of (6B.16) yields

$$(i) \quad 0 + T_1\frac{1}{\beta}\tilde{X}^{-1}A_{12}^T = 0$$

$$(ii) \quad -\frac{1}{\beta}A_{12}^T + \frac{1}{\beta}T_2\tilde{X}^{-1}A_{12}^T = 0$$

Clearly, both equations are met by $T_1 = 0$ and $T_2 = \tilde{X}$ as defined in (6B.19).

Condition 3: Substitution of the definitions of the relevant matrices of (6B.17) yields

$$(i) \quad \frac{1}{\beta}A_{12}T_1 + \frac{1}{\beta}A_{12} = \frac{1}{\beta}A_{12}$$

$$(ii) \quad (\sigma_1\mathbf{P}^T\mathbf{C} + \mathbf{B}\Sigma_2)\Gamma^{-1}T_1 + (I - \mathbf{P}^T\mathbf{P})\mathbf{B}T_2 + \mathbf{P}^T\mathbf{P}\mathbf{B}\tilde{X} = \mathbf{B}\tilde{X}$$

Clearly, (i) is met by $T_1 = 0$ and manipulation of (ii) yields

$$(I - \mathbf{P}^T\mathbf{P})\mathbf{B}T_2 = (I - \mathbf{P}^T\mathbf{P})\mathbf{B}\tilde{X}$$

It is obvious that $T_2 = \tilde{X}$ satisfies this constraint, thus, the parameter $\mathbf{P}_{\tilde{X}}$ combined with the choice of T meets conditions 1 through 3.

Condition 4: Using the definitions for $\mathcal{D}$ and D_x in (6B.18) produces

$$\begin{pmatrix} 1 & 0 \\ 0 & \mathbf{P}^T\mathbf{P} \end{pmatrix}(-\mathbf{e}_1) = (-\mathbf{e}_1)$$

and equality is automatic.

Hence, all four conditions are satisfied by maximizing vector $\mathbf{x}(s)$. The proof of the maximizing property for $\mathbf{y}(s)$ is similar and thus omitted. ■

Proof of Lemma 6.6: (Complementary maximizing vectors)

Given the structure of $\mathbf{y}_\perp(s)$ and $\mathbf{x}_\perp(s)$ and the following equations

$$\hat{B}_1^{\perp T}\hat{B}_1^{\perp} = I - \hat{B}_1^T\hat{B}_1 \qquad \text{and} \qquad \hat{C}_1^{\perp}\hat{C}_1^{\perp T} = I - \hat{C}_1\hat{C}_1^T$$

the proof of innerness and orthogonality is direct and therefore omitted. Equality of $\mathbf{B}^T$ with $\tilde{X}^{-1}\overline{B}_{\tilde{X}}\hat{B}_1^{\perp T}$ and $\Gamma^{-1}\mathbf{C}^T$ with $\tilde{Y}^{-1}\overline{C}_{\tilde{Y}}{}^T\hat{C}_1^{\perp}$ follows from the approximation gramian stationary conditions (6.42) and (6.43) in conjunction with the definitions of $\overline{B}_{\tilde{X}}$ and $\overline{C}_{\tilde{Y}}$ in (6.55) and (6.57) respectively. ■

Proof of Theorem 6.3: (Totally stable projections)

The product of $G_{e_{\tilde{X}}}(s)\mathbf{x}_\perp(-s)$ is given as

$$\left[\begin{array}{cc|c} A & 0 & B \\ 0 & \tilde{A}_{\tilde{X}} & \tilde{B}_{\tilde{X}} \\ \hline C & -\tilde{C}_{\tilde{X}} & \sigma_1 U \end{array}\right] \left[\begin{array}{c|c} -\overline{A}_{\tilde{X}}^T & \tilde{X}^{-1}\overline{B}_{\tilde{X}}\hat{B}_1^{\perp T} \\ \hline \overline{B}_{\tilde{X}}^T & \hat{B}_1^{\perp T} \end{array}\right] = \left[\begin{array}{ccc|c} A & 0 & B\overline{B}_{\tilde{X}}^T & B\hat{B}_1^{\perp T} \\ 0 & \tilde{A}_{\tilde{X}} & \tilde{B}_{\tilde{X}}\overline{B}_{\tilde{X}}^T & \tilde{B}_{\tilde{X}}\hat{B}_1^{\perp T} \\ 0 & 0 & -\overline{A}_{\tilde{X}}^T & \tilde{X}^{-1}\overline{B}_{\tilde{X}}\hat{B}_1^{\perp T} \\ \hline C & -\tilde{C}_{\tilde{X}} & -\tilde{D}_{\tilde{X}}\overline{B}_{\tilde{X}}^T & \sigma_1 U\hat{B}_1^{\perp T} \end{array}\right]$$

Next, apply the state similarity transformation $\left(\begin{smallmatrix} I & 0 & T \\ 0 & I & \tilde{X} \\ 0 & 0 & I \end{smallmatrix}\right)$ to obtain

$$\left[\begin{array}{ccc|c} A & 0 & B\overline{B}_{\tilde{X}}^T & B\hat{B}_1^{\perp T} \\ 0 & \tilde{A}_{\tilde{X}} & \tilde{B}_{\tilde{X}}\overline{B}_{\tilde{X}}^T & \tilde{B}_{\tilde{X}}\hat{B}_1^{\perp T} \\ 0 & 0 & -\overline{A}_{\tilde{X}}^T & \tilde{X}^{-1}\overline{B}_{\tilde{X}}\hat{B}_1^{\perp T} \\ \hline C & -\tilde{C}_{\tilde{X}} & -\tilde{D}_{\tilde{X}}\overline{B}_{\tilde{X}}^T & \sigma_1 U\hat{B}_1^{\perp T} \end{array}\right]$$

$$= \left[\begin{array}{cccc|c} A & 0 & AT + T\overline{A}_{\tilde{X}}^T + B\overline{B}_{\tilde{X}}^T & B\hat{B}_1^{\perp T} - T\tilde{X}^{-1}\overline{B}_{\tilde{X}}\hat{B}_1^{\perp T} \\ 0 & \tilde{A}_{\tilde{X}} & \tilde{A}_{\tilde{X}}\tilde{X} + \tilde{X}\overline{A}_{\tilde{X}}^T + \tilde{B}_{\tilde{X}}\overline{B}_{\tilde{X}}^T & \tilde{B}_{\tilde{X}}\hat{B}_1^{\perp T} - \overline{B}_{\tilde{X}}\hat{B}_1^{\perp T} \\ 0 & 0 & -\overline{A}_{\tilde{X}}^T & \tilde{X}^{-1}\overline{B}_{\tilde{X}}\hat{B}_1^{\perp T} \\ \hline C & -\tilde{C}_{\tilde{X}} & C_2 - \tilde{D}_{\tilde{X}}\overline{B}_{\tilde{X}}^T - \tilde{C}_{\tilde{X}}\tilde{X} & \sigma_1\hat{C}_1^{\perp}\mathbf{P}_{\tilde{X}} \end{array}\right]$$

$$= \left[\begin{array}{c|c} -\overline{A}_{\tilde{X}}^T & \mathbf{B}^T \\ \hline C_2 - \tilde{D}_{\tilde{X}}\overline{B}_{\tilde{X}}^T - \tilde{C}_{\tilde{X}}\tilde{X} & \sigma_1\hat{C}_1^{\perp}\mathbf{P}_{\tilde{X}} \end{array}\right] \qquad (6B.20)$$

where transformation matrix T is defined as $T = \begin{pmatrix} 0 \\ I \end{pmatrix}$ with the top row being an $m-$dimensional zero row vector. Also, $\tilde{X}$ is the approximation system controllability gramian which solves Riccati equation (6.44). The last step in (6B.20) is based on the four conditions below which are proven in turn

$$(1) \quad AT + T\overline{A}_{\tilde{X}}^T + B\overline{B}_{\tilde{X}}^T = 0 \qquad (6B.21)$$

$$(2) \quad B\hat{B}_1^{\perp T} \quad T\tilde{X}^{-1}\overline{B}_{\tilde{X}}\hat{B}_1^{\perp T} = 0 \qquad (6B.22)$$

$$(3) \quad \tilde{A}_{\tilde{X}}\tilde{X} + \tilde{X}\overline{A}_{\tilde{X}}^T + \tilde{B}_{\tilde{X}}\overline{B}_{\tilde{X}}^T = 0 \qquad (6B.23)$$

$$(4) \quad \tilde{B}_{\tilde{X}}\hat{B}_1^{\perp T} - \overline{B}_{\tilde{X}}\hat{B}_1^{\perp T} = 0 \qquad (6B.24)$$

Condition 1: Substitution of the relevant definitions of (6B.21) produces

$$\begin{aligned} AT + T\overline{A}_{\tilde{X}}^T + B\overline{B}_{\tilde{X}}^T & \\ &= \begin{pmatrix} a_{11} & A_{12} \\ A_{21} & A_{22} \end{pmatrix} \begin{pmatrix} 0 \\ I \end{pmatrix} + \begin{pmatrix} 0 \\ I \end{pmatrix} \overline{A}_{\tilde{X}}^T + \begin{pmatrix} B_1 \\ B_2 \end{pmatrix} \begin{pmatrix} -\hat{B}_1^T & \hat{B}_1^{\perp T} \end{pmatrix} \begin{pmatrix} \frac{1}{\beta} A_{12} \\ \mathbf{B}\tilde{X} \end{pmatrix} \\ &= \begin{pmatrix} a_{11} & A_{12} \\ A_{21} & A_{22} \end{pmatrix} \begin{pmatrix} 0 \\ I \end{pmatrix} + \begin{pmatrix} 0 \\ I \end{pmatrix} \overline{A}_{\tilde{X}}^T + \begin{pmatrix} -\beta & 0 \\ -B_2\hat{B}_1^T & \mathbf{B}^T \end{pmatrix} \begin{pmatrix} \frac{1}{\beta} A_{12} \\ \mathbf{B}\tilde{X} \end{pmatrix} \\ &= \begin{pmatrix} 0 \\ 0 \end{pmatrix} \end{aligned}$$

or

$$\begin{aligned} (i) \quad & A_{12} - A_{12} = 0 \\ (ii) \quad & A_{22} + \overline{A}_{\tilde{X}}^T + \frac{1}{\beta^2}\left(\Sigma_2 A_{12}^T + \sigma_1 A_{21}\right) A_{12} + \mathbf{B}^T\mathbf{B}\tilde{X} = 0 \end{aligned}$$

Clearly the first equation is automatically satisfied. The algebra in proving the second equation is long and tedious, and therefore, only an outline is sketched below.

$$\begin{aligned} & A_{22} + \overline{A}_{\tilde{X}}^T + \frac{1}{\beta^2}\left(\Sigma_2 A_{12}^T + \sigma_1 A_{21}\right) A_{12} + \mathbf{B}^T\mathbf{B}\tilde{X} \\ &= A_{22} + \left(\mathbf{A}^T - \mathbf{B}^T\mathbf{B}\left(\tilde{X} - \Sigma_2\Gamma^{-1}\right)\Gamma\right)\Gamma^{-1} + \frac{1}{\beta^2}\left(\Sigma_2 A_{12}^T + \sigma_1 A_{21}\right) A_{12} + \mathbf{B}^T\mathbf{B}\tilde{X} \\ &= A_{22} + \mathbf{A}^T\Gamma^{-1} + \mathbf{B}^T\mathbf{B}\Sigma_2\Gamma^{-1} + \frac{1}{\beta^2}\Sigma_2 A_{12}^T A_{12} + \frac{\sigma_1}{\beta^2}\sigma_1 A_{21} A_{12} \end{aligned}$$

Subsequently, use $\beta = \sqrt{-2a_{11}\sigma_1}$ and the following identities which may be derived from the definition of $\tilde{A}$ given in (6.25) and the Central Glover Solution properties (6.7) through (6.12).

$$\begin{aligned} \mathbf{A} &= \sigma_1^2\left(A_{22} - \frac{1}{2a_{11}}A_{21}A_{12}\right)^T + \Sigma_2\left(A_{22} - \frac{1}{2a_{11}}A_{21}A_{12}\right)\Sigma_2 \\ &\quad -\frac{\sigma_1}{2a_{11}}A_{12}^T A_{12}\Sigma_2 - \frac{\sigma_1}{2a_{11}}\Sigma_2 A_{21}A_{21}^T \\ \mathbf{B}^T\mathbf{B} &= B_2\hat{B}_1^{\perp T}\hat{B}_1^{\perp}B_2^T \\ &= B_2(I - \hat{B}_1^T\hat{B}_1)B_2^T \\ &= -A_{22}\Sigma_2 - \Sigma_2 A_{22}^T \\ &\quad -\frac{1}{\beta^2}\left(\sigma_1^2 A_{21}A_{21}^T + \sigma_1 A_{21}A_{12}\Sigma_2 + \sigma_1\Sigma_2 A_{12}^T A_{21}^T + \Sigma_2 A_{12}^T A_{12}\Sigma_2\right) \end{aligned}$$

Condition 2: This is immediate since both $\mathbf{B}^T = B_2\hat{B}_1^{\perp T} = \tilde{X}^{-1}\overline{B}_{\tilde{X}}\hat{B}_1^{\perp T}$ and $T = \binom{0}{I}$ give

$$B\hat{B}_1^{\perp T} - T\tilde{X}^{-1}\overline{B}_{\tilde{X}}\hat{B}_1^{\perp T} = \begin{pmatrix} B_1 \\ B_2 \end{pmatrix}\hat{B}_1^{\perp T} - \begin{pmatrix} 0 \\ I \end{pmatrix} B_2\hat{B}_1^{\perp T} = \begin{pmatrix} 0 \\ 0 \end{pmatrix}$$

Condition 3: Substitute the relevant definitions of (6B.23) to obtain

$$\Gamma^{-1}(\mathbf{A} - \sigma_1\mathbf{C}^T\mathbf{P}_2\mathbf{B})\tilde{X} + \tilde{X}\left(\mathbf{A}\Gamma^{-1} - \mathbf{B}^T\mathbf{B}(\tilde{X} - \Sigma_2\Gamma^{-1})\right)$$
$$+ \left(\tfrac{1}{\beta}A_{12}^T \quad \Gamma^{-1}(\sigma_1\mathbf{C}^T\mathbf{P}_{\tilde{X}} + \Sigma_2\mathbf{B}^T)\right)\begin{pmatrix} -\hat{B}_1 \\ \hat{B}_1^{\perp} \end{pmatrix}\left(-\hat{B}_1^T \quad \hat{B}_1^{\perp T}\right)\begin{pmatrix} \frac{1}{\beta}A_{12} \\ \mathbf{B}\tilde{X} \end{pmatrix} = 0$$

By carrying out the multiplication and cancelling terms, this reduces to Riccati equation (6.44).

Condition 4: This condition holds automatically for the square case since $\tilde{B}_{\tilde{X}} = \overline{B}_{\tilde{X}}$.

Thus, the fulfillment of all four conditions implies that a minimal realization of the product $G_{e_{\tilde{X}}}(s)\mathbf{x}_\perp(-s)$ is given by (6B.20). To obtain the overall projection, premultiply (6B.20) by $\mathbf{y}_\perp{}^T(-s)$ to obtain the totally stable projection

$$\mathbf{y}_\perp{}^T(-s)G_{e_{\tilde{X}}}(s)\mathbf{x}_\perp(-s) = \left[\begin{array}{cc|c} -\overline{A}_{\tilde{Y}}^T & \overline{C}_{\tilde{Y}}^T(C_2 - \tilde{D}_{\tilde{X}}\overline{B}_{\tilde{X}}^T - \tilde{C}_{\tilde{X}}\tilde{X}) & \sigma_1\tilde{Y}\Gamma^{-1}\mathbf{C}^T\mathbf{P}_{\tilde{X}} \\ 0 & -\overline{A}_{\tilde{X}}^T & \mathbf{B}^T \\ \hline \mathbf{C}\Gamma^{-1} & \mathbf{C}(I - \Sigma_2\tilde{X}) & \sigma_1\mathbf{P}_{\tilde{X}} \end{array}\right]$$

Next, with $T = \Gamma(I - \Sigma_2\tilde{X})$, apply the state similarity transformation $\begin{pmatrix} I & -T \\ 0 & I \end{pmatrix}$ to obtain

$$\left[\begin{array}{cc|c} -\overline{A}_{\tilde{Y}}^T & \overline{C}_{\tilde{Y}}^T(C_2 - \tilde{D}_{\tilde{X}}\overline{B}_{\tilde{X}}^T - \tilde{C}_{\tilde{X}}\tilde{X}) & \sigma_1\tilde{Y}\Gamma^{-1}\mathbf{C}^T\mathbf{P}_{\tilde{X}} \\ 0 & -\overline{A}_{\tilde{X}}^T & \mathbf{B}^T \\ \hline \mathbf{C}\Gamma^{-1} & \mathbf{C}(I - \Sigma_2\tilde{X}) & \sigma_1\mathbf{P}_{\tilde{X}} \end{array}\right]$$

$$= \left[\begin{array}{cc|c} -\overline{A}_{\tilde{Y}}^T & \overline{A}_{\tilde{Y}}^T\Gamma(I-\Sigma_2\tilde{X}) - \Gamma(I-\Sigma_2\tilde{X})\overline{A}_{\tilde{X}}^T + \overline{C}_{\tilde{Y}}^T(C_2 - \tilde{D}_{\tilde{X}}\overline{B}_{\tilde{X}}^T - \tilde{C}_{\tilde{X}}\tilde{X}) & \sigma_1\tilde{Y}\Gamma^{-1}\mathbf{C}^T\mathbf{P}_{\tilde{X}} + \Gamma(I-\Sigma_2\tilde{X})\mathbf{B}^T \\ 0 & -\overline{A}_{\tilde{X}}^T & \mathbf{B}^T \\ \hline \mathbf{C}\Gamma^{-1} & \mathbf{C}(I-\Sigma_2\tilde{X}) - \mathbf{C}\Gamma^{-1}\Gamma(I-\Sigma_2\tilde{X}) & \sigma_1\mathbf{P}_{\tilde{X}} \end{array}\right]$$

$$
\begin{aligned}
&= \left[\begin{array}{cc|c} -\overline{A}_{\tilde{Y}}^T & 0 & \sigma_1 \tilde{Y}\Gamma^{-1}\mathbf{C}^T\mathbf{P}_{\tilde{X}} + \Gamma(I-\Sigma_2\tilde{X})\mathbf{B}^T \\ 0 & -\overline{A}_{\tilde{X}}^T & \mathbf{B}^T \\ \hline \mathbf{C}\Gamma^{-1} & 0 & \sigma_1\mathbf{P}_{\tilde{X}} \end{array}\right] \\
&= \left[\begin{array}{c|c} -\overline{A}_{\tilde{Y}} & -\sigma_1^2\mathbf{B}^T(I-\mathbf{P}_{\tilde{Y}}{}^T\mathbf{P}_{\tilde{X}}) \\ \hline \mathbf{C}\Gamma^{-1} & \sigma_1\mathbf{P}_{\tilde{X}} \end{array}\right] \qquad \text{(6B.25)}
\end{aligned}
$$

where the final form given is the totally stable projection of (6.61). Clearly, the derivation of (6B.25) was based on the fact that

$$
\overline{A}_{\tilde{Y}}^T\Gamma(I-\Sigma_2\tilde{X}) - \Gamma(I-\Sigma_2\tilde{X})\overline{A}_{\tilde{X}}^T + \overline{C}_{\tilde{Y}}^T(C_2 - \tilde{D}_{\tilde{X}}\overline{B}_{\tilde{X}}^T - \tilde{C}_{\tilde{X}}\tilde{X}) = 0 \qquad \text{(6B.26)}
$$

which is proven next. Use of the state-space formulae for $\overline{B}_{\tilde{X}}$, $\overline{C}_{\tilde{Y}}$, $\tilde{C}_{\tilde{X}}$, and $\tilde{D}_{\tilde{X}}$ given in (6.55), (6.57), and (6.50), respectively, yields

$$
\begin{aligned}
&\overline{C}_{\tilde{Y}}(C_2 - \tilde{D}_{\tilde{X}}\overline{B}_{\tilde{X}}^T - \tilde{C}_{\tilde{X}}\tilde{X}) \\
&\quad = \left(-\tfrac{1}{\beta}\Gamma A_{21} \quad \tilde{Y}\Gamma^{-1}\mathbf{C}^T\right)\begin{pmatrix} \hat{C}_1^T \\ \hat{C}_1^{\perp T} \end{pmatrix}\left(\hat{C}_1 \quad \hat{C}_1^{\perp}\right)\begin{pmatrix} \frac{1}{\beta}A_{21}^T\Gamma(\tilde{X}-\Sigma_2\Gamma^{-1}) \\ \mathbf{C}(I-\Sigma_2\tilde{X}) \end{pmatrix} \\
&\quad = -\frac{1}{\beta^2}\Gamma A_{21}A_{21}^T\Gamma(\tilde{X}-\Sigma_2\Gamma^{-1}) + \tilde{Y}\Gamma^{-1}\mathbf{C}^T\mathbf{C}(I-\Sigma_2\tilde{X})
\end{aligned}
$$

Substitution of this together with the definitions of $\overline{A}_{\tilde{Y}}$, $\overline{A}_{\tilde{X}}$ and $\overline{C}_{\tilde{Y}}$ of (6.56), (6.54), and (6.57), respectively, into (6B.26) gives

$$
\begin{aligned}
&(\mathbf{A}^T - \tilde{Y}\Gamma^{-1}\mathbf{C}^T\mathbf{C} + \Sigma_2\mathbf{C}^T\mathbf{C})(I-\Sigma_2\tilde{X}) \\
&\quad -\Gamma(I-\Sigma_2\tilde{X})(\mathbf{A}^T\Gamma^{-1} - \mathbf{B}^T\mathbf{B}(\tilde{X}-\Sigma_2\Gamma^{-1})) \\
&\quad -\frac{1}{\beta^2}\Gamma A_{21}A_{21}^T\Gamma(\tilde{X}-\Sigma_2\Gamma^{-1}) + \tilde{Y}\Gamma^{-1}\mathbf{C}^T\mathbf{C}(I-\Sigma_2\tilde{X}) = 0
\end{aligned}
$$

or

$$
\begin{aligned}
(\mathbf{A}^T + \Sigma_2\mathbf{C}^T\mathbf{C})(I-\Sigma_2\tilde{X}) - \Gamma(I-\Sigma_2\tilde{X})(\mathbf{A}^T\Gamma^{-1} - \mathbf{B}^T\mathbf{B}(\tilde{X}-\Sigma_2\Gamma^{-1})) \\
-\frac{1}{\beta^2}\Gamma A_{21}A_{21}^T\Gamma(\tilde{X}-\Sigma_2\Gamma^{-1}) = 0
\end{aligned}
$$

or

$$
\begin{aligned}
&(\mathbf{A}^T\Gamma^{-1} + \Sigma_2\mathbf{C}^T\mathbf{C}\Gamma^{-1})\Gamma(I-\Sigma_2\tilde{X}) - \Gamma(I-\Sigma_2\tilde{X})\mathbf{A}^T\Gamma^{-1} \\
&\quad + \left(\Gamma(I-\Sigma_2\tilde{X})\mathbf{B}^T\mathbf{B} - \frac{1}{\beta^2}\Gamma A_{21}A_{21}^T\Gamma\right)(\tilde{X}-\Sigma_2\Gamma^{-1}) = 0
\end{aligned}
$$

Hence

$$(\mathbf{A}^T\Gamma^{-1} + \Sigma_2\mathbf{C}^T\mathbf{C}\Gamma^{-1})\Gamma(I - \Sigma_2\tilde{X}) - \Gamma(I - \Sigma_2\tilde{X})\mathbf{A}^T\Gamma^{-1}$$
$$+ \left(\Gamma\mathbf{B}^T\mathbf{B} - \Sigma_2\Gamma\tilde{X}\mathbf{B}^T\mathbf{B} + \sigma_1^2\mathbf{B}^T\mathbf{B} + \Sigma_2\mathbf{A} + \mathbf{A}^T\Sigma_2 + \Sigma_2\mathbf{C}^T\mathbf{C}\Sigma_2\right)(\tilde{X} - \Sigma_2\Gamma^{-1})$$
$$= 0$$

where Hankel singular value property (6.37) has been employed. Carrying out the multiplications produces

$$\begin{aligned}
&\mathbf{A}^T + \Sigma_2\mathbf{C}^T\mathbf{C} - \mathbf{A}^T\Sigma_2\tilde{X} - \Sigma_2\mathbf{C}^T\mathbf{C}\Sigma_2\tilde{X} - \Gamma\mathbf{A}^T\Gamma^{-1} + \Sigma_2\Gamma\tilde{X}\mathbf{A}^T\Gamma^{-1} + \Sigma_2^2\mathbf{B}^T\mathbf{B}\tilde{X} \\
&\quad -\Sigma_2\Gamma\tilde{X}\mathbf{B}^T\mathbf{B}\tilde{X} + \Sigma_2\mathbf{A}\tilde{X} + \mathbf{A}^T\Sigma_2\tilde{X} + \Sigma_2\mathbf{C}^T\mathbf{C}\Sigma_2\tilde{X} - \Sigma_2^2\mathbf{B}^T\mathbf{B}\Sigma_2\Gamma^{-1} \\
&\quad +\Sigma_2\Gamma\tilde{X}\mathbf{B}^T\mathbf{B}\Sigma_2\Gamma^{-1} - \Sigma_2\mathbf{A}\Sigma_2\Gamma^{-1} - \mathbf{A}^T\Sigma_2^2\Gamma^{-1} - \Sigma_2\mathbf{C}^T\mathbf{C}\Sigma_2^2\Gamma^{-1} \\
= \;& -\sigma_1^2(\mathbf{A}^T + \Sigma_2\mathbf{C}^T\mathbf{C})\Gamma^{-1} - \Gamma\mathbf{A}^T\Gamma^{-1} + \Sigma_2\Gamma\tilde{X}\mathbf{A}^T\Gamma^{-1} + \Sigma_2^2\mathbf{B}^T\mathbf{B}\tilde{X} \\
&\quad -\Sigma_2\Gamma\tilde{X}\mathbf{B}^T\mathbf{B}\tilde{X} + \Sigma_2\mathbf{A}\tilde{X} - \Sigma_2^2\mathbf{B}^T\mathbf{B}\Sigma_2\Gamma^{-1} + \Sigma_2\Gamma\tilde{X}\mathbf{B}^T\mathbf{B}\Sigma_2\Gamma^{-1} - \Sigma_2\mathbf{A}\Sigma_2\Gamma^{-1}
\end{aligned}$$

where straightforward cancellations were employed along with the identity

$$(\mathbf{A}^T + \Sigma_2\mathbf{C}^T\mathbf{C})(I - \Sigma_2^2\Gamma^{-1}) = (\mathbf{A}^T + \Sigma_2\mathbf{C}^T\mathbf{C})\Gamma^{-1}(\Gamma - \Sigma_2^2) = -\sigma_1^2(\mathbf{A}^T + \Sigma_2\mathbf{C}^T\mathbf{C})\Gamma^{-1}$$

Next, use $-\Gamma\mathbf{A}^T\Gamma^{-1} = -\Sigma_2^2\mathbf{A}^T\Gamma^{-1} + \sigma_1^2\mathbf{A}^T\Gamma^{-1}$ and regroup terms to obtain

$$\begin{aligned}
&-\sigma_1^2\Sigma_2\mathbf{C}^T\mathbf{C}\Gamma^{-1} - \Sigma_2^2\mathbf{A}^T\Gamma^{-1} \\
&\quad +\Sigma_2\Gamma\tilde{X}\left(\mathbf{A}^T\Gamma^{-1} - \mathbf{B}^T\mathbf{B}(\tilde{X} - \Sigma_2\Gamma^{-1})\right) + \Sigma_2(\mathbf{A} + \Sigma_2\mathbf{B}^T\mathbf{B})(\tilde{X} - \Sigma_2\Gamma^{-1})
\end{aligned}$$

Finally, use (6.42) and (6.44) to transform the above into Riccati equation (6.36) which is satisfied within the Central Glover Solution. This then confirms the validity of the loss of observability in (6B.25) and thus the simplified form of the stable projection given in (6.61). Since the approximation system is entirely antistable, $-\overline{A}_{\tilde{X}}^T$ is entirely stable and thus the projected system is entirely stable. The proof of (6.61) is analogous and therefore omitted. ■

Proof of Lemma 6.7: (Core term minimal realization)

The complementary maximizing vector product $\mathbf{y}_\perp{}^{(r)}(s)F^{(r-1)}(s)\mathbf{x}_\perp{}^{T\,(r)}(s)$ is realized as:

$$\mathbf{y}_\perp{}^{(r)}(s)F^{(r-1)}(s)\mathbf{x}_\perp{}^{T\,(r)}(s) = \left[\begin{array}{ccc|c} \overline{A}_{\tilde{Y}} & \overline{B}_{\tilde{Y}}\tilde{C}_{\tilde{Y}} & \overline{B}_{\tilde{Y}}\tilde{D}_{\tilde{Y}}\overline{C}_{\tilde{X}} & \overline{B}_{\tilde{Y}}\tilde{D}_{\tilde{Y}}\overline{D}_{\tilde{X}} \\ 0 & \tilde{A}_{\tilde{Y}} & \tilde{B}_{\tilde{Y}}\overline{C}_{\tilde{X}} & \tilde{B}_{\tilde{Y}}\overline{D}_{\tilde{X}} \\ 0 & 0 & \overline{A}_{\tilde{X}} & \overline{B}_{\tilde{X}} \\ \hline \overline{C}_{\tilde{Y}} & \overline{D}_{\tilde{Y}}\tilde{C}_{\tilde{Y}} & \overline{D}_{\tilde{Y}}\tilde{D}_{\tilde{Y}}\overline{C}_{\tilde{X}} & \overline{D}_{\tilde{Y}}\tilde{D}_{\tilde{Y}}\overline{D}_{\tilde{X}} \end{array}\right]$$

Apply the state-similarity transformation $\left(\begin{smallmatrix} I & T_2 & T_1 \\ 0 & I & 0 \\ 0 & 0 & I \end{smallmatrix}\right)$ to obtain:

$$\mathbf{y}_\perp{}^{(r)}(s)F^{(r-1)}(s)\mathbf{x}_\perp{}^{T\,(r)}(s) = \left[\begin{array}{ccc|c} \overline{A}_{\tilde{Y}} & 0 & 0 & \overline{B}_{\tilde{Y}}\tilde{D}_{\tilde{Y}}\overline{D}_{\tilde{X}} - T_1\overline{B}_{\tilde{X}} - T_2\tilde{B}_{\tilde{Y}}\overline{D}_{\tilde{X}} \\ 0 & \tilde{A}_{\tilde{Y}} & \tilde{B}_{\tilde{Y}}\overline{C}_{\tilde{X}} & \tilde{B}_{\tilde{Y}}\overline{D}_{\tilde{X}} \\ 0 & 0 & \overline{A}_{\tilde{X}} & \overline{B}_{\tilde{X}} \\ \hline \overline{C}_{\tilde{Y}} & \overline{C}_{\tilde{Y}}T_2 + \overline{D}_{\tilde{Y}}\tilde{C}_{\tilde{Y}} & \overline{C}_{\tilde{Y}}T_1 + \overline{D}_{\tilde{Y}}\tilde{D}_{\tilde{Y}}\overline{C}_{\tilde{X}} & \overline{D}_{\tilde{Y}}\tilde{D}_{\tilde{Y}}\overline{D}_{\tilde{X}} \end{array}\right] \tag{6B.27}$$

where T_1 and T_2 solve the following Sylvester equations:

$$\overline{A}_{\tilde{Y}}T_1 - T_1\overline{A}_{\tilde{X}} - T_2\tilde{B}_{\tilde{Y}}\overline{C}_{\tilde{X}} + \overline{B}_{\tilde{Y}}\tilde{D}_{\tilde{Y}}\overline{C}_{\tilde{X}} = 0 \tag{6B.28}$$

$$\overline{A}_{\tilde{Y}}T_2 - T_2\tilde{A}_{\tilde{Y}} + \overline{B}_{\tilde{Y}}\tilde{C}_{\tilde{Y}} = 0 \tag{6B.29}$$

Note that (6B.29) must be solved prior to computing (6B.28) since T_2 is required to solve for T_1. Next apply the state-similarity transformation $\left(\begin{smallmatrix} I & 0 & 0 \\ 0 & I & T_3 \\ 0 & 0 & I \end{smallmatrix}\right)$ to obtain:

$$\mathbf{y}_\perp{}^{(r)}(s)F^{(r-1)}(s)\mathbf{x}_\perp{}^{T\,(r)}(s) = \left[\begin{array}{ccc|c} \overline{A}_{\tilde{Y}} & 0 & 0 & \overline{B}_{\tilde{Y}}\tilde{D}_{\tilde{Y}}\overline{D}_{\tilde{X}} - T_1\overline{B}_{\tilde{X}} - T_2\tilde{B}_{\tilde{Y}}\overline{D}_{\tilde{X}} \\ 0 & \tilde{A}_{\tilde{Y}} & 0 & \tilde{B}_{\tilde{Y}}\overline{D}_{\tilde{X}} - T_3\overline{B}_{\tilde{X}} \\ 0 & 0 & \overline{A}_{\tilde{X}} & \overline{B}_{\tilde{X}} \\ \hline \overline{C}_{\tilde{Y}} & \overline{C}_{\tilde{Y}}T_2 + \overline{D}_{\tilde{Y}}\tilde{C}_{\tilde{Y}} & \begin{array}{l}\overline{C}_{\tilde{Y}}(T_1 + T_2T_3) \\ +\overline{D}_{\tilde{Y}}\left(\tilde{D}_{\tilde{Y}}\overline{C}_{\tilde{X}} + \tilde{C}_{\tilde{Y}}T_3\right)\end{array} & \overline{D}_{\tilde{Y}}\tilde{D}_{\tilde{Y}}\overline{D}_{\tilde{X}} \end{array}\right] \tag{6B.30}$$

where T_3 solves the following Sylvester equation:

$$\tilde{A}_{\tilde{Y}}T_3 - T_3\overline{A}_{\tilde{X}} + \tilde{B}_{\tilde{Y}}\overline{C}_{\tilde{X}} = 0 \tag{6B.31}$$

Next, perform the state-similarity transformation $\begin{pmatrix} I & 0 & 0 \\ 0 & I & 0 \\ 0 & 0 & T_4^{-1} \end{pmatrix}$ to obtain:

$$\mathbf{y}_\perp{}^{(r)}(s)F^{(r-1)}(s)\mathbf{x}_\perp{}^{T\,(r)}(s) =$$

$$\left[\begin{array}{ccc|c} \overline{A}_{\tilde{Y}} & 0 & 0 & \overline{B}_{\tilde{Y}}\tilde{D}_{\tilde{Y}}\overline{D}_{\tilde{X}} - T_1\overline{B}_{\tilde{X}} - T_2\tilde{B}_{\tilde{Y}}\overline{D}_{\tilde{X}} \\ 0 & \tilde{A}_{\tilde{Y}} & 0 & \tilde{B}_{\tilde{Y}}\overline{D}_{\tilde{X}} - T_3\overline{B}_{\tilde{X}} \\ 0 & 0 & \overline{A}_{\tilde{Y}} & T_4\overline{B}_{\tilde{X}} \\ \hline \overline{C}_{\tilde{Y}} & \overline{C}_{\tilde{Y}}T_2 + \overline{D}_{\tilde{Y}}\tilde{C}_{\tilde{Y}} & \overline{C}_{\tilde{Y}} & \overline{D}_{\tilde{Y}}\tilde{D}_{\tilde{Y}}\overline{D}_{\tilde{X}} \end{array}\right] \tag{6B.32}$$

where the following three conditions have been used and will be subsequently justified:

$$(1) \quad T_4\overline{A}_{\tilde{X}}T_4^{-1} = \overline{A}_{\tilde{Y}} \tag{6B.33}$$

$$(2) \quad T_4 = T_1 + T_2T_3 \tag{6B.34}$$

$$(3) \quad \tilde{D}_{\tilde{Y}}\overline{C}_{\tilde{X}} + \tilde{C}_{\tilde{Y}}T_3 = 0 \tag{6B.35}$$

Condition 1: Since the maximizing vectors $\overline{A}_{\tilde{X}}$ and $\overline{A}_{\tilde{Y}}$ share the same spectrum [Limebeer et al., 1989], there exists a similarity transformation T_4 which satisfies (6B.33), hence T_4 is chosen to meet (6B.33).

Conditions 2 & 3: Post multiply (6B.29) by T_3 and add this to (6B.28) to get:

$$\overline{A}_{\tilde{Y}}(T_1 + T_2T_3) - T_1T_4^{-1}\overline{A}_{\tilde{Y}}T_4 - T_2\left(\tilde{A}_{\tilde{Y}}T_3 + \tilde{B}_{\tilde{Y}}\overline{C}_{\tilde{X}}\right) + \overline{B}_{\tilde{Y}}\left(\tilde{D}_{\tilde{Y}}\overline{C}_{\tilde{X}} + \tilde{C}_{\tilde{Y}}T_3\right) = 0 \tag{6B.36}$$

where (6B.33) has been used. Next, use (6B.31) and combine terms to obtain:

$$\overline{A}_{\tilde{Y}}(T_1 + T_2T_3) - (T_1 + T_2T_3)T_4^{-1}\overline{A}_{\tilde{Y}}T_4 + \overline{B}_{\tilde{Y}}\left(\tilde{D}_{\tilde{Y}}\overline{C}_{\tilde{X}} + \tilde{C}_{\tilde{Y}}T_3\right) = 0 \tag{6B.37}$$

Since $\overline{B}_{\tilde{Y}}$ is "tall" in the square case, first premultiply (6B.37) by its Moore-Penrose pseudo-inverse $\overline{B}_{\tilde{Y}}^{\dagger}$ and next by its orthogonal complement $\overline{B}_{\tilde{Y}}^{\perp}$ to get the following two conditions:

$$(i) \quad \overline{B}_{\tilde{Y}}^{\dagger}\left[\overline{A}_{\tilde{Y}}(T_1 + T_2T_3) - (T_1 + T_2T_3)T_4^{-1}\overline{A}_{\tilde{Y}}T_4\right] + \tilde{D}_{\tilde{Y}}\overline{C}_{\tilde{X}} + \tilde{C}_{\tilde{Y}}T_3 = 0 \tag{6B.38}$$

$$(ii) \quad \overline{B}_{\tilde{Y}}^{\perp}\left(\overline{A}_{\tilde{Y}}(T_1 + T_2T_3) - (T_1 + T_2T_3)T_4^{-1}\overline{A}_{\tilde{Y}}T_4\right) = 0 \tag{6B.39}$$

Equation (ii) clearly implies that sufficiency is met by $T_4 = T_1 + T_2T_3$, hence (6B.34) is satisfied. Using this result in (i) implies that $\tilde{D}_{\tilde{Y}}\overline{C}_{\tilde{X}} + \tilde{C}_{\tilde{Y}}T_3 = 0$ and (6B.35) is met. Thus (6B.32) is valid and its states may be combined to yield:

$$\mathbf{y}_\perp{}^{(r)}(s)F^{(r-1)}(s)\mathbf{x}_\perp{}^{T\,(r)}(s) =$$

$$\left[\begin{array}{cc|c} \overline{A}_{\tilde{Y}} & 0 & \overline{B}_{\tilde{Y}}\tilde{D}_{\tilde{Y}}\overline{D}_{\tilde{X}} - T_2\tilde{B}_{\tilde{Y}}\overline{D}_{\tilde{X}} + T_2T_3\overline{B}_{\tilde{X}} \\ 0 & \tilde{A}_{\tilde{Y}} & \tilde{B}_{\tilde{Y}}\overline{D}_{\tilde{X}} - T_3\overline{B}_{\tilde{X}} \\ \hline \overline{C}_{\tilde{Y}} & \overline{C}_{\tilde{Y}}T_2 + \overline{D}_{\tilde{Y}}\tilde{C}_{\tilde{Y}} & \overline{D}_{\tilde{Y}}\tilde{D}_{\tilde{Y}}\overline{D}_{\tilde{X}} \end{array}\right] \tag{6B.40}$$

where (6B.34) has been employed. By use of (6B.29), this may be put in the following simpler form:

$$\mathbf{y}_\perp{}^{(r)}(s)F^{(r-1)}(s)\mathbf{x}_\perp{}^{T\,(r)}(s) = \left[\begin{array}{cc|c} \overline{A}_{\tilde{Y}} & \overline{B}_{\tilde{Y}}\tilde{C}_{\tilde{Y}} & \overline{B}_{\tilde{Y}}\tilde{D}_{\tilde{Y}}\overline{D}_{\tilde{X}} \\ 0 & \tilde{A}_{\tilde{Y}} & \tilde{B}_{\tilde{Y}}\overline{D}_{\tilde{X}} - T_3\overline{B}_{\tilde{X}} \\ \hline \overline{C}_{\tilde{Y}} & \overline{D}_{\tilde{Y}}\tilde{C}_{\tilde{Y}} & \overline{D}_{\tilde{Y}}\tilde{D}_{\tilde{Y}}\overline{D}_{\tilde{X}} \end{array}\right] \tag{6B.41}$$

(6B.42)

Finally, by adding to this the approximation system $F^{(r)}(s)$ which is matched to the left complementary maximizing vector observability pair $(\overline{A}_{\tilde{Y}}, \overline{C}_{\tilde{Y}})$, the result of (6.66) is obtained. ■

Proof of Theorem 6.4: (Singular value total flatness)

Equation (6B.20) gives:

$$\mathbf{x}_\perp{}^T(s)G_{e_{\tilde{X}}}^T(-s)G_{e_{\tilde{X}}}(s)\mathbf{x}_\perp(-s) =$$

$$\left[\begin{array}{cc|c} \overline{A}_{\tilde{X}} & -\mathbf{M} & -\sigma_1(I - \tilde{X}\Sigma_2)\mathbf{C}^T\mathbf{P}_{\tilde{X}} \\ 0 & -\overline{A}_{\tilde{X}}^T & \mathbf{B}^T \\ \hline \mathbf{B} & \sigma_1\mathbf{P}_{\tilde{X}}{}^T\mathbf{C}(I - \Sigma_2\tilde{X}) & \sigma_1^2\mathbf{P}_{\tilde{X}}\mathbf{P}_{\tilde{X}}{}^T \end{array}\right] \tag{6B.43}$$

where $\mathbf{M}$ is given by

$$\begin{aligned} \mathbf{M} &= \frac{1}{\beta^2}(\tilde{X} - \Sigma_2\Gamma^{-1})\Gamma A_{21}A_{21}^T\Gamma(\tilde{X} - \Sigma_2\Gamma^{-1}) \\ &\quad + \mathbf{C}^T\mathbf{C} - \mathbf{C}^T\mathbf{C}\Sigma_2\tilde{X} - \tilde{X}\Sigma_2\mathbf{C}^T\mathbf{C} + \tilde{X}\Sigma_2\mathbf{C}^T\mathbf{C}\Sigma_2\tilde{X} \end{aligned} \tag{6B.44}$$

Next, let T be given as

$$T = \sigma_1(I - \tilde{X}\Sigma_2)\mathbf{C}^T\mathbf{P}_{\tilde{X}}\mathbf{B}^{T^{-1}} = (I - \tilde{X}\Sigma_2)(\Gamma\tilde{X} - \Sigma_2) \tag{6B.45}$$

where the equality $\sigma_1 \mathbf{C}^T \mathbf{P}_{\tilde{x}} \mathbf{B}^{T^{-1}} = (\Gamma\tilde{X} - \Sigma_2)$ has been used as implied by (6.42). Note that T is symmetric as shown below

$$\begin{aligned} T = (I - \tilde{X}\Sigma_2)(\Gamma\tilde{X} - \Sigma_2) &= \Gamma\tilde{X} + \tilde{X}\Sigma_2^2 - \tilde{X}\Sigma_2\Gamma\tilde{X} - \Sigma_2 \\ &= \Sigma_2^2\tilde{X} - \sigma_1^2\tilde{X} + \tilde{X}\Sigma_2^2 - \tilde{X}\Sigma_2\Gamma\tilde{X} - \Sigma_2 \\ &= (\tilde{X}\Gamma - \Sigma_2)(I - \Sigma_2\tilde{X}) \end{aligned}$$

Therefore, applying the state similarity transformation $\begin{pmatrix} I & T \\ 0 & I \end{pmatrix}$ to (6B.43) and using the symmetry of T, it is deduced that

$$\begin{aligned} \mathbf{x}_\perp{}^T(s) G_{e_{\tilde{X}}}^T(-s) G_{e_{\tilde{X}}}(s) \mathbf{x}_\perp(-s) &= \left[\begin{array}{cc|c} \overline{A}_{\tilde{X}} & -\left(\overline{A}_{\tilde{X}}T + T\overline{A}_{\tilde{X}}^T + \mathbf{M}\right) & 0 \\ 0 & -\overline{A}_{\tilde{X}}^T & \mathbf{B}^T \\ \hline \mathbf{B} & 0 & \sigma_1^2 \mathbf{P}_{\tilde{X}} \mathbf{P}_{\tilde{X}}{}^T \end{array}\right] \\ &= \sigma_1^2 \mathbf{P}_{\tilde{X}} \mathbf{P}_{\tilde{X}}{}^T \end{aligned} \tag{6B.46}$$

The last step in (6B.46) is based on the fact that

$$\overline{A}_{\tilde{X}}T + T\overline{A}_{\tilde{X}}^T + \mathbf{M} = 0 \tag{6B.47}$$

which is proven next. First, $\overline{A}_{\tilde{X}}T$ is given by

$$\begin{aligned} \overline{A}_{\tilde{X}}T &= \Gamma^{-1}\left(\mathbf{A} - (\Gamma\tilde{X} - \Sigma_2)\mathbf{B}^T\mathbf{B}\right)\sigma_1 \mathbf{B}^{-1}\mathbf{P}_{\tilde{X}}{}^T\mathbf{C}(I - \Sigma_2\tilde{X}) \\ &= \Gamma^{-1}\left(\sigma_1\mathbf{A}\mathbf{B}^{-1}\mathbf{P}_{\tilde{X}}{}^T\mathbf{C} - \sigma_1^2\mathbf{C}^T\mathbf{P}_{\tilde{X}}\mathbf{P}_{\tilde{X}}{}^T\mathbf{C}\right)(I - \Sigma_2\tilde{X}) \end{aligned} \tag{6B.48}$$

where (6.42) was used and, hence

$$\begin{aligned} &\overline{A}_{\tilde{X}}T + \mathbf{C}^T\mathbf{C}(I - \Sigma_2\tilde{X}) \\ &\quad = \Gamma^{-1}\left(\sigma_1\mathbf{A}\mathbf{B}^{-1}\mathbf{P}_{\tilde{X}}{}^T\mathbf{C} - \sigma_1^2\mathbf{C}^T\mathbf{P}_{\tilde{X}}\mathbf{P}_{\tilde{X}}{}^T\mathbf{C}\right)(I - \Sigma_2\tilde{X}) + \mathbf{C}^T\mathbf{C}(I - \Sigma_2\tilde{X}) \\ &\quad = \Gamma^{-1}\left(\sigma_1\mathbf{A}\mathbf{B}^{-1}\mathbf{P}_{\tilde{X}}{}^T\mathbf{C} + \Sigma_2^2\mathbf{C}^T\mathbf{C} - \sigma_1^2\mathbf{C}^T(I + \mathbf{P}_{\tilde{X}}\mathbf{P}_{\tilde{X}}{}^T)\mathbf{C}\right)(I - \Sigma_2\tilde{X}) \end{aligned}$$

Observe that $\sigma_1^2\mathbf{C}^T(I + \mathbf{P}_{\tilde{X}}\mathbf{P}_{\tilde{X}}{}^T)\mathbf{C}$ may be obtained from (6B.8). Using this and continuing gives

$$\begin{aligned} \overline{A}_{\tilde{X}}T + \mathbf{C}^T\mathbf{C}(I - \Sigma_2\tilde{X}) &= \Gamma^{-1}\big(\sigma_1\mathbf{A}\mathbf{B}^{-1}\mathbf{P}_{\tilde{X}}{}^T\mathbf{C} + \Sigma_2^2\mathbf{C}^T\mathbf{C} - \sigma_1\mathbf{C}^T\mathbf{P}_{\tilde{X}}\mathbf{B}^{T^{-1}}\mathbf{A}^T \\ &\qquad + \sigma_1\mathbf{A}\mathbf{B}^{-1}\mathbf{P}_{\tilde{X}}{}^T\mathbf{C}\big)(I - \Sigma_2\tilde{X}) \\ &= \Gamma^{-1}\left(\Sigma_2^2\mathbf{C}^T\mathbf{C} - \sigma_1\mathbf{C}^T\mathbf{P}_{\tilde{X}}\mathbf{B}^{T^{-1}}\mathbf{A}^T\right)(I - \Sigma_2\tilde{X}) \end{aligned}$$

Using this together with (6.37) yields

$$\begin{aligned}
&\overline{A}_{\tilde{X}}T + T\overline{A}_{\tilde{X}}^T + \mathbf{M} + \mathbf{C}^T\mathbf{C} - \mathbf{C}^T\mathbf{C} = \\
&\quad \Sigma_2^2\Gamma^{-1}\mathbf{C}^T\mathbf{C} - (\Sigma_2^2\Gamma^{-1}\mathbf{C}^T\mathbf{C}\Sigma_2\tilde{X}) - \sigma_1\Gamma^{-1}\mathbf{C}^T\mathbf{P}_{\tilde{X}}\mathbf{B}^{T^{-1}}\mathbf{A}^T \\
&\quad +\sigma_1\Gamma^{-1}\mathbf{C}^T\mathbf{P}_{\tilde{X}}\mathbf{B}^{T^{-1}}\mathbf{A}^T\Sigma_2\tilde{X} + \mathbf{C}^T\mathbf{C}\Sigma_2^2\Gamma^{-1} - (\tilde{X}\Sigma_2\mathbf{C}^T\mathbf{C}\Sigma_2^2\Gamma^{-1}) \\
&\quad -\sigma_1\mathbf{A}\mathbf{B}^{-1}\mathbf{P}_{\tilde{X}}{}^T\mathbf{C}\Gamma^{-1} + \sigma_1\tilde{X}\Sigma_2\mathbf{A}\mathbf{B}^{-1}\mathbf{P}_{\tilde{X}}{}^T\mathbf{C}\Gamma^{-1} - \tilde{X}\Sigma_2\mathbf{A}\tilde{X} - \tilde{X}\mathbf{A}^T\Sigma_2\tilde{X} \\
&\quad -(\tilde{X}\Sigma_2\mathbf{C}^T\mathbf{C}\Sigma_2\tilde{X}) - [\sigma_1^2\tilde{X}\mathbf{B}^T\mathbf{B}\tilde{X}] + \Sigma_2^2\Gamma^{-1}\mathbf{A}\tilde{X} + \Sigma_2\Gamma^{-1}\mathbf{A}^T\Sigma_2\tilde{X} \\
&\quad +(\Sigma_2^2\Gamma^{-1}\mathbf{C}^T\mathbf{C}\Sigma_2\tilde{X}) + [\sigma_1^2\Sigma_2\Gamma^{-1}\mathbf{B}^T\mathbf{B}\tilde{X}] + \tilde{X}\Sigma_2\mathbf{A}\Sigma_2\Gamma^{-1} + \tilde{X}\mathbf{A}^T\Sigma_2^2\Gamma^{-1} \\
&\quad +(\tilde{X}\Sigma_2\mathbf{C}^T\mathbf{C}\Sigma_2^2\Gamma^{-1}) + [\sigma_1^2\tilde{X}\mathbf{B}^T\mathbf{B}\Sigma_2\Gamma^{-1}] - \Sigma_2^2\Gamma^{-1}\mathbf{A}\Sigma_2\Gamma^{-1} - \Sigma_2\Gamma^{-1}\mathbf{A}^T\Sigma_2^2\Gamma^{-1} \\
&\quad -\Sigma_2^2\Gamma^{-1}\mathbf{C}^T\mathbf{C}\Sigma_2^2\Gamma^{-1} - [\sigma_1^2\Sigma_2\Gamma^{-1}\mathbf{B}^T\mathbf{B}\Sigma_2\Gamma^{-1}] + (\tilde{X}\Sigma_2\mathbf{C}^T\mathbf{C}\Sigma_2\tilde{X}) - \mathbf{C}^T\mathbf{C}
\end{aligned}$$

The terms in parentheses drop out while the terms in square brackets may be replaced using (6.44) by

$$\begin{aligned}
-\sigma_1^2\tilde{X}\mathbf{B}^T\mathbf{B}\tilde{X} + \sigma_1^2\Sigma_2\Gamma^{-1}\mathbf{B}^T\mathbf{B}\tilde{X} + \sigma_1^2\tilde{X}\mathbf{B}^T\mathbf{B}\Sigma_2\Gamma^{-1} - \sigma_1^2\Sigma_2\Gamma^{-1}\mathbf{B}^T\mathbf{B}\Sigma_2\Gamma^{-1} \\
= \; -\sigma_1^2\tilde{X}\mathbf{A}^T\Gamma^{-1} - \sigma_1^2\Gamma^{-1}\mathbf{A}\tilde{X} + \sigma_1^2\Sigma_2\Gamma^{-1}\mathbf{A}^T\Gamma^{-1} \\
+ \sigma_1^2\Gamma^{-1}\mathbf{A}\Sigma_2\Gamma^{-1} + \sigma_1^4\Gamma^{-1}\mathbf{C}^T\mathbf{C}\Gamma^{-1}
\end{aligned}$$

After making this substitution and using $\sigma_1\Gamma^{-1}\mathbf{C}^T\mathbf{P}_{\tilde{X}}\mathbf{B}^{T^{-1}} = (\tilde{X} - \Sigma_2\Gamma^{-1})$, it is true that

$$\begin{aligned}
&\overline{A}_{\tilde{X}}T + T\overline{A}_{\tilde{X}}^T + \mathbf{M} + \mathbf{C}^T\mathbf{C} - \mathbf{C}^T\mathbf{C} = \\
&\quad -\tilde{X}\mathbf{A}^T + \Sigma_2\Gamma^{-1}\mathbf{A}^T + \tilde{X}\mathbf{A}^T\Sigma_2\tilde{X} - \Sigma_2\Gamma^{-1}\mathbf{A}^T\Sigma_2\tilde{X} \\
&\quad -A\tilde{X} + \mathbf{A}\Sigma_2\Gamma^{-1} + \tilde{X}\Sigma_2\mathbf{A}\tilde{X} - \tilde{X}\Sigma_2\mathbf{A}\Sigma_2\Gamma^{-1} \\
&\quad +\Sigma_2^2\Gamma^{-1}\mathbf{C}^T\mathbf{C} + \mathbf{C}^T\mathbf{C}\Sigma_2^2\Gamma^{-1} - \mathbf{C}^T\mathbf{C} + \sigma_1^4\Gamma^{-1}\mathbf{C}^T\mathbf{C}\Gamma^{-1} - \Sigma_2^2\Gamma^{-1}\mathbf{C}^T\mathbf{C}\Sigma_2^2\Gamma^{-1} \\
&\quad +\Sigma_2\Gamma^{-1}\mathbf{A}^T\Sigma_2\tilde{X} + \tilde{X}\Sigma_2\mathbf{A}\Sigma_2\Gamma^{-1} - \tilde{X}\Sigma_2\mathbf{A}\tilde{X} - \tilde{X}\mathbf{A}^T\Sigma_2\tilde{X} \\
&\quad +[\Sigma_2^2\Gamma^{-1}\mathbf{A}\tilde{X} - \sigma_1^2\Gamma^{-1}\mathbf{A}\tilde{X}] + [\tilde{X}\mathbf{A}^T\Sigma_2^2\Gamma^{-1} - \sigma_1^2\tilde{X}\mathbf{A}^T\Gamma^{-1}] \\
&\quad -[\Sigma_2^2\Gamma^{-1}\mathbf{A}\Sigma_2\Gamma^{-1} - \sigma_1^2\Gamma^{-1}\mathbf{A}\Sigma_2\Gamma^{-1}] - [\Sigma_2\Gamma^{-1}\mathbf{A}^T\Sigma_2^2\Gamma^{-1} + \sigma_1^2\Sigma_2\Gamma^{-1}\mathbf{A}^T\Gamma^{-1}]
\end{aligned}$$

Each term in square brackets may be simplified using $\Gamma = \Sigma_2^2 - \sigma_1^2 I$. Using this and

cancelling terms leaves us with

$$\begin{aligned}
&\overline{A}_{\hat{X}}T + T\overline{A}_{\hat{X}}^T + \mathbf{M} + \mathbf{C}^T\mathbf{C} - \mathbf{C}^T\mathbf{C} \\
&= \Sigma_2^2\Gamma^{-1}\mathbf{C}^T\mathbf{C} + \mathbf{C}^T\mathbf{C}\Sigma_2^2\Gamma^{-1} - \mathbf{C}^T\mathbf{C} + \sigma_1^4\Gamma^{-1}\mathbf{C}^T\mathbf{C}\Gamma^{-1} - \Sigma_2^2\Gamma^{-1}\mathbf{C}^T\mathbf{C}\Sigma_2^2\Gamma^{-1} \\
&= -(I - \Sigma_2^2\Gamma^{-1})\mathbf{C}^T\mathbf{C}(I - \Sigma_2^2\Gamma^{-1}) + \sigma_1^4\Gamma^{-1}\mathbf{C}^T\mathbf{C}\Gamma^{-1} \\
&= \Gamma^{-1}\left(-(\Gamma - \Sigma_2^2)\mathbf{C}^T\mathbf{C}(\Gamma - \Sigma_2^2) + \sigma_1^4\mathbf{C}^T\mathbf{C}\right)\Gamma^{-1} \\
&= \Gamma^{-1}\left(-\sigma_1^4\mathbf{C}^T\mathbf{C} + \sigma_1^4\mathbf{C}^T\mathbf{C}\right)\Gamma^{-1} = 0
\end{aligned}$$

Thus it has been shown that $\overline{A}_{\hat{X}}T + T\overline{A}_{\hat{X}}^T + \mathbf{M} = 0$ and (6B.46) is true. Note that what has just been shown implies the following

$$\begin{aligned}
&\mathbf{x}_\perp{}^T(s)G_{e_{\hat{X}}}^T(-s)G_{e_{\hat{X}}}(s)\mathbf{x}_\perp(-s) = \sigma_1^2\mathbf{P}_{\hat{X}}\mathbf{P}_{\hat{X}}{}^T \\
&\quad\Rightarrow\quad \sigma_j\left[G_{e_{\hat{X}}}(s)\mathbf{x}_\perp(-s)\right] = \sigma_j\left[\sigma_1\mathbf{P}_{\hat{X}}\right] = \sigma_1 \times \sigma_j\left[\mathbf{P}_{\hat{X}}\right] \qquad j = 1,\ldots,n-1
\end{aligned}$$

In order to conclude that the original (unprojected) error system $G_{e_{\hat{X}}}(s)$ has singular value total flatness, it only needs to be pointed out that $\|G_{e_{\hat{X}}}(s)\mathbf{x}(-s)\|_\infty = \sigma_1$. This together with what has just been shown confirms (6.71) since the inner operator comprising the maximizing vector and its complement are norm-preserving. The proof of (6.72) is parallel and therefore omitted. ■

Chapter 7

Using the degrees of freedom in the general case

7.1 Introduction

The previous chapter and examples demonstrated how characterizing the degrees of freedom in the H^∞ problem enabled their fruitful use in the context of square case systems. Not only did the matching error systems acquire the total flatness property, but they also yielded completely stable projections which facilitated the development of a computationally efficient super-optimal algorithm. The purpose of this chapter is to extend these results to the general class of stable transfer function matrices in which the number of states differs from the number of inputs and outputs, hereafter referred to as the *nonsquare case*. This general class can be subdivided into the following two types:

Type I: The number of states, n, is less than or equal to the number of inputs and outputs, m and p, respectively. Thus, $n \leq m$ and $m = p$.

Type II: The number of states, n, is greater than the number of inputs and outputs, m and p, respectively. Thus, $n > m$ and $m = p$.

For Type I systems, the stable projection property and the total singular value flatness property can be easily retrieved by simply introducing uncontrollable/unobservable, stable states. In contrast, for Type II systems there are not enough degrees of freedom in the Central Glover Solution to fully achieve these properties. Unlike Type I systems, Type II systems cannot be "squared-up" by introducing "null" inputs and outputs since this would create singular **B** and **C**

matrices as given by (6.33) and (6.34), respectively. Moreover, since the dimensions of the free parameter $\mathbf{P}$ are $(m-1)\times(p-1)$, increasing the number of inputs by appending zero columns to B, for instance, is tantamount to creating nonexistent degrees of freedom. Thus, Type II systems require the development of alternative methods to exploit the limited degrees of freedom available to either minimize the degree of the projected antistable component or achieve singular value near flatness the former of which is examined next.

7.2 Minimal antistable projection

Indeed, the maximizing vectors and their complements as given in Lemma 6.5 and Lemma 6.6, respectively, apply for the general case (see proofs contained in Appendix 6B); however, the construction of a matched error system which leads to a completely stable projection relies on there being sufficient degrees of freedom in the Central Glover Solution. Previously, the degrees of freedom contained in $\mathbf{P}$ were given up in order to match either the Central Glover Solution controllability pair $(\tilde{A}_{\tilde{X}}, \tilde{B}_{\tilde{X}})$ with the right complementary maximizing vector controllability pair $(\overline{A}_{\tilde{X}}, \overline{B}_{\tilde{X}})$ or, alternatively, the Central Glover Solution observability pair $(\tilde{A}_{\tilde{Y}}, \tilde{C}_{\tilde{Y}})$ with the left complementary maximizing vector observability pair $(\overline{A}_{\tilde{Y}}, \overline{C}_{\tilde{Y}})$. In lieu of having sufficient degrees of freedom to completely match the complementary maximizing vectors, it is possible to give up the available degrees of freedom to match a maximal part of one of the complementary maximizing vectors with a view toward minimizing the projected antistable component. The following theorem fulfills this objective:

Theorem 7.1 (Minimal antistable projection)

For Type II systems, the Central Glover Solution degrees of freedom can be used to remove $(m-1)$ states of the antistable projection and the parameters $\mathbf{P}_{\tilde{X}}$ and $\mathbf{P}_{\tilde{Y}}$ used to achieve this are given by

$$\mathbf{P}_{\tilde{X}} = \left(V_{\tilde{c}_{\tilde{X}}}\Gamma^{-1}\mathbf{C}^T\right)^{-1} V_{\tilde{c}_{\tilde{X}}} Z_{\tilde{X}} \tag{7.1}$$

$$\mathbf{P}_{\tilde{Y}} = Z_{\tilde{Y}} W_{\tilde{o}_{\tilde{Y}}} \left(\mathbf{B} W_{\tilde{o}_{\tilde{Y}}}\right)^{-1} \tag{7.2}$$

where $Z_{\tilde{X}}$ and $Z_{\tilde{Y}}$ are given as

$$Z_{\tilde{X}} = \frac{1}{\sigma_1}\left(\tilde{X} - \Sigma_2\Gamma^{-1}\right)\mathbf{B}^T \qquad \text{and} \qquad Z_{\tilde{Y}} = \frac{1}{\sigma_1}\mathbf{C}\Gamma^{-1}\left(\tilde{Y} - \Sigma_2\Gamma\right)$$

Furthermore, $V_{\overline{c}_{\tilde{X}}}$ contains $(m-1)$ rows of the left eigenvector matrix of $\mathbf{A}_{Z_{\tilde{X}}}$ and $W_{\overline{o}_{\tilde{Y}}}$ contains $(m-1)$ columns of the right eigenvector matrix of $\mathbf{A}_{Z_{\tilde{Y}}}$ where $\mathbf{A}_{Z_{\tilde{X}}}$ and $\mathbf{A}_{Z_{\tilde{Y}}}$ are given as

$$\mathbf{A}_{Z_{\tilde{X}}} = \Gamma^{-1}\mathbf{A} - \sigma_1 Z_{\tilde{X}}\mathbf{B} = \begin{pmatrix} W_{\overline{c}_{\tilde{X}}} & W_{c_{\tilde{X}}} \end{pmatrix}\begin{pmatrix} \Lambda_{\overline{c}_{\tilde{X}}} & 0 \\ 0 & \Lambda_{c_{\tilde{X}}} \end{pmatrix}\begin{pmatrix} V_{\overline{c}_{\tilde{X}}} \\ V_{c_{\tilde{X}}} \end{pmatrix} \tag{7.3}$$

$$\mathbf{A}_{Z_{\tilde{Y}}} = \Gamma^{-1}\mathbf{A} - \sigma_1\Gamma^{-1}\mathbf{C}^T Z_{\tilde{Y}} = \begin{pmatrix} W_{\overline{o}_{\tilde{Y}}} & W_{o_{\tilde{Y}}} \end{pmatrix}\begin{pmatrix} \Lambda_{\overline{o}_{\tilde{Y}}} & 0 \\ 0 & \Lambda_{o_{\tilde{Y}}} \end{pmatrix}\begin{pmatrix} V_{\overline{o}_{\tilde{Y}}} \\ V_{o_{\tilde{Y}}} \end{pmatrix} \tag{7.4}$$

where the overbarred subscripts $\overline{c}$ and $\overline{o}$ identify the parts of the spectral decompositions which are decoupled through uncontrollability and unobservability, respectively. Using this notation, the minimal realizations of the antistable projections are given by

$$\begin{aligned} Q^{(1)}_{\tilde{X}}(s) &= \left[\begin{array}{c|c} A_{u_{\tilde{X}}} & B_{u_{\tilde{X}}} \\ \hline C_{u_{\tilde{X}}} & 0 \end{array}\right] \\ &= \left[\begin{array}{c|c} V_{c_{\tilde{X}}}\tilde{A}_{\tilde{X}}W_{c_{\tilde{X}}} & \sigma_1 V_{c_{\tilde{X}}}\left(Z_{\tilde{X}} - \Gamma^{-1}\mathbf{C}^T\mathbf{P}_{\tilde{X}}\right) \\ \hat{C}_1^{\perp T}\tilde{C}_{\tilde{X}}W_{c_{\tilde{X}}} - \mathbf{C}\Gamma^{-1}L_{\tilde{X}} & 0 \end{array}\right] \end{aligned} \tag{7.5}$$

$$\begin{aligned} Q^{(1)}_{\tilde{Y}}(s) &= \left[\begin{array}{c|c} A_{u_{\tilde{Y}}} & B_{u_{\tilde{Y}}} \\ \hline C_{u_{\tilde{Y}}} & 0 \end{array}\right] \\ &= \left[\begin{array}{c|c} V_{o_{\tilde{Y}}}\tilde{A}_{\tilde{Y}}W_{o_{\tilde{Y}}} & \sigma_1 V_{o_{\tilde{Y}}}\tilde{B}_{\tilde{Y}}\hat{B}_1^{\perp T} - L_{\tilde{Y}}\mathbf{B}^T \\ \left(Z_{\tilde{Y}} - \mathbf{P}_{\tilde{Y}}\mathbf{B}\right)W_{o_{\tilde{Y}}} & 0 \end{array}\right] \end{aligned} \tag{7.6}$$

and the minimal realizations of the stable projections are given by:

$$G^{(1)}_{\tilde{X}}(s) = \left[\begin{array}{c|c} -\overline{A}^T_{\tilde{Y}} & \Gamma\left(I - \Sigma_2\tilde{X}\right)\mathbf{B}^T + \sigma_1\tilde{Y}\Gamma^{-1}\mathbf{C}^T\mathbf{P}_{\tilde{X}} + L_{\tilde{X}}B_{u_{\tilde{X}}} \\ \hline \mathbf{C}\Gamma^{-1} & \sigma_1\mathbf{P}_{\tilde{X}} \end{array}\right] \tag{7.7}$$

$$G^{(1)}_{\tilde{Y}}(s) = \left[\begin{array}{c|c} -\overline{A}^T_{\tilde{X}} & \mathbf{B}^T \\ \hline \mathbf{C}\Gamma^{-1}\left(\Gamma - \tilde{Y}\Sigma_2\Gamma^{-1}\right) + \sigma_1\mathbf{P}_{\tilde{Y}}\mathbf{B}\tilde{X} + C_{u_{\tilde{Y}}}L_{\tilde{Y}} & \sigma_1\mathbf{P}_{\tilde{Y}} \end{array}\right] \tag{7.8}$$

where $L_{\tilde{X}}$ and $L_{\tilde{Y}}$ satisfy the following general Sylvester equations

$$\begin{aligned} \overline{A}_{\tilde{Y}}^T L_{\tilde{X}} + L_{\tilde{X}} A_{u_{\tilde{X}}} + \overline{C}_{\tilde{Y}}^T \tilde{C}_{\tilde{X}} W_{c_{\tilde{X}}} &= 0 \\ A_{u_{\tilde{Y}}} L_{\tilde{Y}} + L_{\tilde{Y}} \overline{A}_{\tilde{X}}^T + \sigma_1 V_{o_{\tilde{Y}}} \tilde{B}_{\tilde{Y}} \overline{B}_{\tilde{X}}^T &= 0 \end{aligned}$$

Proof: First note that of the four conditions given in (6B.21) through (6B.24), the first three carry over to the nonsquare case so that (6B.20) can be written as

$$G_{e_{\tilde{X}}}(s)\mathbf{x}_\perp(-s) = \left[\begin{array}{cc|c} \tilde{A}_{\tilde{X}} & 0 & \tilde{B}_{\tilde{X}}\hat{B}_1^{\perp T} - \overline{B}_{\tilde{X}}\hat{B}_1^{\perp T} \\ 0 & -\overline{A}_{\tilde{X}}^T & \tilde{X}^{-1}\overline{B}_{\tilde{X}}\hat{B}_1^{\perp T} \\ \hline -\tilde{C}_{\tilde{X}} & C_2 - \tilde{D}_{\tilde{X}}\overline{B}_{\tilde{X}}^T - \tilde{C}_{\tilde{X}}\tilde{X} & \sigma_1 \hat{C}_1^\perp \mathbf{P}_{\tilde{X}} \end{array}\right]$$

The inability to fulfill the fourth condition by making the antistable components in $\tilde{A}_{\tilde{X}}$ uncontrollable stems from the insufficient degrees of freedom in the parameter $\mathbf{P}_{\tilde{X}}$. This can be seen by expressing $\tilde{B}_{\tilde{X}}\hat{B}_1^{\perp T}$ and $\overline{B}_{\tilde{X}}\hat{B}_1^{\perp T}$ as follows

$$\tilde{B}_{\tilde{X}}\hat{B}_1^{\perp T} = \sigma_1 \Gamma^{-1}\mathbf{C}^T\mathbf{P}_{\tilde{X}} + \Sigma_2\Gamma^{-1}\mathbf{B}^T \qquad \text{and} \qquad \overline{B}_{\tilde{X}}\hat{B}_1^{\perp T} = \tilde{X}\mathbf{B}^T = \sigma_1 Z_{\tilde{X}} + \Sigma_2\Gamma^{-1}\mathbf{B}^T$$

where $Z_{\tilde{X}} = \frac{1}{\sigma_1}\left(\tilde{X} - \Sigma_2\Gamma^{-1}\right)\mathbf{B}^T$ as defined in Theorem 7.1. These alternative forms underscore the intrinsic problem that there are not enough degrees of freedom in $\mathbf{P}_{\tilde{X}}$ to equate $\Gamma^{-1}\mathbf{C}^T\mathbf{P}_{\tilde{X}}$ with $Z_{\tilde{X}}$. Combining the above terms and simplifying gives

$$\begin{aligned} G_{e_{\tilde{X}}}(s)\mathbf{x}_\perp(-s) &= \left[\begin{array}{cc|c} \tilde{A}_{\tilde{X}} & 0 & \sigma_1\left(\Gamma^{-1}\mathbf{C}^T\mathbf{P}_{\tilde{X}} - Z_{\tilde{X}}\right) \\ 0 & -\overline{A}_{\tilde{X}}^T & \tilde{X}^{-1}\overline{B}_{\tilde{X}}\hat{B}_1^{\perp T} \\ \hline -\tilde{C}_{\tilde{X}} & C_2 - \tilde{D}_{\tilde{X}}\overline{B}_{\tilde{X}}^T - \tilde{C}_{\tilde{X}}\tilde{X} & \sigma_1\hat{C}_1^\perp\mathbf{P}_{\tilde{X}} \end{array}\right] \\ &= \left[\begin{array}{cc|c} \mathbf{A}_{z_{\tilde{X}}} - \mathbf{B}_{z_{\tilde{X}}}\mathbf{B} & 0 & \mathbf{B}_{z_{\tilde{X}}} \\ 0 & -\overline{A}_{\tilde{X}}^T & \tilde{X}^{-1}\overline{B}_{\tilde{X}}\hat{B}_1^{\perp T} \\ \hline -\tilde{C}_{\tilde{X}} & C_2 - \tilde{D}_{\tilde{X}}\overline{B}_{\tilde{X}}^T - \tilde{C}_{\tilde{X}}\tilde{X} & \sigma_1\hat{C}_1^\perp\mathbf{P}_{\tilde{X}} \end{array}\right] \end{aligned}$$

where $\mathbf{B}_{z_{\tilde{X}}} = \sigma_1\left(\Gamma^{-1}\mathbf{C}^T\mathbf{P}_{\tilde{X}} - Z_{\tilde{X}}\right)$ and use has been made of the definitions of $\tilde{A}$ and $\mathbf{A}_{z_{\tilde{X}}}$ given in (6.25) and (7.3) respectively. Now, observe that $(\mathbf{A}_{z_{\tilde{X}}} - \mathbf{B}_{z_{\tilde{X}}}\mathbf{B}, \mathbf{B}_{z_{\tilde{X}}})$ may be interpreted as a closed-loop state feedback controllability pair with state feedback gain matrix $\mathbf{B}$. The corresponding open-loop controllability pair is $(\mathbf{A}_{z_{\tilde{X}}}, \mathbf{B}_{z_{\tilde{X}}})$ both terms of which are known independent of the parameter

$\mathbf{P}_{\tilde{X}}$. This, together with the fact that open-loop controllability characteristics are unaltered under state-feedback, implies that $\mathbf{P}_{\tilde{X}}$ can be chosen to decouple $(m-1)$ of the antistable states contained in $\tilde{A}_{\tilde{X}} = \mathbf{A}_{z_{\tilde{X}}} - \mathbf{B}_{z_{\tilde{X}}}\mathbf{B}$. In particular, partition the spectral decomposition of $\mathbf{A}_{z_{\tilde{X}}}$ as

$$\mathbf{A}_{z_{\tilde{X}}} = \begin{pmatrix} W_{\bar{c}_{\tilde{X}}} & W_{c_{\tilde{X}}} \end{pmatrix} \begin{pmatrix} \Lambda_{\bar{c}_{\tilde{X}}} & 0 \\ 0 & \Lambda_{c_{\tilde{X}}} \end{pmatrix} \begin{pmatrix} V_{\bar{c}_{\tilde{X}}} \\ V_{c_{\tilde{X}}} \end{pmatrix}$$

where $\Lambda_{\bar{c}_{\tilde{X}}}$ contains $(m-1)$ eigenvalues of $\mathbf{A}_{z_{\tilde{X}}}$. The $(m-1)$ eigenvalues can always be chosen so that $V_{\bar{c}_{\tilde{X}}}\Gamma^{-1}\mathbf{C}^T$ is full rank. Thus, decoupling the $(m-1)$ eigenvalues contained in $\Lambda_{\bar{c}_{\tilde{X}}}$ requires

$$V_{\bar{c}_{\tilde{X}}}\mathbf{B}_{z_{\tilde{X}}} = \sigma_1 V_{\bar{c}_{\tilde{X}}}\left(\Gamma^{-1}\mathbf{C}^T\mathbf{P}_{\tilde{X}} - Z_{\tilde{X}}\right) = 0 \quad \Longleftrightarrow \quad \mathbf{P}_{\tilde{X}} = \left(V_{\bar{c}_{\tilde{X}}}\Gamma^{-1}\mathbf{C}^T\right)^{-1} V_{\bar{c}_{\tilde{X}}} Z_{\tilde{X}}$$

For this value of $\mathbf{P}_{\tilde{X}}$, the minimal realization of $G_{e_{\tilde{X}}}(s)\mathbf{x}_\perp(-s)$ is given by

$$G_{e_{\tilde{X}}}(s)\mathbf{x}_\perp(-s) = \left[\begin{array}{cc|c} V_{c_{\tilde{X}}}\tilde{A}_{\tilde{X}}W_{c_{\tilde{X}}} & 0 & V_{c_{\tilde{X}}}\mathbf{B}_{z_{\tilde{X}}} \\ 0 & -\overline{A}_{\tilde{X}}^T & \tilde{X}^{-1}\overline{B}_{\tilde{X}}\hat{B}_1^{\perp T} \\ \hline -\tilde{C}_{\tilde{X}}W_{c_{\tilde{X}}} & C_2 - \tilde{D}_{\tilde{X}}\overline{B}_{\tilde{X}}^T - \tilde{C}_{\tilde{X}}\tilde{X} & \sigma_1\hat{C}_1^{\perp}\mathbf{P}_{\tilde{X}} \end{array}\right]$$

and the overall projection $\mathbf{y}_\perp{}^T(-s)G_{e_{\tilde{X}}}(s)\mathbf{x}_\perp(-s)$ is given by

$$\mathbf{y}_\perp{}^T(-s)G_{e_{\tilde{X}}}(s)\mathbf{x}_\perp(-s) = \left[\begin{array}{ccc|c} -\overline{A}_Y^T & -\overline{C}_Y^T\tilde{C}_{\tilde{X}}W_{c_{\tilde{X}}} & \overline{C}_Y^T\left(C_2 - \tilde{D}_{\tilde{X}}\overline{B}_{\tilde{X}}^T - \tilde{C}_{\tilde{X}}\tilde{X}\right) & \sigma_1\overline{C}_Y^T\hat{C}_1^{\perp}\mathbf{P}_{\tilde{X}} \\ 0 & V_{c_{\tilde{X}}}\tilde{A}_{\tilde{X}}W_{c_{\tilde{X}}} & 0 & V_{c_{\tilde{X}}}\mathbf{B}_{z_{\tilde{X}}} \\ 0 & 0 & -\overline{A}_{\tilde{X}}^T & \mathbf{B}^T \\ \hline \mathbf{C}\Gamma^{-1} & -\hat{C}_1^{\perp T}\tilde{C}_{\tilde{X}}W_{c_{\tilde{X}}} & \hat{C}_1^{\perp T}\left(C_2 - \tilde{D}_{\tilde{X}}\overline{B}_{\tilde{X}}^T - \tilde{C}_{\tilde{X}}\tilde{X}\right) & \sigma_1\mathbf{P}_{\tilde{X}} \end{array}\right]$$

Apply the state similarity transformation $\begin{pmatrix} I & 0 & \Gamma(I-\Sigma_2\tilde{X}) \\ 0 & I & 0 \\ 0 & 0 & I \end{pmatrix}$ and remove the unobservable states as was done previously in (6B.25) to obtain

$$\mathbf{y}_\perp{}^T(-s)G_{e_{\tilde{X}}}(s)\mathbf{x}_\perp(-s) = \left[\begin{array}{cc|c} -\overline{A}_Y^T & -\overline{C}_Y^T\tilde{C}_{\tilde{X}}W_{c_{\tilde{X}}} & \sigma_1\tilde{Y}\Gamma^{-1}\mathbf{C}^T\mathbf{P}_{\tilde{X}} + \Gamma(I-\Sigma_2\tilde{X})\mathbf{B}^T \\ 0 & V_{c_{\tilde{X}}}\tilde{A}_{\tilde{X}}W_{c_{\tilde{X}}} & V_{c_{\tilde{X}}}\mathbf{B}_{z_{\tilde{X}}} \\ \hline \mathbf{C}\Gamma^{-1} & -\hat{C}_1^{\perp T}\tilde{C}_{\tilde{X}}W_{c_{\tilde{X}}} & \sigma_1\mathbf{P}_{\tilde{X}} \end{array}\right]$$

Finally, performing the state similarity transformation $\begin{pmatrix} I & L_{\tilde{X}} \\ 0 & I \end{pmatrix}$ yields the following general Lyapunov equation whose solution decouples the stable and antistable

projections.

$$\overline{A}_{\tilde{Y}}^T L_{\tilde{X}} + L_{\tilde{X}} \left(V_{c_{\tilde{X}}} \tilde{A}_{\tilde{X}} W_{c_{\tilde{X}}} \right) + \overline{C}_{\tilde{Y}}^T \tilde{C}_{\tilde{X}} W_{c_{\tilde{X}}} = 0$$

The resulting non-decoupled terms form the minimal antistable and stable projections given in (7.5) and (7.7) respectively. The proof of (7.2) is analogous and therefore omitted. ■

Remark 7.1 In Theorem 7.1, any $(m-1)$ subset of the entire set of $(n-1)$ unstable eigenvalues can be eliminated. One possible strategy could involve removing $(m-1)$ of the most unstable eigenvalues (i.e. those $(m-1)$ eigenvalues with the largest positive real parts). Another strategy might involve removing $(m-1)$ of the unstable eigenvalues with the largest residues.

The descriptions of the complementary maximizing vector projections in Theorem 7.1 are quite detailed; however, the resultant computational savings are significant and therefore worthwhile. In particular, the projections given are minimal which in turn removes the computationally burdensome chore of determining minimal realizations of the projections. These computational improvements are included in the nonsquare super-optimal algorithm presented below:

Super-optimal Algorithm III (Nonsquare Case):
Given a stable n−state, m-input/m-output transfer function matrix $G^{(0)}(s)$, find the super-optimal extension $F_{so}(s)$. In the following, superscripts are used to represent the iteration value.

Step 1. Initialization:

a. Compute $\mathbf{P}_{\tilde{X}}$ and $\mathbf{P}_{\tilde{Y}}$ in accordance with Theorem 7.1.

b. Construct the Central Glover Solution $F_l^{(0)}(s)$ using Lemma 6.1 where the subscript "l" identifies which of the two approximation systems will be constructed according to the following rule:

$$l = \begin{cases} \tilde{X} & \text{if} \quad \|\mathbf{P}_{\tilde{X}}\| \leq \|\mathbf{P}_{\tilde{Y}}\| \\ \tilde{Y} & \text{if} \quad \|\mathbf{P}_{\tilde{X}}\| > \|\mathbf{P}_{\tilde{Y}}\| \end{cases}$$

c. Construct the stable projection $G_l^{(1)}(s)$ and the antistable projection $Q_l^{(1)}(s)$ using Theorem 7.1.

d. Calculate and save the complementary maximizing vectors ${\mathbf{x}_\perp}^{T(0)}(s)$ and ${\mathbf{y}_\perp}^{(0)}(s)$ using Lemma 6.6.

e. Set $F_{so}^{(0)}(s) = F_l^{(0)}(s)$.

Step 2. Iteration: for $i = 1$ to $n-1$ do the following:

a. For each iteration, compute the Central Glover Solution, the complementary maximizing vectors, and the corresponding projections similar to above.

b. Accumulate the super-optimal extension as:

$$F_{so}^{(i)}(s) = F_{so}^{(i-1)}(s) + \left[\prod_{j=0}^{i-1} {\mathbf{y}_\perp}^{(j)}(s)\right]\left[F_l^{(i)}(s) + Q_l^{(i)}(s)\right]\left[\prod_{k=i-1}^{0} {\mathbf{x}_\perp}^{T\,(k)}(s)\right]$$

Prior to demonstrating the efficacy of this algorithm by way of example, the square case matched error system total flatness property will be extended to the nonsquare case.

7.3 Singular value near flatness

Unlike the square case in which the matched error systems possess both totally stable projections *and* totally flat singular values, the "near matched" error systems, resulting from minimizing the antistable components as given in Theorem 7.1, do not generally possess total flatness but can be steered toward "near flatness." A rigorous definition of near flatness remains illusory even though it is relatively easy to identify through numerical observation. In the context of this section, near flatness alludes to the situation that would arise from using solutions for the parameter $\mathbf{P}$ obtained from the approximation gramian stationary conditions (6.42) and (6.43). For the general nonsquare case, (6.42) and (6.43) in general will not admit a solution; therefore, the near flatness solutions emerge as solutions of necessary (but not sufficient) conditions for stationarity and hence flatness. Because of this difficulty with an appropriate definition of near flatness, the result below is a conjecture and not a theorem.

Conjecture 7.1 (Singular Value Near Total Flatness) *For the general case, the parameters* $\mathbf{P}_{\tilde{X}}$ *and* $\mathbf{P}_{\tilde{Y}}$ *which give singular value near flatness may be derived from the destabilizing solutions of the following nonsymmetric Riccati equations:*

$$(i) \quad \mathbf{M}^{T^{-1}}\mathbf{R}\mathbf{P}_{\tilde{X}} + \mathbf{P}_{\tilde{X}}\mathbf{M}^{-1}\mathbf{R}^T - \mathbf{P}_{\tilde{X}}\mathbf{R}\mathbf{P}_{\tilde{X}} - \mathbf{R}^T = 0 \tag{7.9}$$

$$(ii) \quad \mathbf{R}^T\mathbf{M}^{-1}\mathbf{P}_{\tilde{Y}} + \mathbf{P}_{\tilde{Y}}\mathbf{R}\mathbf{M}^{T^{-1}} - \mathbf{P}_{\tilde{Y}}\mathbf{R}\mathbf{P}_{\tilde{Y}} - \mathbf{R}^T = 0 \tag{7.10}$$

where $\mathbf{M}$ *and* $\mathbf{R}$ *are defined as:*

$$\mathbf{M} = \sigma_1\mathbf{C}\mathbf{A}^{T^{-1}}\mathbf{B}^T \tag{7.11}$$

$$\mathbf{R} = \sigma_1\mathbf{B}\Gamma^{-1}\mathbf{C}^T \tag{7.12}$$

An illustration of the error system singular value near flatness property as well as the strength of the super-optimal computational improvements afforded by Theorem 7.1 are demonstrated in the following example.

Example 7.1 Consider the following minimal realization of a three-state, two-input, two-output stable transfer function matrix $G^{(0)}(s)$:

$$G^{(0)}(s) = \left[\begin{array}{ccc|cc} -1 & 0 & 0 & 3 & -3 \\ 0 & -2 & 0 & -1 & 5 \\ 0 & 0 & -3 & 2 & 3 \\ \hline 1 & 2 & 1 & 0 & 0 \\ 3 & 1 & -1 & 0 & 0 \end{array}\right]$$

with Hankel singular values given as $\{5.5741, 2.1330, 0.1299\}$. Based on the corresponding balanced realization, the Central Glover Solution parameters $\mathbf{A}$, $\mathbf{B}$, and $\mathbf{C}$ are calculated as:

$$\mathbf{A} = \begin{pmatrix} -78.6508 & -19.1270 \\ 0.0935 & -90.6818 \end{pmatrix} \quad \mathbf{B} = \begin{pmatrix} 2.9221 & 0.6378 \end{pmatrix} \quad \mathbf{C} = \begin{pmatrix} 3.0885 & -0.0092 \end{pmatrix}$$

In the context of the nonsquare super-optimal algorithm, the problem dimension dictates two Central Glover Solution iterations and after the first iteration, the antistable and stable projections corresponding to the parameter $\mathbf{P}_{\tilde{X}}$ are given by

Theorem 7.1 as:

$$Q_{\hat{X}}^{(1)}(s) = \left[\begin{array}{c|c} A_{u_{\hat{X}}} & B_{u_{\hat{X}}} \\ \hline C_{u_{\hat{X}}} & 0 \end{array}\right] = \left[\begin{array}{c|c} 2.3558 & 0.0256 \\ \hline 0.6383 & 0.0000 \end{array}\right]$$

$$G_{\hat{X}}^{(1)}(s) = \left[\begin{array}{c|c} A^{(1)} & B^{(1)} \\ \hline C^{(1)} & D^{(1)} \end{array}\right] = \left[\begin{array}{cc|c} -2.2798 & 0.0013 & -78.9181 \\ -0.6654 & -2.9203 & -18.8504 \\ \hline -0.1165 & 0.0003 & -1.7964 \end{array}\right]$$

where the value of the parameter $\mathbf{P}_{\hat{X}}$ is given by $\mathbf{P}_{\hat{X}} = -0.3615$. As predicted by Theorem 7.1, $(m-1) = 1$ state has been eliminated from antistable projection $Q_{\hat{X}}^{(1)}(s)$ and, in addition, Theorem 7.1 ensured the minimality of the projections $Q_{\hat{X}}^{(0)}(s)$ and $G_{\hat{X}}^{(1)}(s)$. Upon obtaining the final Central Glover Solution and assembling the super-optimal solution $F_{so}(s)$, the resulting s-numbers are computed to be $s_1^{\infty} = 5.5741$ and $s_2^{\infty} = 2.015972$.

In comparison to the super-optimal solution, consider the near flatness results given by Conjecture 7.1 which requires only a single Central Glover Solution iteration. Since the system for this example has two inputs and two outputs, the parameters $\mathbf{P}_{\hat{X}}$ and $\mathbf{P}_{\hat{Y}}$ are equal scalars and, by using Conjecture 7.1, are given as $\mathbf{P}_{\hat{X}} = \mathbf{P}_{\hat{Y}} = -0.3616$. As predicted by Conjecture 7.1, the second error system singular value does exhibit near flatness as depicted in Fig. 7.1. (The first singular value is not

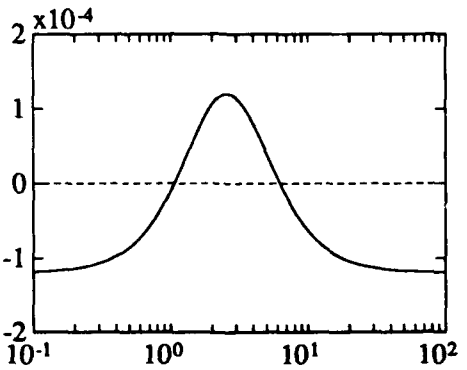

Figure 7.1: Comparison of normalized near flat second singular value (solid line) with normalized super-optimal value (dashed line). Note that the vertical units are measured in increments of 10^{-4}.

shown since it is already all-pass by the Central Glover Solution.) Since the super-

optimal value s_2^∞ is completely flat, the frequency plots of both s_2^∞ and $\sigma_2\left[G_{e_{\tilde{X}}}(j\omega)\right]$ have been normalized by subtracting $s_2^\infty = 2.015972$; hence, the normalized second s-number $\widehat{s_2^\infty} = 0$ is plotted as the dashed line and the normalized near flat second singular value $\sigma_2\left[\widehat{G_{e_{\tilde{X}}}(j\omega)}\right]$ is plotted as the solid line. From this plot it can be seen that the near flat second singular value has the same initial and final value. In fact, the values at d.c. and at infinity are equivalent and are given by

$$\sigma_2\left[G_{e_{\tilde{X}}}(j0)\right] = \sigma_2\left[G_{e_{\tilde{X}}}(j\infty)\right] = \sigma_1 \times |\mathbf{P}_{\tilde{X}}| = 2.015852$$

Although the near flat second singular value deviates from its initial and final values and indeed exceeds the super-optimal value over the frequency range $1\frac{\text{rad}}{\text{sec}}$ to $5\frac{\text{rad}}{\text{sec}}$, the excess is never greater than 1.2×10^{-4} (0.006%). Moreover, the near flat second singular value is actually less than the super-optimal value over the converse range of frequencies and this is achieved with one less state than required by the super-optimal solution. Hence, for this example, giving up the Central Glover Solution degrees of freedom to achieve near flatness virtually obviates the more complex super-optimal solution.

7.4 Super-optimization and early termination

The preceding results based on the solutions $\mathbf{P}_{\tilde{X}}$ and $\mathbf{P}_{\tilde{Y}}$ given in (7.9) and (7.10), respectively, imply that near super-optimality can be attained without fully completing the super-optimal algorithm; this process is referred to as *early termination*. Presently, it is of interest to investigate how the solutions of Conjecture 7.1 can be employed in super-optimization since $(m-1)$ of the corresponding error system singular values are manipulated simultaneously. The explicit algorithm based on these solutions is not given here; however, it is straightforward to modify Super-optimal Algorithm III presented earlier to accommodate $\mathbf{P}_{\tilde{X}}$ and $\mathbf{P}_{\tilde{Y}}$ of Conjecture 7.1. Although the resulting super-optimal algorithm converges correctly to the final super-optimal solution $F_{so}(s)$, some examples have demonstrated that H^∞ optimality can be lost during intervening super-optimization stages, however, the final stage invari-

ably recovers both H^∞ optimality and super-optimality. The intermediate loss of optimality can be traced to violations of the norm constraint on the parameter $\mathbf{P}$ stated in (6.24) and repeated here for convenience:

$$\overline{\sigma}_{\mathbf{P}} \leq 1 \tag{7.13}$$

The reason this norm constraint cannot always be met is that neither of the non-symmetric Riccati equations given in (7.9) and (7.10) imposes *a priori* the necessary upper bound on $\overline{\sigma}_{\mathbf{P}}$. The only notable exception occurs when the parameter $\mathbf{P}$ is scalar; in this case, the parameter $\mathbf{P}$ can be found as the root of the scalar quadratic equation (6.40) which was shown previously to contain a unique root $\mathbf{P}$ given by (6.38) in the open interval $-1 < \mathbf{P} < 1$. Finally, since the super-optimal algorithm terminates after an iteration for which $\mathbf{P}$ is scalar, this establishes that either (7.9) or (7.10) can be employed successfully in the context of a super-optimal algorithm to achieve the overall super-optimal extension. An illustration of this observation is given in the hypothetical example below.

For simplicity, consider a 3-state square case system $G^{(0)}(s)$ with nonrepeated, ordered Hankel singular values $\sigma_1 > \sigma_2 > \sigma_3$. Additionally, suppose that the approximation system $F_{\hat{X}}{}^{(0)}(s)$ is computed from the 2×2 parameter $\mathbf{P}_{\hat{X}}$ which has a norm in excess of unity (i.e. $\overline{\sigma}_{\mathbf{P}_{\hat{X}}} > 1$). In this case, $\|G^{(0)}(s) - F_{\hat{X}}{}^{(0)}(s)\|_\infty > \sigma_1$ and H^∞ optimality is lost. However, consider the following super-optimal diagonalization:

$$\begin{aligned}
\|G^{(0)}(s) - F_{\hat{X}}{}^{(0)}(s)\|_\infty &= \\
&= \left\| \begin{bmatrix} \mathbf{y}^{T\,(0)}(-s) \\ \mathbf{y}_\perp{}^{T\,(0)}(-s) \end{bmatrix} \left(G^{(0)}(s) - F_{\hat{X}}{}^{(0)}(s)\right) \begin{bmatrix} \mathbf{x}^{(0)}(-s) & \mathbf{x}_\perp{}^{(0)}(-s) \end{bmatrix} \right\|_\infty \\
&= \left\| \begin{bmatrix} \sigma_1 & 0 \\ 0 & G_{\hat{X}}^{(1)}(s) + Q_{\hat{X}}^{(1)}(s) \end{bmatrix} \right\|_\infty > \sigma_1
\end{aligned}$$

Here, $G_{\hat{X}}^{(1)}(s)$ and $Q_{\hat{X}}^{(1)}(s)$ are the stable and antistable projections, respectively. Clearly, the Hankel norm of the stable projection $G_{\hat{X}}^{(1)}(s)$ is less than σ_1 since the maximizing/complementary maximizing vectors are norm preserving. Thus, the loss of optimality arises from the antistable projection $Q_{\hat{X}}^{(1)}(s)$; however, this term will

be absorbed in the next optimal approximation and will no longer adversely affect overall optimality. In particular, denote the approximation based on the stable projection $G_{\hat{X}}^{(1)}(s)$ as $F_{\mathbf{P}_{\hat{X}}}^{(1)}(s)$ where $\hat{\mathbf{P}}_{\hat{X}}$ is the scalar parameter derived from (6.38) and satisfies $\overline{\sigma}_{\mathbf{P}_{\hat{X}}} < 1$. Finally, since the optimal approximation $F_{\mathbf{P}_{\hat{X}}}^{(1)}(s)$ accounts for the antistable term $Q_{\hat{X}}^{(1)}(s)$, overall *optimality is recovered.*

The previous example can be easily generalized to confirm that intermediate violations of constraint (7.13) for $\mathbf{P}$ non-scalar have no impact on the final super-optimal extension $F_{so}(s)$ since the *antistable* approximation system $Q(s)$ must be the source of any intermediate loss of optimality. With subsequent iterations however, only the *stable* projections determine the Hankel norm, hence successive applications of the Central Glover Solution in combination with the aforementioned control over $\overline{\sigma}_{\mathbf{P}}$ for $\mathbf{P}$ scalar ensure that the final super-optimal solution is correct.

Even though $\mathbf{P}_{\hat{X}}$ and $\mathbf{P}_{\hat{Y}}$ as defined by (7.9) and (7.10) can be used in generating the unique super-optimal solution, it is desirable to maintain H^∞ optimality during all super-optimal algorithmic stages in order to permit early termination after any iteration. In Example 6.2, for instance, early termination of the super-optimal algorithm after one iteration resulted in virtual super-optimality (to within 0.01%) as confirmed by comparing the singular values given in (6.73) with the s-numbers given in (6.74). Furthermore, the possibility of early termination in that example came about from having one of the parameters satisfy norm constraint (7.13), namely $\mathbf{P}_{\hat{Y}} = 0.2226$.

The feasibility of early termination is contingent upon the development of a method of ensuring that constraint (7.13) is satisfied during all stages of super-optimization. The remainder of the work presented in this chapter fulfills this objective for the general nonsquare case with a view toward obtaining the degree of freedom parameter $\mathbf{P}$ in a manner which not only satisfies the *necessary* approximation gramian stationary conditions, but permits early termination as well. In particular, this work merges the controllability and observability gramian stationary conditions with their respective Riccati equations in a way which generates two related Riccati

equations that share a unique, common solution $\mathbf{P}$. It will be seen that the common solution $\mathbf{P}$ not only ensures H^∞ optimality during all super-optimization stages, but it also supplants the previous Riccati solution procedure which forms the solution from the partitioned eigenvectors of the Hamiltonian matrix. Before this however, the following lemma merges the gramian stationary conditions (6.42) and (6.43) with their respective Riccati equations (6.44) and (6.45).

Lemma 7.1 (Composite Riccati equation construction and solution) *The gramian stationary conditions (6.42) and (6.43) in conjunction with their respective Riccati equations (6.44) and (6.45) have the following modified respective forms:*

$$\mathbf{P}_M{}^T\mathbf{M} + \mathbf{M}^T\mathbf{P}_M - \mathbf{M}^T\mathbf{P}_M\mathbf{P}_M{}^T\mathbf{M} - \mathbf{M}^T\mathbf{M} = 0 \tag{7.14}$$

$$\mathbf{P}_M\mathbf{M}^T + \mathbf{M}\mathbf{P}_M{}^T - \mathbf{M}\mathbf{P}_M{}^T\mathbf{P}_M\mathbf{M}^T - \mathbf{M}\mathbf{M}^T = 0 \tag{7.15}$$

for which the unique solution $\mathbf{P}_M$ may be retrieved from the destabilizing solution of the following composite Riccati equation:

$$\mathbf{S}\tilde{\mathbf{P}} + \tilde{\mathbf{P}}\mathbf{S} - \tilde{\mathbf{P}}\tilde{\mathbf{P}} - I = 0 \tag{7.16}$$

where $\mathbf{S}$ is defined by either of the following equations along with the corresponding parameter $\mathbf{P}_M$:

$$\mathbf{S} = \mathbf{X}\Sigma\mathbf{X}^* \quad \Rightarrow \quad \mathbf{P}_M = \mathbf{Y}\mathbf{X}^*\tilde{\mathbf{P}} \tag{7.17}$$

$$\mathbf{S} = \mathbf{Y}\Sigma\mathbf{Y}^* \quad \Rightarrow \quad \mathbf{P}_M = \tilde{\mathbf{P}}\mathbf{Y}\mathbf{X}^* \tag{7.18}$$

Here, $\mathbf{X}$ and $\mathbf{Y}$ are the principal directions derived from the singular value decomposition of the inverse of $\mathbf{M}$:

$$\mathbf{M}^{-1} = \mathbf{X}\Sigma\mathbf{Y}^* \tag{7.19}$$

where $\mathbf{M}$ is defined by (7.11).

Proof: Equation (7.15) is identical to (6B.10) which was derived as a modified form of Riccati equation (6.45) in the proof of Corollary 6.3. Equation (7.14) can

be derived in a similar manner and the details will be excluded here. In order to cast (7.14) in the form of (7.16), first pre- and post-multiply (7.14) by $\mathbf{M}^{T^{-1}}$ and $\mathbf{M}^{-1}$, respectively, and substitute the singular value decomposition of $\mathbf{M}^{-1}$ to obtain:

$$\mathbf{Y}\Sigma\mathbf{X}^*\mathbf{P}_M{}^T + \mathbf{P}_M\mathbf{X}\Sigma\mathbf{Y}^* - \mathbf{P}_M\mathbf{P}_M{}^T - I = 0$$

Pre- and post-multiplication of this equation by $\mathbf{XY}^*$ and $\mathbf{YX}^*$, respectively, yields Riccati equation (7.16) with the corresponding definitions of $\mathbf{S}$ and $\tilde{\mathbf{P}}$ given by (7.17). The proof that (7.15) leads to (7.16) with the corresponding definitions of $\mathbf{S}$ and $\tilde{\mathbf{P}}$ given by (7.18) is similar and therefore omitted. ■

The special form of the composite Riccati equation given in (7.16) possesses special properties which the next lemma defines. In particular, the following lemma bounds the gain of the singular values of the corresponding error system $G_{e_M}(s)$ both by placing a lower bound on $\underline{\sigma}_{\mathbf{S}} = \underline{\sigma}_{\mathbf{M}^{-1}}$ which in turn places an upper bound on $\overline{\sigma}_{\tilde{\mathbf{P}}} = \overline{\sigma}_{\mathbf{P}}$. Furthermore, these results yield the cross-MPDA property between $\tilde{\mathbf{P}}$ and $\mathbf{S}$ (or equivalently between $\mathbf{P}_M$ and $\mathbf{M}^T$).

Lemma 7.2 (Lower bound on $\underline{\sigma}_{\mathbf{S}}$, upper bound on $\overline{\sigma}_{\tilde{\mathbf{P}}}$ and cross-MPDA of $\mathbf{S}$ and $\tilde{\mathbf{P}}$)

Given the parameters $\mathbf{S}$ and $\tilde{\mathbf{P}}$ defined in either (7.17) or (7.18) which form the composite Riccati equation (7.16), the following conditions hold:

$$\underline{\sigma}_{\mathbf{S}} = \underline{\sigma}_{[\mathbf{M}^{-1}]} > 1 \tag{7.20}$$

$$\overline{\sigma}_{\tilde{\mathbf{P}}} = \overline{\sigma}_{\mathbf{P}_M} = \underline{\sigma}_{\mathbf{S}} - \sqrt{\underline{\sigma}_{\mathbf{S}}^2 - 1} \leq 1 \tag{7.21}$$

$$\underline{x}_{\mathbf{S}} \parallel \overline{x}_{\tilde{\mathbf{P}}} \qquad \text{and} \qquad \overline{x}_{\mathbf{S}} \parallel \underline{x}_{\tilde{\mathbf{P}}} \tag{7.22}$$

Proof: Define the following symmetric singular value decompositions:

$$\tilde{\mathbf{P}} = X_{\tilde{\mathbf{P}}}\Sigma_{\tilde{\mathbf{P}}}X_{\tilde{\mathbf{P}}}^* \qquad \text{and} \qquad \mathbf{S} = X_{\mathbf{S}}\Sigma_{\mathbf{S}}X_{\mathbf{S}}^*$$

Pre- and post-multiply (7.16) by $X_{\tilde{\mathbf{P}}}^*$ and $X_{\tilde{\mathbf{P}}}$ respectively to obtain:

$$\left(X_{\tilde{\mathbf{P}}}^*X_{\mathbf{S}}\Sigma_{\mathbf{S}}X_{\mathbf{S}}^*X_{\tilde{\mathbf{P}}}\right)\Sigma_{\tilde{\mathbf{P}}} + \Sigma_{\tilde{\mathbf{P}}}\left(X_{\tilde{\mathbf{P}}}^*X_{\mathbf{S}}\Sigma_{\mathbf{S}}X_{\mathbf{S}}^*X_{\tilde{\mathbf{P}}}\right) - \Sigma_{\tilde{\mathbf{P}}}^2 - I = 0 \tag{7.23}$$

However, (7.23) implies that $\left(X_{\tilde{\mathbf{P}}}^{*} X_{\mathbf{S}} \Sigma_{\mathbf{S}} X_{\mathbf{S}}^{*} X_{\tilde{\mathbf{P}}}\right)$ is a diagonal matrix; define this matrix as $\tilde{\Sigma}_{\mathbf{S}} = \left(X_{\tilde{\mathbf{P}}}^{*} X_{\mathbf{S}} \Sigma_{\mathbf{S}} X_{\mathbf{S}}^{*} X_{\tilde{\mathbf{P}}}\right)$. Clearly, $\tilde{\Sigma}_{\mathbf{S}}$ contains the singular values of $\Sigma_{\mathbf{S}}$ in some unknown order. Using the definition of $\tilde{\Sigma}_{\mathbf{S}}$, (7.23) can be rewritten as:

$$2\tilde{\Sigma}_{\mathbf{S}} \Sigma_{\tilde{\mathbf{P}}} - \Sigma_{\tilde{\mathbf{P}}}^{2} - I = 0$$

which in turn implies

$$(\sigma_{\tilde{\mathbf{P}}})_i^2 - 2(\sigma_{\mathbf{S}})_j (\sigma_{\tilde{\mathbf{P}}})_i + 1 = 0 \tag{7.24}$$

for the corresponding (i, j) pairings. Using (7.24), any i^{th} singular value of $\tilde{\mathbf{P}}$ can be expressed as:

$$(\sigma_{\tilde{\mathbf{P}}})_i = (\sigma_{\mathbf{S}})_j \pm \sqrt{(\sigma_{\mathbf{S}})_j^2 - 1} \tag{7.25}$$

Equation (7.25), however, must be true for all j and because the singular values of $\tilde{\mathbf{P}}$ are real by definition, the discriminant of (7.25) yields the lower bound on $\underline{\sigma}_{\mathbf{S}}$ given in (7.20). Using (7.24), the largest singular value of $\tilde{\mathbf{P}}$ is given by:

$$\overline{\sigma}_{\tilde{\mathbf{P}}} = (\sigma_{\tilde{\mathbf{P}}})_1 = (\sigma_{\mathbf{S}})_k \pm \sqrt{(\sigma_{\mathbf{S}})_k^2 - 1} \tag{7.26}$$

where $(\sigma_{\mathbf{S}})_k$ is the first diagonal element of $\tilde{\Sigma}_{\mathbf{S}}$ corresponding to the largest singular value of $\tilde{\mathbf{P}}$. The only remaining question is whether (7.26) is computed using the plus or minus sign and this will be determined in the following treatment. The destabilizing solution $\tilde{\mathbf{P}}$ can be formed by partioning the following Hamiltonian matrix as:

$$H = \begin{pmatrix} \mathbf{S} & -I \\ I & -\mathbf{S} \end{pmatrix} = \begin{pmatrix} W_{11} & W_{12} \\ W_{21} & W_{22} \end{pmatrix} \begin{pmatrix} \Lambda_p & 0 \\ 0 & -\Lambda_p \end{pmatrix} \begin{pmatrix} W_{11} & W_{12} \\ W_{21} & W_{22} \end{pmatrix}^{-1}$$

where Λ_p contains the strictly positive eigenvalues of H. It follows from this partitioning that:

$$\mathbf{S} W_{11} - W_{12} = W_{11} \Lambda_p$$

After post-multiplication by $(W_{11})^{-1}$ this becomes:

$$\mathbf{S} - W_{12}(W_{11})^{-1} = \mathbf{S} - \tilde{\mathbf{P}} = W_{11} \Lambda_p (W_{11})^{-1} \tag{7.27}$$

where the equality $\tilde{\mathbf{P}} = W_{12}(W_{11})^{-1}$ defines the destabilizing solution. Pre- and post-multiplication of (7.27) by $X^*_{\tilde{\mathbf{P}}}$ and $X_{\tilde{\mathbf{P}}}$ respectively yields:

$$\tilde{\Sigma}_{\mathbf{S}} - \Sigma_{\tilde{\mathbf{P}}} = \left(X^*_{\tilde{\mathbf{P}}} W_{11}\right) \Lambda_p \left(X^*_{\tilde{\mathbf{P}}} W_{11}\right)^{-1}$$

This equation confirms that $\tilde{\Sigma}_{\mathbf{S}} - \Sigma_{\tilde{\mathbf{P}}}$ must be positive definite in order for $\tilde{\mathbf{P}}$ to correspond to the destabilizing solution. Using this fact in conjunction with (7.26), it follows that:

$$\begin{aligned} (\sigma_{\mathbf{S}})_k - \left[(\sigma_{\mathbf{S}})_k \pm \sqrt{(\sigma_{\mathbf{S}})_k^2 - 1}\right] > 0 \\ \Rightarrow \qquad \mp\sqrt{(\sigma_{\mathbf{S}})_k^2 - 1} > 0 \end{aligned} \tag{7.28}$$

This result in conjunction with (7.20) confirms that the negative sign is used in (7.26). This, in turn, implies that the largest singular value of $\tilde{\mathbf{P}}$ corresponds to the smallest singular value of $\mathbf{S}$ and therefore $(\sigma_{\mathbf{S}})_k = \underline{\sigma}_{\mathbf{S}}$. Furthermore, this gives the constraint on the norm of $\tilde{\mathbf{P}}$ given in (7.21). In addition, when (7.25) is used with the minus sign only and coupled with the realization that $(\sigma_{\mathbf{S}})_j < 1 \ \forall \ j$ it follows that $\overline{\sigma}_{\tilde{\mathbf{P}}}$ is uniquely associated with $\underline{\sigma}_{\mathbf{S}}$; hence, the cross-MPDA property of (7.22) follows directly. ■

The special property (7.21) identified in Lemma 7.2 yields the desired constraint (7.13); therefore, by employing the parameter $\mathbf{P}_M$ derived from (7.17) [or identically (7.18)] early termination can be accomplished while ensuring H^∞ optimality during all stages of super-optimization. This fundamental result, which derives from Riccati equation (7.16), is improved upon in the following theorem which allows the direct solution of the unique parameter $\mathbf{P}_M$ without recourse to the standard Riccati solution procedure as would otherwise be required by Lemma 7.1.

Theorem 7.2 (Closed form Riccati solution)

The unique parameter $\mathbf{P}_M$ *which solves both of the Riccati equations given in (7.14) and (7.15), respectively is given by:*

$$\mathbf{P}_M = \mathbf{M}^{T^{-1}} \left(I - \left(I - \mathbf{M}^T \mathbf{M} \right)^{\frac{1}{2}} \right) \tag{7.29}$$

$$= \left(I - \left(I - \mathbf{M}\mathbf{M}^T \right)^{\frac{1}{2}} \right) \mathbf{M}^{T^{-1}} \tag{7.30}$$

where $\mathbf{M}$ *is defined by (7.11).*

Proof: Since $\mathbf{S}\tilde{\mathbf{P}}$ has been shown to be symmetric in Lemma 7.2, these definitions imply that $\mathbf{M}\mathbf{P}_M{}^T = \mathbf{P}_M\mathbf{M}^T$ and thus (7.14) can be rewritten as:

$$2\mathbf{M}^T\mathbf{P}_M - \left(\mathbf{M}^T\mathbf{P}_M \right)^2 - \mathbf{M}^T\mathbf{M} = 0 \tag{7.31}$$

Define the following:

$$\mathbf{U} = I - \mathbf{M}^T\mathbf{M} \tag{7.32}$$

and substitute (7.29) in (7.31) to obtain:

$$\begin{aligned} 2\left(I - \mathbf{U}^{\frac{1}{2}} \right) - \left(I - \mathbf{U}^{\frac{1}{2}} \right)^2 - (I - \mathbf{U}) &= \left(I - \mathbf{U}^{\frac{1}{2}} \right) \left(2I - I + \mathbf{U}^{\frac{1}{2}} \right) - (I - \mathbf{U}) \\ &= \left(I - \mathbf{U}^{\frac{1}{2}} \right) \left(I + \mathbf{U}^{\frac{1}{2}} \right) - (I - \mathbf{U}) \\ &= 0 \end{aligned}$$

This shows sufficiency. Necessity comes from the uniqueness of the Riccati solution [Kailath, 1980]. The proof of (7.15) and (7.30) is similar and thus omitted. Furthermore, equality of (7.29) and (7.30) is immediate. ■

In addition to yielding the closed form Riccati solution of parameter $\mathbf{P}_M$, Theorem 7.2 also permits the following statement of a singular value property which is a necessary (but not sufficient) condition for singular value flatness.

Corollary 7.1 (Singular value equality at $\omega = 0$ and $\omega = \infty$)

The error system $G_{e_M}(j\omega)$ constructed in the Central Glover Solution and based on the parameter $\mathbf{P}_M$ given by (7.29) or identically (7.30) possess singular values which satisfy:

$$\sigma_i[G_{e_M}(j0)] = \sigma_i[G_{e_M}(j\infty)] \qquad \forall i \tag{7.33}$$

Proof: Consider the normalized parahermitian system $G(s)$ based on the parameter $\mathbf{P}_M$ and defined analogous to (6B.1) as:

$$G(s) = \left[\begin{array}{c|c} \mathcal{A} & \mathcal{B} \\ \hline \mathcal{C} & \mathcal{D} \end{array}\right]$$

$$= \left[\begin{array}{cc|cc} (-\mathbf{A}^T+\sigma_1\mathbf{B}^T{\mathbf{P}_M}^T\mathbf{C})\Gamma^{-1} & \mathbf{B}^T(I-{\mathbf{P}_M}^T\mathbf{P}_M)\mathbf{B} & 0 & -\mathbf{B}^T(I-{\mathbf{P}_M}^T\mathbf{P}_M) \\ 0 & \Gamma^{-1}(\mathbf{A}-\sigma_1\mathbf{C}^T\mathbf{P}_M\mathbf{B}) & \frac{1}{\beta}A_{12}^T & \Gamma^{-1}(\sigma_1\mathbf{C}^T\mathbf{P}_M+\Sigma_2\mathbf{B}^T) \\ \hline \frac{1}{\beta}A_{12} & 0 & 1 & 0 \\ (\sigma_1{\mathbf{P}_M}^T\mathbf{C}+\mathbf{B}\Sigma_2)\Gamma^{-1} & (I-{\mathbf{P}_M}^T\mathbf{P}_M)\mathbf{B} & 0 & {\mathbf{P}_M}^T\mathbf{P}_M \end{array}\right]$$

First note that $\mathcal{A}^{-1}$ is given as:

$$\mathcal{A}^{-1} = \begin{pmatrix} -\tilde{A}^{T^{-1}} & \tilde{A}^{T^{-1}}\mathbf{B}^T(I-{\mathbf{P}_M}^T\mathbf{P}_M)\mathbf{B}\tilde{A}^{-1} \\ 0 & \tilde{A}^{-1} \end{pmatrix}$$

Since $\tilde{A}$ is defined by (6.25) as $\tilde{A} = \Gamma^{-1}(\mathbf{A} - \sigma_1\mathbf{C}^T\mathbf{P}_M\mathbf{B})$, the matrix inversion lemma [Kailath, 1980] may be employed to write $\tilde{A}^{-1}$ as:

$$\tilde{A}^{-1} = \left[\mathbf{A}^{-1} + \sigma_1\mathbf{A}^{-1}\mathbf{C}^T\mathbf{P}_M(I-\mathbf{M}^T\mathbf{P}_M)^{-1}\mathbf{B}\mathbf{A}^{-1}\right]\Gamma \tag{7.34}$$

where $\mathbf{M}$ is defined by (7.11). Using (7.34), the quantity $\mathbf{B}\tilde{A}^{-1}$ is given by:

$$\mathbf{B}\tilde{A}^{-1} = \left[I + \mathbf{M}^T\mathbf{P}_M(I-\mathbf{M}^T\mathbf{P}_M)^{-1}\right]\mathbf{B}\mathbf{A}^{-1}\Gamma$$

This is useful in carrying out the multiplication of $\mathcal{C}\mathcal{A}^{-1}\mathcal{B}$ which is given as:

$$\mathcal{C}\mathcal{A}^{-1}\mathcal{B} = \begin{pmatrix} (\mathcal{C}\mathcal{A}^{-1}\mathcal{B})_{11} & (\mathcal{C}\mathcal{A}^{-1}\mathcal{B})_{12} \\ (\mathcal{C}\mathcal{A}^{-1}\mathcal{B})_{21} & (\mathcal{C}\mathcal{A}^{-1}\mathcal{B})_{22} \end{pmatrix} \tag{7.35}$$

where, by defining $\mathbf{J} = (I - {\mathbf{P}_M}^T\mathbf{P}_M)$, the individual terms become:

$$
\begin{aligned}
(\mathcal{CA}^{-1}\mathcal{B})_{11} &= \frac{1}{\beta^2} A_{12}\tilde{A}^{T^{-1}}\mathbf{B}^T\mathbf{J}\mathbf{B}\tilde{A}^{-1}A_{12}^T \\
(\mathcal{CA}^{-1}\mathcal{B})_{12} &= \frac{1}{\beta} A_{12}\tilde{A}^{T^{-1}}\mathbf{B}^T\mathbf{J}\left(I + \mathbf{B}\tilde{A}^{-1}\Gamma^{-1}(\sigma_1\mathbf{C}^T\mathbf{P}_M + \Sigma_2\mathbf{B}^T)\right) \\
(\mathcal{CA}^{-1}\mathcal{B})_{21} &= (\mathcal{CA}^{-1}\mathcal{B})_{12}^T \\
(\mathcal{CA}^{-1}\mathcal{B})_{22} &= (\sigma_1\mathbf{P}_M{}^T\mathbf{C} + \mathbf{B}\Sigma_2)\Gamma^{-1}\tilde{A}^{T^{-1}}\mathbf{B}^T\mathbf{J} + \mathbf{J}\mathbf{B}\tilde{A}^{-1}\Gamma^{-1}(\sigma_1\mathbf{C}^T\mathbf{P}_M + \Sigma_2\mathbf{B}^T) \\
&\quad +(\sigma_1\mathbf{P}_M{}^T\mathbf{C} + \mathbf{B}\Sigma_2)\Gamma^{-1}\tilde{A}^{T^{-1}}\mathbf{B}^T\mathbf{J}\mathbf{B}\tilde{A}^{-1}\Gamma^{-1}(\sigma_1\mathbf{C}^T\mathbf{P}_M + \Sigma_2\mathbf{B}^T)
\end{aligned}
$$

Given the definition for $\mathbf{U}$ in(7.32), the Hankel singular value relationship given in Lemma 6.3 may be used to give an alternative definition of $\mathbf{U}$, namely:

$$
\begin{aligned}
\mathbf{U} &= \mathbf{V}\mathbf{V}^T + (I + \mathbf{W})\left(I + \mathbf{W}^T\right) \\
&= \mathbf{Q}\mathbf{Q}^T
\end{aligned} \tag{7.36}
$$

where

$$
\begin{aligned}
\mathbf{V} &= \left(\frac{1}{\beta}\right)\mathbf{B}\mathbf{A}^{-1}\Gamma A_{12}^T \\
\mathbf{W} &= \mathbf{B}\mathbf{A}^{-1}\Sigma_2\mathbf{B}^T \\
\mathbf{Q} &= \left[\begin{array}{cc} \mathbf{V} & (I + \mathbf{W}) \end{array}\right]
\end{aligned}
$$

By defining $\mathbf{Z} = (I - \mathbf{U})^{-1}\left(I - \mathbf{U}^{-\frac{1}{2}}\right)$, the desired matrix $G(j0) = -\mathcal{CA}^{-1}\mathcal{B} + \mathcal{D}$ is given as:

$$
-\mathcal{CA}^{-1}\mathcal{B} + \mathcal{D} = \begin{pmatrix} (-\mathcal{CA}^{-1}\mathcal{B} + \mathcal{D})_{11} & (-\mathcal{CA}^{-1}\mathcal{B} + \mathcal{D})_{12} \\ (-\mathcal{CA}^{-1}\mathcal{B} + \mathcal{D})_{21} & (-\mathcal{CA}^{-1}\mathcal{B} + \mathcal{D})_{22} \end{pmatrix} \tag{7.37}
$$

where the individual terms are given as (after much simplification):

$$
\begin{aligned}
(-\mathcal{CA}^{-1}\mathcal{B} + \mathcal{D})_{11} &= 2\mathbf{V}^T\mathbf{Z}\mathbf{V} + 1 \\
(-\mathcal{CA}^{-1}\mathcal{B} + \mathcal{D})_{12} &= 2\mathbf{V}^T\mathbf{Z}(I + \mathbf{W}) \\
(-\mathcal{CA}^{-1}\mathcal{B} + \mathcal{D})_{21} &= 2\left(I + \mathbf{W}^T\right)\mathbf{Z}\mathbf{V} \\
(-\mathcal{CA}^{-1}\mathcal{B} + \mathcal{D})_{22} &= 2\left(I + \mathbf{W}^T\right)\mathbf{Z}(I + \mathbf{W}) + I
\end{aligned}
$$

or in matrix form:

$$\begin{aligned} -\mathcal{C}\mathcal{A}^{-1}\mathcal{B}+\mathcal{D} &= 2\begin{pmatrix} \mathbf{V}^T\mathbf{Z}\mathbf{V} & \mathbf{V}^T\mathbf{Z}(I+\mathbf{W}) \\ \left(I+\mathbf{W}^T\right)\mathbf{Z}\mathbf{V} & \left(I+\mathbf{W}^T\right)\mathbf{Z}(I+\mathbf{W}) \end{pmatrix}+I \\ &= 2\mathbf{Q}^T\mathbf{Z}\mathbf{Q}+I \end{aligned} \tag{7.38}$$

where $\mathbf{Q}$ is defined by (7.36). Thus (7.38) gives:

$$\lambda\left[-\mathcal{C}\mathcal{A}^{-1}\mathcal{B}+\mathcal{D}\right]=\lambda\left[2\mathbf{Q}^T\mathbf{Z}\mathbf{Q}+I\right] \tag{7.39}$$

Use of both the eigenvalue shift theorem and the eigenvalue property $\lambda[AB]=\lambda[BA]$ gives:

$$\lambda\left[-\mathcal{C}\mathcal{A}^{-1}\mathcal{B}+\mathcal{D}\right]=\{1,2\lambda[\mathbf{ZU}]+1\} \tag{7.40}$$

where the form of the parameter $\mathbf{U}$ defined in (7.36) has been employed. Additionally, the first eigenvalue (i.e. 1) corresponds to the largest eigenvalue of the normalized system $G(j0)$. Next the eigenvalues of $G(j0)$ must be compared to those of $G(j\infty)=\mathcal{D}$ which are given by:

$$\lambda[\mathcal{D}]=\left\{1,\lambda\left[\mathbf{P}_M{}^T\mathbf{P}_M\right]\right\} \tag{7.41}$$

Subsequent use of (7.29) along with the definitions of $\mathbf{U}$ and $\mathbf{Z}$ gives:

$$\mathbf{P}_M{}^T\mathbf{P}_M=2\mathbf{ZU}+I \tag{7.42}$$

Hence, the eigenvalues of $\mathcal{D}$ are given by:

$$\lambda[\mathcal{D}]=\{1,2\lambda[\mathbf{ZU}]+1\} \tag{7.43}$$

Comparison of (7.43) with (7.40) confirms that $\sigma_i[G_{e_M}(j0)]=\sigma_i[G_{e_M}(j\infty)]\quad\forall i.$ ■

Thus, the closed form Riccati solution $\mathbf{P}_M$ of Theorem 7.2 not only satisfies norm constraint (7.13), but, it also satisfies a necessary condition for error system singular value flatness. The implications of these results in super-optimization are that *all* of the error system singular values are simultaneously manipulated and *guaranteed* to be less than the infinity norm of the optimal system. Therefore, early termination of

the algorithm yields the implicit assurance that H^∞ optimality is maintained. The corresponding super-optimal algorithm based on the unique parameter $\mathbf{P}_M$ is given below.

Super-optimal Algorithm IV (General Case):
Given a stable n−state, m-input/m-output transfer function matrix $G^{(0)}(s)$, find the super-optimal extension $F_{so}(s)$. In the following, superscripts are used to represent the iteration value.

Step 1. Initialization:

a. Compute the parameter $\mathbf{P}_M$ given in Theorem 7.2.

b. Construct the Central Glover Solution ${F_M}^{(0)}(s)$.

c. Calculate and save the complementary maximizing vectors ${\mathbf{x}_\perp}^{T\ (0)}(s)$ and ${\mathbf{y}_\perp}^{(0)}(s)$ using Lemma 6.6.

d. Compute the stable projection $G_M^{(1)}(s)$ and the antistable projection $Q_M^{(1)}(s)$ using (6.22) and (6.23), respectively.

e. Set $F_{so}^{(0)}(s) = {F_M}^{(0)}(s)$.

Step 2. Iteration: for $i = 1$ to $n-1$ do the following:

a. For each iteration, compute the Central Glover Solution, the complementary maximizing vectors, and the corresponding projections similar to above.

b. Accumulate the super-optimal extension as:

$$F_{so}^{(i)}(s) = F_{so}^{(i-1)}(s) + \left[\prod_{j=0}^{i-1} {\mathbf{y}_\perp}^{(j)}(s)\right] \left[{F_M}^{(i)}(s) + Q_M^{(i)}(s)\right] \left[\prod_{k=i-1}^{0} {\mathbf{x}_\perp}^{T\ (k)}(s)\right]$$

The following example illustrates how the norm of the error system based on either the parameter $\mathbf{P}_{\tilde{X}}$ of (7.9) or the parameter $\mathbf{P}_{\tilde{Y}}$ of (7.10) may exceed the optimal Hankel norm resulting in the loss of H^∞ optimality. In comparison, the example also depicts how the error system based on the parameter $\mathbf{P}_M$ of (7.29) maintains H^∞ optimality during all stages of the super-optimal algorithm presented above.

Example 7.2 Consider the following minimal balanced realization of a 4-state, 3-input, 3-output stable transfer function matrix $G^{(0)}(s)$:

$$G^{(0)}(s) = \left[\begin{array}{cccc|ccc} -0.5293 & 0.0154 & -0.0518 & -0.0467 & 0.9471 & 0.1236 & -0.4243 \\ 0.0273 & -0.4658 & 0.0302 & 0.0366 & -0.1766 & -0.7787 & -0.5192 \\ 0.0037 & 0.0616 & -0.4521 & 0.0947 & 0.0700 & -0.0378 & 0.1502 \\ -0.0185 & -0.0598 & -0.0271 & -0.5783 & 0.0189 & -0.0643 & -0.0219 \\ \hline -0.6339 & 0.6762 & -0.1163 & -0.0361 & 0 & 0 & 0 \\ -0.6395 & -0.0489 & 0.0965 & -0.0569 & 0 & 0 & 0 \\ 0.5305 & 0.6689 & 0.0778 & -0.0207 & 0 & 0 & 0 \end{array}\right]$$

with Hankel singular values given as $\{1.0318, 0.9737, 0.0320, 0.0043\}$. The Central Glover Solution parameters $\mathbf{P}_{\hat{X}}$ and $\mathbf{P}_{\hat{Y}}$ as well as the parameter $\mathbf{P}_M$ are calculated to be (using (7.9), (7.10), and (7.29), respectively):

$$\mathbf{P}_{\hat{X}} = \begin{pmatrix} -0.0913 & -0.1003 \\ 0.7733 & 0.5598 \end{pmatrix} \qquad \mathbf{P}_{\hat{Y}} = \begin{pmatrix} -0.3175 & -0.1076 \\ 0.9380 & 0.2244 \end{pmatrix}$$

$$\mathbf{P}_M = \begin{pmatrix} -0.2410 & -0.2093 \\ 0.7201 & 0.5203 \end{pmatrix}$$

These parameters have the following norms:

$$\overline{\sigma}_{\mathbf{P}_{\hat{X}}} = 0.9639 \qquad \overline{\sigma}_{\mathbf{P}_{\hat{Y}}} = 1.0207 \qquad \overline{\sigma}_{\mathbf{P}_M} = 0.9436$$

and from these, it is clear that the error system based on the parameter $\mathbf{P}_{\hat{Y}}$ of (7.10) will exceed the optimal Hankel norm resulting in the loss of H^∞ optimality. Fig. 7.2a confirms this by depicting the largest singular value of the corresponding error system $G_{e_{\hat{Y}}}(s)$ as the dotted line which has a maximum value of 1.0531. The solid line shown in Fig. 7.2a depicts the largest singular value of the error systems based on either the super-optimal approximation or the parameters $\mathbf{P}_{\hat{X}}$ or $\mathbf{P}_M$ (since the largest singular values of all of these systems equal σ_1) and clearly these error systems achieve H^∞ optimality. Fig. 7.2b depicts the second singular value of all four of the following error systems: $G_{e_{so}}(s)$ (solid line), $G_{e_M}(s)$ (dash-dot line), $G_{e_{\hat{X}}}(s)$ (dashed line), and $G_{e_{\hat{Y}}}(s)$ (dotted line). Since the second singular values corresponding to $G_{e_{so}}(s)$ and $G_{e_M}(s)$, respectively, differ by only 0.0037%, the difference cannot be discerned in Fig. 7.2b; therefore, Fig. 7.3a isolates these singular values on a single plot. This

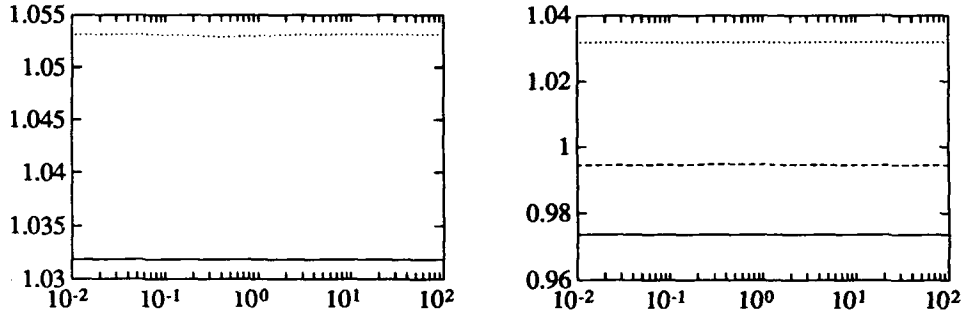

(a) (b)

Figure 7.2: Singular value comparison of the first and second singular values. (a) First singular value of the H^∞ optimal error system (solid line) compared with the first singular value of the error system $G_{e_{\hat{Y}}}(s)$ (dotted line). (b) Second singular value of the following error systems: $G_{e_{so}}(s)$ (solid line), $G_{e_M}(s)$ (dash-dot line), $G_{e_{\hat{X}}}(s)$ (dashed line), and $G_{e_{\hat{Y}}}(s)$ (dotted line).

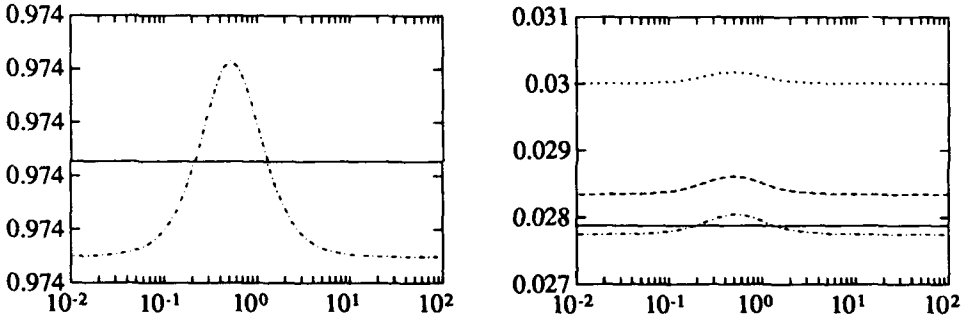

(a) (b)

Figure 7.3: Singular value comparison of the second and third singular values. (a) Second singular value of $G_{e_{so}}(s)$ (solid line) and $G_{e_M}(s)$ (dash-dot line); here, the y-axis increments are 0.00001. (b) Third singular value of the following error systems: $G_{e_{so}}(s)$ (solid line), $G_{e_M}(s)$ (dash-dot line), $G_{e_{\hat{X}}}(s)$ (dashed line), and $G_{e_{\hat{Y}}}(s)$ (dotted line).

figure confirms the efficacy of the parameter $\mathbf{P}_M$ since the corresponding error system second singular value never exceeds the second s-number s_2^∞ by more than 3.7710×10^{-5}. Therefore, early termination after a single iteration not only ensures H^∞ optimality, but also virtually annuls additional super-optimization improvements. Finally, Fig. 7.3b completes the comparison with a depiction of the third singular value the four following error systems: $G_{e_{so}}(s)$ (solid line), $G_{e_M}(s)$ (dash-dot line), $G_{e_{\hat{X}}}(s)$ (dashed line), and $G_{e_{\hat{Y}}}(s)$ (dotted line). Once again, the third singular values follow the same ordering as the second singular values with the error system $G_{e_M}(s)$ comparing favourably with the super-optimal error system $G_{e_{so}}(s)$.

7.5 Summary

Over the past decade, the H^∞ approach has received much attention in the control community since it facilitates the design of robust feedback controllers which maintain stability in the presence of plant uncertainty. In the context of H^∞ optimization problems which can be cast in the 1-block framework, a unique and useful characterization of the degrees of freedom available to the designer was given in Chapter 6. This characterization proved useful originally in deriving expressions for the maximizing vectors and their complementary components which, in turn, allowed the construction of error systems which were uniquely matched to either the left or right maximizing vector observability or controllability dynamics, respectively. Subsequently, the matched error systems enabled the realization of totally stable projections for the square case and minimal antistable projections for the general case which produced significant computational improvements using the super-optimal algorithms presented. Additionally, the singular value total flatness property associated with the matched error systems for the square case was conjectured for the nonsquare case in a manner which, when applied in the square case, maintained approximation gramian stationarity. Although the resulting parameters $\mathbf{P}_{\hat{X}}$ and $\mathbf{P}_{\hat{Y}}$ could be successfully deployed in super-optimization, early termination of the

associated super-optimal algorithm required a strict upper bound on the norm of the parameter $\mathbf{P}$. To achieve this, a composite Riccati equation was derived from the two symmetric Riccati equations previously used to obtain $\mathbf{P}_{\tilde{X}}$ and $\mathbf{P}_{\tilde{Y}}$. The resulting symmetric Riccati equation possessed the required property bounding the norm of the parameter $\mathbf{P}_M$ and, in addition, could be solved without recourse to partitioning the eigenvectors of the Hamiltonian matrix. A super-optimal algorithm employing the parameter $\mathbf{P}_M$ was presented to simultaneously manipulate all of the error system singular values and maintain H^∞ *optimality throughout each cycle of* super-optimization. Finally, the efficacy of the results of this chapter were demonstrated by way of two illustrative examples.

Chapter 8

An evaluation of super-optimality as a control tool: a relative stability perspective

8.1 Introduction

There exist several design philosophies based on H^∞ optimal techniques, such as mixed H^∞/H^2 control [Bernstein and Haddad, 1989; Zhou et al., 1990], μ-synthesis [Doyle, 1984], robustness optimization for coprime factor uncertainty [McFarlane and Glover, 1990], the equalizer principle [Nyman, 1991], and many others. One of the usual control objectives which is considered in the literature [Doyle, 1984; Glover, 1986] is the maximization of a feedback system's tolerance to additive unstructured uncertainty and this, within the methodology of H^∞ design, implies the minimization of the infinity norm of an appropriate transfer function matrix. The controller which achieves this minimization is generally nonunique [Limebeer et al., 1989] and this non-uniqueness may be expressed in degrees of freedom [Glover, 1984; Crews and Kouvaritakis, 1992a] which the designer may use to achieve further control design objectives. Thus, H^∞ optimal design provides a framework which ensures robust stability and permits some degrees of design freedom in the process.

Super-optimal design suggests that the degrees of freedom be exploited to minimize all the singular values in the H^∞ cost function. Although the super-optimal design problem has been successfully solved using mathematically elegant state-space algorithms given in [Limebeer et al., 1989; Tsai et al., 1988; Gu et al., 1989], the control engineering motivation for attaining super-optimality remains ambiguous. For

instance, in a robust stability design problem for which both the plant and the controller are diagonal, super-optimality clearly enhances the robustness of each channel as demonstrated in [Tsai et al., 1988]; by contrast, in [Tsai et al., 1988] it is pointed out that an equalizing solution[1] would be impractical for design. In more general multivariable design problems, the robustness properties resulting from employing a super-optimal design become less clear.

The present chapter shows, by way of an example, that H^∞ super-optimal design does not ensure optimal stability margins when considering additive unstructured uncertainty. Furthermore, the degrees of freedom contained within the H^∞ framework can be used to optimize stability margins, and thereby, attain a clear control engineering objective. The next section gives the necessary background to convey the notation and essential mechanics of the H^∞ design process. Additionally, a formulation of H^∞ optimal design is presented which embodies some of the degrees of freedom in the design process. Subsequently, it is shown how these degrees of freedom may be used to achieve either super-optimality or maximize stability margins for a simple multivariable case. It is noted that, in the maximization, all of the degrees of freedom available in H^∞ design process have not been deployed (the appropriate design procedure for the general case is given in the following chapter), yet the resulting controller affords better stability margins than the super-optimal controller. Finally, an example is given to illustrate the main point of this chapter; interestingly, the solution which optimizes the stability margins, contrary to the intuition presented in [Tsai et al., 1988], turns out to be an equalizing solution. Moreover, the example given is in no way special and a procedure for generating others is given.

[1] An equalizing solution is one in which *all* of the singular values of the error system equal the optimal H^∞-norm.

8.2 Development of main idea

8.2.1 Background

H^∞ design is based on the standard positive feedback configuration which comprises in the forward path a linear dynamical system with transfer function matrix $G(s)$ and a linear controller with transfer function matrix $K(s)$ as depicted in Fig. 8.1. For this structure, the H^∞ design problem which addresses robust stability with

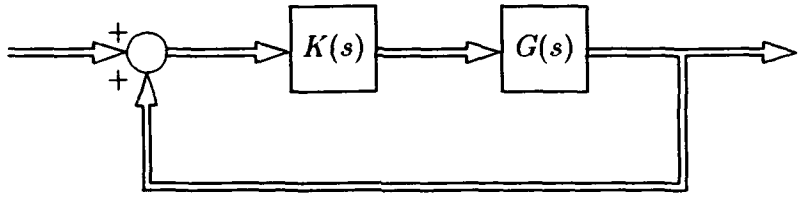

Figure 8.1: Multivariable feedback system

respect to the class $\mathbf{D_u}$ of additive unstructured uncertainty $\Delta(s)$ is given by the following optimization problem:

$$\min_{\text{Stabilizing } K(s)} \left\| p(s)K(s)\left(I - G(s)K(s)\right)^{-1} \right\|_\infty \leq 1 \tag{8.1}$$

where $p(s)$ is a scalar, proper (but not strictly proper), stable, and minimum phase radius function which satisfies:

$$\overline{\sigma}\left[\Delta(j\omega)\right] < |p(j\omega)| \qquad \forall\ \omega \tag{8.2}$$

and $\overline{\sigma}[\,\cdot\,]$ denotes the largest singular value of $[\,\cdot\,]$. As usual, the assumption is made that all the unstable poles of the additive perturbation $\Delta(s)$ are also poles of the nominal plant $G(s)$. As outlined in Chapter 5, the robust stability cost function given in (8.1) is nonlinear in $K(s)$ and can be transformed into the following equivalent cost function which is affine in the Youla parameter $Q(s)$:

$$\min_{Q(s)\in RH_+^\infty} \left\| p(s)\left(M^{-1}(s)U(s) + Q(s)\right) \right\|_\infty \leq 1 \tag{8.3}$$

The mechanics of this transformation require the following coprime factorizations for the plant $G(s)$ and the controller $K(s)$:

$$G(s) = N(s)M^{-1}(s) = \tilde{M}^{-1}(s)\tilde{N}(s) \tag{8.4}$$

$$K(s) = [U(s) + M(s)Q(s)]\,[V(s) + N(s)Q(s)]^{-1} \tag{8.5}$$

In conjunction with these factorizations, if the state-space representation of the plant is given by $G(s) = \left[\begin{array}{c|c} A & B \\ \hline C & D \end{array}\right]$, then the state-space representation for the parameters of (8.4) and (8.5) are given as [c.f. (5.11) and (5.12)]:

$$\begin{bmatrix} M(s) & U(s) \\ N(s) & V(s) \end{bmatrix} = \left[\begin{array}{c|cc} A - BB^TP_c & B & P_oC^T \\ \hline -B^TP_c & I & 0 \\ C - DB^TP_c & D & I \end{array}\right] \tag{8.6}$$

$$\begin{bmatrix} \tilde{V}(s) & -\tilde{U}(s) \\ -\tilde{N}(s) & \tilde{M}(s) \end{bmatrix} = \left[\begin{array}{c|cc} A - P_oC^TC & -B + P_oC^TD & -P_oC^T \\ \hline -B^TP_c & I & 0 \\ C & -D & I \end{array}\right] \tag{8.7}$$

where P_c and P_o satisfy the following algebraic Riccati equations [c.f. (5.13) and (5.14)]:

$$P_cA + A^TP_c - P_cBB^TP_c = 0 \tag{8.8}$$

$$P_oA^T + AP_o - P_oC^TCP_o = 0 \tag{8.9}$$

With the above definitions, the coprime factorization of the plant $G(s)$ given in (8.4) has $M(s)$, $N(s)$, $\tilde{M}(s)$, and $\tilde{N}(s)$ all stable (i.e. in RH_+^∞) and, in addition, has $M(s)$ and $\tilde{M}(s)$ both square and inner.

The state-space formulae of (8.6) and (8.7) can also be used to further simplify the H^∞ cost function (8.3). In particular, it is straightforward to show that state-space representation of $M^{-1}(s)U(s)$ simplifies to:

$$M^{-1}(s)U(s) = \left[\begin{array}{c|c} A & -P_oC^T \\ \hline B^TP_c & 0 \end{array}\right] \tag{8.10}$$

The cost function (8.3) can be solved explicitly [for $Q(s)$] using Glover's state-space formulae [Glover, 1984], referred to previously as the Central Glover Solution in

Chapter 6. For notational convenience, consider the following H^∞ cost function:

$$\min_{F(s)\in RH_-^\infty} \|G(s) - F(s)\|_\infty \tag{8.11}$$

where $G(s)$[2] is a completely stable transfer function matrix in RH_+^∞. The state-space formulae which constitute the Central Glover Solution $F(s)$ were given previously in Lemma 6.1 and the degrees of freedom contained in the Central Glover Solution were characterized in terms of the parameter $\mathbf{P}$ (c.f. Lemma 6.2). Although the parameter $\mathbf{P}$ of (6.24) completely characterizes the degrees of freedom contained within the Central Glover Solution, it is noted that the general Glover solution has more degrees of freedom, but for the present objective, it will be seen that the degrees of freedom available in the central solution are sufficient to demonstrate the main point of this chapter.

8.2.2 H^∞ controller synthesis

The H^∞ optimal design process can be expressed completely in terms of the degree of freedom parameter $\mathbf{P}$. In particular, H^∞ optimal controller synthesis consists of the following steps:

1. Determine the state-space representation of $p(s)M^{-1}(s)U(s)$ using the simplification of (8.10).
2. Separate the state-space representation of $p(s)M^{-1}(s)U(s)$ into a sum of stable and unstable terms, $G_s(s)$ and $G_u(s)$, respectively.
3. Determine the Central Glover Solution $F(s)$ based on $G(s) = G_u^T(-s)$ for a chosen value of $\mathbf{P}$ using (6.25) through (6.31).
4. Solve for $Q(s)$ as $Q(s) = -\left(F^T(-s) + G_s(s)\right)/p(s)$.
5. Construct the H^∞ optimal controller $K(s)$ using (8.5) in conjunction with (8.6).

[2]G(s) here is to be distinguished from the plant transfer function matrix. This conforms to the notation originally given in [Glover, 1984] and previously adhered to in the H^∞ optimization problem (6.1).

Clearly, different H^∞ optimal controllers result by varying the parameter $\mathbf{P}$ as can be seen in step 3 above. The next section describes how the parameter $\mathbf{P}$ can be used to either achieve super-optimality or maximize the relative stability margins for a simple multivariable case.

8.2.3 Computation of P for either super-optimality or the maximization of relative stability margins for a simple case

In the 2-state square case, the parameter $\mathbf{P}$ is a scalar and represents the only degree of freedom in the Central Glover Solution and, as reported in Chapter 6, super-optimality involves the solution of a single quadratic equation [c.f. (6.40)]. In particular, the choice of parameter $\mathbf{P}$ which attains super-optimality in the H^∞ cost function (8.3) is given by:

$$\mathbf{P}_{so} = (\sigma_1 \mathbf{BC})^{-1} \left(\mathbf{A} + \sqrt{\mathbf{A}^2 - (\sigma_1 \mathbf{BC})^2} \right) \tag{8.12}$$

where $\mathbf{A}, \mathbf{B}$, and $\mathbf{C}$ were defined by (6.32) through (6.34) and are all scalars. Subsequent to attaining the super-optimal parameter P_{so}, steps 4 and 5 of the previous section may be used to synthesize the H^∞ super-optimal controller.

In contrast to super-optimality, design for the maximization of relative stability margins seeks to maximize, over the class of uncertainty, the minimum distance from the imaginary-axis to the system's worst case closed-loop poles. Assuming that the dynamics associated with the relevant poles are not negligible (i.e. that the corresponding modes are not nearly decoupled), this measure provides immediate insight into the closed-loop dynamic performance and, in addition, it is unambiguous as compared to alternative measures such as gain/phase margins for the case of multivariable systems. Clearly then, a small relative stability margin would imply a slow and possibly oscillatory dynamic response and thus the maximization of this margin forms an obvious desirable control objective. Note that this objective is sought in addition to the maximization of tolerance to uncertainty which is already achieved

through the use of the H^∞ design process described at the end of Section 8.2.1. In order to maximize relative stability margins within H^∞ optimal design, the degrees of freedom should be used to maximize the "shift ρ" which the H^∞ cost function can sustain while ensuring robust stability. In particular, the parameter $\mathbf{P}$ should be chosen so as to

$$\max_{-1 \leq \mathbf{P} \leq 1} \rho^*[\mathbf{P}] \tag{8.13}$$

where $\rho^*[\mathbf{P}]$ is defined as:

$$\rho^*[\mathbf{P}] = \left\{ - \max_{\Delta(s) \in \mathbf{D_u}} \text{Real}[s] \quad | \, s \in C \quad : \quad \det\{I - (G(s) + \Delta(s)) K(s, \mathbf{P})\} = 0 \right\} \tag{8.14}$$

where the dependence of $K(s)$ on the parameter $\mathbf{P}$ has been made explicit. Additionally, the constraint in (8.13) that the parameter $\mathbf{P}$ lie in the range $-1 \leq \mathbf{P} \leq 1$ arises from (6.24).

Remark 8.1 It should be noted that in the following chapter the associated relative stability margins will be maximized over the entire class of stabilizing controllers whereas here, for purposes of comparison with super-optimality, the stabilizing controller class is limited to the Central Glover Solution in H^∞ optimal design.

Remark 8.2 The aim of (8.14) is to place the worst case poles as far to the left of the imaginary-axis as possible and thus could theoretically result in fast but resonant poles; this is not the case in the numerical example considered in Section 8.3. In parallel with super-optimality, no special consideration has been given to the question of damping. However, a slight modification of the procedure to include a "shift" [as shown in (8.16) below] and a "rotation" of the imaginary-axis would cater for this aspect of design.

Because the additive uncertainty $\Delta(s)$ is unknown, (8.14) does not represent a practical means of computing the parameter $\mathbf{P}$ which maximizes (8.13) denoted $\mathbf{P}_{rsm}$. However, under the assumption that the stable poles of $\Delta(s)$ have a real part

which is less than $-\rho^*[\mathbf{P}_{rsm}]$, an equivalent definition of $\rho^*[\mathbf{P}]$ is given by the smallest solution ρ of

$$\phi(\rho, \mathbf{P}) = 1 \tag{8.15}$$

where $\phi(\rho, \mathbf{P})$ is given by:

$$\phi(\rho, \mathbf{P}) = \left\| p(s-\rho)K(s-\rho, \mathbf{P})\left[I - G(s-\rho)K(s-\rho, \mathbf{P})\right]^{-1} \right\|_\infty \tag{8.16}$$

Here, it is assumed that it is possible to define a "shifted" radius function $p(s-\rho)$ which is proper, stable, and minimum phase and which gives an upper bound on $\overline{\sigma}\left(\Delta(s-\rho)\right)$ when $s = j\omega$. Under the assumption that (8.1) has a solution, it is clear that the shift $\rho = 0$ yields $\phi(0, \mathbf{P}) \leq 1$. On the other hand, $\phi(\rho, \mathbf{P})$ cannot remain less than 1 for ρ positive and increasing because this would correspond to the trivial case of a system with infinite stability margins. Hence, (8.15) will admit a solution $\rho^*[\mathbf{P}]$ for any $\mathbf{P}$ in the range $-1 \leq \mathbf{P} \leq 1$. In addition, the assumption above that the stable poles of $\Delta(s)$ be at least a distance $-\rho^*[\mathbf{P}_{rsm}]$ from the imaginary-axis is not necessary and can be avoided in a manner to be fully described in the following chapter; presently, this assumption is invoked merely to keep the presentation simple.

Equation (8.15) can be solved by any nonlinear equation solver (e.g. regula falsi) and thus generates values of $\rho^*[\mathbf{P}]$ for any value of $\mathbf{P}$. Consequently, any standard optimization technique (e.g. FMIN in MATLAB) can be used to compute $\mathbf{P}_{rsm}$. For the simple case considered, a graph of the variation of $\rho^*[\mathbf{P}]$ as $\mathbf{P}$ varies from $-1 \leq \mathbf{P} \leq 1$ can be deployed to steer the algorithm to the global maximum. Subsequent to computing $\mathbf{P}_{rsm}$, steps 4 and 5 of the previous section may be used to synthesize the H^∞ optimal controller, $K_{rsm}(s)$. It should emphasized that the algorithm above is sufficient to demonstrate that super-optimality does not optimize the relative stability margins; a more general treatment will be given in the following chapter. The next example highlights the distinction between H^∞ optimal designs which use the parameter $\mathbf{P}$ to achieve either super-optimality or the maximization of relative stability margins.

8.3 Illustrative example

Consider the following state-space description of an unstable plant:

$$G(s) = \left[\begin{array}{c|c} A & B \\ \hline C & D \end{array}\right] = \left[\begin{array}{cc|cc} 1 & 0 & -5 & 2 \\ 0 & 2 & 4 & -3 \\ \hline 1 & 2 & 0 & 0 \\ 3 & 4 & 0 & 0 \end{array}\right]$$

This example was chosen to conform to the simple case formulation of the previous section and, other than having integer values in the state-space representation, has no special properties. Suppose next that $G(s)$ is subject to an additive perturbation $\Delta(s)$ which has two unstable poles and whose other poles lie to the left of the point $(-0.2+j0)$. A trivial but nonetheless valid choice of $p(s)$ [and $p(s-\rho)$] is a constant for which $\overline{\sigma}\left[\Delta(j\omega)\right] \leq 1$. Hence, for simplicity the radius function can be taken to be unity, $p(s) = 1$, which yields a shifted radius function which also equals unity, $p(s-\rho) = 1$.

The state-space realization of $M^{-1}(s)U(s)$ may be expressed using (8.10) as:

$$M^{-1}(s)U(s) = \left[\begin{array}{c|c} A & -P_o C^T \\ \hline B^T P_c & 0 \end{array}\right] = \left[\begin{array}{cc|cc} 1 & 0 & -1.3448 & -1.1379 \\ 0 & 2 & 1.6552 & 1.8621 \\ \hline -0.2202 & -0.9454 & 0 & 0 \\ 0.8702 & 1.6867 & 0 & 0 \end{array}\right]$$

For this example, $G_u(s) = M^{-1}(s)U(s)$ and $G_s(s) = 0$ because both $p(s) = 1$ and the original plant $G(s)$ is completely unstable. Hence, the solution submitted for the Central Glover Solution is $G(s) = G_u^T(-s)$. The parameters $\mathbf{A}, \mathbf{B}$, and $\mathbf{C}$ defined in (6.32) through (6.34) are given by:

$$\mathbf{A} = -0.1926 \qquad \mathbf{B} = -0.3633 \qquad \mathbf{C} = 0.2278$$

Using these parameters along with $\sigma_1 = 0.6390$ in (8.12) gives the super-optimal parameter $\mathbf{P}$ as $\mathbf{P}_{so} = 0.1399$. Completing steps 3 through 5 of the H^∞ design process given in the previous section yields the following minimal realization of the

super-optimal controller:

$$K_{so}(s) = \left[\begin{array}{c|cc} -1.7158 & -0.5171 & -0.8441 \\ \hline -0.7826 & -0.2964 & -0.2706 \\ 0.6062 & 0.2620 & 0.4320 \end{array}\right]$$

The nominal closed-loop poles for the super-optimal design may be retrieved from the nominal closed-loop state-space description and are given by:

$$\{-0.5155, -1, -2\} \tag{8.17}$$

A worst case perturbation matrix $\Delta_{wc}(s)$ can be obtained by the following procedure:

1. Determine the minimum shift ρ_t at which a shifted E-Contour plot based on the shifted uncertainty modulus function $p(j\omega - \rho_t)$ and the shifted open-loop transfer function matrix $G(j\omega - \rho_t)K_{so}(j\omega - \rho_t)$ *first* touches the critical point $(1 + j0)$.

2. Determine the frequency ω_t corresponding to the E-Contour in Step 1 which first touched the critical point.

3. Compute the singular value decomposition of the shifted controller sensitivity function evaluated at $s = j\omega_t - \rho_t$:

$$X\Sigma Y^* = R_{so}(j\omega_t - \rho_t) = K_{so}(j\omega_t - \rho_t)(I - G(j\omega_t - \rho_t)K_{so}(j\omega_t - \rho_t))^{-1}$$

4. Since the uncertainty class considered is frequency independent and thus depends on neither the frequency ω_t nor the shift ρ_t, a sufficient worst case uncertainty is given by the following major principal direction dyad:

$$\Delta_{wc} = \overline{y}_{R_{so}}\overline{x}^*_{R_{so}}$$

Note that this worst case perturbation satisfies $\overline{\sigma}[\Delta_{wc}] = 1$ and therefore is on the boundary of the uncertainty class $\mathbf{D_u}$.

Using the procedure outlined above, the shift $\rho_t = 0.1100$ produces the first occurrence of an E-Contour contacting the critical point. The frequency corresponding to this particular E-Contour is given by $\omega_t = 0$; hence, using the major principal directions of the controller sensitivity function $R_{so}(j0 - 0.1100)$ yields the following possible worst case perturbation matrix:

$$\Delta_{wc} = \begin{pmatrix} -0.1690 & -0.1599 \\ 0.7064 & 0.6685 \end{pmatrix}$$

The worst case closed-loop poles for the super-optimal design may be obtained using a worst case closed-loop state-space description using $G(s) + \Delta_{wc}$ in place of $G(s)$. Using Δ_{wc} above gives the following worst case closed-loop poles:

$$\{-0.1100, -1.7353 \pm j0.9829\} \tag{8.18}$$

The maximum singular values of the residues of these closed-loop poles are 1.1768, 4.4025, and 4.4025 respectively, thereby indicating that the dynamics associated with the pole at -0.1100 are by no means negligible.

The controller derived using H^∞ design to maximize relative stability margins chooses the degree of freedom $\mathbf{P}$ to maximize the shift $\rho^*[\mathbf{P}]$ as given in (8.15). Using a nonlinear equation solver, the parameter $\mathbf{P}$ which maximizes (8.15) is given by $\mathbf{P}_{rsm} = -1$ and the maximum shift is $\rho^*[-1] = 0.1254$. Based on this, the resulting controller is given by the following state-space description:

$$K_{rsm}(s) = \left[\begin{array}{c|cc} -3.1139 & -0.5814 & 1.4774 \\ \hline 1.5701 & 0.1577 & -0.6193 \\ -0.2356 & 0.6193 & 0.1577 \end{array}\right]$$

The first evidence of improved relative stability margins is given by the nominal closed-loop poles:

$$\{-0.6832, -1, -2\} \tag{8.19}$$

However, the controller was designed to shift the worst case poles as far to the left as possible within the H^∞ design framework. In order to find a suitable worst case perturbation matrix, the procedure outlined previously can be used with $R_{rsm}(s)$ in place of $R_{so}(s)$. Performing this procedure yields the shift $\rho_t = 0.1254$ and the frequency $\omega_t = 0$ which are used in computing the specific value of the complementary sensitivity function $R_{rsm}(s)$ at $s = j\omega_t - \rho_t$. Using the major principal directions of $R_{rsm}(j0 - 0.1254)$ permits the construction of the following possible worst case perturbation matrix as:

$$\Delta_{wc} = \begin{pmatrix} -0.3898 & -0.3541 \\ 0.6293 & 0.5715 \end{pmatrix}$$

This worst case uncertainty produces the following set of worst case closed-loop poles:

$$\{-0.1254, -1.5220 \pm j0.4170\} \tag{8.20}$$

To illustrate the functional relationship between ρ and $\mathbf{P}$, Fig. 8.2(a) gives a plot of the parameter $\mathbf{P}$ versus the shift $\rho^*[\mathbf{P}]$. From this plot, it can be seen that the

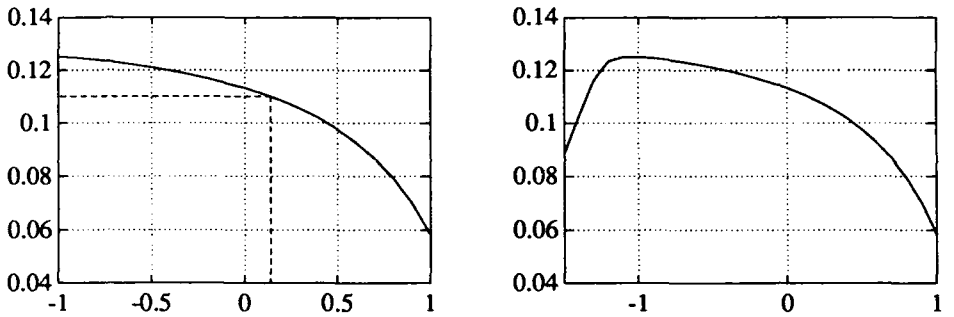

(a) (b)

Figure 8.2: (a) Plot of the Central Glover Solution degree of freedom parameter $\mathbf{P}$ versus the shift $\rho^*[\mathbf{P}]$ where $\mathbf{P}$ satisfies $-1 \leq \mathbf{P} \leq 1$. The dashed line corresponds to the super-optimal shift $\rho^*[0.1399] = 0.1100$. (b) Plot of the shift $\rho^*[\mathbf{P}]$ versus the Central Glover Solution degree of freedom parameter $\mathbf{P}$ where $\mathbf{P}$ ranges from: $-1.5 \leq \mathbf{P} \leq 1$.

maximal shift $\rho^*[\mathbf{P}_{rsm}] = 0.1254$ occurs at $\mathbf{P}_{rsm} = -1$. This data also correlates with the minimum distance from the imaginary-axis to the set of worst case closed-loop poles as given in (8.20). Fig. 8.2(a) also depicts the super-optimal parameter value of $\mathbf{P}_{so} = 0.1399$ and the corresponding shift $\rho^*[\mathbf{P}_{so}] = 0.1100$ as indicated by the dashed line. Similarly, this correlates with the minimum distance from the imaginary-axis to the set of super-optimal closed-loop poles as given in (8.18).

Comparison of (8.18) with (8.20) clearly reveals that the H^∞ super-optimal controller produced worse results with respect to relative stability margins. Interestingly, the singular values of the H^∞ cost function associated with the $\mathbf{P} = -1$ solution are equal over all frequencies [this is an equalizing (or all pass) solution]; hence the second singular value is far from its minimal value as would otherwise be required in super-optimal design.

The maximum of $\rho^*[\mathbf{P}]$ as seen from Fig. 8.2(b) occurs at $\mathbf{P} = -1.0494$ which lies outside the range of interest from $-1 \leq \mathbf{P} \leq 1$. However, this is not always the case and, therefore, the relative stability margin maximizer $\mathbf{P}_{rsm}$ will not always turn out to be the equalizing solution. More importantly, whether $\mathbf{P}_{rsm}$ leads to an equalizing solution or not, $\mathbf{P}_{rsm}$ will not, in general, coincide with $\mathbf{P}_{so}$.

8.4 Summary

Within the framework of H^∞ optimal design which addresses additive unstructured uncertainty, there are degrees of design freedom which may be used to enhance robustness properties. Super-optimal design, albeit mathematically elegant, did not ensure optimal robust stability as was demonstrated by way of a simple example. Alternatively, the degrees of design freedom can be used to optimize relative stability margins and therefore achieve a clear control objective; this objective will be fulfilled for the general case in the following chapter.

Chapter 9

H^∞ design for the maximization of relative stability

9.1 Introduction

The previous chapter set forth a simple design procedure which synthesized optimal relative stability margin controllers for a limited controller class, namely those controllers which could be generated by optimizing the Central Glover Solution degree of freedom parameter **P** in the 2-state square case. The purpose of this chapter is to develop a more general[1] design procedure which attains the optimal relative stability margin when the nominal plant is subject to an additive unstructured uncertainty. As will be seen, the design procedure exploits the degree of freedom made available by the upper bound (i.e. unity) of the robustness to additive unstructured uncertainty H^∞ cost function [c.f. (8.1)]. To see how this degree of freedom arises, it is only necessary to point out that *any* internally stabilizing controller which satisfies the upper bound constraint will, by definition, achieve robust stability. Thus, H^∞ optimality is not the precondition for robust stability; rather, the upper bound defines the robust stability condition. Consequently, when the upper bound is *strictly less than one*, the stabilizing controller class can be enlarged to include those stabilizing controllers which attain the upper bound; hence, there exists some freedom in satisfying the robust stability constraint. Moreover, when the upper bound of the robust stability cost function is strictly less than one, the synthesized controller achieves robust stability not only for the given uncertainty class, but also for the expanded

[1]The number of inputs equals the number of outputs with no state order constraints.

uncertainty class scaled by the maximum gain of the modulus function; therefore, the corresponding H^∞ controller maximizes *tolerance to uncertainty.*

Rather than maximize tolerance to uncertainty, this work seeks to optimize relative stability by deploying the degree of freedom in terms of *shifting* the $j\omega$-axis in the H^∞ cost function until the upper bound either achieves unity or achieves some prescribed upper limit less than unity; thus, the design procedure presented in the sequel employs a shifted H^∞ design technique. Although the concept of designing with a shift has been used extensively in the LQG methodology [Anderson and Moore, 1971; Anderson and Moore, 1989; Medanic et al., 1988; Kim and Furuta, 1988; Kawasaki and Shimemura, 1988], this work constitutes its first application in the context of robust *multivariable* H^∞ design. It is noted that similar work has been accomplished for the *SISO* case in [Kimura et al., 1991]; however, the present work was completed independently [Kouvaritakis et al., 1991] and resolves the unique and critical multivariable design aspects.

It should be pointed out that even though LQG design has previously employed a shift to obtain a guaranteed stability margin, the LQG design process caters only for the nominal case; clearly the optimality of the nominal stability margin does not generally imply the optimality of the perturbed stability margin. In contrast, the optimal relative stability margin design procedure presented in this work directly targets the worst case thereby ensuring optimality over the uncertainty class. It is also recognized that by solving sub-optimal H^∞ problems as outlined in [Doyle et al., 1989], we can deal with the case whereby the modulus function is specified; however, within that approach there exist no systematic means of maximizing relative stability.

In order to support the ultimate development of the optimal relative stability design procedure, the next section begins by distinguishing between the differing design objectives of maximizing uncertainty tolerance and maximizing relative stability. Following this delineation, a SISO treatment is given to motivate the ensuing theoretical development. Finally, the design synthesis is enumerated and its efficacy illustrated by means of two numerical examples.

9.2 Design Objectives

Consider the unity, positive feedback configuration depicted in Fig. 9.1 which comprises in the forward path a perturbed plant transfer function matrix $G(s) + \Delta(s)$ and a controller with transfer function matrix $K(s)$. With regard to this system,

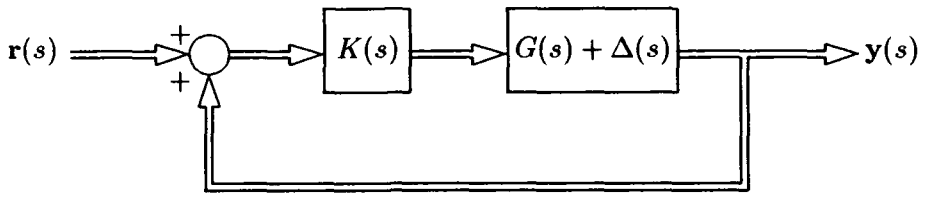

Figure 9.1: Multivariable feedback system with positive feedback and additive uncertainty.

the H^∞ cost function [Glover, 1986] which addresses robust stability with respect to the additive unstructured uncertainty class $\mathbf{D_u}$ is given by (c.f. Section 5.3):

$$\min_{\text{K(s) stabilizing}} \|p(s)R(s)\|_\infty \leq 1 \tag{9.1}$$

where $p(s)$ is a biproper, stable and minimum phase modulus function which bounds the norm of the additive unstructured uncertainty as:

$$\overline{\sigma}\left[\Delta(j\omega)\right] \leq |p(j\omega)| \tag{9.2}$$

and $R(s)$ is the controller sensitivity function given by:

$$R(s) = K(s)\left[I - G(s)K(s)\right]^{-1} \tag{9.3}$$

Assuming that the nominal plant $G(s)$ and the perturbed plant $G(s) + \Delta(s)$ share the same number of unstable poles, it is straightforward to show that the controller which optimizes (9.1) will also stabilize the perturbed system $G(s) + \Delta(s)$ for the same uncertainty class $\mathbf{D_u}$ but whose corresponding modulus function $p(s)$ is scaled as $p(s)/\|p(s)R(s)\|_\infty$. Therefore, the optimization of (9.1) maximizes the amount by which the modulus function $p(s)$ can be increased which, in turn, yields the optimal uncertainty tolerance.

In some instances, maximizing tolerance to additive uncertainty forms a useful design objective; however, this objective is distinct from the aim of maximizing relative stability for a given uncertainty class $\mathbf{D_u}$. At this point, the clear resolution of these differing design objectives requires a concise definition of "relative stability margin." Conventionally, relative stability is measured in terms of gain and phase margins for the case of scalar systems, or in terms of the suitable extension of the classical concepts of gain and phase margins for the case of multivariable systems. Although this measure of relative stability provides useful information concerning closed-loop dynamic performance, the analysis can be misleading except for cases in which either a single pole or a pole-pair dominates the frequency response. Thus, in order to avoid possible ambiguity, the relative stability margin employed here will be defined by the minimum distance from the imaginary axis to the set of *worst case* closed-loop poles. Although this measure also has closed-loop dynamic performance ramifications, the emphasis here remains on the *worst case* robust stability aspect of the measure; hence, this measure correctly indicates when the *perturbed* system can lose stability. Hereon for clarity, the use of the phrase "relative stability" will implicitly convey this worst case aspect of the measure just defined.

It will be seen that, although the direct optimization of (9.1) automatically maximizes uncertainty tolerance, it does not implicitly maximize relative stability; indeed examples will be presented to illustrate that the resulting controller can yield a relative stability margin which is far from optimal. Thus, the delineation of uncertainty tolerance and relative stability raises the question as to whether one should maximize uncertainty tolerance or relative stability. Here, the view is taken that if the uncertainty modulus function $p(s)$ is potentially inaccurate[2], then maximizing uncertainty tolerance constitutes a meaningful design objective. However, if the modulus function $p(s)$ accurately envelopes the uncertainty as often occurs in practice (c.f. Section 9.3), then the alternative view is taken that maximizing relative stability constitutes the more useful design objective. This objective will be accomplished in the

[2]This is tantamount to stating that there is an "uncertain" uncertainty characterization.

sequel; however, we first require additional preliminaries to support the succeeding theoretical development.

9.3 Theoretical preliminaries

In order to motivate the subsequent theoretical development, first consider a simple open-loop unstable, scalar system consisting of a nominal plant $g(s)$ which is subject to an additive uncertainty $\delta(s)$ which also shares the same number of unstable poles as $g(s)$. Additionally, assume that the uncertainty $\delta(s)$ is subject to the following constraint:

$$|\delta(j\omega)| < \alpha\,|p(j\omega)|\ , \qquad 0 < \alpha \tag{9.4}$$

where $p(s)$ is a proper (but not strictly proper) stable and minimum phase, modulus function and α is some positive, real, scalar constant. Based on (9.1), the H^∞ optimal controller which maximizes robust stability satisfies the following optimization:

$$\min_{\mathbf{k(s)\ stabilizing}} \|p(s)r(s)\|_\infty = \min_{\mathbf{k(s)\ stabilizing}} \left\| \frac{p(s)k(s)}{1-g(s)k(s)} \right\|_\infty = \mu \leq 1 \tag{9.5}$$

where μ is the constant modulus of the resulting all-pass system $p(j\omega)r(j\omega)$. The key fact from this simple example confirms the previous observation that the resulting H^∞ controller $k(s)$ will not only achieve robust stability for the given uncertainty class defined by (9.4) with $\alpha \leq 1$, but also for the larger class of uncertainty defined by (9.4) with $\alpha = 1/\mu$.

From this discussion, it is clear that if there is uncertainty concerning the value of α in (9.4), the controller resulting from the minimization (9.5) achieves a useful result. Assuming however that α is known to be 1, it is possible to stipulate an unscaled modulus function $|p(j\omega)|$ which defines a strict upper bound on the modulus of the uncertainty $|\delta(j\omega)|$. Such a stipulation of the modulus function is generally possible as illustrated in three different typical cases below:

Case A: The nominal plant $g(s)$ is determined from a frequency response analysis which yields values for the gain and phase of $g(j\omega)$. Due to noise, such

measurements are subject to a percent error on the basis of which it is possible to stipulate lower and upper values for both the gain and phase of $g(j\omega)$. The circumscription of circles around the implied regions in which $g(j\omega)$ can lie determines the largest value of the uncertainty modulus $|\delta(j\omega)|$.

Case B: The system is described in terms of an ordinary linear differential equation whose coefficients are known to lie within upper and lower limits. These bounds may be used to compute regions in the complex plane within which $g(j\omega)$ must lie. Circumscription of these regions by circles will again yield worst case estimates of the uncertainty modulus $|\delta(j\omega)|$.

Case C: On the basis of a statistical confidence analysis it is possible to determine ellipsoidal regions in which the vector of numerator coefficients and the vector of denominator coefficients must lie [Edmunds, 1984]. Once again these can be mapped to the g-plane in order to determine the largest value of the uncertainty modulus $|\delta(j\omega)|$. It is pointed out that in the case of discrete-time systems which are modelled in terms of a causal weighting sequence (for the case of stable systems) or a bi-causal weighting sequence, the calculation of $p(e^{j\omega T})$ is straightforward and reduces to the computation of the maximum eigenvalue of a known matrix function of $z = e^{j\omega T}$ [Cloud and Kouvaritakis, 1986; Cloud and Kouvaritakis, 1988; Kouvaritakis and Rossiter, 1992].

In all of these cases a suitable modulus function $p(s)$ can be computed from the uncertainty modulus $|\delta(j\omega)|$ and, hence, the maximization of the value of α given in (9.4) for which stability can be maintained is no longer a high priority.

Given that a modulus function $p(s)$ can be computed reliably (therefore removing the uncertainty about α), it is of interest to assess the relative stability margin characteristics of the H^∞ optimal controller resulting from the optimization of (9.5). To enable such an assessment, consider the following definition of the relative stability

margin:

$$\rho[k] = \left\{ - \max_{|\delta(s)| \leq |p(s)|} [\text{Real}(s)] \quad | \quad s \in C \quad : \quad [g(s) + \delta(s)]\, k(s) = 1 \right\} \tag{9.6}$$

where, for consistency with most of the H^∞ literature, the positive feedback convention has been followed (c.f. Fig. 9.1). Thus, the quantity $\rho[k]$ measures the minimum distance over the class of uncertainty from the imaginary-axis to the worst case closed-loop poles. In order to simplify the ensuing presentation, define the following notation:

$$x_\rho(s) \equiv x(s - \rho) \tag{9.7}$$

where $x(s)$ is some proper transfer function and the subscript ρ denotes a shift of the imaginary axis to the left for $\rho > 0$. In addition, if it is assumed that the nominal plant $g(s)$ and the perturbed plant $g(s) + \delta(s)$ have the same number of poles to the right of the line defined by $-\rho[k]$, then an equivalent statement to the relative stability margin definition (9.6) is that the shifted perturbed sensitivity function

$$s_\rho(s) = [1 - (g_\rho(s) + \delta_\rho(s))\, k(\rho, s)]^{-1} \tag{9.8}$$

be analytic in the closed right half complex-plane; here the controller $k(\rho, s)$ is designed at the shift ρ. Furthermore, if $p(\rho, s)$ denotes a modulus function which bounds the shifted perturbation $\delta_\rho(s)$:

$$|\delta_\rho(j\omega)| < |p(\rho, j\omega)| \tag{9.9}$$

then by the definition of the relative stability margin $\rho[k]$ given in (9.6), the shifted H^∞ cost function (9.1) becomes:

$$\min_{\text{k}(\rho,s)\ \text{stabilizing}} \|p(\rho, s) r_\rho(s)\|_\infty = \min_{\text{k}(\rho,s)\ \text{stabilizing}} \left\| \frac{p(\rho, s) k(\rho, s)}{1 - g_\rho(s) k(\rho, s)} \right\|_\infty = 1 \tag{9.10}$$

where the shifted controller $k(\rho, s)$ optimizes (9.10) and stabilizes the closed-loop containing the shifted, perturbed plant $g_\rho(s) + \delta_\rho(s)$. It is pointed out the methods used to compute the modulus function $p(\rho, s)$ which bounds $|\delta_\rho(s)|$ are similar to those used to compute the modulus function $p(s)$ which bounds $|\delta(s)|$; in particular

for cases B and C above, the procedure is identical. It is also pointed out that under some assumptions concerning the pole/zero positions of the uncertainty $\delta(s)$ there will exist a range of values for the shift ρ, $0 \leq \rho \leq \rho_u$, over which it is possible to use:

$$p(\rho, s) = p_\rho(s) \tag{9.11}$$

A more detailed analysis of the constraints required for the validity of (9.11) is given in Section 9.5; for the time being suffice it to say that it possible to define a suitable modulus function $p(\rho, s)$ which is proper but not strictly proper, stable and minimum phase. If $k_{(-\rho)}(\rho, s)$ represents the unshifted controller based on the shifted optimization (9.10), then since $k_{(-\rho)}(\rho, s)$ is based on the maximization of the relative stability margin $\rho\,[k]$ given by (9.6), this controller clearly affords a greater relative stability margin over the controller based on the unshifted optimization (9.5). Thus, given a fixed uncertainty bound $p(s)$ it is perfectly feasible to generate the controller which maximizes the relative stability margin $\rho\,[k]$; the machinery to generate this controller will be developed in the next section after defining further notation as well as the uncertainty class.

In the sequel, $p(\rho, s)$ [or $p_\rho(s)$] will continue to be scalar, however $g(s)$, $\delta(s)$, and $k(s)$ will be taken to be multivariable and will be denoted by $G(s)$, $\Delta(s)$, and $K(s)$. Additionally, $G(s)$ and $p(\rho, s)$ will have the following state-space descriptions:

$$G(s) = \left[\begin{array}{c|c} A & B \\ \hline C & D \end{array}\right] \qquad p(\rho, s) = \left[\begin{array}{c|c} A_p(\rho) & B_p(\rho) \\ \hline C_p(\rho) & D_p \end{array}\right] \tag{9.12}$$

and the corresponding shifted transfer function matrices will have the following state-space descriptions:

$$G_\rho(s) = \left[\begin{array}{c|c} A+\rho I & B \\ \hline C & D \end{array}\right] \qquad p_\rho(s) = \left[\begin{array}{c|c} A_p+\rho I & B_p \\ \hline C_p & D_p \end{array}\right] \tag{9.13}$$

where the assumption has been made that $A_p = A_p(0)$, $B_p = B_p(0)$, and $C_p = C_p(0)$, and where I denotes the identity matrix of conformal dimensions. Moreover, it will be assumed that the perturbed plant $G(s) + \Delta(s)$ can be stabilized over the entire

class of uncertainty. Since only the modulus of $p(\rho, j\omega)$ or $p_\rho(j\omega)$ is of interest, it is always possible to arrange for $p(\rho, s)$ or $p_\rho(s)$ to be stable and minimum phase. Furthermore, both $p(\rho, s)$ and $p_\rho(s)$ will be assumed to be proper but not strictly proper; this can be achieved by the introduction of zeros that lie well to the left of the complex plane so that they will not affect any of the relevant calculations over the desired system bandwidth[3].

Finally, the class of additive unstructured uncertainty $\Delta(s)$ to be considered is defined as

$$\mathbf{D_u} = \left\{ \Delta(s) : \begin{array}{l} (i)\ \text{G(s) and G(s)} + \Delta\text{(s) have the same number of unstable poles} \\ (ii)\ \bar{\sigma}\left[\Delta(j\omega)\right] \leq |p(j\omega)| \quad \forall\, \omega \in R \end{array} \right.$$

Additionally, both the plant $G(s)$ and the controller $K(s)$ will be assumed to have an equal number of inputs and outputs so that the implied H^∞ problem corresponds to the 1-block problem.

9.4 Theoretical development

From the preliminary discussion of the previous section it follows that in the interest of maximizing the relative stability margin of a system subject to an additive perturbation $\Delta(s)$ one should consider the following optimization problem:

$$\begin{aligned} \min_{\mathrm{K}(\rho,\mathrm{s})\ \text{stabilizing}} \|p(\rho,s)R_\rho(s)\|_\infty &= 1 \\ &= \min_{\mathrm{K}(\rho,\mathrm{s})\ \text{stabilizing}} \left\| p(\rho,s)K(\rho,s)\left[I - G_\rho(s)K(\rho,s)\right]^{-1} \right\|_\infty \end{aligned} \tag{9.14}$$

As will be seen, the optimization procedure which solves (9.14) has many close parallels with the standard H^∞ robust stability design procedure and these parallels will be fully exploited. Thus, similar to the standard H^∞ robust stability design procedure, the following lemma determines a doubly coprime factorization for the shifted plant $G_\rho(s)$:

[3]The procedure suggested here is similar to that described in [Francis, 1987], p. 76.

Lemma 9.1 (Inner coprime factorizations at the shift ρ)

For the non-negative shift $\rho \geq 0$, let $P_c(\rho)$ and $P_o(\rho)$ be the stabilizing solutions of the following algebraic Riccati equations:

$$P_c(\rho)\,(A+\rho I) + \left(A^T + \rho I\right) P_c(\rho) - P_c(\rho) B B^T P_c(\rho) \;=\; 0 \qquad (9.15)$$

$$P_o(\rho)\left(A^T + \rho I\right) + (A+\rho I)\,P_o(\rho) - P_o(\rho) C^T C P_o(\rho) \;=\; 0 \qquad (9.16)$$

and define M, $\tilde{M}$, N, and $\tilde{N}$ to be:

$$M(s) = \left[\begin{array}{c|c} A-BB^TP_c(\rho) & B \\ \hline -B^TP_c(\rho) & I \end{array}\right] \qquad \tilde{M}(s) = \left[\begin{array}{c|c} A-P_o(\rho)C^TC & -P_o(\rho)C^T \\ \hline C & I \end{array}\right] \qquad (9.17)$$

$$N(s) = \left[\begin{array}{c|c} A-BB^TP_c(\rho) & B \\ \hline C-DB^TP_c(\rho) & D \end{array}\right] \qquad \tilde{N}(s) = \left[\begin{array}{c|c} A-P_o(\rho)C^TC & B-P_o(\rho)C^TD \\ \hline C & D \end{array}\right] \qquad (9.18)$$

Then the right and left coprime factorizations of $G(s)$ are given, respectively, by:

$$G(s) = N(s)M^{-1}(s) = \tilde{M}^{-1}(s)\tilde{N}(s) \qquad (9.19)$$

with M, N, $\tilde{M}$, $\tilde{N}$, M_ρ, N_ρ, $\tilde{M}_\rho$, and $\tilde{N}_\rho$ all belonging to RH_+^∞ and with the shifted factors M_ρ and $\tilde{M}_\rho$ both being square and inner:

$$M_\rho^T(-s)M_\rho(s) = \tilde{M}_\rho(s)\tilde{M}_\rho^T(-s) = I \qquad (9.20)$$

Proof: Using standard state-space algebra [Francis, 1987] it is straightforward to show that the shifted transfer function matrix $G_\rho(s)$ has the following right and left coprime factorizations, respectively:

$$G_\rho(s) = N_\rho(s)M_\rho^{-1}(s) = \tilde{M}_\rho^{-1}(s)\tilde{N}_\rho(s) \qquad (9.21)$$

This further implies (9.19) as well as ensures that M_ρ, N_ρ, $\tilde{M}_\rho$, and $\tilde{N}_\rho$ belong to RH_+^∞. The subsequent use of standard state-space algebra in conjunction with Riccati equations (9.15) and (9.16) confirms that the shifted transfer matrices M_ρ and $\tilde{M}_\rho$ are inner. Additionally, since the following holds:

$$A - BB^TP_c(\rho) = \left[A + \rho I - BB^TP_c(\rho)\right] - \rho I \qquad (9.22)$$

the poles of M and N are those of M_ρ and N_ρ with a backshift of $-\rho$. This confirms that M and N are both in RH_+^∞; the proof for $\tilde{M}$ and $\tilde{N}$ is similar and thus omitted. ■

Remark 9.1 Note that whereas M_ρ and $\tilde{M}_\rho$ are designed to be inner at the shift ρ, in general the corresponding coprime factors after the backshift $-\rho$, namely M and $\tilde{M}$, will not typically be inner for $\rho > 0$.

As will be seen, the innerness property (9.20) of $M_\rho(s)$ and $\tilde{M}_\rho(s)$ facilitates norm-preserving simplifications of the shifted robust stability cost function (9.14) in a manner analogous to that rendered in Section 5.3. In particular, recall that H^∞ synthesis requires the construction of unshifted inner factors $M(s)$ and $\tilde{M}(s)$ in order to produce the following H^∞-norm equivalence:

$$\|p(s)R(s)\|_\infty = \left\|p(s)M^{-1}(s)U(s) + p(s)Q(s)\right\|_\infty \tag{9.23}$$

Subsequently, the term $p(s)M^{-1}(s)U(s)$ is split into a sum of stable and unstable components in order to combine the stable component with the stable term $p(s)Q(s)$; the following lemma modifies this procedure to accommodate a shifted design by first splitting the term $p(\rho,s)M_\rho^{-1}(s)U_\rho(s)$ (analogous to (9.23)) into a sum of stable and unstable terms. Furthermore, this lemma defines the relative stability optimization function $\phi(\rho)$ which equals the Hankel norm of the complex-conjugated unstable term and, therefore, also equals the infinity norm of the shifted cost function $\|p(\rho,s)R_\rho(s)\|_\infty$.

Lemma 9.2 (Internal stability at shift and relative stability optimization function $\phi(\rho)$)

With the definitions of Section 9.3 and Lemma 9.1 let the term $p(\rho,s)M_\rho^{-1}(s)U_\rho(s)$ be expressed as the following sum of stable and unstable components

$$\left[\begin{array}{c|c} A_p(\rho) & B_p(\rho) \\ \hline C_p(\rho) & D_p \end{array}\right] \times \left[\begin{array}{c|c} A+\rho I & -P_o(\rho)C^T \\ \hline B^T P_c(\rho) & 0 \end{array}\right] = \left[\begin{array}{c|c} A_s(\rho) & B_s(\rho) \\ \hline C_s(\rho) & 0 \end{array}\right] + \left[\begin{array}{c|c} A_u(\rho) & B_u(\rho) \\ \hline C_u(\rho) & 0 \end{array}\right] \tag{9.24}$$

where all the eigenvalues of $A_s(\rho)$ are stable and all the eigenvalues of $A_u(\rho)$ are unstable. Additionally, let the controllability and observability gramians, denoted by $X_u(\rho)$ and $Y_u(\rho)$ respectively, be given by the solutions of the following Lyapunov equations:

$$A_u(\rho)X_u(\rho) + X_u(\rho)A_u^T(\rho) + B_u(\rho)B_u^T(\rho) = 0 \tag{9.25}$$

$$A_u^T(\rho)Y_u(\rho) + Y_u(\rho)A_u(\rho) + C_u^T(\rho)C_u(\rho) = 0 \tag{9.26}$$

and define the relative stability optimization function $\phi(\rho)$ to be the corresponding Hankel norm given by:

$$\phi(\rho) = \sqrt{\lambda_{max}\left[X_u(\rho)Y_u(\rho)\right]} \tag{9.27}$$

Then the optimization function $\phi(\rho)$ also satisfies:

$$\phi(\rho) = \min_{\mathrm{K}(\rho,s)\ \text{stabilizing}} \|p(\rho,s)R_\rho(s)\|_\infty \tag{9.28}$$

where $K(\rho,s)$ achieves internal stability for the feedback system of Fig. 9.1 when $G(s)$ is replaced by $G_\rho(s)$.

Proof: Analogous to (8.5), the class of stabilizing controllers at the shift ρ may be parameterized by the following factorization:

$$K(\rho,s) = \left[U_\rho(s) + M_\rho(s)Q(s)\right]\left[V_\rho(s) + N_\rho(s)Q(s)\right]^{-1} \tag{9.29}$$

where $Q(s)$ is a stable transfer function in RH_+^∞. Additionally, the backshifted, right coprime factors $U(s)$ and $V(s)$ have the following state-space descriptions:

$$U(s) = \left[\begin{array}{c|c} A-BB^TP_c(\rho) & P_o(\rho)C^T \\ \hline -B^TP_c(\rho) & 0 \end{array}\right] \qquad V(s) = \left[\begin{array}{c|c} A-BB^TP_c(\rho) & P_o(\rho)C^T \\ \hline C-DB^TP_c(\rho) & I \end{array}\right] \tag{9.30}$$

Using these definitions in conjunction with the innerness properties of $M_\rho(s)$ and $\tilde{M}_\rho(s)$, it follows that the shifted H^∞ cost function may be expressed as:

$$\begin{aligned} &\min_{K(\rho,s)\ Stabilizing} \|p(\rho,s)R_\rho(s)\|_\infty \\ &\qquad = \min_{Q(s)\in RH_+^\infty} \left\|p(\rho,s)M_\rho^{-1}(s)U_\rho(s) + p(\rho,s)Q(s)\right\|_\infty \end{aligned} \tag{9.31}$$

In addition, a minimal realization of the term $M_\rho^{-1}(s)U_\rho(s)$ can be found by carrying out the multiplication and removing the unobservable/uncontrollable states to obtain:

$$M_\rho^{-1}(s)U_\rho(s) = \left[\begin{array}{c|c} A+\rho I & -P_o(\rho)C^T \\ \hline B^T P_c(\rho) & 0 \end{array}\right] \tag{9.32}$$

Hence, by its definition the function $\phi(\rho)$ can be shown [Glover, 1984] to be the Hankel norm of the unstable part of the term $p(\rho,s)M_\rho^{-1}(s)U_\rho(s)$. Moreover, this Hankel norm defines the minimal value of $\|p(\rho,s)R_\rho(s)\|_\infty$ which can be achieved by the controller of (9.29) for

$$Q(s) = -\frac{1}{p(\rho,s)}\left(Q_{\text{opt}}(s) + \left[\begin{array}{c|c} A_s(\rho) & B_s(\rho) \\ \hline C_s(\rho) & 0 \end{array}\right]\right) \tag{9.33}$$

where $Q_{\text{opt}}(s)$ denotes any of the Central Glover Solutions (c.f. Lemma 6.1) which satisfies (9.31). Finally it is noted that the modulus function $p(\rho,s)$, by its definition (c.f. Section 9.3), is stable, biproper, and minimum phase so that the unknown transfer function matrix $Q(s)$ of (9.33) is guaranteed to be in RH_+^∞. ■

The relative stability margin optimization function $\phi(\rho)$ defined by (9.27) will play a central role in determining the optimal controller, however, prior to employing $\phi(\rho)$ in actual design, we must first show the following:

(i) for $\phi(\rho) \leq 1$, the resulting controller will be stabilizing,

(ii) the optimal relative stability margin (or shift) ρ^* can be computed using (9.27) without converging to local phenomena, and

(iii) the optimal relative stability margin can computed while respecting the constraints on the number of unstable poles shared by $G_\rho(s)$ and $G_\rho(s) + \Delta_\rho(s)$.

Each of these issues will be addressed in turn beginning with the first:

Theorem 9.1 (Robust stability in terms of $\phi(\rho)$)

Let the nominal plant $G(s)$ and the perturbed plant $G(s)+\Delta(s)$ have the same number of poles to the right of the line that is perpendicular to the real axis and passes through the point $(-\rho + j0)$ and let the uncertainty $\Delta(s)$ be defined by the class $\Delta \in \mathbf{D_u}$.

Then under the assumptions and definitions of Section 9.3 and Lemmata 9.1 and 9.2 the condition

$$\phi(\rho) \leq 1 \tag{9.34}$$

ensures the following robust stability condition:

$$\det\left\{I - [G(s) + \Delta(s)]\, K_{(-\rho)}(\rho, s)\right\} \neq 0$$
$$\forall \quad s: \text{ Real(s)} > -\rho, \text{ and } \forall \quad \Delta(s) \in \mathbf{D_u} \tag{9.35}$$

where $K(\rho, s)$ is the shifted controller given by (9.29) and $K_{(-\rho)}(\rho, s)$ denotes the corresponding controller after applying the backshift $-\rho$.

Proof: (9.28) in conjunction with (9.34) implies that robust stability is maintained at the shift ρ:

$$\det\{I - [G_\rho(j\omega) + \Delta_\rho(j\omega)]\, K(\rho, j\omega)\} \neq 0 \quad \forall \quad \omega \in R \tag{9.36}$$

Now by assumption the nominal plant $G(s)$ and the perturbed plant $G(s) + \Delta(s)$ have the same number of poles to the right of the vertical line through the point $(-\rho + j0)$ and hence, $G_\rho(s)$ and $G_\rho(s) + \Delta_\rho(s)$ share an equal number of unstable poles. This, in combination with (9.36) together with the fact that $K(\rho, s)$ stabilizes $G_\rho(s)$ implies (by homotopy arguments) that the shifted sensitivity function

$$S_\rho(s) = \{I - [G_\rho(s) + \Delta_\rho(s)]\, K(\rho, s)\}^{-1} \tag{9.37}$$

is stable for all the perturbations $\Delta_\rho(s)$ in the class considered by the theorem. After application of the backshift $-\rho$, the sensitivity function may be expressed as

$$S(s) = \left\{I - [G(s) + \Delta(s)]\, K_{(-\rho)}(\rho, s)\right\}^{-1} \tag{9.38}$$

Finally, since the sensitivity function $S(s)$ is analytic everywhere to the right of the line through $(-\rho + j0)$, robust stability is ensured by (9.34). ■

The next theorem derives the important monotonicity property of the optimal relative stability cost function $\phi(\rho)$, hence enabling the use of simple and efficient

bracketing methods (such as regula falsi) to determine the optimal relative stability margin (or shift) ρ^*.

Theorem 9.2 (Monotonicity of the function $\phi(\rho)$)

The relative stability optimization function $\phi(\rho)$ of Theorem 9.1 is a monotonically increasing function of the shift ρ.

Proof: Since the definition of $\phi(\rho)$ depends on the modulus function $p(\rho, s)$ and not on the actual class of perturbations considered, we are at liberty to assume for the moment that the stable poles of the perturbation $\Delta(s)$ all have real parts less than $-\rho$ for the range of values of ρ of interest. Thus, for simplicity and without loss of generality, consider the hypothetical class of uncertainty for which

$$\overline{\sigma}\left[\Delta_\rho(j\omega)\right] \leq |p(\rho, j\omega)| \quad \forall \quad \omega \in R \quad \text{and} \quad 0 \leq \rho \leq \rho_1 \tag{9.39}$$

and for which all the stable poles of $\Delta(s)$ lie to the left of the vertical line through $(-\rho_2 + j0)$ where $0 < \rho_2$. Next let ρ_1 lie in the following interval:

$$0 \leq \rho_1 < \rho_2 \tag{9.40}$$

and assume in contradiction to the statement of the theorem that

$$\phi(\rho_2) \leq \phi(\rho_1) \tag{9.41}$$

Then by Theorem 9.1, the sensitivity function

$$S(\rho_2) = \left\{I - \left[G(s) + \Delta(s)/\phi(\rho_2)\right] K_{(-\rho_2)}(\rho_2, s)\right\}^{-1} \tag{9.42}$$

is analytic everywhere to the right of the vertical line through the point $(-\rho_2 + j0)$, and thus also to the right of the vertical line through $(-\rho_1 + j0)$. This together with the fact that $K(\rho_2, s)$ stabilizes $G_{\rho_2}(s)$ or equivalently that $K_{\rho_1-\rho_2}(\rho_2, s)$ stabilizes $G_{\rho_1}(s)$ implies that

$$\sup_\omega \overline{\sigma}\left\{p(\rho_1, s) K_{\rho_1-\rho_2}(\rho_2, s)\left[I - \left[G_{\rho_1}(s) K_{\rho_1-\rho_2}(\rho_2, s)\right]\right]^{-1}\right\} < \phi(\rho_2) \leq \phi(\rho_1) \tag{9.43}$$

which contradicts the definition of $\phi(\rho)$ according to which $\phi(\rho_1)$ is the minimal value that the left hand side of (9.43) can attain over all possible controllers which stabilize $G_{\rho_1}(s)$. ■

The previous lemmata and theorems combine to give the main result of this work:

Theorem 9.3 (Computation of the optimal relative stability margin ρ^*) *Let ρ_1 be the value of the shift ρ for which $\phi(\rho) = 1$ and let ρ^* be the largest value of the shift ρ such that both $\rho^* \leq \rho_1$ and the nominal plant $G(s)$ and the perturbed plant $G(s) + \Delta(s)$ have the same number of poles to the right of the line through the point $(-\rho^* + j0)$ making right angles with the real axis. Then ρ^* is the optimal (maximal) value of the relative stability margin. By maximal stability margin, we mean*

$$\max_K \rho[K] \tag{9.44}$$

where $\rho[K]$ is the multivariable extension of (9.6) given by

$$\rho[K] = \left\{ - \max_{\Delta(s) \in \mathbf{D_u}} [\text{Real}(s)] \quad | \quad s \in C \quad : \quad \det\{I - [G(s) + \Delta(s)]\, K(s)\} = 0 \right\} \tag{9.45}$$

The controller which achieves the optimal relative stability margin ρ^* is given by (9.29) and (9.33) for the shift $\rho = \rho^*$.

Proof: Consider first the case when $\rho^* = \rho_1$. By Theorem 9.2, the function $\phi(\rho)$ satisfies $\phi(\rho) > 1$ for all shifts $\rho > \rho^*$ which in turn implies that for any controller $K(\rho, s)$ which stabilizes the shifted plant $G_\rho(s)$ there exists a perturbation in the class $\Delta(s) \in \mathbf{D_u}$ such that for some frequency ω, the following instability condition is met:

$$\det\{I - [G_\rho(j\omega) + \Delta_\rho(j\omega)]\, K(\rho, j\omega)\} = 0 \tag{9.46}$$

Hence, there does not exist a controller which will stabilize the shifted perturbed plant $G_\rho(s) + \Delta_\rho(s)$ for all perturbations $\Delta_\rho(s)$ or equivalently there does not exist a controller which will place all of the closed-loop poles of the perturbed plant $G(s) +$

$\Delta(s)$ to the left of the vertical line through $(-\rho + j0)$ for shifts $\rho > \rho^*$. Finally, consider the case when $\rho^* < \rho_1$. By the arguments above it is known that

$$\rho^* = \max \rho\,[K] < \rho_1 \tag{9.47}$$

and for all shifts ρ between ρ^* and ρ_1, the shifted nominal plant $G_\rho(s)$ and the shifted perturbed plant $G_\rho(s) + \Delta_\rho(s)$ will have a different number of unstable poles for some perturbation in the class $\Delta(s) \in \mathbf{D_u}$. It is therefore not possible to find a controller which stabilizes $G_\rho(s) + \Delta_\rho(s)$ for all $\Delta_\rho(s)$ which is equivalent to saying that there does not exist a controller which can place all of the closed-loop poles of the perturbed plant $G(s) + \Delta(s)$ to the left of the vertical line through the point $(-\rho^* + j0)$. ■

Corollary 9.1 (Relative stability margin improvement with shift)
With the definitions of Theorem 9.3 the controller designed at the optimal shift ρ^* yields a relative stability margin which is greater than or equal to that of the controller designed with no shift:

$$\rho\left[K_{(-\rho^*)}(\rho^*, s)\right] \geq \rho\,[K(0, s)] \tag{9.48}$$

Furthermore, equality is possible only when $\rho^* < \rho_1$ and even in this case, (9.48) can be made a strict inequality by replacing $p(\rho, s)$ by $p(\rho, s)/\phi(\rho^*)$.

Proof: Use of the alternative definition of $\phi(\rho)$ given in (9.28) implies the following:

$$\begin{aligned} \phi(\rho^*) &= \left\| p(\rho^*, s) K(\rho^*, s) \left[I - G_{\rho^*}(s) K(\rho^*, s)\right]^{-1} \right\|_\infty \\ &< \left\| p(\rho^*, s) K_{\rho^*}(0, s) \left[I - G_{\rho^*}(s) K_{\rho^*}(0, s)\right]^{-1} \right\|_\infty \end{aligned}$$

where $K(\rho^*, s)$ denotes the optimal relative stability margin controller designed at the optimal shift $\rho = \rho^*$ and $K_{\rho^*}(0, s)$ denotes the H^∞ optimal controller designed at the shift $\rho = 0$ and subsequently employed at the shift $\rho = \rho^*$. The strict inequality above is due to the implicit exclusion of the trivial case $K(\rho^*, s) = K_{\rho^*}(0, s)$. If the optimal shift satisfies $\rho^* = \rho_1$, by Theorem 9.3 we have

$$\rho\left[K_{(-\rho^*)}(\rho^*, s)\right] = \rho^* > \rho\,[K(0, s)] \tag{9.49}$$

and the result of the theorem clearly holds. However, if the optimal shift satisfies $\rho^* < \rho_1$, two possibilities exist for the function $\phi(\rho^*)$:

$$\phi(\rho^*) < 1 < \left\| p(\rho^*, s) K_{\rho^*}(0, s) \left[I - G_{\rho^*}(s) K_{\rho^*}(0, s) \right]^{-1} \right\|_\infty \tag{9.50}$$

$$\phi(\rho^*) < \left\| p(\rho^*, s) K_{\rho^*}(0, s) \left[I - G_{\rho^*}(s) K_{\rho^*}(0, s) \right]^{-1} \right\|_\infty \leq 1 \tag{9.51}$$

Of these the first implies (9.49) whereas (9.51) does not preclude the possibility of (9.49) holding with equality in place of the inequality. However, in this latter case, scaling the perturbation class by replacing $p(\rho, s)$ with $p(\rho, s)/\phi(\rho^*)$ yields $\phi(\rho^*) = 1$ and, hence the previous analysis leading to (9.49) would hold. ■

The conclusion to be drawn from Corollary 9.1 is as follows: if the optimal shift satisfies $\rho^* = \rho_1$, then the H^∞ controller designed to minimize the infinity norm of $p(s)R(s)$ will not be optimal with respect to the relative stability margin $\rho[K(0, s)]$. Moreover, if the optimal shift satisfies $\rho^* < \rho_1$, the H^∞ controller $K(0, s)$ will not be optimal for the augmented class of perturbations with modulus function $p(s)/\phi(\rho^*)$ and may well not be optimal for the class with the unscaled modulus function $p(s)$. In contrast, the controller $K_{(-\rho^*)}(\rho^*, s)$ designed at the optimal shift and subsequently backshifted is guaranteed to yield the optimal relative stability margin.

9.5 Synthesis of the optimal controller

This section describes the controller design procedure which achieves the optimal relative stability margin ρ^*. However, the precise statement of the procedure requires the resolution of both of the following issues:

(*i*) An analysis of the constraints required for the use of the shifted modulus function $p_\rho(s)$ in place of $p(\rho, s)$ as per (9.11).

(*ii*) The computation of the optimal relative stability margin ρ^*.

Each of these issues will be addressed in turn below.

The resolution of issue (*i*) above arises more as a matter of convenience rather than necessity; as discussed in Section 9.3, the modulus function $p(\rho, s)$ can be

determined at each shift ρ in a manner analogous to the three typical situations presented in Cases A through C. However, given the following state-space description of the unshifted modulus function $p(0,s) = p(s)$:

$$p(s) = \left[\begin{array}{c|c} A_p & B_p \\ \hline C_p & D_p \end{array}\right]$$

it is clearly more efficient to simply shift the eigenvalues by ρ and use the shifted modulus function $p_\rho(s) = \left[\begin{array}{c|c} A_p+\rho I & B_p \\ \hline C_p & D_p \end{array}\right]$ rather than recompute $p(\rho,s) = \left[\begin{array}{c|c} A_p(\rho) & B_p(\rho) \\ \hline C_p(\rho) & D_p \end{array}\right]$ at each value of the shift ρ. Hence, it is desireable to know *a priori* the upper shift limit ρ_u (i.e. $0 \leq \rho < \rho_u$) over which the following choice of $A_p(\rho)$, $B_p(\rho)$, and $C_p(\rho)$ will be valid:

$$A_p(\rho) = A_p + \rho I \qquad B_p(\rho) = B_p \qquad C_p(\rho) = C_p \tag{9.52}$$

It will be assumed that the upper shift limit ρ_u over which (9.52) is valid can be obtained from the possible pole and zero locations of the unshifted modulus function $p(s)$ as discussed next.

To gain insight into the determination of the upper shift limit ρ_u, consider the following descriptions of a nominal, open-loop unstable plant and the corresponding perturbed plant:

$$g(s) = \frac{1}{s-a} \qquad \text{and} \qquad g(s) + \delta(s) = \frac{1}{s-(a-\epsilon)} \tag{9.53}$$

where $g(s)$ has a simple pole which satisfies $a > 0$ and ϵ is an unknown real number which satisfies $|\epsilon| < a$. Based on this information, a suitable choice for the unshifted modulus function for $\delta(s)$ is given by:

$$p(0,s) = \frac{\varepsilon}{(s+a)(s+a-\varepsilon)} \tag{9.54}$$

where ε satisfies: $|\epsilon| \leq \varepsilon < a$. Additionally, a suitable choice for the modulus function of the shifted perturbation $\delta_\rho(s)$ is[4]:

$$p(\rho,s) = \frac{\varepsilon}{(s-\rho+a)(s-\rho+a-\varepsilon)} \tag{9.55}$$

[4]Although (9.54) and (9.55) are strictly proper, they can be made proper by introducing minimum phase zeros as discussed in [Francis, 1987].

The modulus function $p(\rho, s)$ is valid for all shift values which satisfy $0 \leq \rho < a - \varepsilon = \rho_u$ and, therefore for this example, (9.52) holds true for all shifts in the interval $0 \leq \rho < \rho_u = a - \varepsilon$. As a further example, consider the unshifted modulus function $p(0, s) = \varepsilon(s + z)/(s + \alpha)$ with $0 < \alpha < z$. If it is known that $\delta(s)$ has one pole and one zero both of which lie to the left of the vertical line through $(-\alpha + j0)$ then (9.52) will hold true for all ρ in the range $0 \leq \rho < \rho_u = \alpha$. Thus, it will be assumed that the upper shift limit ρ_u can be determined from the possible pole and zero locations of the modulus function.

The remaining issue (i.e. (ii) above) to be resolved is the actual computation of the optimal relative stability margin ρ^*. However, given the monotonically increasing nature of the function $\phi(\rho)$ it is obvious that any bracketing method for the solution of (9.27) [say the bi-section or the regula falsi method] can be used to converge to ρ_1 (i.e. the value of the shift ρ for which the function $\phi(\rho)$ satisfies $\phi(\rho_1) = 1$). Providing that the point $(-\rho_1 + j0)$ is sufficiently far away from the real part of the poles of the nominal plant $G(s)$ so that the point $(-\rho_1 + j\omega)$ cannot be made to be a pole of the perturbed plant $G(s) + \Delta(s)$ for any frequency ω and any perturbation $\Delta(s)$ in the uncertainty class $\mathbf{D_u}$, the value of the optimal shift ρ^* will be given by $\rho^* = \rho_1$. This presupposes that bounds on the possible locations of the poles of the perturbed plant $G(s) + \Delta(s)$ can be stipulated, however this is possible in most practical situations. For example, information concerning the upper and lower bounds of system time constants or the natural frequencies and damping ratios can be used to determine upper and lower bounds on the real part of the system poles. This information can then be exploited to verify if the point $(-\rho_1 + j0)$ is sufficiently far away from the real part of a pole of the perturbed plant $G(s) + \Delta(s)$. Therefore, by using the monotonicity of the function $\phi(\rho)$ and using information on the possible pole locations of $G(s) + \Delta(s)$, the actual computation of the optimal shift ρ^* is relatively straightforward.

The resolution of both of the issues listed at the beginning of this section enables the following description of the design procedure to construct the optimal controller

$K_{(-\rho^*)}(\rho^*, s)$ which maximizes the relative stability margin ρ^*:

1. Determine the upper shift limit ρ_u to preclude a shift across the stable poles and zeros of $p(s)$ and such that $G(s)$ and $G(s) + \Delta(s)$ have the same number of poles to the right of the line that is perpendicular to the real axis and passes through the point $(-\rho_u + j0)$.
2. Compute ρ_1 such that $\phi(\rho_1) = 1$ using any bracketing method.
3. Compute the optimal relative stability margin $\rho^* = \min(\rho_1, \rho_u)$.
4. Determine the state-space representation of $p_{\rho^*}(s)M_{\rho^*}^{-1}(s)U_{\rho^*}(s)$ using the simplification of (9.32).
5. Separate the state-space representation of $p_{\rho^*}(s)M_{\rho^*}^{-1}(s)U_{\rho^*}(s)$ into a sum of stable and unstable terms.
6. Determine the Central Glover Solution $Q_{\text{opt}}(s)$ and retrieve $Q(s)$ as given in (9.33).
7. Construct the optimal relative stability margin controller $K_{(-\rho^*)}(\rho^*, s)$ using (9.29) in conjunction with (9.30).

This synthesis procedure is deployed in the following illustrative examples.

9.6 Illustrative examples

9.6.1 Scalar case

The following nominal plant transfer function was selected by some random means

$$g(s) = \frac{1.9235s^3 + 24.6926s^2 + 154.3848s + 302.1600}{s^4 + 3.2045s^3 - 21.5806s^2 - 42.9658s + 107.2208} \tag{9.56}$$

and has two unstable poles at $\{1.6412, 3.6804\}$ and two stable poles at $\{-3.6133, -4.9128\}$. Let this plant be subject to an additive perturbation $\delta(s)$ which has two unstable poles and whose other poles lie to the left of the vertical line through the point $(-2+j0)$. In addition, let the uncertainty class $\mathbf{D_u}$ be defined by the following modulus function

$$|\delta_\rho(j\omega)| \leq |p(\rho, j\omega)| \quad \forall \quad \rho: \quad 0 \leq \rho \leq 1 \tag{9.57}$$

where the unshifted modulus function is given by

$$p(s) = \frac{1}{s+2} + 0.1 \tag{9.58}$$

To check how realistic the uncertainty class $\mathbf{D_u}$ is for the given plant $g(s)$, Fig. 9.2 gives a plot of the frequency response of $g(s)$ with uncertainty circles of radius $|p(j\omega)|$ superimposed. From this figure it can be seen that the size of the uncertainty ranges

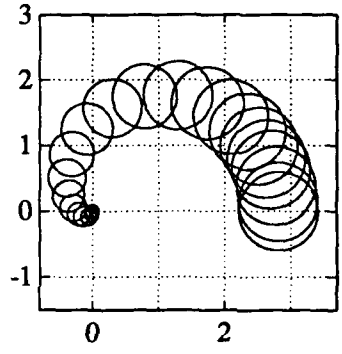

Figure 9.2: Scalar example frequency response plot of the perturbed plant $g(j\omega) + |p(j\omega)|$.

from about 20% of the magnitude of the plant $|g(j\omega)|$ at low frequencies to more than 100% at high frequencies. This sort of behaviour is typical of many practical applications [Doyle et al., 1992], and if anything it can be argued that the modulus function $p(j\omega)$ is chosen to be too large rather than too small. This observation is made to emphasize the point that in many practical instances *increasing tolerance to uncertainty beyond ihe bounds set by* $p(s)$ *does not necessarily form a useful design objective.*

The unshifted H^∞ optimal controller $k(0,s)$ which stabilizes the feedback system of Fig. 9.1 for the plant $g(s)$ of (9.56) is given by

$$k(0,s) = \frac{-6.950\,(s^4 + 10s^3 + 29.2603s^2 + 17.1797s - 18.6886)}{s^4 + 18.3279s^3 + 149.1335s^2 + 471.0315s + 478.1706} \tag{9.59}$$

This controller minimizes the infinity norm of $[p(s)r(s)]$ and yields the following

all-pass transfer function:

$$\left|\frac{p(j\omega)k(0,j\omega)}{1-g(j\omega)k(0,j\omega)}\right| = 0.6950 \quad \forall \quad \omega \tag{9.60}$$

The implication of (9.60) is that the unshifted H^∞ optimal controller $k(0,s)$ not only stabilizes the nominal plant $g(s)$, but also the perturbed plant $g(s)+\delta(s)$, for all $\delta(s) \in \mathbf{D_u}$, as well as all as the augmented class $\mathbf{D_{u_a}}$ defined by $\mathbf{D_u}$ when the modulus function $p(s)$ is replaced by $p(s)/0.6950$. A convenient alternative way of representing this information graphically is to plot $g(j\omega)k(0,j\omega)$ and superimpose circles of radius $|p(j\omega)k(0,j\omega)|$ with center $g(j\omega)k(0,j\omega)$. This is done in Fig. 9.3a to show that, as expected the band swept by the circles avoids the critical point[5] $(1+j0)$ and encircles it twice in a counter-clockwise sense, thereby ensuring the closed-loop stability of both the nominal plant $g(s)$ and the perturbed plant $g(s)+\delta(s)$ where $\delta(s) \in \mathbf{D_u}$. It can be seen that the band of circles would still just miss the critical

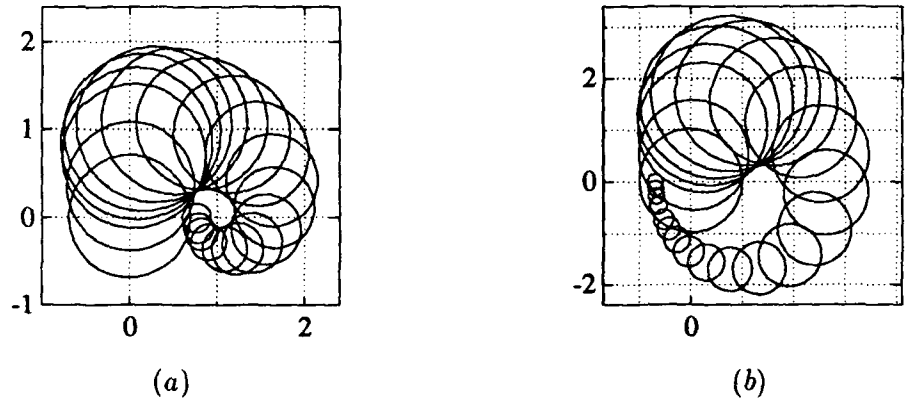

Figure 9.3: Comparison of the relative stability margin based on the open-loop frequency plots: (a) $[g(j\omega)+|p(j\omega)|]\,k(0,j\omega)$ where $k(0,s)$ denotes the unshifted H^∞ optimal controller (b) $[g(j\omega)+|p(j\omega)|]\,k_{(-\rho^*)}(\rho^*,j\omega)$ where $k_{(-\rho^*)}(\rho^*,s)$ denotes the controller which yields the optimal stability margin $\rho^* = 0.7612$.

point $(1+j0)$ [and encircle it twice counter-clockwise] if the circles are all scaled by a factor $1/0.6950$. In conclusion therefore the unshifted H^∞ optimal controller $k(0,s)$ appears to have done well as is further evidenced by the positions of the nominal

[5]This is the critical point for the positive feedback system of Fig. 9.1.

closed-loop poles which are at:

$$\{-0.5264, -1.6412, -3.6003, -3.6923, -4.9124, -12\}$$

To obtain the controller that maximizes the relative stability margin, $\rho[k]$, (in contrast to $k(0,s)$ above which maximizes the tolerance to uncertainty), regular falsi was applied using the brackets $\rho = 0$ and $\rho = 1.999$ [this latter value being dictated by the upper shift limit $\rho_u = 2$ based on the pole positions of $\delta(s)$]. For this example, the value of ρ_1 which makes the relative stability margin function satisfy $\phi(\rho_1) = 1$ is obtained after 4 iterations to within 4 decimal places and is given by $\rho_1 = 0.7612$. By assumption all perturbations in the uncertainty class $\mathbf{D_u}$ have the same number of poles to the left of the vertical line through $(-2 + j0)$ and so by Theorem 9.3 the optimal shift is given by

$$\rho^* = \rho_1 = 0.7612$$

The optimal relative stability margin controller based on the shift ρ^* is given by

$$k_{(-\rho^*)}(\rho^*, s) = \frac{-10\,(s^4 + 10.8174s^3 + 37.8698s^2 + 45.6415s + 10.3426)}{s^4 + 16.2096s^3 + 133.0385s^2 + 424.0444s + 423.1013} \qquad (9.61)$$

The open-loop frequency response information based on this controller, analogous to that already presented for $k(0,s)$, is depicted in Fig. 9.3b, and at first sight appears to have achieved the worst results. In particular it can be seen that the uncertainty circles at high frequencies nearly touch the critical point $(1 + j0)$. The implication of this is that any increase in the size of the modulus function $p(j\omega)$ could result in instability; however, as was observed earlier, if anything $|p(j\omega)|$ gives an overestimate of uncertainty, especially at high frequencies, and thus there is no need to consider an even more pessimistic modulus function. Inspection of the nominal closed-loop poles gives the first evidence of the improved relative stability margin achieved by $k_{(-\rho^*)}(\rho^*, s)$:

$$\{-1.2310, -3.2246, -3.6132, -4.9129, -5.2027, -12\}$$

However this controller was designed to shift the worst case poles as far to the left as possible, and it has achieved this as demonstrated by the shifted open-loop frequency

response evaluated at the shift $\rho = \rho^* = -0.7612$ as displayed in Fig. 9.4b. The

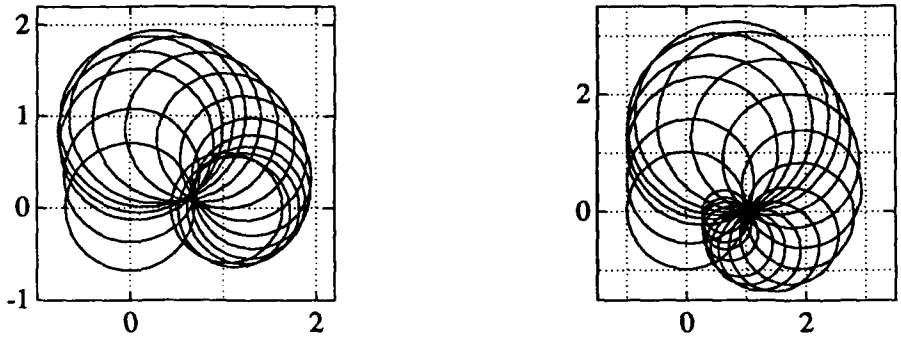

Figure 9.4: Relative stability comparison of the open-loop shifted frequency response plots using the optimal shift $\rho^* = \rho_1 = 0.7612$: (a) the shifted frequency response plot of $[g_{\rho^*}(j\omega) + |p_{\rho^*}(j\omega)|]\, k_{\rho^*}(0, j\omega)$ reveals that the unshifted H^∞ optimal controller is not robustly stabilizing at this shift and therefore has a worse stability margin (b) the shifted frequency response plot of $[g_{\rho^*}(j\omega) + |p_{\rho^*}(j\omega)|]\, k(\rho^*, j\omega)$ reveals the optimal relative stability margin controller maintains stability since all of the uncertainty circles touch the critical point but do not encircle it.

corresponding circles touch the critical point $(1 + j0)$ [at all ω frequency points] indicating that there is a worst case perturbation Δ for which the closed-loop poles lie on the vertical line through the point $(-0.7612 + j0)$. Indeed for the perturbation $\delta(s) = p(s)$ [which is clearly a member of the class] the closed-loop poles using the optimal relative stability margin controller $k_{(-\rho^*)}(\rho^*, s)$ are

$$\{-0.7612, -0.7612 \pm j3.7264, -3.6133, -4.9128, -12\}$$

The corresponding open-loop shifted frequency response plot for the optimal tolerance to uncertainty controller $k_{\rho^*}(0, s)$, shown in Fig. 9.4a, on the other hand suggests that the worst case poles for this controller will certainly lie to right of the line through the point $(-0.7612 + j0)$ since the uncertainty circles include the critical point. The precise location of the worst case pole using the controller $k(0, s)$ can be determined by plotting the open-loop frequency response of Fig. 9.4a for different values of the shift ρ and choosing the value of the shift ρ for which the band of circles

for the controller $k(0,s)$ just touches the critical point $(1+j0)$. This, as is shown in Fig. 9.5 happens for the shift $\rho = 0.0652$ which indicates that the worst case closed-loop poles can lie within a distance of only 0.0652 from the imaginary axis. Indeed

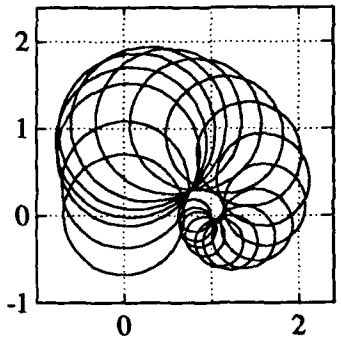

Figure 9.5:
The open-loop shifted frequency response plot of $[g_\rho(j\omega) + |p_\rho(j\omega)|]\, k_\rho(0,j\omega)$ based on the shift $\rho = 0.0652$ clearly demonstrates the reduced stability margin (i.e. $\rho = 0.0652$) of the unshifted H^∞ controller $k(0,s)$.

this is confirmed by the values below which indicate the positions of the closed-loop poles achieved by the controller $k(0,s)$ for the perturbation $\delta(s) = p(s)$:

$$\{-0.0652, -0.4936 \pm j2.9212, -3.6133, -4.9128, -12\}$$

Clearly then, although the H^∞ controller did very well by way of tolerance to uncertainty, it produced very poor results with respect to the relative stability margin. This statement is reinforced by the fact that the worst case closed-loop poles corresponding to the H^∞ controller lie an order of magnitude closer to the imaginary axis than those corresponding to the controller designed to maximize the relative stability margin.

9.6.2 Multivariable example

The procedure followed above can be repeated for a multivariable example, the only difference being that instead of the Nyquist diagram of $g(s)k(s)$ together with associated uncertainty circles, here one has to plot the generalized Nyquist diagrams with

the associated E-Contours [Daniel and Kouvaritakis, 1985] which define the regions within which the eigenvalues of $(G(s) + \Delta(s))\,K(s)$ can lie.

Consider the following state-space description of an open-loop unstable plant $G(s)$:

$$G(s) = \left[\begin{array}{c|c} A & B \\ \hline C & D \end{array}\right] = \left[\begin{array}{cccc|cc} -4 & 0 & 0 & 0 & 8 & 3 \\ 0 & -3 & 0 & 0 & 4 & 2 \\ 0 & 0 & 1 & 0 & -9 & -6 \\ 0 & 0 & 0 & 2 & 4 & 7 \\ \hline -0.3288 & -0.1644 & 0.3288 & 0.4932 & 0 & 0 \\ 0.1644 & 0.3288 & 1.3152 & 0.6576 & 0 & 0 \end{array}\right]$$

Let this plant be subject to an additive perturbation $\Delta(s) \in \mathbf{D_u}$ where the uncertainty class $\mathbf{D_u}$ is defined by the following modulus function:

$$p(s) = \frac{1}{s+2} + 0.1$$

Hence, all possible perturbations $\Delta(s)$ satisfy $\overline{\sigma}\,[\Delta(j\omega)] \leq |p(j\omega)|$. Additionally, suppose that it is known that the perturbed plant $G(s) + \Delta(s)$ has the same number of poles to the right of the vertical line through the point $(-2 + j0)$. Analogous to the previous example, this establishes an upper bound on the permissible shift (i.e. $\rho_u = 2$) and therefore yields an upper bracket for the computation of the shift ρ_1 such that the relative stability function $\phi(\rho_1) = 1$. The following results were obtained and are presented in summary form:

The nominal closed-loop poles for the unshifted H^∞ controller $K(0, s)$ are:

$$\{-0.8581, -1, -3, -4, -12, -12\}$$

The worst case closed-loop poles for the unshifted H^∞ controller $K(0, s)$ are:

$$\{-0.1812, -1.8289 \pm j0.2747, -3, -4, -12, -12\}$$

The optimal shift ρ^* for the optimal relative stability margin controller $K_{(-\rho^*)}(\rho^*, s)$ is:

$$\rho^* = 0.7266$$

The nominal closed-loop poles for the optimal relative stability margin controller $K_{(-\rho^*)}(\rho^*, s)$ are:

$$\{-2.2602, -2.4532, -3, -3.4532, -4, -12, -12\}$$

The worst case closed-loop poles for the optimal relative stability margin controller $K_{(-\rho^*)}(\rho^*, s)$ are:

$$\{-0.7266, -2.6212, -3, -3.2583, -4, -12, -12\}$$

The open-loop frequency response diagrams using $K(0, j\omega)$ and $K_{(-\rho^*)}(\rho^*, s)$ are shown in Figs. 9.6a and 9.6b, respectively. These confirm that closed-loop stability results with either controller since both plots encircle the critical point $(1 + j0)$ twice in a counter-clockwise sense.

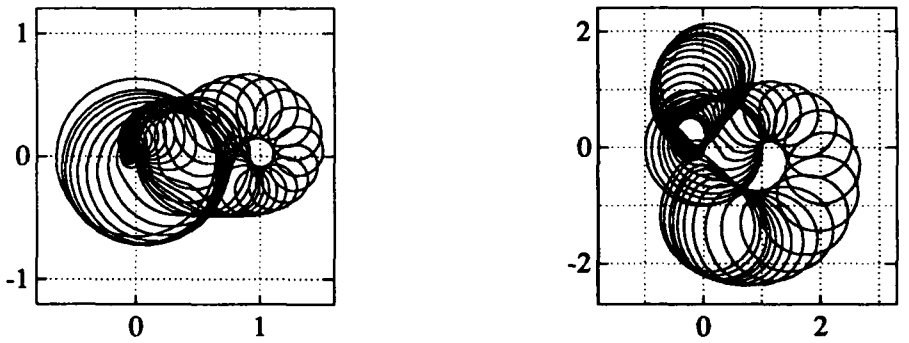

(a) (b)

Figure 9.6: Comparison of the relative stability margin based on the open-loop frequency response plots where the uncertainty $\Delta(s)$ satisfies $\overline{\sigma}\left[\Delta(j\omega)\right] \leq |p(j\omega)|$: (a) $[G(j\omega) + \Delta(j\omega)]\, K(0, j\omega)$ where $K(0, s)$ denotes the unshifted H^∞ optimal controller (b) $[G(j\omega) + \Delta(j\omega)]\, K_{(-\rho^*)}(\rho^*, j\omega)$ where $K_{(-\rho^*)}(\rho^*, s)$ denotes the controller which yields the optimal stability margin $\rho^* = 0.7266$.

Fig. 9.6b also confirms that the worst case closed-loop poles using the controller $K_{(-\rho^*)}(\rho^*, s)$ can lie within a distance of 0.7266 from the imaginary axis. The shifted open-loop frequency response diagrams based on the shift $\rho^* = 0.7266$ and using the H^∞ controller $K_{\rho^*}(0, j\omega)$ in comparison with the optimal relative stability margin controller $K(\rho^*, j\omega)$ are shown in Figs. 9.7a and 9.7b, respectively. Fig. 9.8 depicts

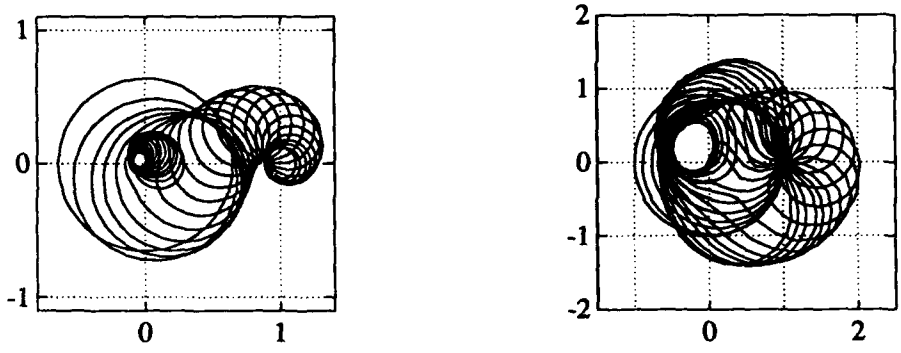

(a) (b)

Figure 9.7: Comparison of the relative stability margin using the open-loop shifted frequency response plots where the optimal shift $\rho^* = \rho_1 = 0.7266$ has been used: (a) the shifted frequency response plot of $[G_{\rho^*}(j\omega) + \Delta_{\rho^*}(j\omega)]\, H_{\rho^*}(0, j\omega)$ reveals that the unshifted H^∞ optimal controller is unstable at this shift and therefore has a worse stability margin (b) the shifted frequency response plot of $[G_{\rho^*}(j\omega) + \Delta_{\rho^*}(j\omega)]\, K(\rho^*, j\omega)$ reveals that all of the uncertainty circles touch the critical point for the controller designed at the optimal shift ρ^* and stability is maintained.

the worst case shifted open-loop frequency response using $K_\rho(0, j\omega)$ for the shift value $\rho = 0.1812$. Since the E-Contours touch the critical point $(1 + j0)$, the worst case closed-loop poles using this controller can lie within a distance of only 0.1812 from the imaginary axis. The conclusion here is the same as for the scalar case: the unshifted H^∞ controller $K(0, s)$ gave optimal results with respect to tolerance to uncertainty, but very poor results with respect to the relative stability margin, especially when these are compared with the optimal results achieved by the controller $K_{(-\rho^*)}(\rho^*, s)$.

9.7 Summary

This work has shown that when accurate upper bounds on the size of additive uncertainty are known, maximizing tolerance to uncertainty beyond such bounds does not form a useful design objective whereas maximizing the relative stability margin constitutes the clear robust design aim. In order to achieve this robustness objective, a shifted H^∞ design technique was developed along with the necessary theory govern-

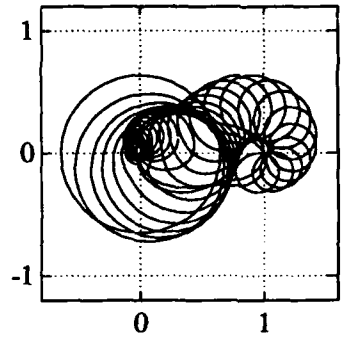

Figure 9.8:
The open-loop shifted frequency response plot of $[G_\rho(j\omega) + \Delta_\rho(j\omega)]\, K_\rho(0, j\omega)$ using the shift $\rho = 0.1812$ clearly demonstrates the reduced stability margin (i.e. $\rho = 0.1812$) of the unshifted H^∞ controller $K(0, s)$.

ing uncertainty bounding functions and the relative stability optimization function. This work represents the first application of applying a shift in the context of multivariable H^∞ design and aims directly at the maximization of the worst case relative stability margin as measured by the position of the worst case closed-loop poles. The approach was outlined and its superiority was clearly demonstrated in both scalar and multivariable examples.

Chapter 10

Conclusions and future work

10.1 Restatement of objectives

Nominal system models are subject to an unavoidable amount of uncertainty and effective control strategies must address this issue; therefore, this work was directed at advancing the theory and understanding of robust multivariable control methods. In this undertaking, a principal objective was the development of a robust interaction analysis technique which exploits the geometric eigen-structure of the generalized Nyquist/characteristic locus framework. In order to address robust design, this work turned to H^∞ optimal techniques and during this process, investigated the related aim of characterizing and using the degrees of freedom to develop new mathematical theory pertaining to H^∞ optimization. Following this, the objective of developing a robust design procedure was pursued in order to optimize relative stability. All of these objectives have been fulfilled in this work as expounded in the preceding chapters. The remainder of this chapter summarizes this work in more detail and proposes how it may be extended in the future.

10.2 Summary

Chapter 1 provided the background necessary to place this work in a proper historical context. From this perspective, the general thesis objectives were stated in terms of advancing the theory and understanding of robust multivariable control methods pertaining to perturbed interaction, H^∞ super-optimization, and H^∞ design for the maximization of relative stability. In accordance with these objectives, the work

of this thesis was divided into two main parts relating to the characteristic locus approach and the H^∞ optimal framework.

Preliminary material pertaining to uncertainty characterizations and the E-Contour method was presented in Chapter 2. Moreover, an overview of the relevant nominal and robust aspects of the generalized Nyquist/characteristic locus approach was given in order to properly orient and motivate the ensuing discussion of interaction. By way of counterexample, Chapter 3 confirmed that perturbed multivariable interaction is *not* inherently an open-loop property.

Chapter 4 characterized the worst case uncertainty which yields the maximum interaction as measured by the misalignment angles. This characterization of the worst case uncertainty enables an efficient determination of the worst case misalignment angles and, taken together with the E-Contour method, provides a convenient tool for assessing perturbed interaction using open-loop quantities.

Chapter 5 reoriented the thesis toward H^∞ optimal techniques with a presentation of the general H^∞ optimization problem. The Youla parametrization of internally stabilizing controllers not only transforms the nonlinear optimization into an affine optimization, but it also facilitates the application of Hankel approximation theory. Finally, the robust stability to additive unstructured uncertainty problem was introduced to set the stage for the following theoretical development and robust design treatment.

In Chapter 6, the degrees of freedom appertaining to the Central Glover Solution within H^∞ optimization were characterized in a manner which could be naturally exploited to achieve some well-defined mathematical properties. First, the degrees of freedom were used for square case systems to obtain the stationarity of either of the approximation system gramians. This, in turn, imposed singular value total flatness on the corresponding matched error system. Moreover, since the matched error systems shared either the controllability or observability dynamics with one of the complementary maximizing vectors, the dimensionally reduced projections were totally stable. The reduced computational complexity afforded by the stable

projections was presented in an attendant super-optimal algorithm. Finally, the computational efficiency was enhanced even further by the subsequent super-optimal algorithm which exploited the minimal realization of the core recursion term.

Chapter 7 extended the results of Chapter 6 by considering general nonsquare systems. The degrees of freedom were deployed to yield either singular value near flatness or minimal antistable projections in the context of a super-optimal algorithm. Although the near flatness solutions could be successfully deployed in super-optimization, early termination of the associated super-optimal algorithm required a strict upper bound on the norm of the degree of freedom parameter. To achieve this, a composite Riccati equation was derived by merging the necessary conditions for approximation gramian stationarity with the respective gramian Riccati equations. The composite Riccati equation gave a unique solution which not only ensured H^∞ optimality throughout each cycle of super-optimization, but the solution could also be found in closed form without recourse to the standard Riccati solution procedure.

Chapter 8 evaluated a simple class of H^∞ super-optimal controllers from a relative stability perspective. In support of this, a simple procedure was developed in order to demonstrate that super-optimal design does not implicitly optimize relative stability.

Chapter 9 presented a newly developed robust design technique to maximize the worst case relative stability margin. This work represented the first application of applying a shift in the context of multivariable H^∞ design and aimed directly at the maximization of the worst case relative stability margin as measured by the position of the worst-case closed-loop poles. The specific cost function required to maximize the relative stability margin was formulated along with the theory required to optimize the cost function. Finally, the design process itself was given along with illustrative examples.

10.3 Recommendations for future research

The work presented in this thesis suggests several avenues leading to potentially rewarding future research in the area of robust multivariable control. From the wealth of robust frequency domain results, most of the fruitful work apparently originates from the classical approach initiated by Bode and Nyquist. Therefore, the following suggestions for ensuing work all emanate from the frequency domain.

- A key direction of future research involves the development of a robust generalized Nyquist/characteristic locus design procedure. The E-Contour method enables a worst case relative stability assessment from the perturbed characteristic locus bands. In addition, the work of this thesis enables a worst case interaction assessment from the misalignment angles of the perturbed system. Hence, the robust analysis tools are in place for potential extension to robust *design*.

- A related direction of research encompasses the characterization of commutative commutative controllers based on the Youla parametrization. Since this parametrization embraces the entire class of stabilizing controllers generated by a *free* transfer function matrix $Q(s) \in RH_+^\infty$, future research could examine how to use this degree of freedom to achieve controller commutativity with the plant transfer function matrix. This would have the concomitant benefit of removing previous artificial design constraints needed to ensure stability.

- Future research can also be focused on applications of the real rational singular value decomposition resulting from super-optimization. In particular, the super-optimal error system has the following real rational singular value decomposition:

$$G_{e_{so}}(s) = \mathbf{Y}(s)\, \mathbf{\Sigma}\, \mathbf{X}^T(s)$$

where $\mathbf{X}(-s)$ and $\mathbf{Y}(s)$ are the dynamic input and output principal directions (i.e. maximizing vectors), respectively, and $\mathbf{\Sigma}$ contains the ordered, constant

s-numbers [c.f. (6.21)]. Hence, prospective research could explore possible applications of this dynamic singular value decomposition.

- A *final suggestion for future work* lies in the extension of the shifted H^∞ design technique to additional H^∞ control problems. For example, it would be interesting to determine the impact of shifted design in the mixed disturbance rejection performance and multiplicative output uncertainty robustness problem; however in this case, a prime challenge would be in formulating a meaningful and precise measure analogous to the relative stability measure defined in this work.

Bibliography

Adamjan, V. M., Arov, D. Z., and Krein, M. G. (1978). Infinite block matrices and related extension problems. *AMS Transactions*, 111(2):133–156.

Anderson, B. D. O. and Moore, J. B. (1971). *Linear Optimal Control.* Prentice Hall, Englewood Cliffs, New Jersey.

Anderson, B. D. O. and Moore, J. B. (1989). *Optimal Control: Linear Quadratic Methods.* Prentice Hall, Englewood Cliffs, New Jersey.

Bernstein, D. and Haddad, W. M. (1989). LQG control with an H^∞ performance bound. *IEEE Transactions on Automatic Control*, 34(3):293–305.

Cameron, R. and Kouvaritakis, B. (1979). The relative stability margins of multivariable systems: A characteristic locus approach. *International Journal of Control*, 30(4):629–651.

Chang, M. and Rhodes, I. B. (1975). Disturbance localization in linear systems with simultaneous decoupling, pole assignment or stabilization. *IEEE Transactions on Automatic Control*, 20(4):518–523.

Chiang, R. Y. and Safonov, M. G. (1988). *MATLAB Robust-Control Toolbox.* The MathWorks, Inc., South Natick, Massachusetts.

Chu, C. C., Doyle, J. C., and Lee, E. B. (1986). The general distance problem in H^∞ optimal control theory. *International Journal of Control*, 44(2):565–596.

Cloud, D. J. and Kouvaritakis, B. (1986). Statistical bound on multivariable frequency response: an extension of the generalized nyquist criterion. *Proceedings of the IEE, Part D*, 133(3):97–109.

Cloud, D. J. and Kouvaritakis, B. (1988). A frequency response-based model order selection criterion. *IEEE Transactions on Automatic Control*, 33(6):582–585.

Crews, M. C. and Kouvaritakis, B. (1992a). Characterization and use of the degrees of freedom in the H^∞ problem. *International Journal of Control.* To appear.

Crews, M. C. and Kouvaritakis, B. (1992b). An evaluation of super-optimality as a control tool: a relative stability perspective. *International Journal of Control.* To appear.

da Silva, P. S. P. and Leite, V. M. P. (1992). Decoupling by dynamic measurement feedback with stability: Necessary and sufficient conditions. *IEEE Transactions on Automatic Control*, 35(5):620–623.

Daniel, R. W. and Kouvaritakis, B. (1984). Analysis and design of linear multivariable feedback systems in the presence of additive perturbations. *International Journal of Control*, 39(2):551–580.

Daniel, R. W. and Kouvaritakis, B. (1985). A new robust stability criterion for linear and non-linear multivariable feedback systems. *International Journal of Control*, 41(6):1349–1379.

Daniel, R. W., Kouvaritakis, B., and Latchman, H. (1986). Principal direction alignment: a geometric framework for the complete solution to the μ-problem. *Proceedings of the IEE, Part D*, 133(2):45–56.

Descusse, Y., Lafay, J. F., and Kačera, V. (1984). Decoupling by restricted static-state feedback: The general case. *IEEE Transactions on Automatic Control*, 29(1):79–81.

Descusse, Y., Lafay, J. F., and Malabre, M. (1988). Solution to Morgan's problem. *IEEE Transactions on Automatic Control*, 33(8):732–739.

Desoer, C. A., Liu, R. W., Murray, J., and Saeks, R. (1980). Feedback system design: The fractional representation approach to analysis and synthesis. *IEEE Transactions on Automatic Control*, 25(3):399–411.

Desoer, C. A. and Nasli Gündes, A. (1986). Decoupling linear multiinput plants by dynamic output feedback: An algebraic theory. *IEEE Transactions on Automatic Control*, 31(8):744–750.

Dorf, R. C. (1989). *Modern Control Systems.* Addison Wesley, Wokingham, England, fifth edition.

Doyle, J. C. (1978). Guaranteed margins for LQG regulators. *IEEE Transactions on Automatic Control*, 23(4):756–757.

Doyle, J. C. (1984). Lecture notes for ONR/Honeywell Workshop on Advances in Multivariable Control. ONR/Honeywell, Minneapolis, Minnesota.

Doyle, J. C., Francis, B. A., and Tannenbaum, A. R. (1992). *Feedback Control Theory.* Maxwell Macmillan International, Oxford.

Doyle, J. C., Glover, K., Khargonekar, P. P., and Francis, B. A. (1989). State-space solutions to standard H^2 and H^∞ control problems. *IEEE Transactions on Automatic Control*, 34(8):831–846.

Doyle, J. C. and Stein, G. (1979). Robustness with observers. *IEEE Transactions on Automatic Control*, 24(4):607–611.

Doyle, J. C. and Stein, G. (1981). Multivariable feedback design: Concepts for a classical/modern synthesis. *IEEE Transactions on Automatic Control*, 26(1):4–16.

Edmunds, J. M. (1984). Confidence limits on identified frequency responses. Technical Report 607, University of Manchester Institute of Science and Technology, Manchester, England. Control System Center Report.

Fabian, E. and Wonham, W. M. (1975). Decoupling and disturbance rejection. *IEEE Transactions on Automatic Control*, 20(3):399–401.

Foo, Y. K. and Postlethwaite, I. (1986). An H^∞-minimax approach to the design of robust control systems, Part II: All solutions, all-pass form solutions and the 'best' solution. *Systems & Control Letters*, 7:261–268.

Francis, B. A. (1987). *A Course in H_∞ Control Theory.* Springer-Verlag (Lecture Notes in Control and Information Sciences), London.

Francis, B. A. and Doyle, J. C. (1987). Linear control theory with an H^∞ optimality criterion. *SIAM Journal of Control and Optimization*, 25:815–844.

Glover, K. (1984). All optimal Hankel-norm approximations of linear multivariable systems and their L_∞-error bounds. *International Journal of Control*, 39(6):1115–1193.

Glover, K. (1986). Robust stabilization of linear multivariable systems: Relations to approximation. *International Journal of Control*, 43(3):741–766.

Glover, K. and Doyle, J. C. (1988). State-space formulae for all stabilizing controllers that satisfy an H^∞-norm bound and relations to risk sensitivity. *Systems & Control Letters*, 11:167–172.

Golub, G. H. and Van Loan, C. F. (1983). *Matrix Computations.* The John Hopkins University Press, Baltimore, Maryland.

Gu, D.-W., Tsai, M.-C., and Postlethwaite, I. (1989). An algorithm for super-optimal H^∞ design: the two-block case. *Automatica*, 25(2):215–221.

Horowitz, I. (1963). *Synthesis of Feedback Systems.* Academic Press.

Horowitz, I. (1982). Quantitative feedback theory. *Proceedings of the IEE, Part D*, 129(6):215–226.

Hvostov, H. S. (1990). Simplifying H^∞ controller synthesis via classical feedback system structure. *IEEE Transactions on Automatic Control*, 35(4):485–488.

Ingpen, R. and Wilkinson, P. (1991). *Encyclopedia of World Events: Eighty turning points in history.* Dragon's World, London.

Kailath, T. (1980). *Linear Systems.* Prentice-Hall Publishing Company, Inc., Englewood Cliffs, New Jersey.

Kalman, R. E. (1964). When is a linear control system optimal? *Journal of Basic Engineering, Series D*, 86:51–60.

Kalman, R. E., Falb, P. L., and Arbib, M. A. (1964). *Topics in Mathematical Systems Theory.* McGraw-Hill, New York.

Kawasaki, N. and Shimemura, E. (1988). Pole placement in a specified region based on a linear quadratic regulator. *International Journal of Control*, 48(1):225–240.

Kim, S. and Furuta, K. (1988). Regulator design with poles in a specified region. *International Journal of Control*, 47(1):143–160.

Kimura, H., Oike, T., Miura, A., Akai, K., and Kida, T. (1991). Robust stability-degree assignment and its applications to the control of flexible structures. *International Journal of Robust and Nonlinear Control*, 1:153–169.

Kouvaritakis, B. (1988). A short course on multivariable control. Oxford University.

Kouvaritakis, B. and Crews, M. C. (1991). Uncertainty and interaction of linear multivariable feedback systems. *International Journal of Control*, 54(4):849–865.

Kouvaritakis, B., Crews, M. C., and Daniel, R. W. (1991). H^∞ design for the maximization of relative stability margins. Technical Report 1901/91, Oxford University, Oxford, England.

Kouvaritakis, B. and Latchman, H. (1985). Necessary and sufficient stability criterion for systems with structured uncertainties: The major principle direction alignment property. *International Journal of Control*, 42(3):575–598.

Kouvaritakis, B. and Latchman, H. (1986). Necessary and sufficient stability criterion for the case of dependent additive perturbations. *International Journal of Control*, 43(6):1615–1630.

Kouvaritakis, B. and Rossiter, J. A. (1992). Use of bicausal weighting sequences in least squares identification of open-loop unstable dynamic systems. *Proceedings of the IEE, Part D*, 139(3):328–336.

Kouvaritakis, B. and Trimboli, M. S. (1988). Dynamic performance, interaction, and the characteristic locus method: A quantitative approach. *International Journal of Control*, 47(4):915–936.

Kouvaritakis, B. and Trimboli, M. S. (1989). Robust multivariable feedback design. *International Journal of Control*, 50(4):1327–1377.

Kwakernaak, H. (1986). A polynomial approach to minimax frequency domain optimization of multivariable feedback systems. *International Journal of Control*, 44(1):117–156.

Laub, A. J., Heath, M. T., Page, C. C., and Ward, R. C. (1987). Computation of balancing transformations and other applications of simultaneous diagonalization algorithms. *IEEE Transactions on Automatic Control*, 32:115–122.

Limebeer, D. J. N., Halikias, G. D., and Glover, K. (1989). State-space algorithm for the computation of super-optimal matrix interpolating functions. *International Journal of Control*, 50(6):2431–2466.

MacFarlane, A. G. J., editor (1980). *Complex Variable Methods for Linear Multivariable Feedback Systems.* Taylor and Francis, London.

MacFarlane, A. G. J. and Kouvaritakis, B. (1977). A design technique for linear multivariable feedback systems. *International Journal of Control*, 25(6):837–874.

MacFarlane, A. G. J. and Postlethwaite, I. (1977a). Characteristic frequency functions and characteristic gain functions. *International Journal of Control*, 26(2):265.

MacFarlane, A. G. J. and Postlethwaite, I. (1977b). The generalized Nyquist stability criterion and multivariable root loci. *International Journal of Control*, 25(1):81–128.

Maciejowski, J. M. (1989). *Multivariable Feedback Design.* Addison-Wesley Publishing Company, Inc., Wokinghan, England.

Mårtensson, K. (1971). On the matrix Riccati equation. *Information Sciences*, 3:17–49.

Maxwell, J. C. (1868). On governors. *Proc. of the Royal Society of London.* in *Selected Papers on Mathematical Trends in Control Theory.* Dover, New York, 1964; pp. 270–283.

McFarlane, D. C. and Glover, K. (1990). *Robust Controller Design Using Normalized Coprime Factor Plant Descriptions.* Springer-Verlag (Lecture Notes in Control and Information Sciences), London.

Medanic, J., Tharp, H. S., and Perkins, W. R. (1988). Pole placement by performance criterion modification. *IEEE Transactions on Automatic Control*, 33(5):469–472.

Moore, B. C. (1981). Principal component analysis in linear systems: Controllability, observability, and model reduction. *IEEE Transactions on Automatic Control*, 26(1):17–32.

Moore, J. B., Glover, K., and Telford, A. (1990). All stabilizing controllers as frequency-shaped state estimate feedback. *IEEE Transactions on Automatic Control*, 35(2):203–208.

Morse, A. S. and Wonham, W. M. (1971). Status of noninteracting control. *IEEE Transactions on Automatic Control*, 16(6):568–581.

Nehari, Z. (1957). On bounded bilinear forms. *Annals of Math*, 65:153–162.

Nett, C. N., Jacobson, C. A., and Balas, M. J. (1984). A connection between state-space and doubly coprime representations. *IEEE Transactions on Automatic Control*, 29(9):831–832.

Nyman, P. O. (1991). Equalizer principle of H^∞-optimal control and its application to super-optimization. *International Journal of Control*, 54(2):393–415.

Pernebo, L. and Silverman, L. M. (1982). Model reduction via balanced state space representations. *IEEE Transactions on Automatic Control*, 27(2):382–387.

Postlethwaite, I., Tsai, M.-C., and Gu, D.-W. (1989). Super-optimal H^∞ design. In *Internation Symposium on the Mathematical Theory of Networks and Systems*, Amsterdam (Amsterdam: North-Holland).

Potter, J. E. (1966). Matrix quadratic solutions. *Journal SIAM*, 14(3):497–501.

Rosenbrock, H. H. (1974). *Computer-Aided Control System Design.* Academic, New York.

Safonov, M. G. and Athans, M. (1977). Gain and phase margins of multiloop LQG regulators. *IEEE Transactions on Automatic Control*, 22(2):173–179.

Safonov, M. G. and Verma, M. S. (1985). L^∞ optimization and Hankel approximation. *IEEE Transactions on Automatic Control*, 30(3):279–280.

Sideris, A. (1990). H^∞ optimal control as a weighted Wiener-Hopf problem. *IEEE Transactions on Automatic Control*, 35(3):361–366.

Siebert, W. M. (1986). *Circuits, Signals, and Systems.* McGraw-Hill, New York.

Trimboli, M. S. (1989). *Generalized Nyquist Design for Uncertain Linear Feedback Systems.* PhD thesis, Oxford University, Oxford, England.

Tsai, M.-C., Gu, D.-W., and Postlethwaite, I. (1988). A state-space approach to super-optimal H^∞ control problems. *IEEE Transactions on Automatic Control*, 33(9):833–843.

Tsai, M.-C., Gu, D.-W., Postlethwaite, I., and Anderson, B. D. O. (1990). Inner functions and a pseudo-singular-value decomposition in super-optimal H^∞ control. *Internation Journal of Control*, 51(5):1119–1131.

Van Trees, H. L. (1968). *Detection, Estimation, and Modulation Theory.* Wiley, New York.

Wicks, M. A. and DeCarlo, R. A. (1990). Gramian assignment based on the Lyapunov equation. *IEEE Transactions on Automatic Control*, 35(4):465–468.

Wiener, N. (1948). *Cybernetics, or Control and Communication in the Animal and the Machine.* John Wiley, New York.

Wonham, W. M. (1979). *Linear Multivariable Control: A Geometric Approach.* Springer-Verlag, New York, second edition.

Youla, D. C., Jabr, H. A., and Bongiorno, J. J. (1976). Modern Weiner-Hopf design of optimal controllers: Part II. *IEEE Transactions on Automatic Control*, 21(3):319–338.

Young, N. J. (1983). The singular-value decomposition of an infinite-Hankel matrix. *Linear Algebra and its Applications*, 18:639–656.

Young, N. J. (1986a). An algorithm for the super-optimal sensitivity minimising controller. *Proc. Workshop on New Perspectives in Industrial Control System Design Using H^∞ Methods.*

Young, N. J. (1986b). The Nevanlinna-Pick problem for matrix-valued functions. *J. Operator Theory*, pages 239–265.

Zames, G. (1981). Feedback and optimal sensitivity: Model reference transformations. *IEEE Transactions on Automatic Control*, 26(2):301–320.

Zames, G. and Francis, B. A. (1983). Feedback, minimax sensitivity, and optimal robustness. *IEEE Transactions on Automatic Control*, 28(5):585–601.

Zhou, K., Doyle, J. C., and Glover, K. (1990). Mixed H^2 and H^∞ control. *American Control Conference.*